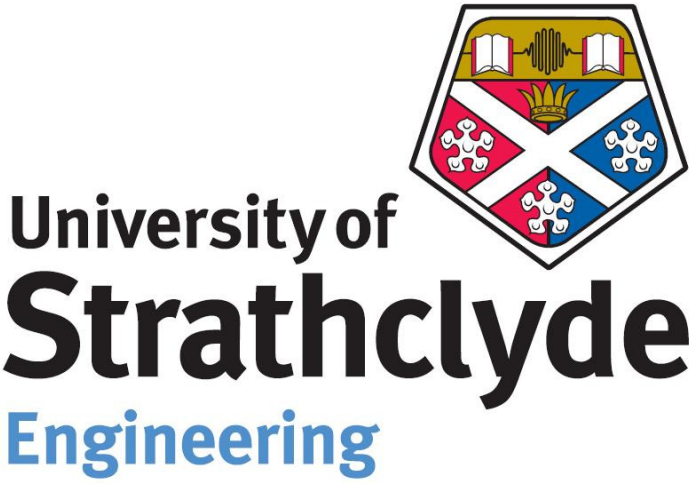

Department of Chemical & Process Engineering

Effect of Density Change on Flux Response Systems

Alexis McDonald

Degree of Doctor of Philosophy

2018

This thesis is the result of the author's original research. It has been composed by the author and has not been previously submitted for examination which has led to the award of a degree.

Signed:
Date:

Acknowledgements

I would like to thank my supervisors, Dr M.J. Heslop and Dr E. Ventura-Medina, for all their help and support throughout the duration of this project. Thank you Dr Heslop for your patience and guidance through all the issues faced during this time. Also thank you to Dr Ventura-Medina for taking on my case! I appreciate all that you both have done to enable me to submit this work.

My thanks are extended to all the departmental staff who contributed in many ways from technical, laboratory and secretarial support to lengthy discussions concerning this topic and more.

I thank my colleagues in the Department of Chemical and Process Engineering. Though most have moved on to various areas, of study and geography, I wish them all the best and cherish the time which we all spent together, supporting each other through the ups and downs of our work.

Also, thank you to my colleagues at Collagen Solutions (UK) Ltd. Without your support, help and giving me time, I would not have been able to complete this thesis.

I will be eternally grateful to the NHS staff in various departments that have educated me in controlling the challenges faced in the past decade and made them manageable.

Many thanks to my friends for their continuous support and humour throughout the long, extensive, lengthy journey of this project. Some thought this submission might never happened but better late than never.

Finally, I'd like to thank my family for their unceasing and unconditional support. For this I will always be grateful.

Abstract

Flux response technology is a technique for using differential measurements of flow rates as changes occur caused by adsorption, reaction and desorption in a continuous flow reactor. This work looks at using a gas chromatographic column as the reactor and uses the concepts of capillary and perturbation viscometry to quantify the effects of density change on flux response on the reactor.

Experiments were conducted using basic equipment including a volume and different resistance set up in a Wheatstone bridge arrangement so that differential measurements can be obtained. Firstly, changes were made by perturbing the flow into the system with pressure. Secondly, changes were made to the system by perturbing with a gas flow. Measurements were taken using a differential pressure transducer (DPT) to measure the flux response and the results were used to determine the volume in the system.

Further experiments were conducted to validate theoretical derivations of the operation of a gas density detector (GDD) which could be used as a gas chromatographic detector. Experiments using nitrogen and argon as the main and perturbation gases were completed. Results were obtained using the DPT and the GDD and verified the theoretical derivations. The results showed that when the perturbation gas is of a higher density to that of the main gas, there is a distinct positive step in the both the DPT and GDD readings. There is negative step when the perturbation gas has a lower density which was as expected.

Helium experiments proved problematic as there were potential issues with viscosity change affecting the detector response producing some anomalous results so further work is required to investigate this. Additional work using different gas components would be advantageous.

Table of Contents

1. Introduction

Gas chromatography is a common separation technique. It is used in many industries including the drug and pharmaceutical industry for quality control purposes and in the analysis of new products, the petroleum industry to separate and determine the components in the petroleum products and in the food industry including the analysis of wines and the determination of antioxidants and food preservatives [1-7].

Gas chromatography (GC) is a popular method because of its simplicity. GC is different from other separation techniques in that one phase moves while the other phase is stationary. It involves chemical equilibria between the phases to bring about a separation. GC is a non-laborious procedure with minimal equipment involved which gives very concise results. The four essential components to carry out a chromatographic separation are a column, a mobile phase, a sample injector and a detector [2]. The detectors measure a physical property of the gas mixture components in the GC system. It is desirable for the detector response to be equal for all sample components present in the carrier gas and give a linear response with concentration. It is also preferable for the detector response to be insensitive to flow rate and pressure changes. The mostly commonly used chromatographic detectors are thermal conductivity detectors (TCDs) and flame ionization detectors (FIDs). Both have some limitations.

TCDs can be used to detect any component other than the carrier gas if their thermal conductivities are different to that of the carrier gas at the detector temperature. The TCD operates with an electrically heated element situated in the gas stream. The resistance of the element is continuously measured by a Wheatstone bridge arrangement which supplies an electrical current. The thermal conductivity is constant when there is just the pure carrier gas being passes through the system. If another component is present in the carrier gas, the equilibrium is disturbed and the change in resistance in the element causes the bridge to become unbalanced. The resultant chromatogram allows the component to be identified and quantified.

FIDs usually involve a hydrogen-air flame which burns the sample to be analysed, pyrolyzing the organic compounds and produces positively charged ions and electrons. Two electrodes are used to provide a potential difference and so ions are detected. The positive electrode is a

nozzle head where the flame is produced. The negative electrode is the collector plate, positioned above the flame. The positively charged ions are attracted to the negatively charged collector plate. As the ions hit the plate a current is induced. The current is measured by an electrometer. The current measured corresponds to the proportion of reduced carbon atoms in the flame. This makes the FID sensitive to mass rather than concentration. The FID has the advantage that it responds to virtually all organic compounds but it destroys the sample being tested.

A gas density detector to be used as a chromatographic detector. A gas density balance was first postulated and developed by Martin and James [8]. They recognised the importance of developing a gas chromatographic detector where its response is dependent on the differences in molecular weights of the substances being separated and independent of the chemical structures. Their design consisted of tubes being arranged in a Wheatstone bridge type arrangement.

Their design was simplified in both design and construction by Nerheim [9] but the principles of the initial design were still the same. Nerheim patented his design and later Gow-Mac Instrument Co. developed the design into a commercial model. Papers have been published looking at the optimum operating conditions and suitable carrier gases and comparisons have been made with other gas chromatographic detectors including the thermal conductivity detector and flame ionization detector [10-18]. The gas density detector was found to give comparable results to both detectors and had the advantages that no calibration was required and that the detector could be used with corrosive samples. The last publication relating to the gas density detector was written by Brandes, Kirchner and Richter [19] comparing the GDD to other chromatographic detectors including TCD and FID and again highlighted the advantages using the GDD.

The work presented here includes deriving theoretical equations for the operation of the gas density detector when changes in flow rates, density and pressure are made to the system. An experimental arrangement was set-up to validate the derivations developed using different gas components in the system.

Combining this new work with previous work, an innovative theme was considered; applications of gas density in flux-response systems. Flux response technology is based on capillary viscometry for the measurement of small changes in flow and viscosity between two

gas streams. The technique enables small changes in volumetric flow rate to be used to make differential measurements in a range of applications. The experimental set-up developed to complete the gas density detector work was used to determine the flux response in the system, with the flux response being the flow rate changes caused by adsorption, reaction and desorption within the continuous flow system. In all experiments conducted, a change is made to the system, either pressure, flow rate or composition, and the flux response to recorded using a differential pressure transducer (DPT). The results from the DPT are then used to quantify the pressure or volume change resulting from the change in the system inputs. The gas density detector was then incorporated into the arrangement to allow another physical property to be measured.

In this work, flux response technology is used investigate the effect of a change in gas density in a system by adding a perturbation flow to the sample flow of the system. The experimental work was separated into three separate projects, each with the common theme of density change. Each project is considered separately, and results are analysed to form conclusions.

The first project involved a completely new arrangement to measure volume using perturbations in pressure. An adjustment to the system was achieved by a change in the resistance which results in a change in pressure as opposed to a change in the flow entering the system. Therefore, the flow remains constant while there is a step change in pressure. A new pneumatic Wheatstone bridge arrangement of resistances was used to achieve results using a differential pressure transducer. The results from the differential pressure transducer were used to measure the volume in the system.

The second project modified the original arrangement for volume measurement using a two-sided arrangement, larger flows and different resistance ratios. A perturbation flow is used to make a change to the system instead of the resistance change used in the first part. In these experiments, there is a step change in flow and pressure with the addition of the perturbation flow. Delay lines were incorporated into the apparatus so that the resulting effect of that change in viscosity due to the addition of the perturbation flow can be seen separately from the effect of the change in flow rate. A differential pressure transducer was used to measure changes when the perturbation flow is added to the measurement side of the system. The result graphs and the theoretical equations derived in this work were used to calculate the change in the pressure in the system when the perturbation flow is added and from these changes the volume could be measured.

Finally, the third project involved the investigation of the operation of the gas density detector (GDD). Theoretical derivations of the operation of the GDD were developed. Experiments were conducted to validate the theories. The double-sided arrangement used in the second project is expanded to include a novel third branch of equal resistance to allow there to be minimal disturbance to the system when changes were made to the system. The gas density detector is incorporated into the apparatus to verify if the hypothetical equations developed in the theory section can corroborate the effect of adding the perturbation flow. In all previous work considering the theory of the GDD, it has been assumed that the flow stays constant. In the work done here, this assumption has not been made and so a new theory has been developed for changing flow. The experiments carried out involve step changes in flow, composition and density while the pressure remains constant. Like in the second project, a differential pressure transducer is used to monitor the changes in the system from perturbing the sample flow with a known component. This project uses the GDD to investigate if a relationship can be found between the GDD results and the change in flow rate, pressure and density due to the addition of the perturbation flow.

The first two projects were carried out using single component systems so that the composition would be the same. The third project considers multi-component systems so that there is a change in composition as well as flow and density. The pressure was maintained at a constant level.

To summarise, the three main aims of this work were: -

1. To develop a new pneumatic Wheatstone bridge arrangement of resistances which allows a pressure perturbation to be used to measure system volumes.
2. To use existing flux response technology to improve this arrangement by developing a two-sided apparatus with changes made by adding a perturbation flow to one side of the system to measure volume.
3. To investigate the operation of the gas density detector and to introduce a new method of measurement through the inclusion of the gas density detector to the experimental arrangement, allowing binary component systems to be considered.

2. Background and Literature Review

2.1. Introduction

This section will give some background into the subjects fundamental to this work and look at previous work conducted in these areas. Firstly, gas chromatography (GC) will be considered and detectors used in this technique. Secondly, using a gas density detector as a means of GC detection will be investigated. Finally, the sorption effect will be explored along with how it is used to determine adsorption isotherms. The sorption effect principles were then used to make viscosity measurements through perturbation viscometry. The basic experimental arrangement used in the sorption effect method was then used as the basis for the apparatus design of flux response measurements.

2.2. Gas Chromatography (GC) and GC Detectors

Most separation techniques involve the formation of at least two phases in which the objective is to separate and measure the various constituents. By choosing the appropriate conditions (temperature and pressure), the phase of the original mixture can be changed. When this phase transition is complete, one phase will contain the component of interest and the other phase the component or components that are not of interest. Phases can be mechanically or physically separated and the phase with the component of interest is retained [20].

Chromatography is a relatively simple experimental technique. It is used in organic chemistry for separating and analysing compounds that can be vaporized without decomposition. The technique can be used for testing the purity of a particular substance or separating the different components of a mixture [1-7].

Gas chromatography (GC) is different from other separation techniques in that one phase moves and the other phase is stationary. GC involves chemical equilibria between phases to bring about a particular separation. Different chromatographic techniques are observed by combining different phase pairs, e.g. by using gas as the mobile phase and solids as the stationary phase gives gas-solid chromatography (GSC).

Four components are essential in a chromatographic separation; a column, a mobile phase, a sample injector and a detector [2]. The mobile phase is a carrier gas, usually an inert gas like helium or unreactive gas like nitrogen. Helium is the most common carrier gas because it can be used in a high range of flow rates, it is non-flammable and works well in most detectors. The sample injector is used to introduce the sample into the column and transport through by the carrier gas. The choice of injection technique or inlet type depends on if the sample is in liquid, gas, adsorbed or solid form.

The column is a piece of glass or metal tubing where the stationary phase is situated. The column is usually contained in an oven for the temperature to be precisely controlled electronically. The stationary phase used to separate the components is an inert solid support (GSC) or a microscopic layer of liquid on the column walls as in gas liquid chromatography (GLC). The gaseous compounds in the mobile phase being analysed will interact with the stationary phase in the column causing each compound to elute at a different time known as the retention time of the compound. The rate at which the molecules progress along the column depends on the strength of adsorption. Each component has a different rate of progression through the column. The various components in the gas mixture are separated as they progress along the column and so reach the end of the column at different times. Therefore, each chemical compound has a different retention time. The retention time can be affected by the carrier gas flow rate and temperature so these must be kept constant. Carrier gas flow rate and temperature affect the chromatographic analysis in the same way, the higher the flow rate or temperature, the faster the sample moves through the column but the lower the separation between analytes as there is less interaction with the stationary phase. Therefore, flow rate and temperature selection is a compromise between the level of separation and the length of analysis.

The comparison of the retention times makes gas chromatography such a useful analytical technique. A detector is used to monitor the outlet stream from the column electronically. The time at which each component reaches the outlet and the amount of that component can be determined by the detector and can be seen on a chromatogram. A chromatogram, shown in Figure 2.1, is a recording from the detector. It shows straight lines when the carrier gas is pure, giving a baseline, and shows peaks corresponding to the presence of other components in the gas.

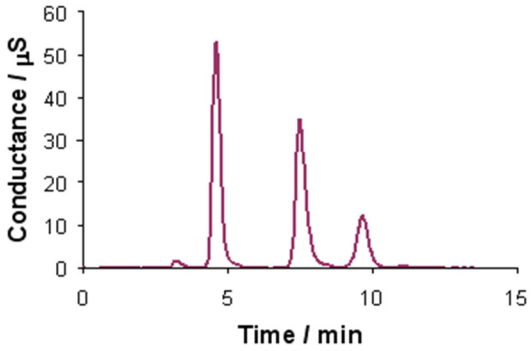

Figure 2.1 - Example of a chromatogram [21]

A lot of information can be obtained from a chromatogram. It can show whether or not a sample is pure. The number of peaks on the chromatogram corresponds to the number of components in the gas mixture. It can be used to identify the individual components of a mixture qualitatively by measuring the retention time. The chromatogram can also be used to obtain a quantitative analysis of the gas mixture. In most detectors, the deflection of the meter from the base line is proportional to the concentration of the gas. So, if the flow rate is constant, the area of the peak will give the total amount of gas present.

When choosing a detector for quantitative analysis, there are a few characteristics which are desirable [22]. An equal response for all sample components present in the carrier gas as well as a linear response with concentration is advantageous. It is preferable for the detector response to be quick whilst being insensitive to flow rate and pressure changes. It is also beneficial to have a high signal to noise ratio and long-term stability.

The most common detectors used are thermal conductivity detectors (TCDs) and flame ionisation detectors (FIDs). Both detectors are sensitive to a wide range of components and concentrations.

Thermal conductivity detectors (also known as katharometers) are essentially universal gas chromatographic detectors [2, 6, 7, 23]. They can be used to detect any component other than the carrier gas if their thermal conductivities are different from that of the carrier gas at the detector temperature.

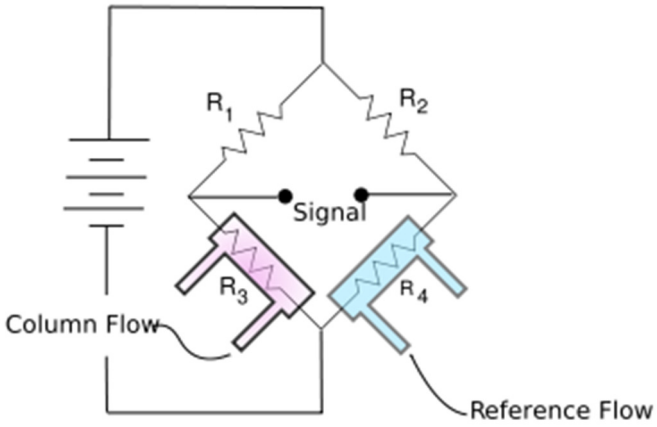

Figure 2.2 - Schematic of Wheatstone bridge arrangement in a TCD [24]

The detector consists of an electrically heated element situated in the gas stream. The resistance of the electrical element is measured continuously by a Wheatstone bridge which supplies the electrical heating current (see Figure 2.2). The thermal conductivity is constant when there is only pure carrier gas passing through the system. When this is happening, the heating element is continually losing heat by conduction to the detector walls. An equilibrium is reached where the rate of heat input by the electrical current is balanced by the rate of heat lost by conduction. Therefore, the temperature and the resistance of the heating element is constant. If another gas or component is present, the thermal conductivity of the carrier gas changes and so the equilibrium is disturbed. More or less heat is conducted to the walls and so the temperature of the heating element changes. The change in resistance causes the bridge to go off balance.

Thermal conductivity detectors are non-destructive to the sample, unlike flame ionisation detectors that are destructive. Flame ionisation detectors are sensitive primarily to hydrocarbons although an FID cannot detect water [6, 7, 23]. An FID has the advantages of responding to virtually all organic compounds, not responding to common carrier gas impurities, it has minimal effects from changes in flow, pressure or temperature, in the absence of sample it has virtually no response to gives a stable baseline, it has good linearity and there are few adjustments that are required for operation. Analysis using an FID involves, as the name suggests, the detection of ions. The source of the ions is usually a hydrogen-air flame but sometimes a hydrogen-oxygen flame is used. The flame burns, pyrolyzing most organic compounds and so produces positively charged ions and electrons. Two electrodes are used to provide a potential difference and so the ions can be detected. The positive electrode is the

nozzle head where the flame is produced. The negative electrode is positioned above the flame. This is known as the collector plate. The positively charged ions are attracted to the negatively charged collector plate. As the ions hit the plate a current is induced. The current is measured by an electrometer. The current measured corresponds to the proportion of reduced carbon atoms in the flame. This makes the FID sensitive to mass rather than concentration.

There are other gas chromatographic detectors available for use including the gas density detector which will be looked at in this work.

2.3. Gas Density Detector

The gas density balance is a gas chromatographic detector first developed by Martin and James (1956) [8]. They recognised that it was important to have a highly sensitive detector whose response was independent of the chemical structure of the substances being separated. The density of a gas stream emerging from the chromatogram is an attractive measurement since the response is dependent on the differences of molecular weights of the gas and vapour only.

Martin and James [8] designed an instrument in which tubes were arranged into a bridge circuit so that two points could be found vertically displaced from one another, where the pressure difference is independent of the gas flow rate. It is possible to combine two such bridges, one with the chromatogram gas flowing through it and the other with a reference stream flowing through, so the difference in head due to the density difference of the two gases is directly measurable.

Figure 2.3 shows a schematic diagram of the gas density meter with two bridges combined. The gas from the chromatograph enters at *A* and splits into two, approximately equal, streams along *B* and *B'* and inclined *C* and *C'* and combine at *E*. The reference gas enters at *F* and again splits into two approximately equal streams along *G* and *G'* and flow through channels *H*, *J* and *K* and *H'*, *J'* and *K'* and combine at *E*. *N* and *N'* are needle valves which can be pushed into or withdrawn from channels *D* and *D'* until the ratio of resistances to flow in the channel is equal to that in channels *B, C* and *B', C'*. The pressure difference between the points where *C* joins *D* and where *C'* joins *D'* is then independent of the rate of gas flow through *A*. A similar arrangement is observed in channels *G* and *G'* with rods *P* and *P'*. If

the resistance to flow in *J, K* and *J', K'* is the same, the pressure difference between the ends of the tube *L, L'* which passes through the detector *M*, is independent of the gas flow rate through either *A* or *F* and is zero if the density of the gas at *A* and *F* are identical. If, however, the density of the gas entering at *A* is greater than that at *F*, the pressure at *L'* is greater than that at *L* and so a flow of gas passes through the detector *M*. If all the velocities are low, the rate of gas through *L, L'* will be proportional to the density difference.

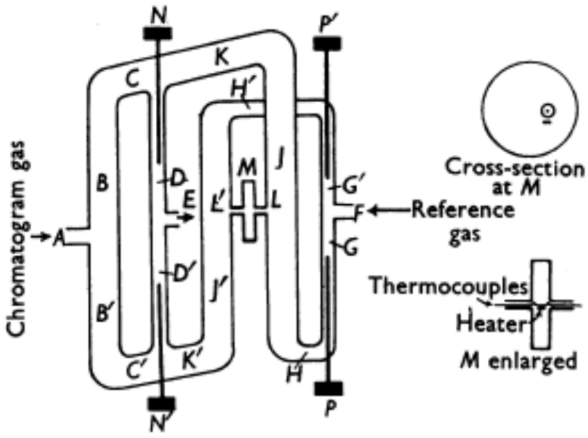

Figure 2.3 - Schematic diagram of the gas-density meter [8]

The detector, *M*, consists of a disc-shaped cavity on a horizontal axis which lies midway between tubes *J* and *J'* and is connected to them by the tube *L, L'*. A pair of thermocouples were strung along the axis of tube *L, L'*. Beneath the thermocouples is a small heater. This circulates a stream of hot convected gas which circulates within the disc-shaped cavity. The thermocouples and heater are placed so that when no gases pass along the tube *L, L'*, the thermocouples are at the same temperature. A flow of gas through the tube causes the hot convected stream to be displaced and so the thermocouples will not be balanced at the same temperature. The outputs of the thermocouples provide a measure of the direction and velocity of the gas flow and therefore the density difference of the chromatogram and reference gas streams. Only the reference gas passes through *L, L'* so the heater and the thermocouples do not need to be chemically resistant to the substances being separated in the column. Therefore, the arrangement is suitable for corrosive gases.

Martin and James [8] found that the sensitivity of the detector depends on the power dissipated by the heater. The slope of the thermal gradient will increase with the heater output. Also, the temperature gradient along the thermocouple is reduced by conduction of heat along the

wire. Therefore, the thinner the wire, the more sensitive the detector will be. The density difference between the two gas streams can be converted into an electromotive force in the sensitive thermocouple. They found that the sensitivity of the detector can be greatly affected by the nature of the gas filling the detector (main/reference flow) i.e. the sensitivity of hydrogen is an order of magnitude lower than that of nitrogen. This is because hydrogen has a higher thermal conductivity, therefore reduces the thermal gradient.

Liberti *et al.* (1956) [25] carried out experiments using the apparatus developed by Martin and James. They added a pure substance of known molecular weight to the unknown mixture from the column. This was referred to as the 'internal standard'. A chromatogram of the mixture on the same column was obtained using to two different elution gases. The gas flow was kept constant so that the volume of elution gas will be the same for both components. However, the peak heights and areas were different for the different elution gases. Measuring the peak areas from the chromatograms for the two elution gases, the following expression was used to find the unknown molecular weight

$$\frac{A}{A_1}\left(\frac{M_1 - m}{M - m}\right) = \frac{A'}{A_1{}'}\left(\frac{M_1 - m'}{M - m'}\right) \qquad 2.1$$

where M and M_1 are the molecular weights of the known and unknown compounds, m and m' are the molecular weights of the carrier gases and A, A', A_1 and $A_1{}'$ are the peak areas with the two carrier gases of known and unknown compounds. It was found that this expression was valid providing the gas flow was kept strictly constant and the density changes were small. This method of molecular weight determination is very attractive as it allows the molecular weights of all the peaks in a chromatogram to be determined without prior separation, provided that one molecular weight is known.

Liberti *et al*. demonstrated that the electromotive force of the thermocouple in the detector is proportional to the density difference for small density differences and reported that a molecular weight accuracy of about 4% could be obtained.

Phillips and Timms (1961) [26] continued the work of Liberti *et al*. They found that there were several difficulties with the previous method that were not immediately apparent. Small percentage errors in the peak areas became significantly magnified in the final molecular

weight. Also, they found that it was essential that the ratio of the two components (known and unknown molecular weights) in the two experiments using the different elution gases should be constant to within 1%.

The authors developed an alternative method for finding molecular weights using the Martin and James gas density balance. They rearranged a previously derived equation from the Liberti paper so that by making pressure-volume measurements on a vapour, then passing it through the density balance, the molecular weight, M, can be found. The equation used was

$$PV = \frac{KA}{(M - m)} \qquad 2.2$$

where P and V are the pressure and volume of the vapour entering the balance, A is the peak area from the chromatogram and K is a constant. Unlike Liberti's method, pure components are required here. Using this method, Phillips and Timms could determine molecular weights with an accuracy of better than 1%.

Nerheim (1963) [9] recognised that the Martin density balance was so complex in design and construction that they had not come into wide spread use and so a simpler gas density detector was needed. He developed a concept based on the conservation of energy in the gas to explain the response of the detector to changes in density.

Figure 2.4 shows the basic flow pattern in a gas density detector as defined by Nerheim. This simplifies the arrangement in Figure 2.3.

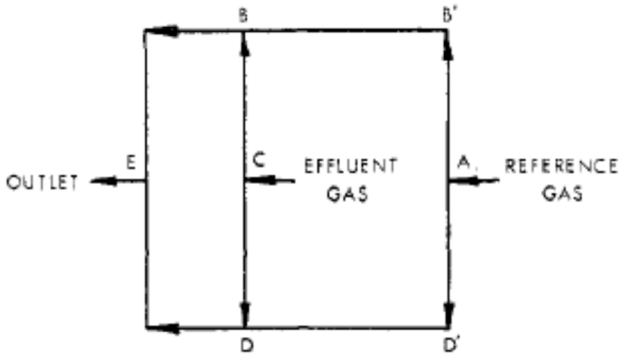

Figure 2.4 - Flow in gas density detector [9]

The reference and effluent gas enter the network at *A* and *C* respectively. Both streams divide with part of each stream flowing upwards to *B* and part flowing down to *D*. The divided reference and effluent streams flow through *BE* and *DE* and exit together at *E*. The total flow rate at the exit, *E*, remains constant. Only the interior flow rates of the gas streams change creating a variation in pressure within the circuit. Conduit *BD* is always filled with effluent gas. When components heavier than the carrier gas are present, the density of the gas in *BD* is greater and so the pressure at *D* increases. When components lighter than the carrier gas are present, the gas density in *BD* is smaller and so the pressure at *D* decreases.

The change in this pressure can be measured in two ways: -

1. As used in the Martin gas density detector, a flowmeter in a channel parallel to BD senses a change in flow caused by changes in pressure at *B* and *D*.
2. Measure all the changes in flows in the conduits *AB* and *AD* and therefore eliminate the parallel circuit that was described above.

Nerheim [9] developed a simple form of Bernoulli's theorem by assuming that pressure drop develops as potential energy and dissipates as friction. The pressure drop around loop *ABCDA* is zero because the terms derived for the development and dissipation of energy balance out. Any changes in pressure drop around the loop *ABCDA* are related to changes in density and flow rate. The equation derived for the change in pressure drop around the loop is

$$\Delta(\Delta P) = \Delta\rho(X_B - X_D) - \sum F_{ABCD}(\Delta U) = 0 \qquad 2.3$$

where $\Delta(\Delta P)$ is the change in pressure drop, $\Delta\rho$ is the change in density, $(X_B - X_D)$ is the height of the gas in vertical conduit *BD*, *F* is the constant for friction and ΔU is the change in flow rate.

The first term in the equation represents the development of potential energy because of the change in density of the gas in *BD*. The second term represents the dissipation of energy because of the change in flow caused by the change in density. By assuming viscous flow, factors from Poiseuille's equation could be substituted into the second term of the equation. So,

$$\Delta(\Delta P) = \Delta\rho(X_B - X_D) - \frac{128\mu L\Delta U}{\pi g D^4} = 0 \qquad 2.4$$

where μ is the viscosity, L is the length of the conduit, *g* is the gravitational constant and *D* is the diameter of the conduit. It was assumed that the effect of any change in viscosity is negligible.

The equation was then rearranged to give

$$\Delta\rho = \frac{128\mu L\Delta U}{\pi g D^4 (X_D - X_B)} \qquad 2.5$$

Nerheim [28] verified this theory by connecting filament flowmeters located in channels *BB'* and *DD'* to a recording potentiometer via an electrical bridge. He wanted to establish a relationship between the change in flow rate and the electrical response. He did this by removing conduits *BCDE,* and connecting rotameters with needle valves to the flowmeter conduits. With nitrogen flow maintained at a constant flow of 50 ml/min, flow was diverted from *AD* to *AB* and vice versa by adjusting the needle valves. For each conduit, it was found that the response varied linearly with flow. The linearity, unlike the nonlinear relationship of conventional flowmeters, may be explained as a direct response to the change in flow rate as the flow is diverted from one flowmeter to the other.

Experiments showed that for a carrier gas of nitrogen, data for components heavier than nitrogen fit the theoretical curve with a positive slope while data for components lighter than nitrogen fit the theoretical curve with a negative slope as shown in Figure 2.5.

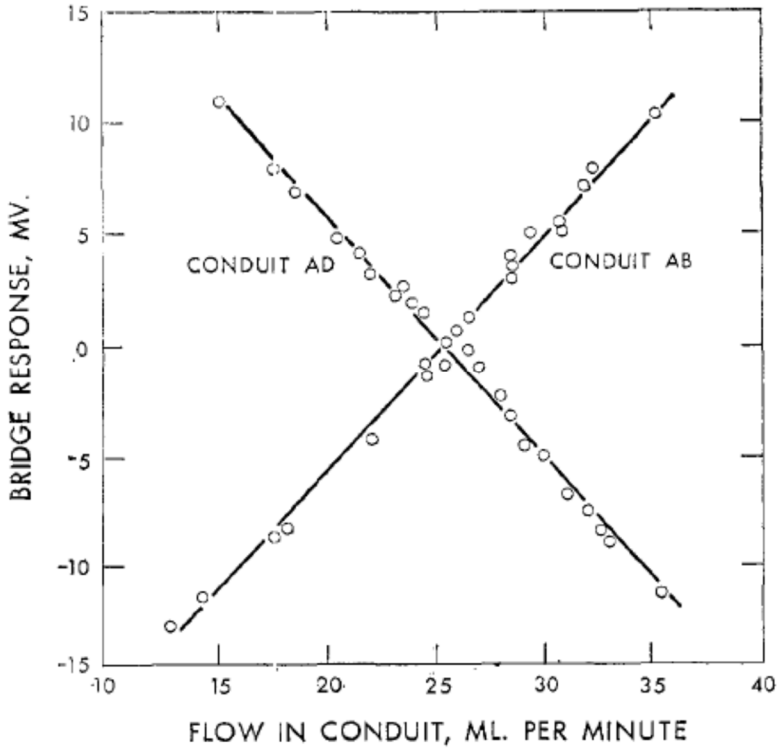

Figure 2.5 - Effect of changing flow on response [9]

In Figure 2.5, it can be seen that the positive slope shows that increased density diverts flow through *AB* while the negative slope shows that decreased density diverts flow through *AD*. These correlations provided fundamental evidence that Equation 2.4 describes the operation of the detector and justifies the simplifying assumptions.

Nerheim found that there were some practical problems involved in designing and operating the detector. He assessed these by looking at Equation 2.4. The flow rates of reference and effluent gas had to be high enough to maintain the difference in flow rate and so dissipate the energy developed by the changing density. He found that increasing the flow rates of the reference and effluent gases increased the linear dynamic range. Also, increasing the effluent gas flow rate decreased response time as the volume of the channel *BD* was filled and emptied more quickly. Therefore, linear dynamic range and response time may be enhanced by increasing flow rate. Both may also be enhanced by decreasing detector dimensions but this is at the expense of sensitivity. It was found that restricting the diameter around the flowmeters to increase the flow velocity increases both the sensitivity and the dynamic range. Also, it was discovered that restricting the diameter and length of the effluent gas conduit *BD* while increasing the diameter of the reference gas channels *AB* and *AD* can reduce response time without loss of sensitivity.

Nerheim [9] considered using two different kinds of flowmeters, one with thermistors and one with filaments. Different electrical bridges were used for each flowmeter so they could be utilized more effectively. A parallel bridge was used for thermistors while a series bridge was used with filaments. These are shown in Figure 2.6. In the parallel bridge, the current through the element with lower resistance increases and vice versa. The negative temperature coefficient of the thermistors means that the change in current in the parallel bridge causes a decrease in the resistance in the heated element and an increase in the resistance in the cooled element. This cumulative effect results in a larger net change in resistance than that obtained using a series bridge.

In a series bridge, the same amount of current goes through each of the sensing elements. The positive temperature coefficient of the filaments means that the net change in resistance is larger than that obtainable with a parallel bridge.

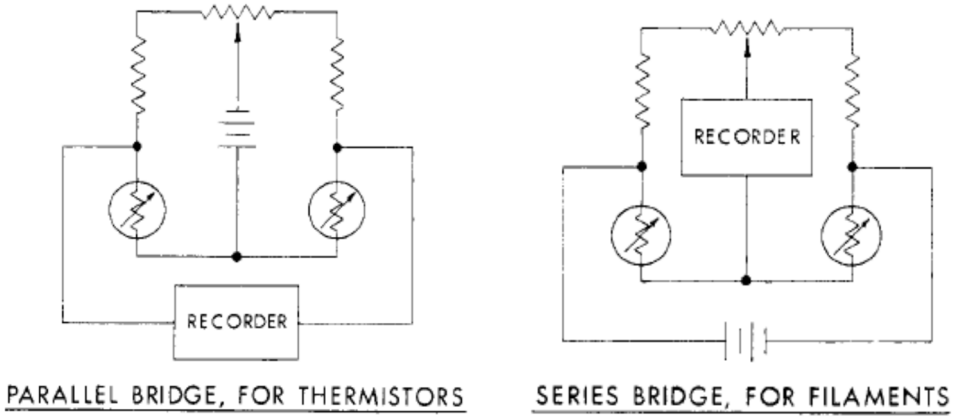

Figure 2.6 - Electrical bridges for flowmeters [9]

Nerheim tested the detector performance by investigating the response time. He found that the response time is directly proportional to the time it takes to fill and empty conduit *BD* and that it decreases with flow for both detectors. As the gas density detector is a flow-through rather than a diffusion device, only the peak shape, but not the peak area, was affected by the response time. After the performance tests, the thermistor detector was preferred to the filament detector at room temperature as the limit of detection was found to be six times better for the thermistor. The greater sensitivity of the thermistors resulted from the advantages of a higher temperature coefficient and resistance outweighing the disadvantages of small current and element area when used in the parallel bridge.

Nerheim patented this new design for the gas density detector for Standard Oil Company (Indiana, U.S.A.) and commercial models of the detector were developed by the Gow-Mac Instrument Co.

Guillemin and Auricourt (1963) [10] presented a study to define the optimum operating conditions of the Gow-Mac gas density balance designed by Nerheim from a quantitative analysis perspective. They studied the detector's response to changes in carrier gas, flow rates, the amount of the sample injected into the column and the temperature.

Experiments were carried out with argon, nitrogen and carbon dioxide. In each case, the maximum response for given measuring flow rates while varying the reference flow rate was investigated. It was observed that the response curves, as a function of the reference to measuring flow rate ratio, displayed a maximum for each value of the measuring flow rate. The value of this maximum varied inversely with the flow rate in the measuring circuit. It was found that carbon dioxide gave the highest sensitivity. This was because it has the greatest density and smallest viscosity. It was also established that the gas density balance was most sensitive when operated with the greatest possible reference to measurement ratio and with a constant reference flow for a given carrier gas. They also reported that care had to be taken when injecting the principal component of the mixture to be analysed into the column. Peak broadening and deformation was observed when the component amount exceeded 5 microliters.

When considering the effect of temperature, the authors looked at the equation for pressure drop as derived by Nerheim (Equation 2.5). For a given flow rate, the second term in the equation depends only on the viscosity of the gas. As explained previously, carbon dioxide as the carrier gas gave the highest sensitivity because it is a dense gas with a low viscosity. Therefore, it was predicted that temperature would have a negative effect on the balance response. It was found that the sensitivity of the balance was 5 times less at 250ºC than at 50ºC.

The gas density balance gives the response in weight per cent if the peak areas are multiplied by a factor, K, which is based on the molecular weights of the solute and the carrier gas. This factor is defined as

$$K = \frac{M_s}{M_s - m_g} \qquad 2.6$$

where M_s is the molecular weight of the solute and m_g is the molecular weight of the carrier gas.

To test the quantitative response of the detector, Guillemin and Auricourt [10] analysed two mixtures of chlorinated hydrocarbons whose compositions were known in weight per cent. The precision of quantitative analyses for a given concentration is a function of numerous parameters including the sensitivity of the detector. It was found that under the best Gow-Mac operating conditions, the gas density balance was 4 to 5 times less sensitive than a thermal conductivity detector. However, it was also concluded that the precision obtained at concentrations of 5 to 10% was satisfactory in comparison with other detection systems and was sufficient for numerous industrial analytical problems. They proposed that when the prospect of eliminating the need for quantitative calibration of the balance was considered, interest in use of the gas density balance as a detector would significantly increase. Also, the simplicity of its operation and indestructibility, as the solutes never come in contact with the sensing elements, were also attractive features of the detector.

Guillemin and Auricourt concluded that the Gow-Mac balance gives adequate results when used for quantitative analysis, it eliminates the need for quantitative calibration so has the advantages of rapidity and economy and has a sensitivity that is sufficient to solve many industrial analytical problems.

Guillemin and Auricourt (1964) [11] continued their investigation into the Gow-Mac balance by considering the choice of carrier gas. They looked at the use of sulphur hexafluoride (SF_6) as a carrier gas in the gas density balance. As discussed in their previous paper, the most appropriate carrier gas used in the gas density balance should have a high density. The authors chose this because it is a chemically inert gas and has a density 5 times greater than that of air. They postulated that when using SF_6 as the carrier gas, the response from the detector would be approximately 4 to 5 times greater than that attained with nitrogen and 2 to 3 times greater than that with carbon dioxide. Upon completion of experiments, it was confirmed that by using SF_6 as the carrier gas, the sensitivity of the gas density detector approached that of a thermal conductivity detector and so would be a valuable detector.

Guillemin *et al.* (1966) [12] compared the work that was carried out and reported in their previous papers to summarise the optimum operating conditions for the Gow-Mac gas density balance. On comparison of their results from their previous work, they found that from the carrier gases they used, Ar, N_2, CO_2 and SF_6, the gas density balance gave a maximum response when the value of the reference flow rate for each of the gases satisfied a constant of the apparatus: a Reynolds number equal to 20 whatever the value of the measuring flow rate. This means that the reference flow rate determines the intrinsic sensitivity of the detector. They also determined that it is preferable to operate with a reference to measuring flow-rate ratio of R/M > 1. The results obtained from previous experiments showed that the response curves vary inversely with the measuring flow rate as the peak areas increase when the measuring flow rate decreases. Therefore, the authors found that the measuring flow rate determines the apparent sensitivity of the balance.

The authors reported that the choice of carrier gas for the gas density balance is a function of the density, or the molecular weight, of the vapour of the compounds being analysed. With a thermal conductivity detector, the carrier gas is almost always hydrogen or helium because these gases have a relatively high thermal conductivity when compared to any compounds encountered. The maximum response of the balance can be obtained under the condition that the proportionality constant, K, is as small as possible or $K \leq 1$. This means that the chosen carrier gas should have a molecular weight as remote as possible from the molecular weights of the different components in the mixture.

Guillemin *et al.* also discussed the dynamic range of linearity of the gas density balance. They found that the range of linearity was well defined being limited by non-proportionality and the lower limit of detection. The lower limit of detection is the minimum quantity of substance that gives a signal that is twice that of the background noise. Background noise in the balance is mostly created when the flow in the measuring circuit meets the perpendicular flow of the reference circuit. The effect of both flows meeting can affect the sensing elements and so creates some background noise. This effect will become more evident as the R/M ratio approaches 1. Any external variations in pressure can also create background noise that can be reflected in the balance operation. It was suggested that a muffler constructed of a series of resistances and capacitors could be used to absorb any variations in pressure. The authors considered the linearity for three carrier gases, He, N_2 and SF_6. They found that the three gases had an identical maximum linearity but the lower limits of detection were different. It was found that SF_6 had a low range of linearity due to the high levels of background noise. This

was shown to be because of a poor R/M ratio. When helium was used, the noise level was nil due to the favourable R/M ratio but also a lack of sensitivity in the sensing elements due to insufficient feed. With helium, to stop any back diffusion, the reference flow rate had to be 50 l/hr or 25 l/hr through each branch. This resulted in intense cooling of the sensing elements and so a high current was required to supply the sensing elements. With nitrogen, a total reference flow of 6 l/hr and a current of 170 mA were found to be sufficient to obtain maximum sensitivity.

Guillemin *et al*. concluded their research by highlighting some of the advantages of the gas density balance over other detectors. They found that the sensitivity was equal to and sometimes superior to that of thermal conductivity detectors using the same sensing elements and that its linearity was of the same order of magnitude as that of these detectors. They found the balance to be versatile, capable of operation with any carrier gas, is non-selective so allows analysis of all gaseous compounds from heavy components to corrosive gases, is non-destructive and is simple, robust and reliable.

The use of the Gow-Mac gas density balance for quantitative analysis was further investigated by Walsh and Rosie (1967) [14]. They recognised that, at that time, gas chromatographic detectors were being developed with sensitivity being the primary interest. They thought that it was important to explore the potential of the gas density balance to provide accurate quantitative and molecular weight information for sample sizes within the sensitivity range of thermal conductivity detector. Most of the previous work carried out using the gas density balance was in highly specific areas. Therefore, the authors wanted to consider evaluating the gas density detector regarding its response, operational parameters and quantitative measurements for different compounds over a wide range of concentrations and molecular weight ranges.

Several experiments were carried out as part of the author's investigation. The detector response to flow rate measurements was looked at in numerous ways including varying the reference flow while holding the sample flow constant, varying the sample flow while keeping the reference flow constant and setting the reference and measuring flows to be equal over a range of different flow rates. The change in filament voltage in the detector was recorded at different reference gas flow rates. This was carried out by connecting the two filaments in the density balance to a potentiometer which was then connected to a galvanometer to measure the difference in current in the filaments. Finally, experiments were carried out to determine

the percentage weight and molecular weight of the samples. This was completed using an internal standard method. Known mixtures of an internal standard and sample were prepared on a weight per cent basis. Peak areas of the standard and sample were measured and the percentage weight and molecular weights were calculated.

The detector response at various reference to measuring gas flow rate ratios (R/M) showed that when the detector response is plotted against the flow rate ratio, the maximum of the curve represents the optimum reference flow for highest balance response. This agrees with results obtained by Guillemin and Auricourt (1963) [10]. The same result was obtained when the reference and measuring flow rate were equal flows (R/M=1). However, there was also found to be a minimum measuring flow below which response decreases. The authors reported that the reference and measuring gas flow rates must be high enough to maintain and reflect any changes in flow caused by the presence of the sample vapour. They found that with the reference flow rate and the sample size being kept constant, there is a minimum measuring flow which will not reflect the flow rate change due to the sample vapour. At this point the linearity of the detector response was lost. The determination of flow rate effects on the detector response is complicated by the fact that more than one flow path is involved. At the point where the reference and measuring flow combine, the measuring flow can act as a resistance to the reference flow. This accounts for the fact that when the reference and measuring flows are equal, the detector displays its lowest response as the measuring flow offers its greatest resistance to the exiting reference flow. As the R/M ratio is increased and so the measuring flow is decreasing, there is less resistance to the reference flow so the reference flow can approach its optimum value and the detector response will increase. The R/M ratio is increased until it reaches its optimum value at a lower measuring flow rate. The measuring flow rate at this point is the optimum minimum measuring flow for the highest detector response.

The authors described the measurement of detector response as an electrical measure of the voltage drop change in the sensing elements produced by a reference gas flow rate change. The principle of operation of the gas density detector is that only the presence of the sample should cause a change in the reference flow rate and so a change in voltage. Conversely, it was found that the voltage change was also influenced by the nature of the reference gas. Measurements were taken with no measuring gas flow and no sample present so any voltage drop or response at each flow rate was due to the nature of the reference gas. It was found that the magnitude of the voltage drop in the filaments increased with increase in molecular weight

of the reference gas. It was also reported that when tungsten filaments are used, the voltage drop is temperature dependent so any physical property of the reference gas that would change the filament temperature would result in a voltage drop change. Density, thermal conductivity, viscosity and heat capacity are all properties that could be related to the changes. It is unsure which of these properties is the most significant in affecting detector response. It was found that viscosity and heat capacity were the most influential when changing the flow rate. As expected, it was found that density was the most influential property of the sample. The larger the density change produced in the reference gas by the sample, the greater the detector response. The greatest density change is obtained when the density difference or the molecular weight difference between the reference gas and the sample are large. The sample gas does not pass the filaments so other physical properties are not considered. Therefore, the detector response is related to density only which can then be related to the absolute amount and the molecular weight of the sample.

Walsh and Rosie (1967) [14] considered using the gas density balance to make quantitative measurements like per cent weights and molecular weight determinations. They reported that percentage weights could be determined with an accuracy of about ±1.6% while the molecular weights were ±2.9%. These determinations were made on a variety of compounds with a concentration range of 20-80% by weight and a molecular weight range of 30 to 202. The detector response was found to have a linear relationship with the molecular weight difference between the reference gas and the sample.

The density balance response is proportional to the density change produced in the reference gas by sample vapour under specific experimental conditions. From previous work, it is known that the nature of the reference gas and the sample, and the relation between the two are important factors affecting the detector response. It was proven experimentally that equal amounts of different samples will cause different density changes in each reference gas. Also, equal amounts of a given sample will cause different density changes in different reference gases. Therefore, the authors recommended that response measurements and comparisons should not be based on equal sample sizes but instead should be based on equal density changes produced either in the reference gas or with sample sizes.

Dimbat, Porter and Stross [22] derived a sensitivity factor which was used to express the response from a detector. The authors discovered that the equation for the sensitivity factor does not adequately define the density balance response because it does not account for the

density difference between the reference gas and the sample. If the amount of sample is expressed as vapour volume (E) in millilitres instead of weight and if the density difference (ΔM) between the reference gas and sample are substituted into the sensitivity equation it becomes

$$S_d = \frac{A\ F\ R\ C}{E\ \Delta M} \qquad 2.7$$

where A is the peak area (cm^2), F is the carrier gas flow rate (ml/min), R is the recorder sensitivity (mV/cm) and C is the reciprocal chart speed (min/cm). This expression has the advantage of being able to compare sensitivities or response of density detectors regardless of the reference gas or sample used. By incorporating the density difference into the sensitivity factor equation, a more accurate evaluation of density balance response can be made.

Walsh and Rosie (1967) [14] concluded that there are definite reference and measuring gas flow rate values for a maximum gas density balance response. Also, it was concluded that reliable quantitative and molecular weight measurements can be made with this detector and suggested that to compare the gas density balance with other detectors, the detector response should be expressed as a function of the density difference between the reference gas and the sample vapour.

Guillemin *et al.* (1969) [27] suggested a different use for the Gow-Mac gas density balance. An advantage of the gas density balance is that it is a differential detector with predictable response that can obtain quantitative measurements without calibration because its response is directly linked to the molecular weights of the solutes. The gas density balance has the characteristics of predictable response, non-specificity, linearity, sufficient sensitivity and is very versatile in that it can be used with any carrier gas. These qualities suggest that the gas density balance could be employed to calibrate other industrial detectors like thermal conductivity or flame ionization detectors. The gas density detector can be connected in parallel with the detector to be calibrated to obtain substance-specific correction factors which can be used for reliable quantitative analysis.

The authors carried out experiments by assembling a chromatographic column where the outlet is divided into two streams by a flow divider. One stream leads to the gas density balance while the other leads to the detector to be calibrated. A mixture of known qualitative composition was injected into the column. The responses from both the detectors were

recorded simultaneously. This allowed the exact weight concentrations of the components to be obtained from the gas density balance and by referring to the chromatogram of the detector to be calibrated, the calculation of the substance-specific correction factor could be established. The advantages of calibrating a detector in this way were found to be

1. Elimination of pure calibration standards as the method only requires a separation of the identified components of a mixture whose qualitative composition is known.
2. Elimination of the problem of sampling simultaneously for all possible cases.
3. It allows the substance-specific correction factors for all components without restriction to be obtained easily in cases where the classical calibration methods do not apply.
4. Better accuracy is obtainable at reduced cost and with considerable time saving.

Overall, Guillemin (1969) [27] concluded that their proposed method offered a new calibration technique that was more reliable than classical calibration methods as random errors associated with these methods, like weighing, sample preparation, sample injection, are reduced. They also proposed the new technique could be improved to be of more universal value by paying more attention to the quality of chromatographic equipment, in particular temperature constancy.

Vermont and Guillemin (1973) [15] published another paper developing the calibration technique they had previously created by incorporating the suggestions they proposed in the previous paper. They considered improving the apparatus by including ovens so that the temperature could be kept constant. Two ovens were added to the system. Both ovens have an injection port and a column in them. The gas density balance, the detector to be calibrated and a flow divider were placed in the second oven.

They also proposed a new procedure which involves the separate injection of components and so eliminates quantitative blending of samples. This new procedure is simple, more accurate and is considerably more time saving and cost reducing. It does not require pure standards. The most important point of the new procedure is the possibility of getting any relative response factor with equal accuracy with respect to any reference compound.

Heggie and Reeburgh (1974) [16] carried out experiments with the Gow-Mac gas density balance using the method proposed above to inject the sample. They were looking to evaluate

the suitability of the gas density balance for quantitative measurements of Ar, N_2, CH_4, CO_2 and H_2S in aqueous solutions. It was important to determine the concentration range over which the gas density balance response is linear as it is only within this region that the detector response is predictable. It was found that the maximum gas concentrations for which the detector response was linear was inversely proportional to the difference in molecular weight between the sample and the carrier gas.

While Vermont and Guillemin (1973) [15] used a parallel flow system when using the gas density balance in calibrating other detectors, Barry and Rosie (1975) [17] constructed a thermal conductivity detector-gas density balance detector system connected in series. The gas density balance was added downstream of the thermal conductivity detector. They maintained the apparatus at 100ºC in one chromatographic oven. This arrangement had many attractive features. The gas density balance responds to the effluent of the thermal conductivity detector and not to what is injected into the column and so any problems associated with purity of standards and preparation of standard mixtures are eliminated. Also, the series arrangement does not require a flow divider or thermally stable needle valves which are required in the parallel system.

Kiran and Gillham (1975) [18] published a paper presenting an analysis of the hydrodynamics of the gas density detector. They identified that, even though the gas density balance was one of the first gas chromatographic detectors designed, there had been no investigation into the hydrodynamics of its operation.

The authors first considered the kind of flow patterns that were prevalent in the gas density balance. They did this by looking at the Knudsen number, the Mach number and the Reynolds number. All are dimensionless quantities. The Knudsen number (Kn) is the ratio of the mean free path of the molecules (λ) to a characteristic length of the conduit in the flow system (l). A fluid is treated as in the continuum flow regime if $\lambda \ll l$ so $Kn \ll 1$. If $\lambda \gg l$ so $Kn \gg 1$ then the molecular flow is free from collisions. If $\lambda \approx l$ and so $Kn \approx 1$, then the flow is in a transitional phase between continuum and collisionless flow. The Mach number (Ma) is the ratio of some characteristic velocity of the fluid (υ) to the velocity of sound in the fluid (c). It gives a measure from which it can be decided if the fluid can be treated as incompressible. The relative change in density ($\Delta\rho/\rho_0$) due to a pressure increase Δp is related to the Mach number through

$$\frac{\Delta\rho}{\rho_0} \approx \left(\frac{\upsilon}{c}\right)^2 = [Ma]^2 \qquad 2.8$$

The fluid can be treated as incompressible when $\Delta\rho/\rho_0 \ll 1$ so $Ma \ll 1$. The Reynolds number (Re) is the ratio of the inertial forces to the viscous forces. It is used to determine if the flow conditions are laminar or turbulent. In pipe flow, when $Re < 2100$, the flow is laminar and is characterised by smooth motion. At higher Reynolds number, the flow is turbulent and is characterised by irregular and random motions. It was found that, based on the dimensions of the Gow-Mac gas density balance and using carbon dioxide as the fluid, the gas flow in the conduits of the balance can be treated as continuum, incompressible and laminar. The dynamics of the flow under these conditions were then analysed.

The authors evaluated the pressure drop in the conduits of the gas density detector. The gas density detector is shown diagrammatically in Figure 2.7.

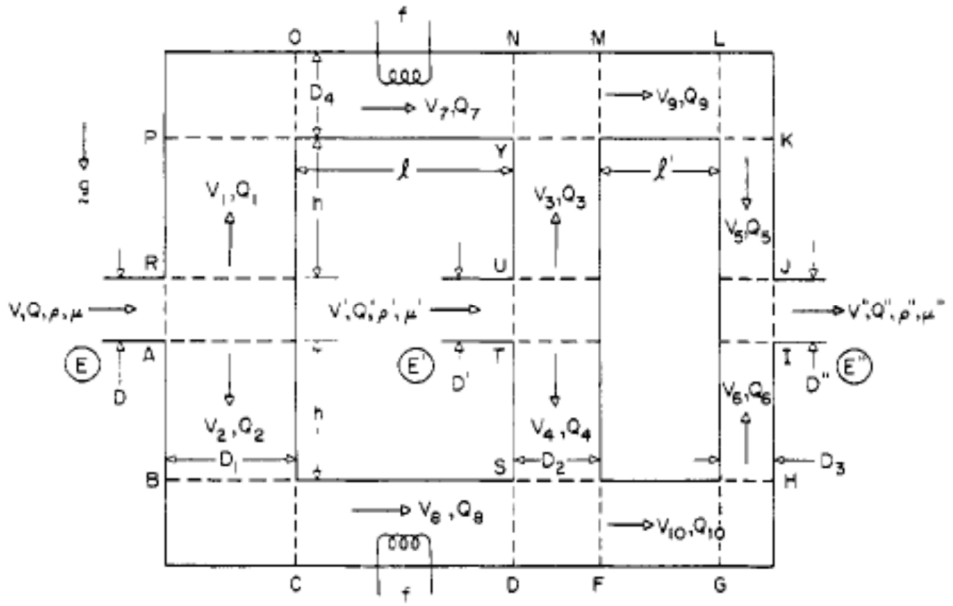

Figure 2.7 - Schematic diagram of the gas density balance [18]

The vertical conduit RP was initially examined. The gas stream in the conduit RP flows at an average velocity, υ_1, and in the opposite direction of gravity. Also, with the fluid being treated as incompressible, the density is taken as being constant. With these points being taken into consideration, the equation for the pressure drop along conduit RP is given by

$$(P_P - P_R) = -\rho gh - \frac{8\mu h}{R_1^2}\upsilon_1 \qquad 2.9$$

where P_P and P_R represent the pressures at P and R and h is the height of the conduit RP. The ρgh term represents the static losses in the balance and the $\frac{8\mu h}{R_1^2}\upsilon_1$ term the dynamic losses. Both terms being negative means that the pressure decreases from point R to P.

The pressure drop in conduit AB was then evaluated in a similar way. In this instance, the fluid stream is flowing at an average velocity, υ_2, and in the same direction as gravity so the equation for the pressure drop along conduit AB is given by

$$(P_B - P_A) = \rho gh - \frac{8\mu h}{R_1^2}\upsilon_2 \qquad 2.10$$

From point A to point B, the pressure decreases due to the dynamic contributions, however, it increases due to the static contributions.

Similar pressure drop equations were evaluated for the other vertical conduits in the gas density balance. These are shown below

$$(P_Y - P_U) = -\rho' gh - \frac{8\mu' h}{R_2^2}\upsilon_3 \qquad 2.11$$

$$(P_S - P_T) = \rho' gh - \frac{8\mu' h}{R_2^2}\upsilon_4 \qquad 2.12$$

$$\left(P_J - P_K\right) = \rho'' gh - \frac{8\mu'' h}{R_3^2}\upsilon_5 \qquad 2.13$$

$$(P_I - P_H) = -\rho'' gh - \frac{8\mu'' h}{R_3^2}\upsilon_6 \qquad 2.14$$

where ρ and μ represent the density and viscosity of the reference gas in conduit PB, ρ' and μ' represent the density and viscosity of the sample flow entering the detector into conduit YS

and ρ'' and μ'' are the density and viscosity of the exit gas in conduit KH after both the reference and sample flows have combined. Also,R_1, R_2 and R_3 allow for the radii in each conduit to differ.

The horizontal conduits were also examined. The gas is flowing horizontally so the gravity effect is zero. Therefore, the pressure drop equations for the horizontal conduits are

$$(P_N - P_O) = -\frac{8\mu l}{R_4^2}\upsilon_7 \qquad 2.15$$

$$(P_D - P_C) = -\frac{8\mu l}{R_4^2}\upsilon_8 \qquad 2.16$$

$$(P_L - P_M) = -\frac{8\mu'' l'}{R_4^2}\upsilon_9 \qquad 2.17$$

$$(P_G - P_F) = -\frac{8\mu'' l'}{R_4^2}\upsilon_{10} \qquad 2.18$$

where l and l' represent the lengths and R_4 is the radius of the horizontal conduits. From the equations, the pressure decreases along the length of the conduit.

The authors knew that the sum of the pressure drops around a circuit must be zero as so they looked at the two loops in the balance separately. Firstly, the initial loop in the system, loop ABCDSTUYNOPRA from Figure 2.7 above, where the reference flow enters is investigated. This gave an overall pressure drop around the loop of

$$\begin{aligned}(P_A - P_B) + (P_B - P_C) + (P_C - P_D) + (P_D - P_S) + (P_S - P_T) \\ + (P_T - P_U) + (P_U - P_Y) + (P_Y - P_N) + (P_N - P_O) \\ + (P_O - P_P) + (P_P - P_R) + (P_R - P_A) = 0\end{aligned} \qquad 2.19$$

The equations for pressure drop defined above were inserted into the above equation and rearranged to give

$$2gh(\rho' - \rho) + \frac{8\mu h}{R_1^2}(\upsilon_2 - \upsilon_1) + \frac{8\mu l}{R_4^2}(\upsilon_8 - \upsilon_7) + \frac{8\mu' h}{R_2^2}(\upsilon_3 - \upsilon_4) + \sum \Delta P_M = 0 \quad (2.20)$$

where $\sum \Delta P_M$ is the sum of all the pressure drops at the elbows and T-joints in the initial loop of the balance.

It is necessary to try to simplify this further. Knowing that velocities υ_1 and υ_2 are related to υ_7 and υ_8 through material balances, an expression for $(\upsilon_2 - \upsilon_1)$ was determined

$$(\upsilon_2 - \upsilon_1) = \left(\frac{R_4}{R_1}\right)^2 (\upsilon_8 - \upsilon_7) \quad (2.21)$$

This can be substituted into the equation above eliminating $(\upsilon_2 - \upsilon_1)$ to give

$$2gh(\rho' - \rho) + \left\{\frac{8\mu l}{R_4^2} + \frac{8\mu h}{R_1^2}\left(\frac{R_4}{R_1}\right)^2\right\}(\upsilon_8 - \upsilon_7) + \frac{8\mu' h}{R_2^2}(\upsilon_3 - \upsilon_4) + \sum \Delta P_M = 0 \quad (2.22)$$

The same procedure was followed for the sample flow loop. In Figure 2.10, the sample flow loop is represented by TSFGHIJKLMYUT. The pressure drop around this loop is zero. The overall pressure drop around the loop is given by

$$(P_T - P_S) + (P_S - P_F) + (P_F - P_G) + (P_G - P_H) + (P_H - P_I) + (P_I - P_J) + (P_J - P_K) + (P_K - P_L) + (P_L - P_M) + (P_M - P_Y) + (P_Y - P_U) + (P_U - P_T) = 0 \quad (2.23)$$

Again, the equations for pressure drop defined above were inserted into the above equation and rearranged to give

$$2gh(\rho'' - \rho') + \frac{8\mu' h}{R_2^2}(\upsilon_4 - \upsilon_3) + \frac{8\mu'' l'}{R_4^2}(\upsilon_{10} - \upsilon_9) + \frac{8\mu'' h}{R_3^2}(\upsilon_6 - \upsilon_5) + \sum \Delta P_M' = 0 \quad (2.24)$$

where $\sum \Delta P_M{}'$ is the sum of all the pressure drops at the elbows and T-joints in the sample loop of the balance.

Like the previously investigated loop, it is necessary to simplify this equation further. It was known that υ_5 and υ_6 are related to υ_9 and υ_{10} through material balances, an expression for $(\upsilon_6 - \upsilon_5)$ was determined

$$(\upsilon_6 - \upsilon_5) = \left(\frac{R_4}{R_3}\right)^2 (\upsilon_{10} - \upsilon_9) \qquad 2.25$$

Similarly, velocities υ_9 and υ_{10} are related to υ_8, υ_4, υ_7 and υ_3 through material balances. An expression for $(\upsilon_{10} - \upsilon_9)$ was determined

$$(\upsilon_{10} - \upsilon_9) = \left(\frac{\rho}{\rho''}\right)(\upsilon_8 - \upsilon_7) + \left(\frac{\rho'}{\rho''}\right)\left(\frac{R_2}{R_4}\right)(\upsilon_4 - \upsilon_3) \qquad 2.26$$

Inserting this into Equation 2.25 gives

$$(\upsilon_6 - \upsilon_5) = \left(\frac{\rho}{\rho''}\right)\left(\frac{R_4}{R_3}\right)^2 (\upsilon_8 - \upsilon_7) + \left(\frac{\rho'}{\rho''}\right)\left(\frac{R_2}{R_3}\right)^2 (\upsilon_4 - \upsilon_3) \qquad 2.27$$

Equations 2.26 and 2.27 can be inserted into Equation 2.24 to give

$$\begin{aligned} 2gh(\rho'' - \rho') + \left\{\frac{8\mu' h}{R_2^2} + \frac{8\mu'' l'}{R_4^2}\left(\frac{R_2}{R_4}\right)^2 \left(\frac{\rho'}{\rho''}\right) + \frac{8\mu' h}{R_3^2}\left(\frac{R_2}{R_3}\right)^2 \left(\frac{\rho'}{\rho''}\right)\right\}(\upsilon_4 \\ - \upsilon_3) + \left\{\frac{8\mu'' l'}{R_4^2}\left(\frac{\rho}{\rho''}\right) + \frac{8\mu' h}{R_3^2}\left(\frac{R_4}{R_3}\right)^2 \left(\frac{\rho}{\rho''}\right)\right\}(\upsilon_8 - \upsilon_7) \\ + \sum \Delta P_M{}' = 0 \end{aligned} \qquad 2.28$$

Equations 2.24 and 2.28 can be solved simultaneously for either $(\upsilon_4 - \upsilon_3)$ or $(\upsilon_8 - \upsilon_7)$. It was preferential to develop an equation for $(\upsilon_8 - \upsilon_7)$ as υ_7 and υ_8 are the velocities of the flows passing the filaments in the gas density balance.

Equation 2.24 was rearranged for $(\upsilon_4 - \upsilon_3)$ and inserted into Equation 2.28. Equation 2.28 was in turn rearranged for $(\upsilon_8 - \upsilon_7)$ to give

$$(\upsilon_8 - \upsilon_7) = \frac{2gh\left\{(\rho'' - \rho) + \frac{\mu''}{\mu'}\left(\frac{\rho'}{\rho''}\right)[A](\rho' - \rho)\right\} + \left\{1 + \frac{\mu''}{\mu'}\left(\frac{\rho'}{\rho''}\right)[A]\right\}\sum \Delta P_M + \sum \Delta P_M{}'}{\frac{8\mu l}{R_4^2}\left\{[B] + \frac{\mu''}{\mu}\left(\frac{\rho}{\rho''}\right)[C] + \frac{\mu''}{\mu'}\left(\frac{\rho'}{\rho''}\right)[D]\right\}} \quad 2.29$$

where

$$[A] = \left(\frac{R_2}{R_3}\right)^4 + \frac{l'}{h}\left(\frac{R_2}{R_4}\right)^4 \quad 2.30$$

$$[B] = 1 + \frac{h}{l}\left(\frac{R_4}{R_1}\right)^4 \quad 2.31$$

$$[C] = \frac{l'}{l} + \frac{h}{l}\left(\frac{R_4}{R_3}\right)^4 \quad 2.32$$

$$[D] = \left(\frac{R_2}{R_3}\right)^4 + \frac{l}{h}\left(\frac{R_2}{R_4}\right)^4 + \frac{l'}{l}\left(\frac{R_2}{R_1}\right)^4 + \frac{h}{l}\left(\frac{R_2}{R_3}\right)^2\left(\frac{R_4}{R_1}\right)^4 \quad 2.33$$

Equations 2.30 to 2.33 give detector parameters in terms of dimensions.

The volumetric flow rates of the gas passing the filaments in the detector are given by

$$Q_7 = \pi {R_4}^2 v_7 \quad 2.34$$

$$Q_8 = \pi {R_4}^2 v_8 \quad 2.35$$

The difference in flow rates between the upper and lower filaments of the gas density detector can be expressed using Equations 2.29, 2.34 and 2.35 as

$$(Q_7 - Q_8) = \frac{\pi g H {R_4}^4}{8\mu l}\left\{\frac{(\rho'' - \rho) + \frac{\mu''}{\mu'}\left(\frac{\rho'}{\rho''}\right)[A](\rho' - \rho) + \frac{\sum \Delta P_M}{\mathrm{gH}}\left\{1 + \frac{\mu''}{\mu'}\left(\frac{\rho'}{\rho''}\right)[A]\right\} + \frac{\sum \Delta P_M{}'}{\mathrm{gH}}}{[B] + \frac{\mu''}{\mu}\left(\frac{\rho}{\rho''}\right)[C] + \frac{\mu''}{\mu'}\left(\frac{\rho'}{\rho''}\right)[D]}\right\} \quad 2.36$$

This equation gives a relationship between the difference in flow rates in terms of the fluid parameters of the substances used in the balance, the dimensions of the detector and any pressure losses occurring at the bends and T-joints.

It is essential to find the actual size of the loss terms ($\sum \Delta P_M$ and $\sum \Delta P_M{}'$). As Kiran and Gillham (1975) [18] discussed earlier in their paper, it is assumed that the fluid is flowing in the laminar flow regime. The empirical information required to determine the magnitude of the loss terms is very scarce for laminar flow conditions. In the turbulent flow regime, these terms are often considered negligible as any losses are inconsequential. The authors estimated the magnitude of the loss terms by considering the case where no solute enters the system. In this situation only pure gases enter the system therefore $\rho = \rho' = \rho''$ and $\mu = \mu' = \mu''$. Equation 2.36 becomes

$$(Q_7 - Q_8) = \frac{\pi g H {R_4}^4}{8\mu l}\left\{\frac{\sum \Delta P_M{}' + (\sum \Delta P_M)\{1 + [A]\}}{\{[B] + [C] + [D]\}gH}\right\} \quad 2.37$$

According to this equation, if the loss terms are negligible, the difference in flow rates over the upper and lower filaments will also be negligible. Therefore, for simplicity it is assumed that the loss terms are negligible. Without the loss terms Equation 2.36 becomes

$$(Q_7 - Q_8) = \frac{\pi g H {R_4}^4}{8\mu l}\left\{\frac{(\rho'' - \rho) + \frac{\mu''}{\mu'}\left(\frac{\rho'}{\rho''}\right)[A](\rho' - \rho)}{[B] + \frac{\mu''}{\mu}\left(\frac{\rho}{\rho''}\right)[C] + \frac{\mu''}{\mu'}\left(\frac{\rho'}{\rho''}\right)[D]}\right\} \quad 2.38$$

The authors reported some observations from this equation. If $\rho' > \rho$, then $\rho'' > \rho$ as ρ'' is the flow leaving the detector where the flows with ρ and ρ' combine. In this case, $Q_7 - Q_8 > 0$ as the flow rate of the gas flowing over the upper filament will be higher than that at the

lower filament. The opposite situation occurs when $\rho' < \rho$. The authors also noted that the relationship between $(Q_7 - Q_8)$ and $(\rho' - \rho)$ is not exactly linear.

On inspection of Equation 2.38 some design considerations were observed that could maximise the sensitivity of the detector. By maximising $\frac{\pi g H {R_4}^4}{8\mu l}$ and $[A]$ in the numerator and minimising$[B]$, $[C]$ and $[D]$, the detector sensitivity is optimised. All these specifications cannot be satisfied concurrently. It is more important that $[A]$ is maximised than to minimise $[D]$ as $[A]$ directly amplifies the change in density. With this in mind, the authors concluded that the detector dimensions were chosen to satisfy the following conditions:

$$R_4 \ll R_1$$
$$R_4 \ll R_3$$
$$R_2 > R_3$$
$$R_4 < R_2 < R_1$$
$$l' < l < h$$

Taking these conditions into consideration, the detector dimension parameters are approximated as

$$[B] \approx 1$$
$$[C] \approx \frac{l'}{l}$$
$$[D] \approx \frac{l'}{h}\left(\frac{R_2}{R_4}\right)^4 + \left(\frac{R_2}{R_3}\right)^4 \approx [A]$$

To further reduce Equation 2.38, it was considered that the reference flow rate was significantly greater than the sample flow rate so that ρ'' and μ'' could be assumed to be equal to ρ and μ respectively. Taking the above into consideration, Equation 2.39 can be condensed to

$$(Q_7 - Q_8) = \frac{\pi g H {R_4}^4}{8\mu l}(\rho' - \rho) \qquad 2.39$$

By changing the radius term into a diameter term gives

$$(Q_7 - Q_8) = \frac{\pi g H D^4}{128 \mu l}(\rho' - \rho) \qquad 2.40$$

This equation is the same as the linear relationship derived in Equation 2.5 by Nerheim (1963) [9].

In this paper, Kiran and Gillham (1975) [18] also looked at what happens in the vertical channel YS where the sample flow enters the detector and splits before mixing with the reference flow. As previously mentioned, when considering the pressure drop in a vertical conduit, there are both static and dynamic contributions. The authors concluded that the dynamic contribution to the pressure drop can be considered to be negligible when compared to the static contribution. Therefore, the pressure drop Equation 2.10 can be reduced to

$$(P_P - P_R) = -\rho g h \qquad 2.41$$

The overall pressure drop equations around the initial and sample loop equations can be reduced to

$$2gh(\rho' - \rho) + \frac{8\mu l}{R_4^2}(\upsilon_8 - \upsilon_7) + + \sum \Delta P_M = 0 \qquad 2.42$$

and

$$2gh(\rho'' - \rho') + \frac{8\mu'' l'}{R_4^2}\left(\frac{R_2}{R_4}\right)^2 \left(\frac{\rho'}{\rho''}\right)(\upsilon_4 - \upsilon_3) + \frac{8\mu'' l'}{R_4^2}\left(\frac{\rho}{\rho''}\right)(\upsilon_8 - \upsilon_7) + \sum \Delta P_M{}' = 0 \qquad 2.43$$

Again, the pressure losses at the junctions can be ignored. Equation 2.42 can be rearranged to give

$$(\upsilon_7 - \upsilon_8) = \frac{2gh{R_4}^2}{8\mu l}(\rho' - \rho) \qquad 2.44$$

This can be rearranged to give Equation 2.39 and so changed to diameter terms and give Equation 2.40. Inserting Equation 2.44 into 2.43 and rearranging gives

$$(\upsilon_4 - \upsilon_3) = \frac{ghR_4{}^2}{8\mu l}\left(\frac{\mathrm{R}_4}{\mathrm{R}_2}\right)^2 \left\{\left(\frac{\rho}{\rho'}\right)(\rho' - \rho) + \frac{\mu}{\mu''}\left(\frac{l}{l'}\right)\left(\frac{\rho''}{\rho'}\right)(\rho' - \rho'')\right\} \qquad 2.45$$

Changing from velocities to flow rates, the equation becomes

$$(\mathrm{Q}_4 - \mathrm{Q}_3) = \frac{\pi gHR_4{}^2}{8\mu l}\left\{\left(\frac{\rho}{\rho'}\right)(\rho' - \rho) + \frac{\mu}{\mu''}\left(\frac{l}{l'}\right)\left(\frac{\rho''}{\rho'}\right)(\rho' - \rho'')\right\} \qquad 2.46$$

This equation shows that if a sample flow with a greater density than the reference flow enters the detector, ρ' is greater than ρ and ρ'' and so the downward flow in the vertical conduit YS will be greater than the upward flow. Also, if a sample flow with a lower density than the reference flow enters the detector, ρ' is less than ρ and ρ'' and so the upward flow in the vertical conduit YS will be greater than the downward flow.

The detector operates with the reference flow being significantly greater than the sample flow. With this in mind it could be approximated that $\rho'' \approx \rho$ and $\mu'' \approx \mu$. Therefore Equation 2.46 becomes

$$(\mathrm{Q}_4 - \mathrm{Q}_3) = \frac{\pi gHR_4{}^2}{8\mu}\left[\frac{1}{l} + \frac{l}{l'}\right]\left(\frac{\rho}{\rho'}\right)(\rho' - \rho) \qquad 2.47$$

This equation implies that the relationship is only linear for low solute concentrations.

The detector operates by the filaments in the upper and lower conduits sensing differences in the flow rates $(\mathrm{Q}_7 - \mathrm{Q}_8)$ flowing over the elements. Any change in the filament temperatures due to changes in flow rates generates an electrical signal. This was described by Nerheim (1963) [9]. He found that the electrical response, *E*, is linearly related to the change in flow rate. The authors of this work have proved that the change in flow rates over the upper and lower filaments is related to the change in density in the sample flow $(\rho' - \rho)$. Therefore, the electrical response is related to the change in density.

Nerheim (1977) [28] recognised that the design of the gas density detector had not been improved with time while other detectors were undergoing improvements. In this paper, investigations were carried out into how the gas density detector could be changed to improve

response. In particular, the effect of the outlet tube was looked at. It was predicted that by reducing the diameter of the outlet tube, the speed and amount of response could be enhanced.

The author reported that the reference and sample flow rates entering the detector must be kept high for greatest accuracy and sensitivity. Increasing these flow rates means that the dynamic range increases with the same detector response to the change in density. It was discussed that when designing for a maximum or optimum detector response with a change in density, the effects of frictional losses must be determined. Frictional resistance includes the effects of viscosity. This effect can be constant for pure carrier gases in the reference flow tubes. It can also be a complex expression for gas mixtures in the sample and outlet tubes. It was thought that it was more practical to minimise the effects of viscosity of the gas mixtures rather than trying to quantify the effects.

The previous paper by Kiran and Gillham (1975) [18] showed that the tube dimensions in the detector affect the detector response to changes in density of the sample flow. This paper states that the dimensions of the sample and outlet tubes also affect the filling and emptying time of the detector and so affects the response time. The response time influence the peak shapes of the result graphs but not the peak areas. A compromise must be found between the response time and the effect of viscosity when deciding the size of the sample flow and outlet tubes. It was found that increasing the reference flow will reduce the effect of changing the viscosity.

Nerheim (1977) [28] concluded that the potential energy that develops due to the change in density from the sample flow reduces the detector response caused by this density change. Reducing the outlet tube diameter minimises the ratio of frictional losses in the sample flow to the outlet flow. The response can be enhanced by increasing the reference flow rate which also increases the detector response. The tube dimensions in the detector can be used to optimise the balance between potential energy and friction. The dimensions of the sample and outlet tubes determine the response time but when the viscosity changes due to composition changes, the friction effects in the sample and outlet tubes reduces accuracy. The composition and hence the viscosity in the reference tubes are not affected by changes in viscosity and so will not reduce accuracy. By taking these points into consideration, the author suggests that an improved gas density detector could be developed.

Brandes, Kirchner and Richter (1984) [19] were the last to publish a paper discussing the gas density detector. The paper compares the gas density detector to other chromatographic detectors including the thermal conductivity detector and flame ionization detector. It highlights that while these detectors need careful calibration, the gas density detector can avoid this disadvantage. Other advantages of the gas density detector over other detectors are that it directly gives the mole fractions of the mixtures and it can be applied to corrosive gases. The paper aimed to show that gas analytical problems can be solved with a sufficient accuracy using a gas density detector with no need for calibration.

In this paper, experiments were carried out to determine the suitability of the gas density detector for gaseous analysis. Firstly, the gas density detector was used to determine mole fractions of various known gas mixtures. The mole fractions were determined with maximum uncertainties of ±0.5% for values above 0.2, ±1% for values between 0.04 and 0.2 and ±10% for values between 0.01 and 0.04. Corrosive gas mixtures were analysed with the same accuracy and after numerous repetitions, the detector properties did not change during the analytical process. Secondly, the gas density detector was used to determine the percentage mole fraction of gas mixtures of unknown compositions. As the compositions were unknown, the accuracy of the results were compared using the physical quantities calculated from the results of the analyses, like the gross calorific value and density, with the measured values. The calorific value from the detector analyses only deviated from the measured value by a maximum of 0.2%. The densities calculated from the analyses deviates from the measured value by a maximum of 0.2%. These results show that a high reliability can be attained. Finally, the gas density detector was used to determine the mole fraction of some binary mixtures. A thermal conductivity detector (TCD) and flame ionisation detector (FID) were also used to determine the mole fractions of the same mixtures and the results were compared. It was found that the binary mixture measurements agreed with the TCD and FID to within ±0.8%. However, the TCD and FID both had to be calibrated for the substances present.

In this paper, the authors also looked at the suitability of different gases to be used as carrier gases. It was found that when helium was used as the carrier gas, with a reference gas flow rate of less than 180 ml/min, results with some errors were obtained. It was thought that this was due to back diffusion of the sample flow into the reference flow. When considering the optimum operating temperature it was found that detector sensitivity increases with temperature of the filaments and so with the heating current. It was concluded that a very good reproducibility of measurements was observed.

After this paper on the gas density detector there has been no new information published about the device. In all the papers published, there have been no results graphs shown and so no peak shapes or areas could be obtained.

2.4. Sorption Effect

As previously discussed, gas chromatography is a technique in which a carrier gas flows through a column containing a material that will adsorb gas components temporarily. The sample to be analysed is injected into the carrier gas which carries it into the column. The different components in the sample gas are adsorbed by the adsorbent to different extents. The adsorbed components are almost stationary within the column and the non-adsorbed components in the sample will flow through the column with the carrier gas. Therefore, the more strongly adsorbed the component of the sample gas, the slower it moves through the column. The sample gas is thus separated into its components. As the components flow through the column, their presence is detected by monitoring a physical property of the gas stream (i.e. thermal conductivity, gas density, etc.). The adsorption of the gas components within the sample gas by the stationary material causes changes in the flow rate and pressure of the gas leaving the column. This was first described by Bosanquet and Morgan (1957) [29] as the sorption effect.

2.4.1. Sorption-Effect Chromatography

In 1986, Buffham *et al.* [30] published a paper discussing sorption-effect chromatography to show how the sorption effect could be used as a new detection method. They considered what happens when the sample enters and leaves the column. They postulated a simple case where an adsorbable sample is injected into a non-adsorbable carrier gas upstream of the column. As the sample enters the column and is adsorbed, there is an immediate pause in flow at the outlet. The effluent flow rate will remain constant as the adsorbed band travels through the column. When the band reaches the column outlet it desorbs and there is a surge in flow. It was reported that the time integral of the incremental flow rate equals the quantity of material desorbed, measured as a gas volume. Therefore, if a mixture of strongly adsorbed species is separated chromatographically, it is possible to calculate the composition from the flow rate record as

gas volume fractions without the need for calibration. The separated components of the sample leaving the column produce surges in flow rate so if these surges can be measured with a sensitive differential flow meter then it is possible to use this measurement to detect the adsorbed bands. The authors described this measurement of changes in flow rate as 'sorption-effect chromatography' as it depends on the sorption effect. It differs from conventional chromatography as it is the flow that is measured instead of the composition. The sorption-effect chromatogram is different from a conventional chromatogram given by another GC detector like a thermal conductivity detector in that the flow detector responds the moment the sample is injected. It responds again as the sample is adsorbed by the material in the column and will respond again as each component band desorbs and exits the column. This final part of the chromatogram resembles a conventional chromatogram but the areas on the sorption effect chromatogram represent gas volumes.

In a simple case where the carrier gas is non-adsorbable and a strongly adsorbable gas mixture sample is injected, the area of the peak caused by the injection is the volume of the sample. The area of the negative absorption peak also is the injected sample volume. The areas of the desorption peaks represent the volume of each component in the sample.

In another case where the carrier gas is adsorbable and the sample is not strongly adsorbed, the injection peak area will still represent the sample volume but the negative absorption peak will be the net volume adsorbed as this will represent the difference between the volume of sample adsorbed and the volume of the carrier gas that desorbs. The areas of the desorption peaks will also be net volumes.

Buffham et el. (1986) [30] described their set up of the sorption effect chromatograph that was used to gain some results. They used a conventional katharometer chromatograph but made some amendments so that the sorption effect could be measured. They ensured that the carrier gas in the chromatographic columns was at a constant flow rate by introducing a pressure regulator and matched capillary tubes. The column outlets were connected to the katharometer and the outlets from this were connected to a pair of matched chokes. The variations in effluent flow rates were measured using a differential pressure transducer (DPT) connected to these capillary tubes. This arrangement of a differential pressure transducer and matched capillary tubes act as a differential flow meter which can detect very small differences between the flows leaving the columns. This differential flow meter is measuring the pressure drop which

is dependent on the flow rate and the viscosity of the gas. In this paper, it is assumed that the effect of viscosity is very small.

The authors carried out some experiments using the sorption-effect chromatograph. They found that the sorption-effect detector had about the same sensitivity as the katharometer and that the response from the detector is approximately proportional to the amount of adsorbed material that is desorbed as a peak leaves the column. It was reported that sorption-effect chromatography has the advantage of measuring the changes in flow and composition in the column so it can be used as an additional measurement to conventional detectors that measure changes in a physical property. A differential flow meter can show the sorption effect instantaneously when the sample is injected and again when the sample is adsorbed and then when the bands desorb and exit the column. This means that residence times can be accurately determined from the chromatogram. The detector can be small and is simple in construction so it is reasonably inexpensive.

Experiments carried out by the authors also showed that there are some disadvantages to using the sorption-effect detector. The method was shown to lack sensitivity when hydrogen or helium was used as the carrier gas when compared to results from the thermal conductivity detector but with other gases the results were comparable. During experiments, it was discovered that the apparatus was sensitive to small changes in atmospheric pressure. Due to the nature of the equipment where there are two matched streams, any imbalance in the streams can cause drift in the baseline.

Meacham, Buffham and Mason (1990) [31] carried on this work to investigate the role viscosity plays in sorption effect chromatography. They considered finding an explanation as to why adding a sample of hydrogen into a carrier gas of helium reacts differently to other gases in the sorption-effect chromatograph. Figure 2.8 shows the difference between the chromatograms when an argon sample is added to a carrier gas of helium (**A**) and when a sample of hydrogen is added to a sample gas of helium (**B**). It also has a depiction of the experimental set-up used to produce these results (**C**).

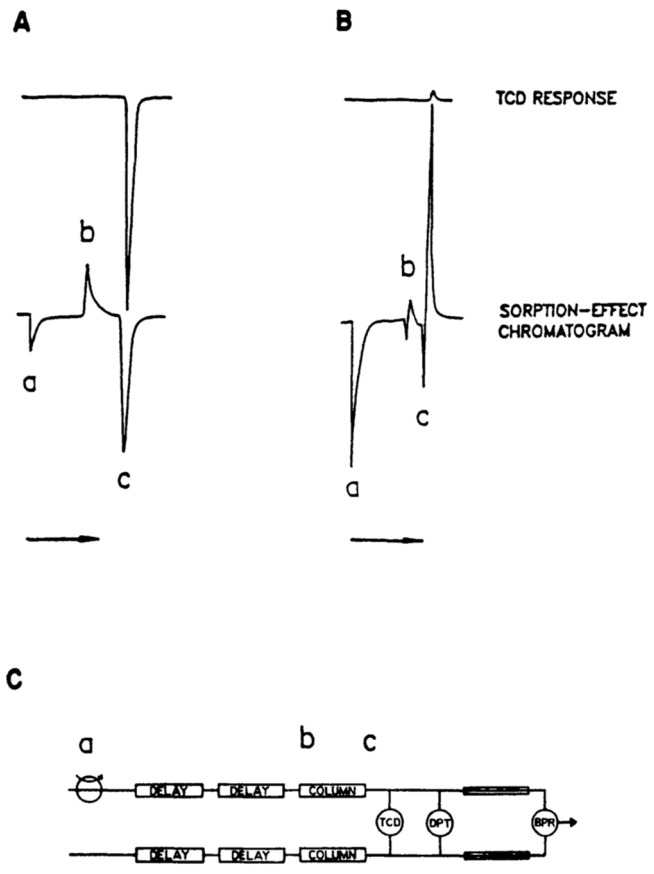

Figure 2.8 - Sorption effect chromatograms and experimental set-up (from [31]*)*

In the figure, part **A** shows a resulting sorption effect chromatogram when a sample gas of argon is injected into helium carrier gas. This is a typical sorption effect chromatogram where α is the injection peak as the sample is added to the system, b is the absorption peak as there is a pause in flow rate as the sample adsorbs in the column and c is the desorption peak as the previously adsorbed band desorbs and leaves the column. The upper trace on the diagram shows the thermal conductivity detector (TCD) response to the addition of the sample. There is only a peak as the sample passes through the detector and leaves the column.

Part **B** in Figure 2.8 shows the chromatograms when a hydrogen sample is added to a helium carrier. The injection peak α is similar to that in part A. In the absorption peak, b, there is a dip in the opposite direction. In the previous paper [30], this was thought to be due to the reduced viscosity at the start of the column. In the desorption peak, c, again there is an initial surge followed by a larger pause in flow that coincides with the peak from the TCD.

Part **C** depicts the experimental arrangement used to obtain these results.

The purpose of this paper was to introduce delay lines in the sorption-effect chromatograph to investigate the response of the capillary flow detector when a hydrogen sample is injected to a carrier gas of helium and to find an explanation for the anomalous behaviour.

The authors tried different experimental configurations to find an explanation for the anomalous behaviour of hydrogen. They found that by introducing delay lines between the column and the DPT, it was possible to separate the desorption peak into two peaks. The first peak occurs when the sample desorbs at the end of the column. The second peak occurs when the sample has reached the flow detector. The experiment was repeated for adding a sample of argon into a helium carrier and the desorption peak had separated into two. Therefore, by the introduction of the delay lines between the column and the capillary flow detector, four peaks are observed on the chromatogram, an injection peak, an adsorption peak, a desorption peak and a peak caused by the viscosity effect when the viscosity changes in the flow-detecting capillaries.

Buffham *et al.* (1993) [32] continued this work to report that sorption-effect chromatography could be used as an absolute method. It was shown that the molar composition of a sample could be determined without the need for calibration. In thermodynamic terms, the capillary flow meter measures an extensive property and conventional detectors measure intensive properties. Therefore, the flow rate record alone can contain enough information for analysis so the method can be absolute.

It was reported that for sorption-effect chromatography to become an absolute method, a flow meter had to be provided that was not dependent on composition and could account for any unadsorbed molecules. As previously discussed above, the area under the flow rate peaks gives the volume of each sample species desorbed. If the sample species are strongly adsorbed and the carrier is not then the volumes desorbed from the column are the partial volumes of the various species in the sample. This method is absolute. A correction factor is required to make the method absolute in cases where the sample species are not so strongly adsorbed and the carrier is adsorbed. The necessary correction factor, F, is the ratio of the quantity of the solute in the band, m_B, to the quantity of gas released when the band desorbs, m_D.

2.4.2. Determination of Binary Gas Adsorption Isotherms

The sorption effect is also used to determine multicomponent gas adsorption isotherms and the sorption-effect chromatogram is used to calculate retention times of transients passing through a column. These values are used to find the slopes of phase equilibrium curves and adsorption isotherms [33-37].

Buffham (1978) [33] published a paper reporting that the chromatographic retention times when step or pulse perturbations are added to a gas flowing into a chromatographic column are independent of the nature of mass transfer processes within the column. The retention times were proved to be solely dependent on equilibrium properties and so could be determined from the sorption-effect chromatogram. It was proved that when a perturbation flow is added to a column, the retention time for a species in the sample is equal to the ratio of the change in equilibrium hold-up of the species in the column to the change in the rate at which it is transmitted through the column.

Buffham *et al.* (1985) [34] continued this work to include binary gas mixtures. They considered adding a perturbation flow to change the composition of a binary gas mixture flowing into a column which adsorbs both species in the gas mixture. A chromatographic transient could be seen by the change in concentration with time of the outlet gas flowing from the column. There was also a flow rate fluctuation due to the addition of the perturbation flow.

The authors developed a theory to relate the composition and flow rate transients to the phase equilibrium properties. It was shown that the slope of the phase equilibrium curve is a function of the retention time. The retention times for the transients were defined using the sorption-effect chromatogram so are dependent on the equilibrium properties and are independent of the mechanism of the rate processes, mass transfer rates and the degree of departure from equilibrium.

The model independent theory starts with a material balance and avoids the need to specify mass transfer rates. It shows that the retention times depend on conditions before and after the transient and not on the rate processes. It is assumed that the column is initially in a steady state. The feed is changed and the column evolves to a new steady state. The material balances represent the change in the inventory of each species in the column in response to this change.

For binary chromatography, the differential signal from the detector is proportional to the difference in mole fractions. Assuming the gas is at low pressure and constant temperature, the volumetric flow rate from the column (measured using a bubble flow meter) is proportional to the molar flow rate. Therefore, transient analysis can be carried out in terms of mole fractions and molar flow rates. In these experiments, the chromatographic transient was produced by changing the feed composition while maintaining the flow rate steady.

Further work was carried out by Mason and Buffham (1996a) [35] where the transient was produced by simultaneously changing the feed composition and its flow rate. As in previous experiments, a perturbation flow was added to the system to change the system from an initial steady state to a new steady state. The flow rate change was measured by a capillary flowmeter and the composition by a katharometer.

The basis of the author's method is simply mass balances. Mass balances were carried out over the chromatographic column at the initial steady state, when a change is made to the system and when a new steady state is reached and so an equation could be derived for the change in hold-up in the system. An equation to determine the gradient of the adsorption isotherm for binary gas mixtures was obtained using these mass balances and retention time transient analyses from the chromatograms.

Apparatus similar to that shown in Figure 2.8 was used in these experiments. Some pieces of equipment were included to allow the addition of the perturbation gas stream to the main gas flow stream as shown in figure 2.9. The experiments were carried out by adding a small perturbation stream to a stream of gas mixture which passed into a column. The effluent flow-rate and composition transients were then measured.

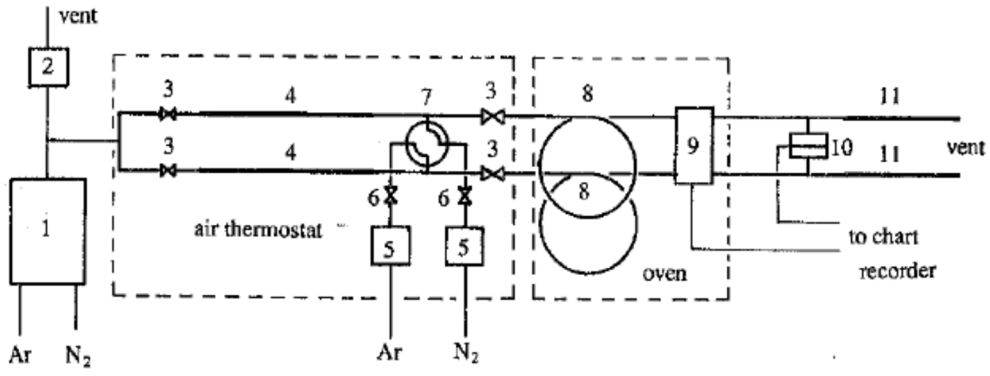

Figure 2.9 – Apparatus used in the determination of gas adsorption isotherms (Figure 10 from [35]*)*

It can be seen from the figure that it is a binary system the main flow is split into two equal streams of identical flow. Each side of the binary system pass through a capillary choke and column before passing the katharometer, differential pressure transducer and flow-sensing capillary. The capillary chokes act as the main flow setting devices. The apparatus is set up so that the perturbation flow can be added to either of the streams. The perturbation gas is added to one of these streams while the other acts as a dummy stream allowing for differential measurements to be made from changes in flow-rate and composition. Experiments were conducted by adding a perturbation stream of either pure argon or pure nitrogen to one of the columns of the apparatus containing the main argon-nitrogen mixture. When the baselines on both the katharometer and the flow recordings were steady, the perturbation stream was switched from one side to the other. In this case, the signals from the katharometer and the flowmeter were recorded using a chart recorder. When a new equilibrium was reached, the results from the chart recorder gave enough information for the retention time of the composition transient to be determined as the response from the katharometer is linear with changes in composition. The differential pressure transducer recorded simultaneously in the same way however the interpretation of the results is different. Since the pressure drop along a pipe varies with flow-rate and viscosity and viscosity of gas mixtures depends on composition, the flowmeter therefore responds to both composition fluctuations and flow-rate. It was assumed in this work that the flowmeter is ideal and so the retention time of the flow-rate transient was calculated. The effect of viscosity was looked at in a later paper [36].

The results of these experiments showed that the time for the composition transient to pass is not dependant on which perturbation gas is used and that the main flow-rate varies with composition as the flow is set by a fixed pressure drop across a capillary tube and so varies with the viscosity of the gas mixture.

In the next paper in this series, Mason and Buffham (1996b) [37] looked at including the effect of pressure changes in the system to get more accurate results. The effect of the increased mean pressure in the column caused by the small increase in flow was investigated. A correction factor for the concentration change caused by the increase in pressure when the perturbation gas is added was incorporated into the equation to determine the gradient of the adsorption isotherm and gave more accurate results to the same experiments carried out in the previous paper. It was found that using argon as the perturbation to determine the nitrogen

adsorption and nitrogen as the perturbation to determine the argon adsorption along with a flow-rate measured at atmospheric pressure compensates for the pressure effect.

In the final paper in the series, Mason *et al.* (1997) [36] included the effect of changes in gas viscosity produced by a change in gas mixture composition in the previous work completed. This has two main effects. The first is that the pressure drop down the column is altered and so changes the amount of gas adsorbed. This effect is quite small. The second effect is concerned with the flow rate measurement method. As mentioned in the other papers in the series, a capillary flowmeter is used in the experiments to monitor flow and that these flowmeters respond to viscosity as well as flow. This effect can be quite significant. The paper has looked at corrections for the viscosity effect. The authors showed that by the addition of a delay line between the column and the flowmeter, this effect can be removed. A delay line is simply an empty tube which delays the arrival of gas of different viscosity. If a sufficient length of tubing is used, the composition of the gas in the flowmeter will remain constant for the time the composition front is travelling and then leaving the column. When the composition front has passed through the delay line, there will be another change in the measurement from the flowmeter. This is due to the change in viscosity.

The three Buffham papers combined [35-37] developed an accurate way of determining the adsorption isotherm gradient using the principles of sorption effect.

2.4.3. Perturbation Viscometry

In 1998, Mason *et al.* [38] continued their work using the sorption effect principles and applied them to develop a new technique for making viscosity measurements, perturbation viscometry. In this paper, two new concepts for viscosity measurements were introduced.

The first concept involved measuring the gradient of the viscosity-composition function instead of measuring the gas viscosity directly. To achieve this, the composition of the gas mixture was changed slightly by the introduction of a small perturbation stream and so the small change in viscosity was measured. This approach has the advantage of differential measurements followed by integration which is more accurate than direct measurement.

The second concept involved the apparatus design and the theory of laminar flow through tubes. A capillary tube was introduced into the equipment. Like the delay line described previously [36], the capillary tube is used first as a flow meter and shortly afterwards as a viscometer. The basic apparatus used in the perturbation viscometer includes four main items, a valve, a delay line, a pressure gauge and a capillary tube as shown in Figure 2.10.

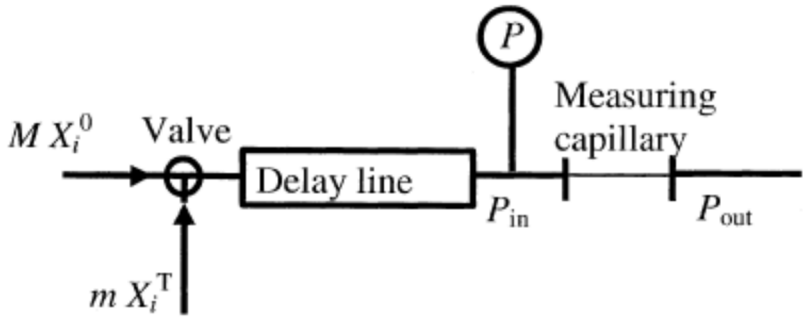

Figure 2.10 – Basic apparatus for perturbation viscometry
(from Figure 1 in [39]*)*

Experiments involve adding a perturbation stream of molar flow rate m to a main stream of molar flow rate M which flows through the delay line and capillary tube. The mole fractions of the main gas and perturbation gas are X_i^0 and X_i^T respectively. Pressure changes at the upstream end of the capillary tube are measured.

When the response due to the change in flow rate is divided by the response due to the change in viscosity, the gradient of viscosity with composition is obtained. The authors showed that the inlet pressure of the capillary tube increases as the perturbation gas is added and this pressure increase is proportional to the change in flow rate. The delay line, between the point where the perturbation gas is added, and the capillary tube means there is empty volume in the system and so there is a delay before the pressure changes again when the composition of the gas flowing through the capillary tube changes again. This second pressure change is proportional to the change in viscosity. The ratio of the two pressure steps is proportional to $\mathrm{d} \ln \mu / \mathrm{d}X_i$ where μ is the viscosity and X_i is the mole fraction of component *i,* and so gives the gradient of the viscosity with composition of the gas mixture. If the viscosity gradients across the composition range are known, then integration of these gradients gives viscosities across the composition range relative to one of the pure components in the mixture. This method has the advantage that the only properties of the gas in the capillary tube are measured so the result is not dependent on the properties of the capillary tube.

Another advantage that the authors proposed is the use of a differential apparatus design, as used in other chromatography systems, to overcome some potential difficulties in maintaining a constant gas flow. Using a differential pressure transducer between the reference and measurement streams has the benefit of common upstream and downstream pressures in both streams. The differential measurement followed by the integration is more accurate than direct measurement of the viscosity.

The theory of this new technique for making viscosity measurements was further modified Mason *et al.* (2000) [40] by the addition and removal of finite perturbations. A pressure record is shown in Figure 2.11 where an argon perturbation gas is added and then removed from a main flow of nitrogen.

When the perturbation gas is added, the pressure instantly increases from P_0 to P_1. When the composition front reaches the capillary tube, the change in viscosity causes a pressure change from P_1 to P_2. This can either increase or decrease the pressure depending on the viscosity of the perturbation gas being greater than or less than the viscosity of the main gas. When the perturbation gas is removed the pressure changes from P_2 to P_3 as the flow rate decreases and from P_3 to P_4 as the viscosity changes again.

In this paper [40], it was shown that there are systematic differences between the results of adding the perturbation gas and removing it. The perturbation gas flow rate would have to be very small to eliminate the effect from these differences. The authors concluded that the major correction in the theory for measuring the gradient of the viscosity-gradient function for finite changes in composition is for the size of the perturbation flow relative to the main flow of gas. They also reported that this correction is only required for results obtained when the perturbation flow is removed. Experiments were carried out in a nitrogen-argon system. The authors further concluded that it would be better to determine the composition of the main flow by making two measurements of $\mathrm{d} \ln \mu / \mathrm{d}X_i$, one measurement using argon as the perturbation gas and the other using nitrogen while keeping the main flow rate constant. This allowed for internal consistency checks to be made.

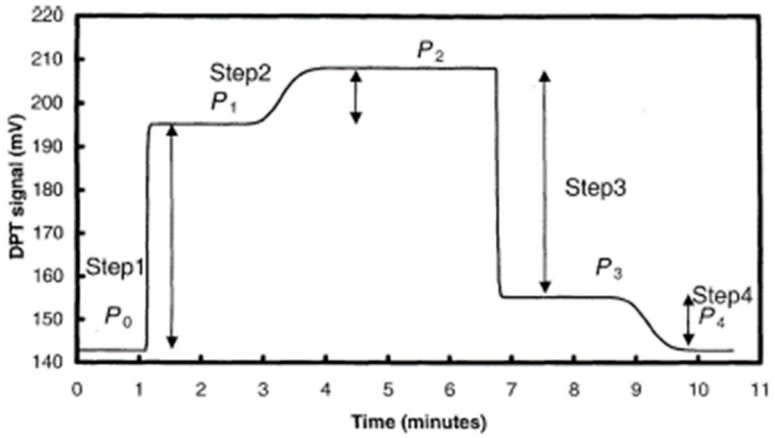

Figure 2.11 - Actual pressure record for an experimental run where an argon perturbation gas is added to a main flow of nitrogen (Figure 2 from [39]*)*

Integration of the logarithmic viscosity gradient measurements obtained from the perturbation viscometer could be completed by either applying the trapezium rule or numerical integration of a polynomial fitted to the data. Buffham *et al*. [41] considered other methods of processing the gradients measured over a full composition range. It was reported that a differential form of the Sutherland equation could be used to generate viscosity gradients. Experiments were carried out using the Sutherland equation and calculated values for the gradients. Both methods showed good agreement.

Russell *et al*. [39] continued work on the perturbation viscometer by carrying out experiments using fully thermostatted apparatus. Previous experiments had been carried out using basic apparatus. This paper looked at refining the apparatus to identify any potential flaws. Improvements were made to the experimental apparatus design.

A flow setting block was designed and included in the equipment to produce very stable, matched flows between the measurement and reference flows. The block has ample thermal mass and conducts heat well enough to maintain all components in the block at the same temperature. A single stream of gas enters the block and this then splits the gas internally into two equal gas streams.

A perturbation switching valve was included in the equipment design to allow the addition of the perturbation flow to the measurement side of the apparatus.

A special pressure transducer was commissioned with extra ports to let the main gas flow pass through its measurement chambers. An extra pressure channel was applied to each side of the transducer so that the main flow entered each side of the transducer through the original ports and would leave through new ports. This allowed the gas composition inside the transducer to be the same as the main flow, eliminating the systematic drift.

A counter current heat exchanger was added after the pressure transducer to increase the temperature of the gas to the operating temperature of the capillaries. It is important for the temperature of the gases in the heat exchanger to remain constant. Changes in the temperature will result in expansion or contraction of the gas and so produces flow rate changes that would appear as noise on the pressure readings.

Finally, a perturbation flow supply system was integrated into the apparatus. This included a mass flow controller to set the perturbation flow downstream of a pressure regulator. A bypass was added around the mass flow controller to permit the perturbation system to be purged with a new perturbation gas when the perturbation gas is to be changed.

The authors carried out experiments for viscosity gradients for a helium-nitrogen mixture at 360ºC. To achieve this temperature, a section of the apparatus was assembled in an oven. The technique and new apparatus were shown to work with no reduction in performance at 360ºC. It was shown that the apparatus produced viscosity-gradient data of a very high quality and integration of the experimental gradient data was as good as existing data.

Up to this point, all perturbation viscometry experiments were carried out with small perturbation flow rates being added to the main gas. In 2005, Russell *et al*. [42] considered using larger perturbation flows being added to the main gas. The existing method was modified to calculate the viscosity gradients from large perturbation flows.

The upstream and downstream pressures in the experimental set-up are fixed. Experiments were carried out as previously discussed where a perturbation flow is added to the main flow. The first change in pressure is due to the change in flow rate so when the perturbation flow is added, the pressure at the capillary will result in a reduction in the main flow rate by a small amount, Δm_1. This amount is dependent on the pressure drop across the upstream resistance and the size of the perturbation flow being added. If the perturbation flow is small, Δm_1 is negligible. The second pressure change due to viscosity after the perturbation flow is added

can also alter the main flow. This change was denoted by Δm_2. These flow rate changes were integrated into the previously derived equations for the effects of adding and removing the perturbation flow and a correction term was added to the viscosity gradient calculations. With the addition of the correction term for adding very large perturbation flows, results of equal accuracy to those obtained using small perturbations were obtained.

Further work was completed using perturbation viscometry to measure the viscosity gradient of ternary gas mixtures [43] and mixtures of non-ideal gases [44]. In both investigations and after further internal tests for direct comparisons, it was found that the perturbation viscometry method gave highly accurate, consistent results.

2.4.4. Flux Response Systems

The flux response is a method for measuring the rates of heterogeneous catalytic and other gas-solid reactions. The flux response is described as the way the net rate at which molecules leave a reactor changes when some input, or other variable, is changed. It depends on the combined effect of adsorption, reaction and desorption of the gases in a reactor. The apparatus used in the sorption effect method was used as the basis for the apparatus design of flux response measurement [45].

Sorbable-band scanning [46] and composition-front scanning [47] have previously been investigated to identify adsorptive and non-adsorptive zones in a packed column. By passing a sorbable band or composition front through a column, the presence of internal anomalous zones can be revealed which causes downstream flow-rate changes that are detectable by a sensitive flow meter. In adsorption, the downstream flow-rate is changed by the capture and release of molecules in the anomalous zones. In a reactive solid, molecules can be removed from or added to the gas phase in the vicinity of that solid in the same way by adsorption or desorption from the solid. In addition, if a reaction occurs, the number of molecules desorbing may be different from the number adsorbing and so the timing may be modified by the reaction taking place. Therefore, within a reactive zone, adsorption, desorption and reaction can take place leading to a net flux of molecules within the zone. A perfect molar flow meter can be used as a downstream device to monitor the passage of molecules and so will be able to record how the net flow, or flux, of molecules from the reactive zone varies with time. This record of flow-rate changes is called the flux response.

Buffham *et al*. [45] carried out flux response experiments using the catalytic decomposition of methanol over platinised alumina. The authors chose this reaction for a first test of the method as three moles (one mole of carbon monoxide and two moles of hydrogen) are produced from the decomposition of one mole of methanol.

An experimental set-up like that of sorption effect chromatography was used as seen in Figure 2.12 below (Fig 3 from [45]).

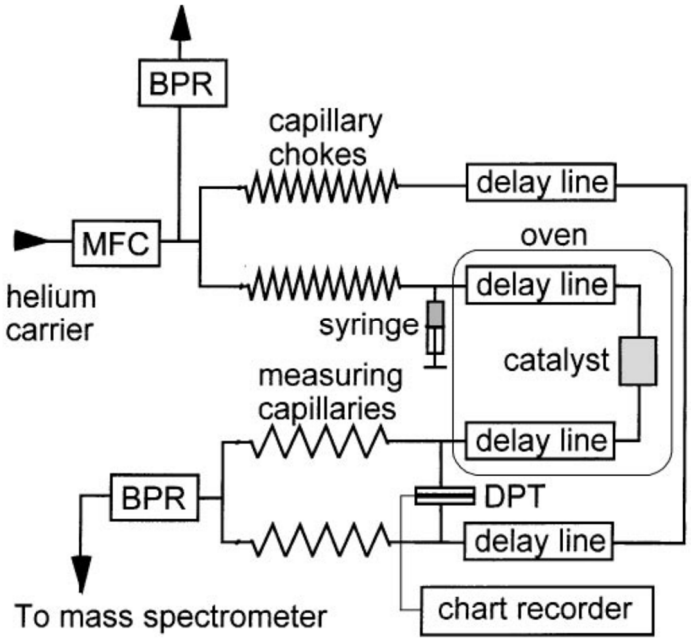

Figure 2.12 – Experimental Set-up to determine flux response (Figure 3 from [45]*)*

The carrier gas is supplied by a mass flow controller to the two parallel channels, a reference and an experimental channel. A differential flow meter was formed by a series of matched capillary chokes, delay lines, flow-sensing capillaries and a pressure transducer. The difference in the pressure measured is proportional to the difference in the flow rates.

The expected result plot of effluent flow rate versus time for a pulse response experiment is shown below in Figure 2.13. The initial baseline is shown by (1). When the pulse of reactant is injected into the system there is a sudden peak from the baseline (2). When the reactant is carried into the inert packing, the response returns to the baseline (3). When the reactant reaches the catalyst, the number of moles changes and causes a flux response (4). The flow

meter response then returns to the baseline again (5). If a capillary meter is used to measure the flow rate, there can be a viscometric response when the products arrive (6).

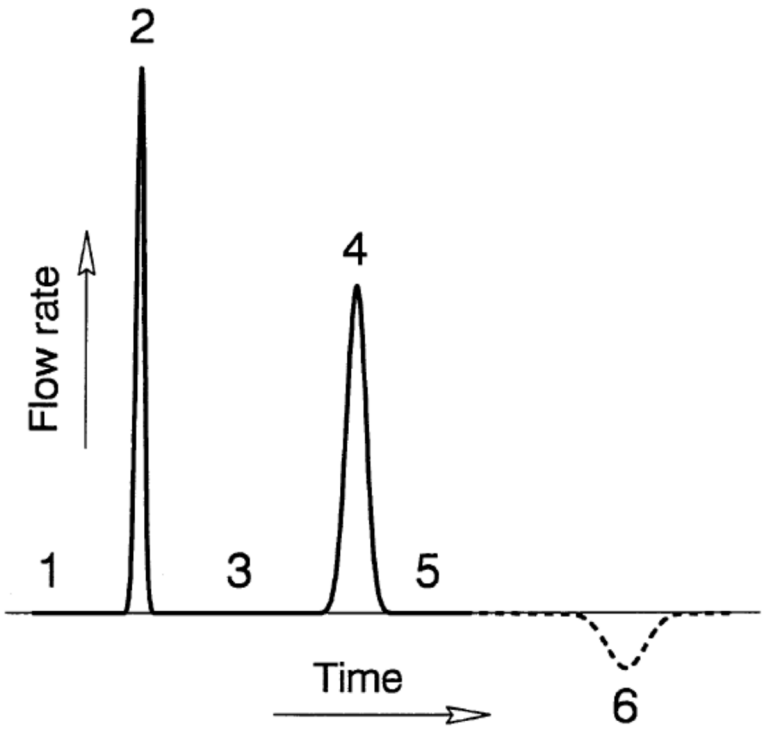

Figure 2.13 – Expected profile during a pulse-response experiment

The integral with time from points 1 to 3 corresponds to the quantity of reactant admitted. The second peak is the flux response due to adsorption, reaction and desorption. Assuming that no reactant or product becomes permanently attached to the catalyst, the integral with time from point 3 to 5 is a measure of the change in volume of the reaction mixture. If the number of moles remains constant there is no change in gas volume but the gas volume changes when the number of moles increases or decreases.

Experiments were carried out at different temperatures. The results obtained were followed the expected result plot. The first peak on the result plot is due to the injection of reactant. The authors observed different flux responses at different temperatures. At lower temperatures, there was more adsorption and the reaction proceeded more slowly.

Along with flux response measurements, a mass spectrometric analysis was carried out to identify and quantify the components present in the effluent stream. Their experiments

confirmed that the flux response can be used to measure the adsorption, reaction and desorption mechanisms in heterogeneous catalysis.

In 2002, Buffham *et al*. [48] used the previous work to develop a mathematical model of the flux responses of gas-solid catalytic reactors. It was assumed that the pressure drop was low enough that the gas be treated as being ideal. It was also assumed that the reactor was isothermal so the gas phase molar density was constant. Mass balances were carried on the reactants adsorbed by the catalyst, on the products and on any inert species in the reactor that neither adsorbs or react. These led to the development of an expression for the reaction rate per unit volume of solid in the catalytic reactor.

In this work, a simulation was also established to allow flux responses to be estimated. The simulations were validated by results from experimental flux responses. There some between the simulated and experimental responses. The simulations were constrained to be within the range of the mass transfer correlation. The authors described future work to address this issue and improve the simulation for use in different reactors.

2.5. Summary

This section provided some background to subjects central to this research. To develop this project further, there is some other general theory that will be used in this work. This will be discussed in the next section.

3. Theory

This chapter discusses some of the general theory that is fundamental to this work. Throughout this thesis, flow of materials along various tubes and resistances will be considered. The Hagen Poiseuille equation defines an equation for the pressure gradient along a length of tubing and will be used in Chapters 4 and 5.

The density of gas mixtures will be investigated throughout so the ideal gas law is rearranged to give equations for the change in density caused by a change in mole fraction, pressure or temperature.

The concept of gas being held up within a system is also a common theme in this work. Equations to determine the change in hold-up with flow rate or pressure change is found and used throughout.

Bernoulli's equation is explained to show that if the velocity of fluid flowing through the system increases, the system pressure decreases. This concept is used in the determining the operation of the gas density detector (Chapter 6).

3.1. Hagen Poiseuille Equation

The Hagen-Poiseuille equation defines the flow of a Newtonian fluid through a tube and how this flow is affected by the attributes of the tube and the fluid [49, 50]. It is defined by the formula:

$$Q = \frac{\Delta P \pi r^4}{8 \mu l} \qquad 3.1$$

For fully-developed laminar flow, it relates the volumetric flow rate (Q), the viscosity (μ), the change in pressure (ΔP) and the tube dimensions (radius, r and tube length, l). In this work, k will be used as a tubing constant to incorporate the tube dimensions.

Equation 3.1 can be rearranged to give the pressure gradient along the length of the tubing, z, as follows:

$$\frac{\mathrm{d}P_z}{\mathrm{d}z} = -k\mu Q \qquad 3.2$$

This is fairly standard to integrate for an incompressible liquid, since flow rate, Q, can be taken as a constant. However, it is more difficult for a gas, since the volumetric flow rate will change with pressure. Q can be modelled using the ideal gas equation as follows:

$$Q = \frac{MRT}{P_z} \qquad 3.3$$

where M is the molar flowrate of gas, R is the universal gas constant, T is the absolute temperature and P_z is the pressure at distance z along the length of tubing.

By substituting Equation 3.3 into Equation 3.2, the pressure gradient can then be expressed as

$$P_z \frac{\mathrm{d}P_z}{\mathrm{d}z} = -k\mu MRT \qquad 3.4$$

At low pressures, the viscosity of a gas is almost independent of pressure. If the viscosity μ is assumed to be constant with temperature then Equation 3.4 can be integrated along a whole length of tubing from 1 to 2 to give:

$$P_1^2 - P_2^2 = 2kRT\mu M \qquad 3.5$$

This equation will be used throughout the experimental and results sections (Sections 4.6.6 and 5.3.3).

3.2. Definition of Ideal Mixture

For an ideal gas mixture of two components A and B, the total specific volume is given by [49, 50]:

$$V = v_A x_A + v_B x_B \tag{3.6}$$

where V is the total specific volume (m^3/kg)

v_A and v_B are the specific volumes of components A and B respectively (m^3/kg)

x_A and x_B are the mass fractions of A and B respectively.

The specific volume is the inverse of density. Therefore, in terms of density, this equation becomes

$$\frac{1}{\rho} = \frac{1}{\rho_A} x_A + \frac{1}{\rho_B} x_B \tag{3.7}$$

where ρ is the density of the gas mixture (kg/m^3)

ρ_A and ρ_B are the densities of components A and B respectively (kg/m^3).

The mass fraction of component A can be obtained by

$$x_A = \frac{y_A w_A}{w_B + y_A(w_A - w_B)} \tag{3.8}$$

where y_A is the mole fraction of component A

w_A and w_B are the molecular weights of components A and B respectively (kg/kmol).

For a binary gas mixture

$$x_B = 1 - x_A \tag{3.9}$$

Therefore, Equation 3.8 can be rearranged to give

$$x_B = \frac{w_B(1 - y_A)}{w_B + y_A(w_A - w_B)} \tag{3.10}$$

Substituting Equations 3.8 and 3.10 into Equation 3.7 gives

$$\frac{1}{\rho} = \frac{1}{\rho_A} \frac{y_A w_A}{w_B + y_A(w_A - w_B)} + \frac{1}{\rho_B} \frac{w_B(1 - y_A)}{w_B + y_A(w_A - w_B)} \tag{3.11}$$

Multiplying through by $\rho_A\rho_B$ and rearranging gives

$$\frac{\rho_A\rho_B}{\rho} = \frac{y_A(w_A\rho_B - \rho_A w_B) + \rho_A w_B}{w_B + y_A(w_A - w_B)} \qquad 3.12$$

Equation 3.12 can be rearranged to obtain the density of the mixture as a function of the components mole fractions, y_i, molecular weight, w_i, and their densities, ρ_i, as;

$$\frac{\mathrm{d}P_z}{\mathrm{d}z} = -k\mu Q\frac{\rho_A\rho_B}{\rho} = \frac{y_A(w_A\rho_B - \rho_A w_B) + \rho_A w_B}{w_B + y_A(w_A - w_B)} \qquad 3.13$$

The ideal gas equation is

$$PV = nRTZ \qquad 3.14$$

where P is the absolute pressure of the gas
V is the volume of the gas
n is the number of moles of gas
R is the universal gas constant (J/mol.K)
T is the absolute temperature of the gas
Z is the compressibility factor.

For an ideal gas, it is assumed that the compressibility factor is 1. Rearranging this equation in terms of concentration (n/V) gives

$$\frac{n}{V} = \frac{P}{RT}\frac{1}{Z} \qquad 3.15$$

And in terms of density;

$$\rho = \frac{n}{V} \times w = \frac{P}{RT}\frac{1}{Z}w \qquad 3.16$$

For components *A* and *B*, the density, ρ_A and ρ_B, can be written as per Equation 3.16 as;

$$\rho_A = \frac{P}{RT}\frac{1}{Z_A}\, w_A \qquad 3.17$$

$$\rho_B = \frac{P}{RT}\frac{1}{Z_B}\, w_B \qquad 3.18$$

If it is assumed that *P*, *R* and *T* are all constant and that *A* and *B* are pure components (ideal gas Z=1) then the ratio of the component densities can be reduced to

$$\frac{\rho_A}{\rho_B} = \frac{w_A}{w_B} \qquad 3.19$$

Taking this into consideration, the $(w_A\rho_B - \rho_A w_B)$ term in the denominator of Equation 3.13 will be zero so the equation becomes

$$\rho = \left[1 + y_A\left(\frac{w_A - w_B}{w_B}\right)\right]\rho_B \qquad 3.20$$

If the mole fraction of A is zero (i.e. there is only B), $y_A = 0$ then $\rho = \rho_B$ as expected and when $y_A = 1$, $\rho = \rho_A\frac{w_B}{w_A}$. From Equation 3.19, this equals ρ_A as expected.

When evaluating changes in density of a mixture with respect to the total pressure P and components mole fraction and molecular weight, Equations 3.18 and 3.20 can be combined to give;

$$\rho = \left[1 + y_A\left(\frac{w_A - w_B}{w_B}\right)\right]\frac{P}{RT}\frac{1}{Z_B}\, w_B \qquad 3.21$$

or

$$\rho = \left[w_B + y_A(w_A - w_B)\right]\frac{P}{RT}\frac{1}{Z_B} \qquad 3.22$$

This shows that the density of the gas mixture, ρ, depends on the mole fraction (y_A), the pressure (P) and the temperature (T). The molecular weights, compressibility factor and the universal gas constant are all constant.

Therefore, if a change in density of the gas mixture is caused by a change in mole fraction, Δy_A, then the equation can be written as;

$$\Delta\rho_1 = \Delta y_A(w_A - w_B)\frac{P}{RT}\frac{1}{Z_B} \tag{3.23}$$

If a change in density is caused by a change in pressure,ΔP, then the equation becomes

$$\Delta\rho_2 = [w_B + y_A(w_A - w_B)]\frac{\Delta P}{RT}\frac{1}{Z_B} \tag{3.24}$$

If a change in density is caused by a change in temperature,ΔT, then the equation becomes

$$\Delta\rho_3 = [w_B + y_A(w_A - w_B)]\frac{P}{RT}\frac{1}{Z_B}\left(\frac{-\Delta T}{T}\right) \tag{3.25}$$

3.3.Hold-Up Theory

The gas hold-up, *H*, in a system is the amount of gas held within the system.

From the previous section, it is known that the perfect gas equation is

$$PV = nRT \tag{3.26}$$

Incorporating the hold-up into the perfect gas equation ($H = n$) and rearranging gives

$$H = \frac{PV}{RT} \tag{3.27}$$

Consider a system with an input, a volume and an output as shown in Figure 3.1. A gas flow enters the system and flows into the volume, V, at a flowrate M_1 and leaves the volume at a flowrate of M_2. Any gas held within the steady state system is the hold-up, H.

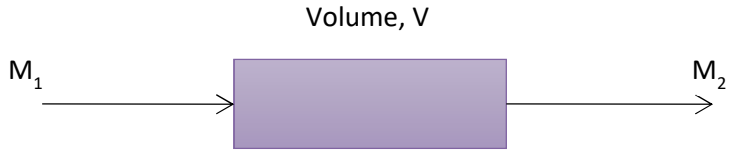

Figure 3.1 - Flow diagram of mass entering, M_1, and leaving, M_2, and a control volume, V.

If either the flow in (M_1) or the flow out (M_2) of the system changes, the hold-up in the system will change. Any change in hold-up is represented by a balance equation;

$$\frac{dH}{dt} = (M_1 - M_2) \tag{3.28}$$

For a constant volume, according to the ideal gas law, the hold-up can alter due to changes in temperature or pressure. When the temperature is constant, the equation for hold-up change with changes in pressure is given by

$$dH = \frac{V}{RT} dP \tag{3.29}$$

For the purposes of the experiments which were carried out for this thesis, the flow into the volume was held at a constant rate. The outlet flow from the volume was changed. When a change is made to the system, a new steady state is achieved. The net change in hold-up from the initial state, M_1, to the final state, M_2, can be found by integrating Equation 3.28 resulting;

$$\Delta H = \int_0^\infty \big(M_1 - M_2(t)\big)\, dt \tag{3.30}$$

The infinity limit refers to the time when the new steady state is reached.

Again, assuming ideal gas behaviour, the total change in hold-up is given by

$$\Delta H = \frac{V}{RT}\left(P_1(\infty) - P_1(0)\right) \qquad 3.31$$

This equation will be used throughout this work when interpreting results.

3.4. Bernoulli's Principle

Bernoulli's principle is important in fluid mechanics [49, 50]. It can be applied to various types of fluid flow. In its simplest form, Bernoulli's principle applies to incompressible flows and to compressible flows that flow at low Mach numbers (gases). It can be derived from the principle of conservation of energy where the total amount of energy in a system remains constant.

Consider a basic system, where a fluid is flowing through a pipe in steady state as shown in Figure 3.2.

Figure 3.2 - Streamline of fluid

where P_1 and P_2 are the pressures at points 1 and 2 on the streamline
v_1 and v_2 are the velocities of the fluid at points 1 and 2
h_1 and h_2 are the static heads at points 1 and 2

According to the energy of conservation principle in this system,

$$Work\ done + Potential\ Energy = Kinetic\ Energy \qquad 3.32$$

Therefore, from the entry point 1 to the exit point 2, the energy equation can be written as;

$$(P_1 - P_2)V + \rho g V(h_1 - h_2) = \frac{\rho V}{2}({v_1}^2 - {v_2}^2) \qquad 3.33$$

where P_1 and P_2 are the pressures at points 1 and 2 on the streamline

V is the volume between these two points

ρ is the density of the fluid flowing through the volume

g is the gravitational acceleration

h_1 and h_2 are the static heads at points 1 and 2

v_1 and v_2 are the velocities of the fluid at points 1 and 2.

Equation 3.33 can be rearranged to

$$\frac{P_1}{\rho g} + \frac{{v_1}^2}{2g} + h_1 = \frac{P_2}{\rho g} + \frac{{v_2}^2}{2g} + h_2 \qquad 3.34$$

This equation applies when points 1 and 2 lie on a streamline, the fluid has a constant density, the flow is steady and there is no friction.

From this, the simplest form of Bernoulli's equation is derived. It states that

$$P + \frac{1}{2}\rho v^2 + \rho g h = constant \qquad 3.35$$

where P represents the static pressure

$\frac{1}{2}\rho v^2$ is the dynamic pressure

$\rho g h$ is the potential energy.

The equation relates the pressure at a point in the system to the fluid velocity and position. From this it can be seen that increasing the fluid velocity, decreases the system pressure or decreases the potential energy in the system.

All the theories discussed in this section will be used in the derivations of experimental work investigated in the next three chapters of this thesis.

4. Volume Determination by Flow-Rate Measurements

4.1. Introduction

This section focuses on the feasibility of using gas flow to measure volume. This work presents a very different approach to measurement of volumes. This is carried out by changing the flow resistance and therefore the pressure of the gas in a system. The experimental arrangement is simple, cheap and robust and can detect very small changes in volume. The method is distinctive in that it involves an increase in system pressure followed by a decrease in pressure. This provides a check on the final result.

As previously discussed in Section 2.4, previous work has been carried out using a microplant by Mason *et al*. (1998) [38], Mason *et al.* (2000) [40] and Russell *et al.* (2005) [42]. This work uses similar concepts in that the experiments involve a change being made to a system which includes two resistances in series but it differs in several ways. Firstly, the inlet is maintained at a constant flow rate throughout the experiments. The step-change is made by changing the resistance as opposed to adding a perturbation flow. Secondly, the system is single sided. A pneumatic Wheatstone bridge arrangement of resistances is used to obtain results using a differential pressure transducer. Thirdly, the procedure can be used as a means to measure volume. Finally, the arrangement can be used to compare the dynamics of the simplest system.

4.2. Background

The measurement of volume is important in many industrial, scientific and domestic situations. For a regular shape such as a rectangular box, cylinder or sphere, the dimensions can be measured and from the appropriate equations, the volume can be determined subject to the standard errors. This approach is not possible if the shape is deformed, or if the total volume includes many small chambers. In this case, the conventional approach of Archimedes principle has been to submerge the object in a known volume of water and assess the internal volume from the change in weight. However, there are two possible problems with this

approach: the water may not be able to reach into all the volume where the dimensions are small and contact with water may prove to be irreversible or destructive to the material: for example, porous materials.

The measurement of volume can be divided into two categories: internal (for example, the volume of a chamber) and external (the volume of a solid object).

One healthcare application of internal volume is in the determination of the body mass index (BMI). This is used to measure of the density of a person: the reason being that fat has a lower density than the rest of the body. The approximate approach is to measure the person's weight in kilograms and divide by their height squared (m^2). This is because there is an approximate correlation between the volume of a person and the height squared. For some people, it is quite clear if they are overweight or underweight, but for a significant proportion the situation is a grey area. The conventional way is to measure the weight of the person when under water, and then to use Archimedes principle to determine the volume of water displaced. There are several limitations to this technique. The equipment is bulky and requires intense maintenance and a large tank of water must be maintained at constant temperature: this is because the density of water varies with temperature. The total test procedure may take one hour. Other potential problems are: fear of immersion, possibility of infection, and a lack of dignity.

There are many applications and techniques listed in the literature for the measurement of volume. For example, Segnini *et al.* (2004) [51] proposed that the volume of potato chips could be determined by measuring the displaced volume of a fine granular material. The reason for this investigation was to determine the volume change after the various stages of cooking. Continuing with the culinary theme, Drazeta *et al.* (2004) [52] used a standard gravimetric technique based on Archimedes principle to determine the volume fraction of air present in a Braeburn apple. The purpose of this study was to assess the degradation problems of apples in storage and transport over long distances. Finally, Frattolillo (2006) [53] proposed an airtight variable volume to measure the volume of complex manifolds. The variable volume is initially filled with a suitable test gas at a known pressure. A valve is opened and the test gas is allowed to expand into the previously evacuated unknown volume. A feedback control loop reacts to the resulting finite pressure drop, thus contracting the variable volume until the pressure exactly retrieves its initial value. The overall reduction of the variable volume achieved at the end of the process gives a direct measurement of the unknown volume.

There are several reasons why this alternative method for the measurement of volume is of interest. First, this is a robust and cheap method, capable of detecting very small changes in volume. Second, the method is distinctive in that it involves an increase in system (volume) pressure followed by a reduction in pressure. This provides a check on the final result. Third, this method involves the continuous flow of gas into the volume. This should make it applicable to situations in which the unknown volume might change with time.

4.3. Theory

This section aims to investigate whether basic principles, including material balances and flow measurements, can be used in the determination of volume.

For a system with a single component – in this case we term air as the single component because there is no change in composition – we write the material balance as:

$$Input = Accumulation + Output \qquad 4.1$$

Figure 4.1 shows the simple arrangement of a volume and then two resistances in series which is used to establish a relationship between the change in pressure and the change in resistance in the system.

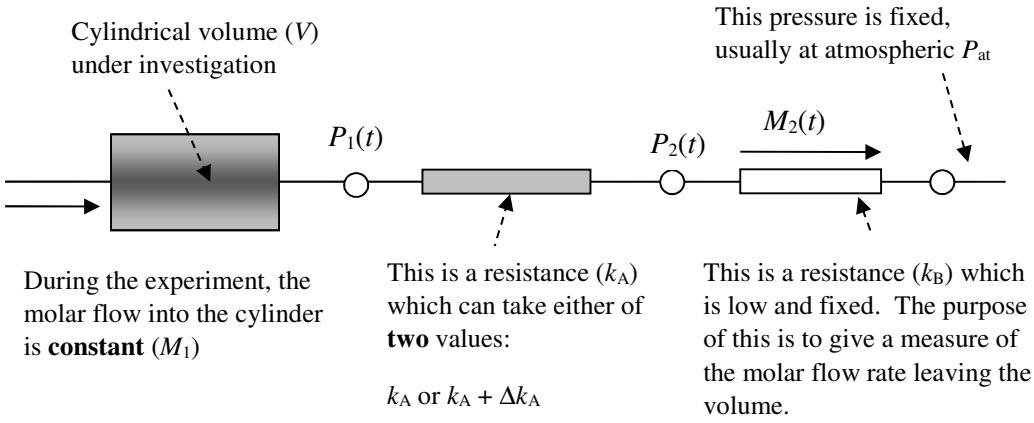

Figure 4.1 - Sketch representing the material balance

The main assumption here is that during the course of an experiment, the molar flow rate into the volume remains constant: this is termed M_1. The flow leaving the cylinder then passes into

two resistances in series: one is variable (of resistance k_A) and the other is fixed (of resistance k_B). Let us assume that we have some method of measuring the pressures upstream and downstream of this variable resistance (k_A): these are termed $P_1(t)$ and $P_2(t)$. The molar flow rate leaving the volume will be the same as that flowing through the two resistances: this is termed M_2(t). This molar flow will vary with time during the experiment.

The system is initially at steady-state. The flow rate into the system (M_1) is equal to the flow rate out of the system, which is $M_2(0)$. At time zero, we make a change to the value of the variable resistance (k_A). This is achieved by a sudden step-change in resistance, for example by Δk_A. This will cause an abrupt drop in the molar flow rate leaving the column – that is the value of $M_2(t)$ – which will eventually return to the original value at the new steady-state. In the new steady-state, the hold-up (H) in the volume will have increased, but the molar flow rate into and out of the volume will be the same. This gives rise to an important experimental requirement: that we have a device that will deliver a constant mass flow into the volume.

We first of all consider a material balance for a small time interval, dt, over which the hold-up in the volume changes by dH:

$$(M_1 - M_2)\, dt = dH \qquad 4.2$$

This means that the total change in holdup (ΔH) is obtained by integration

$$\Delta H = \int_0^\infty \big(M_1 - M_2(t)\big) dt \qquad 4.3$$

The limit of infinity in Equation 4.3 is to show that the integration should be carried out over the time it takes the apparatus to reach the new steady-state.

We now consider how we might measure the variable molar flow rate $M_2(t)$ in more detail. We can use the Hagen-Poiseuille equation as defined in Chapter 3.1. For the initial and time-varying situations, the equations are:

$$P_2^2(0) - P_{at}^2 = 2k_B RT\mu M_2(0) \qquad 4.4$$

$$P_2^2(t) - P_{at}^2 = 2k_B RT\mu M_2(t) \qquad 4.5$$

These can be substituted into Equation 4.3 and accounting that $M_1 = M_2(0)$ then:

$$\Delta H = \frac{1}{2k_B \mu RT} \int_0^\infty (P_2^2(0) - P_2^2(t)) dt \qquad 4.6$$

At this stage, it is helpful to define a perturbation variable (y) as the difference between the baseline value and the value at any time t, and so this gives:

$$y = P_2(0) - P_2(t) \qquad 4.7$$

Substitution of this variable for $P_2(t)$ allows Equation 4.6 to be written as:

$$\Delta H = \frac{1}{2k_B \mu RT} \int_0^\infty y\,(2P_2(0) + y)\,dt \qquad 4.8$$

This can be written in a more convenient form:

$$\Delta H = \frac{1}{2k_B \mu RT} \left[2P_2(0) \int_0^\infty y\,dt - \int_0^\infty y^2\,dt \right] \qquad 4.9$$

In terms of the response of the system to the perturbation, the first integral is the peak area, and the second can be determined by squaring the peak area deviations. For the sake of convenience, we assume that the second integral will be insignificant compared with the value of the first integral.

We now consider the two experiments in which the value of P_1 is first increased and then decreased back to the original value. The sum of the values of ΔH for the two experiments will be zero.

If we assume perfect gas behaviour, which is appropriate for nitrogen gas at ambient temperature and pressure, then we can also write the change in hold-up in the system volume as:

$$\Delta H = \frac{V}{RT} (P_1(\infty) - P_1(0)) \qquad 4.10$$

We now return to the situation of laminar flow through both resistances. The before and after perturbation can be written as:

$$P_1^2(0) - P_{at}^2 = 2(k_A + k_B)RT\mu M_1 \quad 4.11$$

$$P_1^2(\infty) - P_{at}^2 = 2(k_A + \Delta k_A + k_B)RT\mu M_1 \quad 4.12$$

Equations 4.11 and 4.12 can be subtracted to give a more convenient equation:

$$P_1^2(\infty) - P_1^2(0) = 2\Delta k_A\, RT\mu M_1 \quad 4.13$$

Like before, it is helpful to define a perturbation variable (x) as the difference between the initial and final value of the system (volume) pressure:

$$x = P_1(\infty) - P_1(0) \quad 4.14$$

This substitution allows us to write:

$$x[2P_1(0) + x] = 2\Delta k_A\, RT\mu M_1 \quad 4.15$$

As expected, for a particular value of initial system pressure (P_1) and inlet molar flow rate (M_1), the change in system pressure is roughly proportional to the change in resistance (Δk_A).

4.4. Experimental arrangement and procedure

The experimental set-up used in this work consists of a test volume connected to a 6-port valve. This allows the gas to flow through either a lower resistance (k_A) or a higher resistance ($k_A + \Delta k_A$). The outlet pressure from the 6-port valve, $P_2(t)$, is monitored using a differential pressure transducer (DPT) before flowing into another fixed resistance, k_B.

Figure 4.2 gives a representation of the actual experimental arrangement. The value of V for the cylindrical test volume was approximately 2 litres. The constant flow of nitrogen was achieved using a *Porter* VC1000 mass flow controller. The flow leaving the test volume can take one of two different routes depending on the position of the *Valco* 6-port chromatographic valve. The working of the 6-port valve is such that adjacent sets of ports are connected. For

one route, the connecting tube is a 20 cm length of nylon tubing with internal diameter of 1 mm. For the other route, the connecting tube is a choice of lengths of stainless-steel tubing with a bore of 0.5 mm. The pressure $P_2(t)$ is monitored using a Furness Controls Differential Pressure Transducer with an output of ±1000 mV corresponding to an input of ± 100 Pa and this is recorded using *Pico* 16-bit resolution software. The software was programmed to record the differential pressure readings every 200 milliseconds. The graphs of the readings were plotted using *Microsoft* Excel.

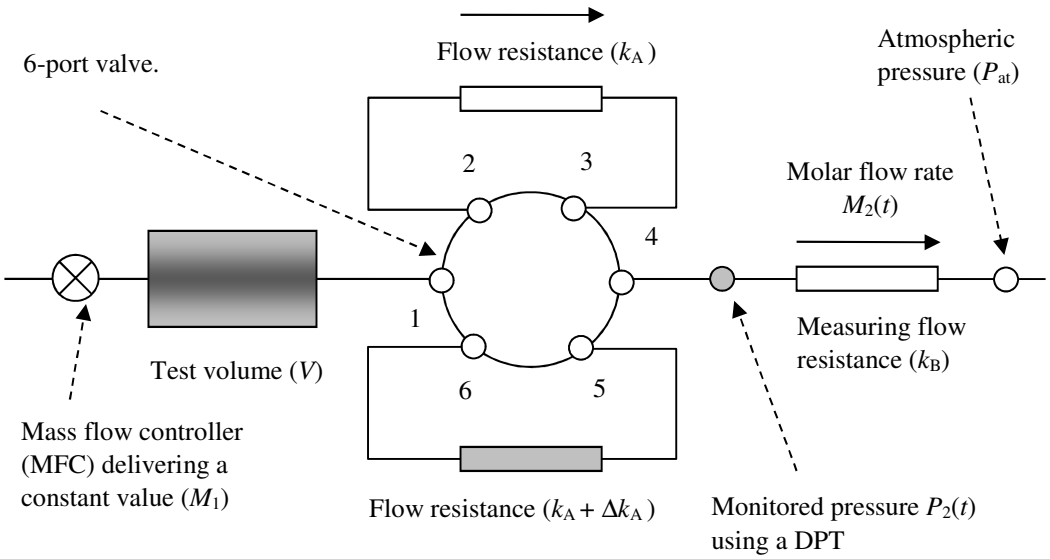

Figure 4.2 - Schematic representation of experimental arrangement

In Figure 4.2, the flow is shown directed through the upper path, which is the lower value (k_A) of resistance. This is because the ports connected are 1 to 2, 3 to 4 and 5 to 6. This is considered as the zero time condition. This is a steady-state because the monitored pressure $P_2(t)$ remains constant with time.

An experiment is conducted by switching the valve and connecting ports 1 to 6, 5 to 4 and 3 to 2, directing the outlet flow from the test volume through the flow resistance with the additional (Δk_A) term. Switching the valve will provide an (almost immediate) step-change in resistance.

One problem with this approach compared to the material balance theory is that there will be a mid-valve position at which the flow is cut off: this is the nature of switching valves. The

increase in resistance will cause a reduction in pressure $P_2(t)$, but eventually the final baseline $P_2(\infty)$ should be exactly the same as the initial baseline $P_2(0)$. Any difference would indicate the likelihood of a leak in one of the paths.

Note that the path not being used is considered a stagnant zone, and as such there may be diffusion of nitrogen out, and air in causing a change in composition of gas. This can be alleviated by first switching the valve a number of times before the experiments are recorded.

Four separate experiments were carried out; a baseline determination followed by using varying the tubing length, short, medium and long, to change the resistance. For the first experiment, the baseline value of $P_2(t)$ was simply recorded for 600 seconds, with no change in the valve position. This was to determine the magnitude of any drifting in the baseline. This is an important parameter, because if the drifting is excessive then this will affect the viability of the method and will require an improved or modified experimental arrangement. For the second experiment, a short length (about 5 cm) of stainless-steel tubing was used to give the value of Δk_A. For the third experiment, the length of tubing was increased to 10 cm, and for the fourth experiment the length was increased further to 20 cm. Each experiment consisted of two parts: switching the valve one way and then the other.

4.4.1. Actual arrangement used to measure flow rate leaving volume

In the previous section, the apparatus for flow rate measurement has been represented as a device to measure the pressure drop across a flow resistance of value k_B. However, in this work a flow version of an electrical Wheatstone bridge assembly was used.

A conventional electrical Wheatstone bridge is used to measure an unknown electrical resistance by balancing two legs in a bridge circuit where one leg contains the unknown resistance. An example of an electrical Wheatstone bridge can be seen in Figure 4.3(a). Previous work has been completed using a pneumatic Wheatstone bridge arrangement where gas molecules represent electrons and flow capillaries represent resistors [54]. Figure 4.3(b) shows the assembly used by Palmer *et al.* (2011) [54] where one leg of the bridge is referred to as the system side while the other leg is referred to as the reference side. The flow setting

and flow sensing capillaries cause a fixed pressure difference between each side of the Wheatstone bridge. This results in a constant flow rate through the assembly. When the flow rates are the same both sides of the bridge, an initial pressure difference is detected by the DPT. A perturbation flow is added to the system side which causes an imbalance in the bridge assembly. The imbalance between the system and reference sides in the system is measured as a voltage difference using a differential pressure transducer (DPT).

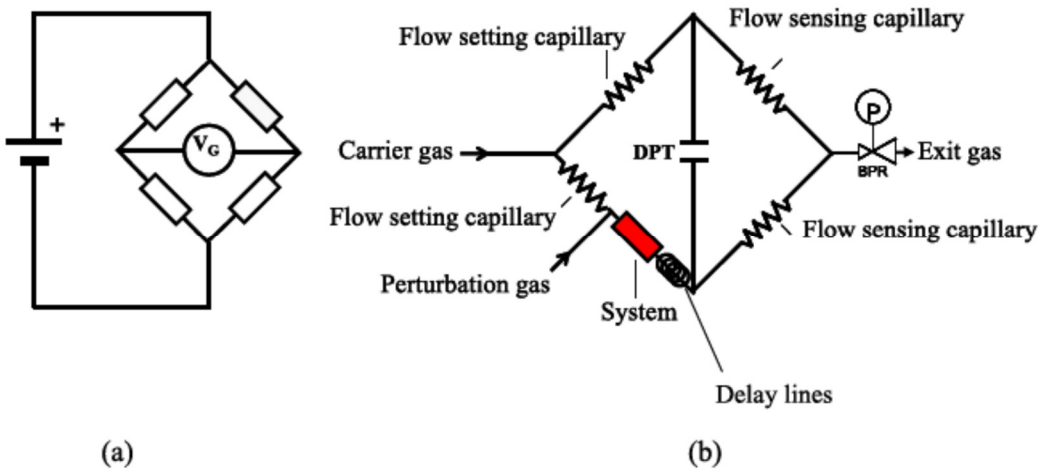

Figure 4.3 - Schematic representations of (a) a conventional electrical Wheatstone bridge and (b) a pneumatic Wheatstone bridge assembly for flow measurements (Fig 1 from [54])

In this work, a pneumatic Wheatstone bridge with a different arrangement of resistances is introduced. The arrangement is shown in Figure 4.4. This was used as opposed to the simplified arrangement shown in the corner of the figure.

As in the previously discussed assembly, the DPT is located across the bridge, measuring the pressure difference between the pressures $P_3(t)$ and $P_4(t)$. Unlike the previous pneumatic bridge, the first resistance in each side is different. The total resistance in each of the upper and lower branches are equal. This means that the values of $M_3(t)$ and $M_4(t)$ are equal. In these experiments, it is necessary to have the resistances set up in this way so that the DPT signal changes with flow rate.

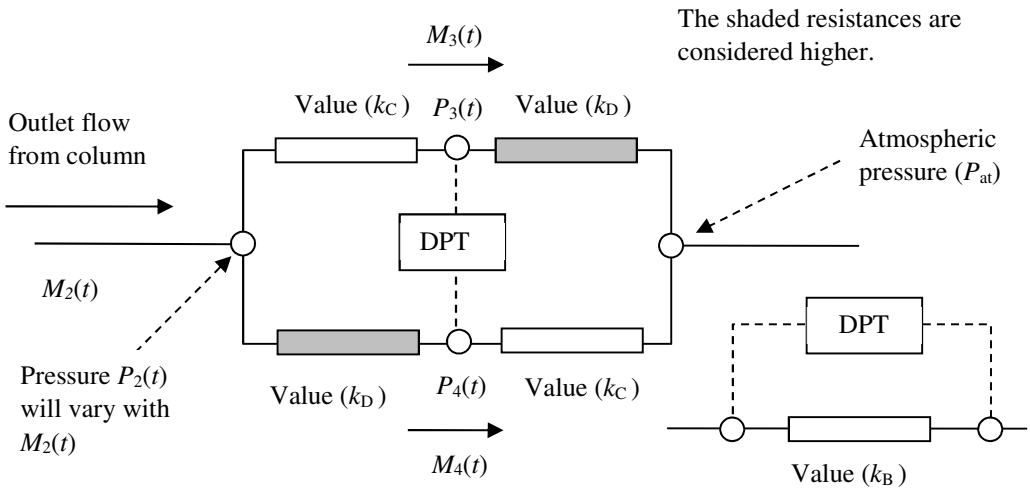

Figure 4.4 - Schematic representation of a Wheatstone bridge for flow measurements

One advantage of the Wheatstone bridge over the conventional arrangement is that it is insulated from any variations in local pressure, and so should be relatively free from noise. Another advantage is that this arrangement gives larger peak areas. There are more possible arrangements with the Wheatstone bridge. For example, one could select resistances such that the total resistance in the top branch is much greater than the total resistance in the lower branch. This would mean that the molar flow rate in the lower branch being much greater than that in the upper branch.

From a consideration of the resistances and flows in each branch we can write:

$$P_3^2(t) - P_4^2(t) = (k_D - k_C)M_2\,\mu RT \qquad 4.16$$

Obviously, the sensitivity will depend on the difference between the two flow resistances. For the purposes of this investigation, the larger resistance (k_C) is a 20-cm length of nylon tubing with a diameter of 1.5 mm and the smaller resistance (k_D) is a 10-cm length of nylon tubing.

4.4.2. Volume Determination using Experimental Arrangement

The determination of volume using the experimental arrangement involves various steps. Firstly, the relationship between the flow rate and the differential pressure transducer (DPT)

readings must be found. This was done by taking mean DPT values at two different flow rates. These were plotted on an Excel graph, then using the trend line function, a linear equation of the relationship and so the line gradient could be found.

Secondly, the areas under the pressure change graphs were found. The baseline was calculated by taking an average of the DPT readings before any change was made so that,

$$DPT_B = \frac{\sum DPT_{0 \to t}}{Number\ of\ samples} \tag{4.17}$$

The area under the graph was then calculated using the trapezoidal rule. The difference between the baseline and each of the DPT readings were calculated using

$$\Delta DPT_t = DPT_t - DPT_B \tag{4.18}$$

where DPT_t is the DPT reading at any time, t and DPT_B is that of the baseline.

The trapezoidal rule to determine the area under the pressure graph was

$$A_p = \left(\frac{\Delta DPT_1 + \Delta DPT_2}{2}\right) \times \Delta t \tag{4.19}$$

The total graph area was then found by

$$A_T = \sum A_p \tag{4.20}$$

Thirdly, an equation for the calculation of volume was determined. This was based on the ideal gas equation

$$\Delta n = \frac{\Delta PV}{RT} \tag{4.21}$$

This can be expressed in terms of flow rate, Q, and change in time, dt, as

$$\Delta n = \frac{P}{RT} \int Q \, \mathrm{d}t \tag{4.22}$$

It is known that

$$\int Q \, \mathrm{d}t = A_T \frac{g}{60} \tag{4.23}$$

where $\frac{g}{60}$ is the line gradient in units ml/s.mV

Substituting 4.22 into 4.21 and equating 4.20 and 4.21 gives

$$V = \frac{P}{\Delta P} A_T \frac{g}{60} \tag{4.24}$$

The pressure change across the stainless steel tubing, ΔP, can be measured using a digital manometer.

4.5.Results

This section will present and interpret the results of the experiments described in Section 4.4 including the baseline determination and experiments using different resistances.

4.5.1. First Experiment – Baseline Test

An important part of the investigation is to ensure that the baseline has a good quality, with limited noise and drift. The baseline is described as drifting if it changes over a period of time. If the baseline increases or decreases with time it is described as drifting. This can be due to a leak in the system, changes in the flow entering the system or environmental changes around the system i.e. temperature or pressure changes. If the baseline has any of these parameters, it may affect the accuracy with which we can determine areas.

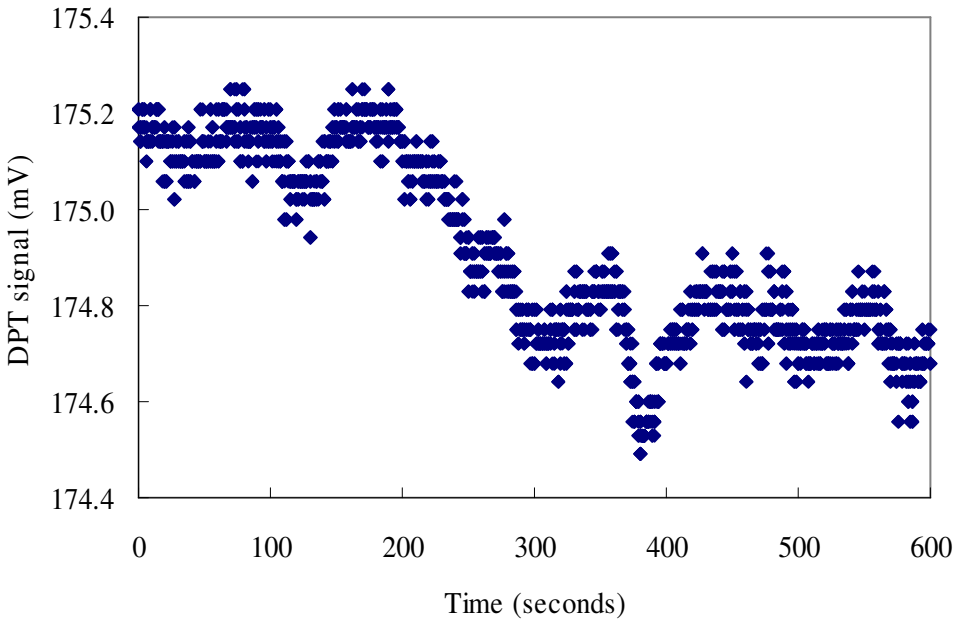

Figure 4.5 - Baseline signal of DPT with the 6-port valve position unchanged

Figure 4.5 shows the baseline for a period of 10 minutes with readings taken from the differential pressure transducer every 100 milliseconds. We can see that the baseline is within a 0.2 mV band for the first 200 seconds. Within this time, there is an oscillation with a period of about 50 seconds. There is then a drift by about 0.4 mV followed by another constant value within a band of 0.2 mV. To put some perspective on these figures, a baseline change of about 1 mV corresponds to a pressure change of about 0.1 Pa so is consistent.

4.5.2. Second Experiment – 5cm length of Tubing

Figure 4.6 shows the results obtained for the second experiment, switching the 6-port valve one way (at t = 30 seconds), allowing a new steady-state to be achieved, and then switching it back the other way (at t = 150 seconds). The main flow flowing through the system was 90 mL/min. The frequency of sampling was every 200 milliseconds for 300 seconds. The first peak corresponds to the increase in resistance/pressure and the second peak corresponds to the reduction in the resistance/pressure. It can be seen that there is a distinct difference in shape between the two peaks. In each case there is a sharp step followed by a slow decay. The step is sharper for (i) the pressure increasing and the decay is longer for (ii) the pressure decreasing. A cursory look would suggest that the areas are in fact of a similar magnitude.

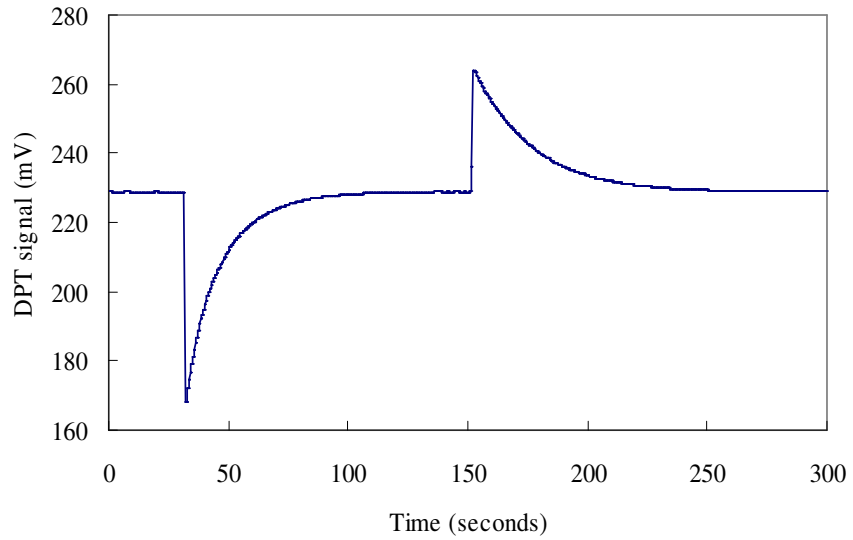

Figure 4.6 - DPT signal for the second experiment.

Figure 4.7 shows a magnification of the baseline and shows that there may be a small problem for the second part of the experiment: the baseline does not return to the original value. The initial value of $P_2(0)$ is around 228.8 mV, but by the end of the experiment this is close to 229.0 mV. This may be because the experiment was not run for long enough – for the next two investigations, the experimental time is doubled to 600 seconds.

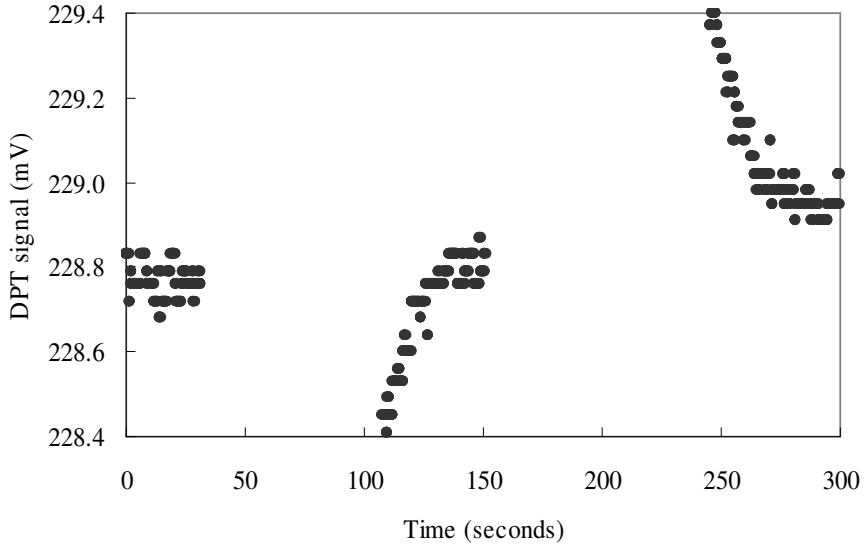

Figure 4.7 - Magnified baseline signal for the second experiment

4.5.3. Third Experiment – 10cm Length of Tubing

Figures 4.8 and 4.9 show the corresponding results for the third experiment. For this, the length of stainless-steel tubing corresponding to the increase of resistance (Δk_A) is increased to 10 cm. Samples were taken every 200 milliseconds for 800 seconds. The first change was made at t = 90 seconds and the signal was allowed to settle back to the baseline before the second change was made. Figure 4.8 shows similarities to the second experiment. There is a distinct difference between the increasing-pressure and decreasing-pressure stages of the experiment. Comparing Figure 4.8 to Figure 4.6, it can be seen that both the spikes and the peak areas are increased. As expected, the increase in resistance (Δk_A) caused a greater increase in hold-up.

Comparing Figure 4.9 to Figure 4.7, it can be seen that the baseline can return to the original value when the valve is switched for the second time, although there may be a slight amount of drifting. The initial value of $P_2(0)$ is around 282.9 mV, but by the end of the experiment this is close to 283.0 mV.

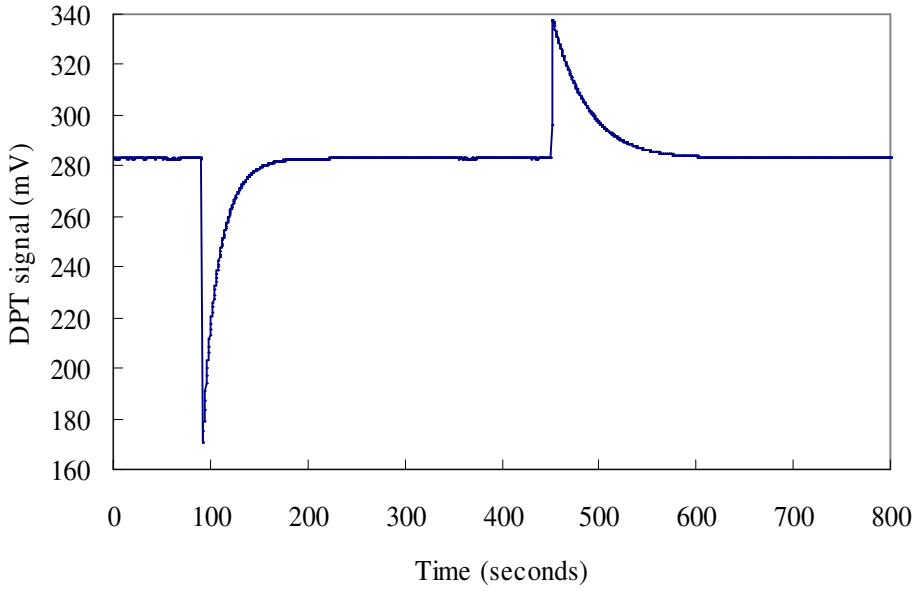

Figure 4.8 - DPT signal for the third experiment

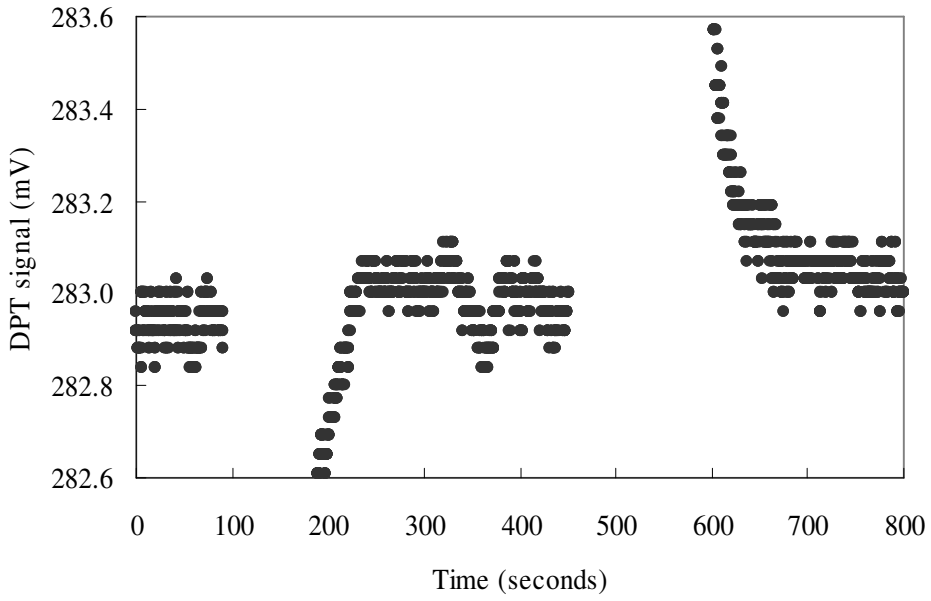

Figure 4.9 - Magnified baseline signal for the third experiment

4.5.4. Fourth Experiment – 20cm Length of Tubing

Finally, Figures 4.10 and 4.11 show the corresponding results for the fourth experiment. For this, the length of stainless-steel tubing corresponding to the increase of resistance (Δk_A) is increased to 20 cm. DPT readings were taken every 200 milliseconds for 600 seconds. The first change was made at t = 30 seconds and the signal was allowed to settle back to the baseline before the second change was made at t = 200 seconds. Comparing Figure 4.10 to Figure 4.8, both the spikes and the peak areas have increased, the peak shapes are different, and the hold-up has increased with the further increase in resistance.

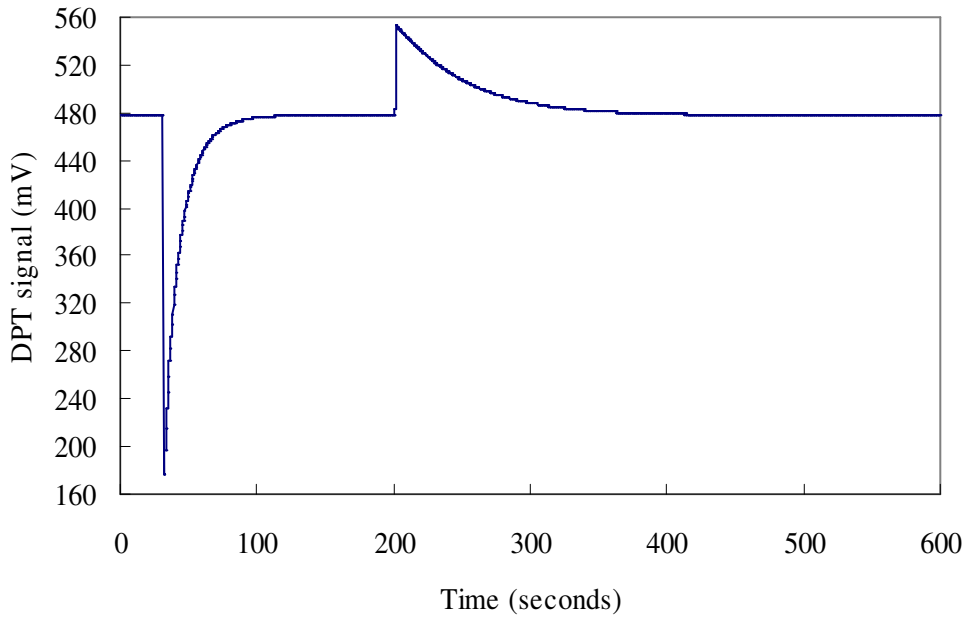

Figure 4.10 - DPT signal for the fourth experiment

Comparing Figure 4.11 to Figure 4.9, it can be seen that with the longer experiment time, the baseline can return to the original value when the valve is switched for the second time. The initial value of $P_2(0)$ is around 477.9 mV, but by the end of the experiment this is close to 478.0 mV. Therefore, there is a minimal amount of drifting and the baseline can be considered consistent.

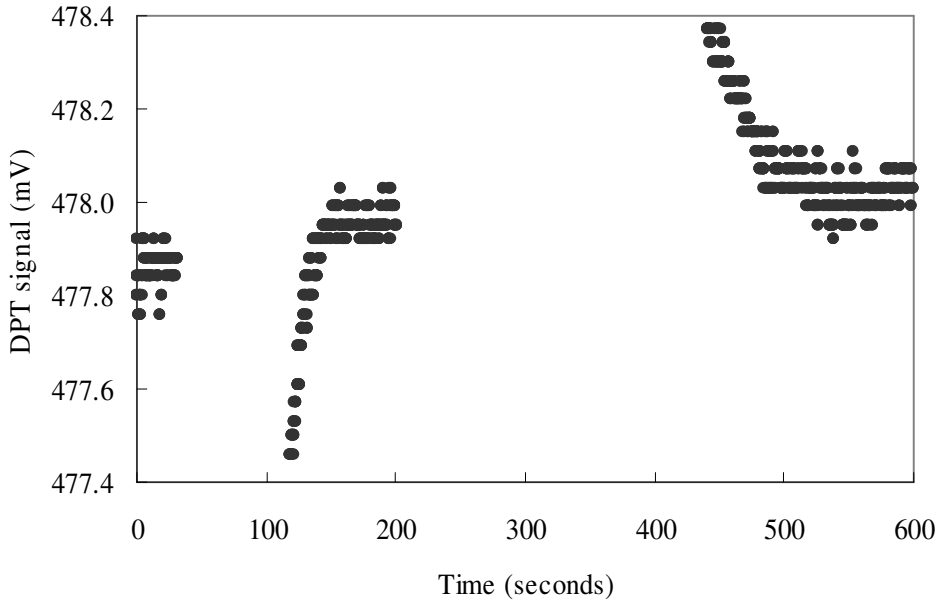

Figure 4.11 - Magnified baseline signal for the fourth experiment

4.6.Discussion

4.6.1. The baseline test for first experiment

An important part of the investigation is to ensure that the baseline has a good quality, with limited noise and drift. If the baseline has any of these parameters, it may affect the accuracy with which we can determine areas. Figure 4.5 shows the baseline for a period of 600 seconds. We can see that the baseline is within a 0.2 mV band for the first 200 seconds. Within this time, there is an oscillation with a period of about 50 seconds. Then the baseline drifts by decreasing slowly by about 0.4 mV followed by another constant value within a band of 0.2 mV. To put some perspective on these figures, a baseline change of about 1 mV corresponds to a pressure change of about 0.1 Pa. The baseline pressure varies by less than 0.1 Pa over the 600 second period.

4.6.2.Importance of selecting the correct baseline to determine peak areas

From Equation 4.8 in the theory section, the volume of the system (which we are trying to measure) depends on the difference of two integrals. To calculate these integrals numerically, it is necessary to select the correct baseline value of P_2. To this end, it is instructive to carry out a sensitivity analysis to see how the calculated peak area depends on the selected value of baseline. For this investigation, we focus on experiment 3, which is shown in Figures 4.8 and 4.9. The results of making slight adjustments in the baseline are shown in Table 4.1. Peak type A refers to an increase in system pressure, and peak type B refers to a reduction in system pressure.

Table 4.1 - Variation of peak area with selected baselines for experiment 3

Peak type	Baseline $P_2(0)$	Peak area (mVs)	Peak type	Baseline $P_2(0)$	Peak area (mVs)
A	283.00	1944	B	283.00	– 1952
A	282.98	1940	B	283.02	– 1942
A	282.96	1935	B	283.04	– 1935
A	282.94	1931	B	283.06	– 1927
A	282.92	1927	B	283.08	– 1923
A	282.90	1922	B	283.10	– 1918

There are two factors which determine the confidence limits which we can assign to a measurement of peak area. The first is the short-term noise in the signal and the second is the baseline drift over the peak time. Obviously, the latter will be more of a problem for large peak times since there is more time for the baseline to shift, and this drifting may not necessarily be linear with time. Consider the first factor for Figure 4.9. It is reasonable to assume that the true value of $P_2(0)$ lies somewhere between 282.9 and 283.0 mV. We can tell that the resolution of the data acquisition system is 0.04 mV. Each change in baseline by 0.02 mV changes the peak area (type A) by 0.2%. The effect is greater for peak type B: each change in baseline by 0.02 mV changes the area by 0.5%. This is because for the pressure-reduction experiment, the experimental time and peak base is longer. Our best guess for the area of the pressure-increase experiment (type A) is 1922 mVs and for the pressure-reduction experiment (type B) is – 1935 mVs.

4.6.3. Comparison of peak areas for each experiment

There are several ways in which this data can be discussed. The first stage is to return to Equation 4.8 where area A_1 refers to the peak area and area A_2 refers to a function of the square of the peak height. According to Equation 4.8, the values of ΔH for the pressure-increase and pressure-reduction experiments must have the same magnitude. The values of y for the pressure-increase and pressure-reduction experiments are positive and negative respectively. The value of y^2 is always positive for each case. This means that the peak areas will not be exactly the same, therefore the peak area for the pressure-increase part should be slightly

greater, but whether this difference can be detected will depend on the magnitude of A_2 (see Table 4.2).

Table 4.2 - Complete Information for each peak for each experiment

Expt	Pressure-increasing step			Pressure-reducing step		
	Peak height (mV)	Area A_1 (mVs)	Area A_2 $(mV)^2$ s	Peak height (mV)	Area A_1 (mVs)	Area A_2 $(mV)^2$ s
2	– 60	893	2.6×10^4	35	(– 853)	1.5×10^4
3	– 113	1922	1.1×10^5	53	– 1935	5.5×10^4
4	– 300	3771	5.5×10^5	73	– 3769	1.5×10^5

We need to check the relative sizes of the two terms to see whether the second integral is significant, or can be ignored: note that the peak area (A_1) is multiplied by a factor of two times the value of $P_2(0)$. If we assume this to be about 1000 mbar, then according to the DPT calibration this is equivalent to 10^6 mV. For experiment 2, the importance of the second integral is obtained from:

$$\frac{A_2(mV^2s)}{A_1(mVs) \times 10^6(mV)} = \frac{2.6 \times 10^4}{893 \times 10^6} = 3 \times 10^{-5} \qquad 4.25$$

and for experiment 4, the importance of the second integral is obtained from

$$\frac{A_2(mV^2s)}{A_1(mVs) \times 10^6(mV)} = \frac{5.5 \times 10^5}{3771 \times 10^6} = 1.5 \times 10^{-4} \qquad 4.26$$

At the most significant level, we would be looking for a difference in area of less than 1 mVs. This would suggest that from now on it is safe to ignore the second integral and just work in terms of the area of the peak.

We can see that going from experiment 2 to 3, the area increases by a factor of 2.1. This is in accordance with the fact that the approximate lengths of tubing are 5 cm and 10 cm.

Furthermore, going from experiment 3 to experiment 4, the area increases by a factor of 2.0; once again, this is in accordance with the approximate lengths of tubing of 10 cm and 20 cm. As the length of stainless-steel tubing is increased, this increases the value of Δk_A which increases the holdup (ΔH) and increases the peak area.

Obviously, the importance of selecting the correct value of baseline signal becomes less significant as the peak area and height are increased. For experiment 3, the area magnitudes are within 0.5% and for experiment 4 the area magnitudes are within 0.1%.

4.6.4. Implications for experimental arrangement

The advantage of the "system perturbation" approach to the measurement of changes in volume and hold-up is that the system pressure can be increased and then decreased back to the original value. This provides a check on the results because the hold-up changes should have equal and opposite values. There is an obvious problem for experiment 2, since the peak areas are 893 and –853 mVs. However, close inspection of Figure 4.6 shows that the baseline did not have enough time to return to the original value. For experiments 3 and 4 the experiment time was increased to allow time for the baseline to settle and return to the original value.

There are obvious experimental implications for very accurate work. At present, the equipment is simply located on the bench-top and is subject to fluctuations in ambient temperature and pressure. Another limiting factor might be the choice of mass flow controller (MFC). This is supposed to deliver a constant mass flow rate regardless of changes in downstream pressure, and the fact that the baseline remains constant after peaks A and B is reassuring. Another assumption is that there are no leaks in either the two parallel paths or in the common path. This was a problem initially, since there was a shift in baseline of 1 mV after each of the peaks A and B. This shift was reproducible and was eventually alleviated by replacing a seal in one of the fittings. The experimental arrangement is shown discharging into the atmosphere, however other possibilities might be to allow discharge through a back-pressure regulator (BPR) or another flow resistance.

4.6.5. Sensitivity of equipment and implications for improved design

The results tell us that for a flow rate of approximately 90 mL/min and a volume of approximately 2000 mL, we obtain peak area of approximately 1940 mVs when using a resistance tubing of length 10 cm. If we were then to place a solid object in the Perspex container and then repeat the experiment, we would expect a reduced peak area. We can say approximately that for this resistance/flow rate arrangement, the sensitivity is that 1 mL is approximately equivalent to 1 mVs. This would suggest that the equipment should be capable of measuring volume changes of the order of 0.1 mL.

It is also appropriate to consider what might be the optimum design for this type of volume, as well as much smaller (the order of mL) and much larger (the order of m^3) volumes. There are three parameters that we can change: the molar flow-rate in (M_1), the length of resistance (value of Δk_A) and the value of the flow-measuring resistance (which is convenient to represent as k_B, even though it consists of a Wheatstone bridge). We can combine Equations 4.10, 4.11 and 4.16 to give a relationship for the peak area:

$$A_1 = \frac{V \Delta k_A k_B M_1 R T \mu^2}{4 P_1(0) P_2(0)} \qquad 4.27$$

This means that as expected, the peak area can be increased by increasing the various resistances. Care should be taken when assessing the effect of increasing the fixed molar flow rate through the system. As the value of M_1 is increased, this will also increase both the values of $P_1(0)$ and $P_2(0)$, but only slightly. In the current experimental arrangement, the pressure drop across the 10cm-length of stainless-steel tubing (Δk_A) is 16 mbar and the pressure drop across the measurement system (k_B) is 0.3 mbar. Thus, doubling the value of M_1 will effectively double the area of the peak.

4.6.6. Dynamics of system – comparison of peak shapes

The shape of the peaks is interesting. For both the pressure-increasing and pressure-reducing steps, there is a sharp step followed by a slow (possibly exponential) return to the original

baseline. For each of the pressure-increase steps, the time taken to return to the original baseline is about 100 seconds. However, for the pressure-reduction step, the time taken to return to the original baseline is about 100 seconds in experiment 2, 200 seconds in experiment 3 and 300 seconds in experiment 4. Also, it is expected that the larger the resistance the greater the temporary reduction in flow rate. This is reflected in the negative peak height in Table 4.2: -60, -113 and -300 mV. However, for the reduction in pressure experiment, the peak heights are lower: 35, 53 and 73 mV. This shows that there is certainly a systematic difference between the shapes of the two types of peak.

In order to explain to the difference between the two peaks shapes, let us consider what happens when the valve is switched to introduce an extra resistance downstream of the column. The initial system is shown in Figure 4.12(a). Then, a change is made to the system so that the resistance k_A is increased to ($k_A + \Delta k_A$) as shown in 4.12(b).

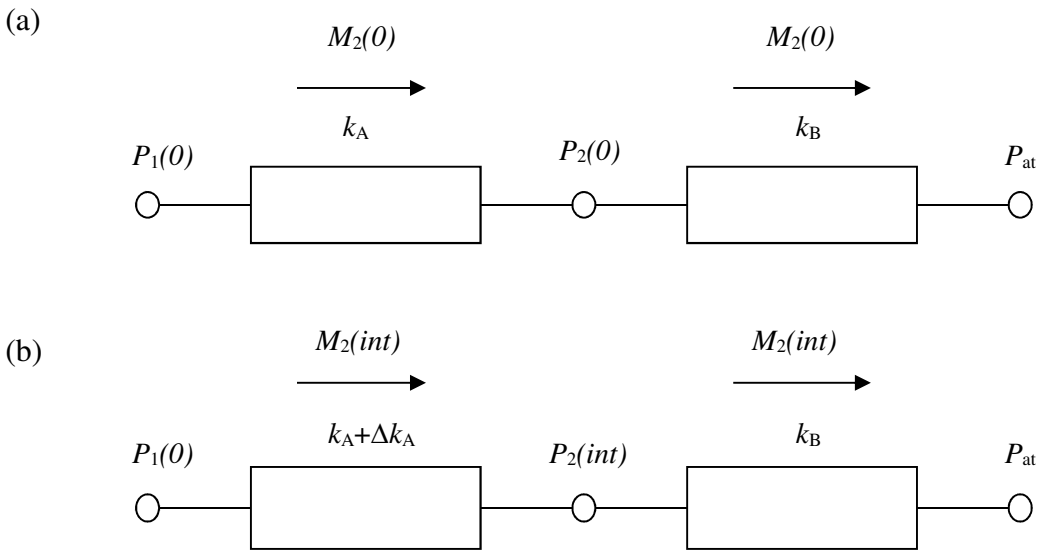

Figure 4.12 - Pressures and flows through the resistances for the increasing resistance experiment

Increasing the resistance suddenly will drop the flow through both resistances and the value P_2 will drop from $P_2(0)$. The flow rate $M_2(int)$ will be less than $M_2(0)$.

As the resistance increases (from k_A to $k_A + \Delta k_A$), the pressure at P_1 increases to $P_1(\infty)$. The hold-up in the volume gradually increases until the system reaches a new steady state. The pressure P_2 decreases sharply to $P_2(int)$ but then gradually increases back up to $P_2(0)$ when the new steady state is reached.

Let us now consider what happens when the valve is switched and the system returns to the initial system without the extra resistance. The new steady state is described above is represented in Figure 4.13(a). This shows the initial system for the resistance reduction experiment. The valve is switched so that the resistance is reduced from ($k_A + \Delta k_A$) back to k_A as shown in Figure 4.13(b).

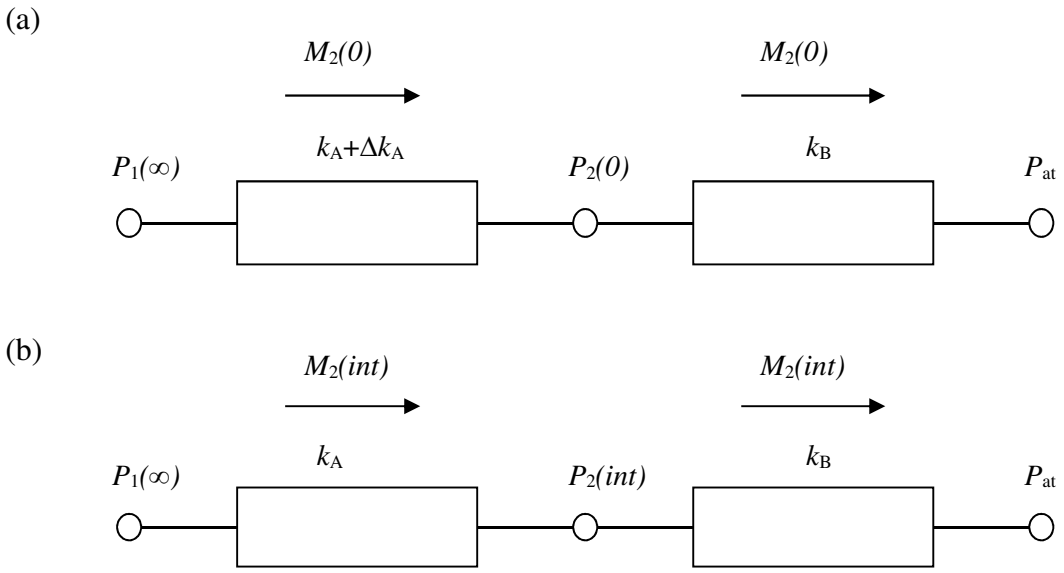

Figure 4.13 - Pressures and flows through the resistances for the decreasing resistance experiment

The sudden decrease in resistance results in an increase in flow through the resistances. The value P_2 will increase from $P_2(0)$. The flow rate $M_2(int)$ will be more than $M_2(0)$.

As the resistance decreases (from $k_A + \Delta k_A$ to k_A), the pressure at P_1 decreases back to $P_1(0)$. The hold-up in the volume gradually decreases until the system returns to the original steady state. The pressure P_2 increases sharply to $P_2(int)$ but then gradually decreases back down to $P_2(0)$ when the steady state is reached.

For the dynamics of the system to be understood the Hagen-Poiseuille equations for the flows across the resistances must be looked at (see Section 3.1).

Across the fixed resistance k_B, the equations are

Initially

$$P_2(0)^2 - {P_{at}}^2 = 2k_B\mu RTM_2(0) \quad 4.28$$

Intermediate

$$P_2(int)^2 - {P_{at}}^2 = 2k_B\mu RTM_2(int) \quad 4.29$$

At any time, *t*

$$P_2(t)^2 - {P_{at}}^2 = 2k_B\mu RTM_2(t) \quad 4.30$$

Finally

$$P_2(0)^2 - {P_{at}}^2 = 2k_B\mu RTM_2(0) \quad 4.31$$

The initial and final equations are the same as the pressure P_2 returns to the original value as the new steady state is reached.

For the increasing resistance experiment, the equations are

Initially

$$P_1(0)^2 - P_2(0)^2 = 2\ k_A\ \mu\ R\ T\ M_2(0) \quad 4.32$$

Intermediate

$$P_1(0)^2 - P_2(int)^2 = 2\ (k_A + \Delta k_A)\ \mu\ R\ T\ M_2(int) \quad 4.33$$

At any time, *t*

$$P_1(t)^2 - P_2(t)^2 = 2\ (k_A + \Delta k_A)\ \mu\ R\ TM_2(t) \quad 4.34$$

Finally

$$P_1(\infty)^2 - P_2(0)^2 = 2\ (k_A + \Delta k_A)\ \mu\ R\ TM_2(0) \quad 4.35$$

For the decreasing resistance experiment, the equations are

Initially

$$P_1(\infty)^2 - P_2(0)^2 = 2\,(k_A + \Delta k_A)\,\mu\,R\,TM_2(0) \qquad 4.36$$

Intermediate

$$P_1(\infty)^2 - P_2(int)^2 = 2\,k_A\,\mu\,R\,T\,M_2(int) \qquad 4.37$$

At any time, *t*

$$P_1(t)^2 - P_2(t)^2 = 2\,k_A\,\mu\,R\,T\,M_2(t) \qquad 4.38$$

Finally

$$P_1(0)^2 - P_2(0)^2 = 2\,k_A\,\mu\,R\,T\,M_2(0) \qquad 4.39$$

A material balance over a small time interval, *dt*, where the hold-up volume changes by *dH* is carried out. This gives

$$M_1 dt = M_2(t)dt + dH \qquad 4.40$$

Initially, the flow into the system, M_1, is equal to the flow out, $M_2(0)$. Rearranging the above equation for the change in hold-up gives

$$\frac{dH}{dt} = M_2(0) - M_2(t) \qquad 4.41$$

where *dH* can be positive or negative.

Assuming perfect gas behaviour, the hold-up change can also be written as

$$dH = \frac{V}{RT}\,dP_1 \qquad 4.42$$

From the Hagen Poiseuille Equations 4.28 and 4.31, subtracting the initial and time varying equations gives

$$M_2(0) - M_2(t) = \frac{P_2(0)^2 - P_2(t)^2}{2\, k_{\mathrm{B}}\, \mu\, R\, T} \qquad 4.43$$

From 4.41, the hold-up equation can therefore also be written as

$$dH = \frac{P_2(0)^2 - P_2(t)^2}{2\, k_{\mathrm{B}}\, \mu\, R\, T} dt \qquad 4.44$$

Equating the hold-up terms in 4.42 and 4.44 and rearranging gives

$$V k_{\mathrm{B}} \mu \frac{dP_1}{dt} = P_2(0)^2 - P_2(t)^2 \qquad 4.45$$

Differentiating and using the chain rule, this equation becomes

$$V k_{\mathrm{B}} \mu \frac{d^2 P_1}{dt^2} = -2P_2(t) \frac{dP_2}{dt} \qquad 4.46$$

To process the material balance, we need to substitute for $P_2(t)$ giving an expression for P_1 only, which can be integrated to give $P_1(t)$.

Let us first consider the increasing resistance experiment. Two equations for $M_2(t)$ are compared. Rearranging 4.30 and 4.34 gives

$$M_2(t) = \frac{P_2(t)^2 - P_{\mathrm{at}}{}^2}{2\, k_{\mathrm{B}}\, \mu\, R\, T} \qquad 4.47$$

$$M_2(t) = \frac{P_1(t)^2 - P_2(t)^2}{2\, (k_A + \Delta k_A)\, \mu\, R\, T} \qquad 4.48$$

Equating and rearranging gives

$$P_2(t)^2 \left[\frac{k_B + k_A + \Delta k_A}{k_B (k_A + \Delta k_A)}\right] = \frac{P_1(t)^2}{k_A + \Delta k_A} + \frac{P_{\mathrm{at}}{}^2}{k_B} \qquad 4.49$$

Rearranging for $P_2(t)^2$ gives

$$P_2(t)^2 = P_1(t)^2\left[\frac{k_B}{k_B + k_A + \Delta k_A}\right] + {P_{\text{at}}}^2\left[\frac{k_A + \Delta k_A}{k_B + k_A + \Delta k_A}\right] \tag{4.50}$$

Substituting the above equation into Equation 4.45 gives

$$\begin{aligned} Vk_{\text{B}}\mu\frac{dP_1}{dt} = {} & P_2(0)^2\left[\frac{k_B + k_A + \Delta k_A}{k_B + k_A + \Delta k_A}\right] - P_1(t)^2\left[\frac{k_B}{k_B + k_A + \Delta k_A}\right] \\ & - {P_{\text{at}}}^2\left[\frac{k_A + \Delta k_A}{k_B + k_A + \Delta k_A}\right] \end{aligned} \tag{4.51}$$

Therefore

$$Vk_{\text{B}}\mu\frac{dP_1}{dt} = \frac{\left[P_2(0)^2 - {P_{at}}^2\right](k_A + \Delta k_A) + [P_2(0)^2 - P_1(t)^2]k_B}{k_B + k_A + \Delta k_A} \tag{4.52}$$

Rearranging this equation for $\frac{dP_1}{dt}$ gives

$$Vk_{\text{B}}\mu\frac{dP_1}{dt} = \frac{\left[P_2(0)^2 - {P_{at}}^2\right](k_A + \Delta k_A) + [P_2(0)^2 - P_1(t)^2]k_B}{k_B + k_A + \Delta k_A} \tag{4.53}$$

The initial values will then be

$$\frac{dP_1}{dt}(t = 0) = \frac{\left[P_2(0)^2 - {P_{at}}^2\right](k_A + \Delta k_A) + [P_2(0)^2 - P_1(0)^2]k_B}{Vk_{\text{B}}\mu(k_B + k_A + \Delta k_A)} \tag{4.54}$$

Inserting the Hagen Poiseuille Equations 4.28 and 4.32, the expression becomes

$$\frac{dP_1}{dt}(t = 0) = \frac{\Delta k_A RTM_2(0)}{V(k_A + \Delta k_A + k_B)} \tag{4.55}$$

Therefore, we have an expression for the change in pressure, P_1, with time for the increasing resistance experiment. This expression will give a positive answer as the pressure, P_1, will increase with time until the new steady state is reached after the resistance is increased.

The same procedure is carried out with the decreasing resistance experiment. Again, the two equations for $M_2(t)$ are compared.

$$M_2(t) = \frac{P_2(t)^2 - {P_{\text{at}}}^2}{2\, k_{\text{B}}\, \mu\, R\, T} \tag{4.56}$$

$$M_2(t) = \frac{P_1(t)^2 - P_2(t)^2}{2\, k_A\, \mu\, R\, T} \tag{4.57}$$

Equating and rearranging gives

$$P_2(t)^2 \left[\frac{k_B + k_A}{k_A k_B}\right] = \frac{P_1(t)^2}{k_A} + \frac{{P_{\text{at}}}^2}{k_B} \tag{4.58}$$

Rearranging for $P_2(t)^2$ gives

$$P_2(t)^2 = P_1(t)^2 \left[\frac{k_{\text{B}}}{k_{\text{A}} + k_{\text{B}}}\right] + {P_{\text{at}}}^2 \left[\frac{k_{\text{A}}}{k_{\text{A}} + k_{\text{B}}}\right] \tag{4.59}$$

Substituting the above equation into Equation 4.45 gives

$$V k_{\text{B}} \mu \frac{dP_1}{dt} = P_2(0)^2 \left[\frac{k_B + k_A}{k_B + k_A}\right] - P_1(t)^2 \left[\frac{k_B}{k_B + k_A}\right] - {P_{\text{at}}}^2 \left[\frac{k_A}{k_B + k_A}\right] \tag{4.60}$$

Therefore

$$V\, k_{\text{B}}\, \mu\, \frac{dP_1}{dt} = \frac{k_A\left[P_2(0)^2 - {P_{at}}^2\right] + k_B[P_2(0)^2 - P_1(t)^2]}{k_B + k_A} \tag{4.61}$$

Rearranging this equation for $\frac{dP_1}{dt}$ gives

$$\frac{dP_1}{dt} = \frac{\left[P_2(0)^2 - {P_{at}}^2\right](k_A + \Delta k_A) + [P_2(0)^2 - P_1(t)^2]k_B}{V k_{\text{B}} \mu (k_B + k_A + \Delta k_A)} \tag{4.62}$$

The initial values will then be

$$\frac{dP_1}{dt}(t = 0) = \frac{\left[P_2(0)^2 - {P_{at}}^2\right]k_A + [P_2(0)^2 - P_1(\infty)^2]k_B}{V k_{\text{B}} \mu (k_A + k_B)} \tag{4.63}$$

Inserting the Hagen Poiseuille equations, the expression becomes

$$\frac{dP_1}{dt}(t=0) = \frac{(-\Delta k_A)RTM_2(0)}{V(k_A + k_B)} \qquad 4.64$$

Again, we have an expression for the change in pressure with time for the decreasing resistance experiment. This expression will give a negative answer.

Comparing the two expressions, if $\Delta k_A > k_A + k_B$, then the decreasing resistance spike will be much sharper than the increasing spike. Therefore, according to the mathematics and intuition, it is expected that the removal experiment should be much faster as the reduction in resistance should result in a rush of flow through the system and an acute increase in pressure at P_2 across the low resistance. However, in practice, this is not the case and is consistent behaviour for all the experiments. A possible explanation for this could be that the sudden surge in nitrogen flow through the resistance causes some type of cooling effect.

4.6.7. Calibration of system – how to use in practice

So far, we have presented many experimental data files, each consisting of the variation of DPT signal with time. In this work, we have concentrated on the consistency and reliability of such measurements – that is, if we report the peak area as 1922 mVs, what are our confidence limits in such a value. However, the final outcome is to be able to report a value for the volume: that is, we require a value in mL. One way of achieving this would be to calibrate the response using a known volume. For example, if a peak area of 1922 mVs corresponds to the calibration volume of 1980 mL, then a peak area of 1890 mVs would correspond to an "unknown" volume of 1947 mL. For the case of measuring much smaller volumes (say the order of a few mL), then it would be normal to select larger values of the various flow resistances (k_B and Δk_A) in order to give a measurable peak area according to Equation 4.16. For the case of measuring much larger volumes (say of the order of m^3), a further consideration is the value of the molar flow rate into the system volume (M_1) to ensure that the experimental time (time to reach the new steady state) is not excessive.

4.6.8. Future Work

Future work could be completed on the apparatus to improve and better understand the system. The experimental arrangement could be improved by enclosing the apparatus to shield it from external factors. The inclusion of a back pressure regulator to the system could also minimise these effects.

Additional experiments could be carried out using needle valves instead of the lengths of tubing. The length of tubing will adjust the system volume. The use of needle valves eliminates this issue but can alter the resistance in the system by restricting the flow. An improved method of delivering a constant flow to system would also beneficial.

Further tests could be conducted without the test volume or with very small volumes to determine the limit of detection of the apparatus. Extra experiments could also be carried out to try this theory on a bigger scale so that it could be used in industrial applications.

4.7.Conclusions

We have shown from a series of experiments that it is possible to use the chemical engineering concept of a material balance to measure volumes and changes in volumes. A gas (such as nitrogen) flows into the volume of interest at a constant rate. Then a change to the system is made by introducing an extra resistance, which causes a slow increase in pressure in the volume and subsequent reduction in the flow rate of gas leaving the volume. For our investigation, we have used a volume of approximately 2 litres and a nitrogen flow rate of 90 mL/min. The extra resistance increases the pressure by about 15 mbar, and the time taken to reach the new steady state is about 100 seconds. The “perturbation” or “system change” approach has several advantages over a “single” measurement: there are two parts to the experiment, and after the second part the system should return to the original state. With the current preliminary arrangement – produced from available equipment – the results suggest that the sensitivity is such that volume changes of the order of 0.1 mL can be determined. The limiting factors in the accuracy and reproducibility of this technique are ensuring that the baseline pressure remains constant over the course of the experiment and selecting a mass flow controller (MFC) does indeed maintain a constant mass flow rate over the course of the experiment.

5. Volume Determination using Perturbation Flows

5.1. Introduction

This section considers another technique that can be used for the measurement of volume. It uses the same basic equipment that is described in Chapter 4 but the experiments differ in several ways. Firstly, a perturbation flow is added to the main flow to make a change to the system rather than changing the resistance in the system. Secondly, back pressure regulators and resistances are used so that the main flow will change when the perturbation flow is added to the main flow rather than a mass flow controller delivering a fixed flow. Thirdly, step areas are calculated rather than peak areas. Finally, a length of 0.25 inch nylon tubing is used as a volume instead of the Perspex volume. The experimental arrangement is also changed from a one-sided to a two-sided system. The two-sided arrangement allows differential measurements to be made reducing any potential errors from environmental issues which could affect the pressure in the system.

A similar system has been used in previous work by Mason *et al*. (1998) [38], Mason *et al*. (2000) [40] and Russell *et al.* (2005) [42] where it has been assumed that the main flow is fixed throughout the experiment. However, in this work, we are looking at the possibility of the main flow rate changing as the perturbation flow is added.

This work differs from previous work by Mason [38,40] and Russell [42] in numerous ways. Firstly, as previously mentioned, in this work, the possibility of the main flow changing as the perturbation flow is added is considered, rather than remaining constant. Secondly, in previous work, conclusions are drawn through examination of changes in step sizes in result graphs when the perturbation flow is added and removed from the main flow. However, in this work the areas under the steps are studied. Thirdly, larger downstream resistances are used in the experimental arrangement and finally, gas mixtures and changes in compositions are also investigated.

Also, previously the pressure differences have been looked at in order to draw conclusions from the experiments. In this section, we will look at the areas under the results graphs to be used as another method of volume determination.

5.2. Background

As previously mentioned in Section 4.2, the measurement of volume is important in many industrial, scientific and domestic situations. Some recent techniques for volume measurement include Kobata *et al.* (2004) [55] who used an acoustic volumeter to measure the volumes of metal weights ranging from 100 g to 10 kg. The volume is required for the buoyancy correction to determine the mass of the weight. Also, Tosti and Bettinali (2006) [56] presented a generic technique for the determination of a container volume with an irregular shape based on the permeation of gas through a membrane. For this technique, the container is pressurised and the volume is determined from the variation of pressure with time and a material balance.

The work in this chapter continues from previous findings by Mason *et al.* (1998) [38], where a new technique for making viscosity measurements on gas mixtures was introduced. This technique involved adding a small, infinitesimal stream of perturbation gas to a gas mixture flowing through a capillary tube. This causes a change in the composition and flow rate. The pressure at the inlet of the capillary tube rises when the perturbation gas is added. This increase in pressure is proportional to the flow rate change. Sometime later the pressure changes again when the composition of the gas flowing through the tube changes. This delay happens because of the empty volume between the point where the perturbation gas is added and the capillary tube. This second pressure change is proportional to the change in viscosity. The ratio of these two pressure steps is proportional to $\mathrm{d} \ln \mu / \mathrm{d}X_i$ where μ is viscosity and X_i is the mole fraction of component i.

This method used by Mason *et al*. (1998) [38] is new in both concept and application. There are two new ideas. The first idea is that instead of measuring the gas viscosity directly, the gradient of the viscosity-composition function is measured. The composition is changed slightly and the small change in viscosity is measured. This approach has the advantage of measurement of differentials followed by integration is more accurate than direct measurement. The second idea involves the detail of the apparatus and the theory of laminar flows through tubes. A capillary tube is first used as a flow meter and then shortly afterwards as a viscometer. When one response is divided by the other, the gradient of viscosity with composition is obtained. The advantage of this is that the result of the experiment will not depend on the properties of the capillary tube. Only the properties of the gas in the capillary tube are measured.

Mason *et al*. (1998) [38] obtained an equation determining the gradient d ln μ/dX_i from the ratio of pressure changes and knowledge of the main flow and perturbation flow compositions, as follows

$$\frac{d\ln\mu}{dX_i} = \frac{p_2 - p_1}{p_1 - p_0}\,\frac{1}{\left(X_i^T - X_i^0\right)} \qquad 5.1$$

where $p_1 - p_0$ is the pressure change due to the change in flowrate and $p_2 - p_1$ is the pressure change due to the change in viscosity. Also, X_i^T and X_i^0 are the compositions of the perturbation flow and the main flow respectively.

This paper also shows that a differential apparatus design overcomes many potential difficulties. Duplicating the upstream capillary choke, the delay line and the downstream capillary choke overcomes some of the difficulties caused by having to keep the main gas flow constant to precise limits. The reference stream provides a similar pressure to the measurement stream pressure and the pressure gauge can be replaced by a differential pressure transducer (DPT).

The main benefit of the differential design is that the pressures upstream and downstream are common to both the measurement and reference streams and any small changes in pressure of both chokes caused by drift in a pressure regulator affects both streams together and cause little change at the differential pressure transducer. This differential design overcomes the difficulty of maintaining the upstream and downstream pressures constant to 1 part to 100,000.

Mason *et al.* (2000) [40] expanded this theory. In this work, experiments were carried out by adding a small, finite perturbation flow to a gas mixture flowing through a capillary tube. When these small finite perturbations are made, there are systematic differences between the ratio of the two pressure steps depending on whether the perturbation flow is being added or removed. In their experiments, the ratio of perturbation gas flow rate, *m*, to the main gas flow rate, *M*, is one to a hundred. This small, finite step makes a perceptible difference in the interpretation of results, particularly when the perturbation stream is removed. The ratio of the pressure ratios when the perturbation ratio is added and removed was found to be

$$\frac{R_{add}}{R_{rem}} = \left(1 + \frac{m}{M}\right)\left(1 + \frac{\Delta\mu}{\mu}\right) \qquad 5.2$$

This shows that the pressure ratio when the perturbation is added, R_{add}, is not exactly the same as the pressure ratio when the perturbation is removed, R_{rem}. It also shows that the ratio depends on the relative size of the perturbation (m/M) and the relative change in viscosity ($\Delta\mu/\mu$). For an experiment where R_{add} is about 0.1 and m/M is about 0.01, the ratio of the pressure ratios, R_{add}/R_{rem}, was found to be about 1.01. Therefore, it is expected that the experimental value of R_{add} to always be 1.01 times the size of the ratio, R_{rem}.

Mason *et al.* (2000) [40] also showed that the twin-channel, differential design is beneficial in that any environmental fluctuations affect the two sides equally and so their effects are eliminated by making differential measurements. The use of a back-pressure regulator was also used to protect the apparatus from atmospheric pressure fluctuations.

Russell *et al.* (2005) [42] investigated the effects of using very large perturbation flows on the same apparatus as used in the previously discussed experiments. It was discovered that when the perturbation stream, *m*, is added, the pressure rise at the capillary will simultaneously reduce the main flow rate, *M*, by a small amount, Δm_1, since the upstream and downstream pressures are fixed. The size of Δm_1 depends upon the size of the perturbation flow used. For small perturbation flow, this will be negligible. The pressure change due to viscosity can also alter the main flow by a small amount, Δm_2. With larger perturbation flows, these changes in flow rate had to be incorporated into the equation for the viscosity gradient.

5.3. Theory

5.3.1. Addition of Perturbation Flow

Figure 5.1 below shows a schematic diagram of the basic experimental arrangement when the perturbation flow is added to the system. It includes a large resistance, a volume, with zero resistance, and a low resistance, all in series.

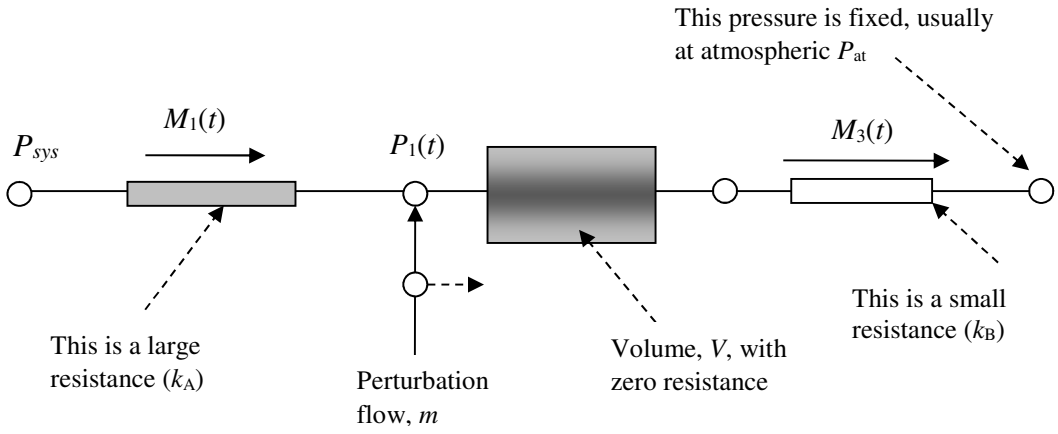

Figure 5.1 - Basic experimental arrangement with perturbation being added to the system

Initially, a flow is passed through the system at a flow rate, $M_1(0)$. The flow enters the system with a viscosity, μ, and passes through a large resistance (k_A). It then passes through a volume which is assumed to have zero resistance and then a small resistance (k_B). P_{sys} and P_{at} are both fixed pressures.

At time t=0 seconds, a small perturbation flow, m, is added to the system. The addition of this perturbation flow results in an increase in the main flow rate, M_1, and the pressure, P_1. The inclusion of a volume in the system means that, after the perturbation flow has been added, the pressure changes in two steps. The pressure change due to the change in flow can be seen separately from that of the change in pressure due to the change in viscosity as shown in Figure 5.2. The figure shows the initial pressure, $P_1(0)$. At this point the viscosity is μ and the flow rate is $M_1(0)$. The perturbation flow, m, is added and the pressure increases to an intermediate stage, $P_1(int)$. The pressure change due to change in flow ($P_1(int)$- $P_1(0)$) is represented by ΔP_1. At this point, the viscosity is μ and the flow rate is now ($M_1(int)+m$). The pressure then increases further to $P_1(\infty)$. This represents the pressure change due to the change in the viscosity, ΔP_2. Here, the flow rate is ($M_1(\infty)+m$) and the viscosity is ($\mu+\Delta\mu$).

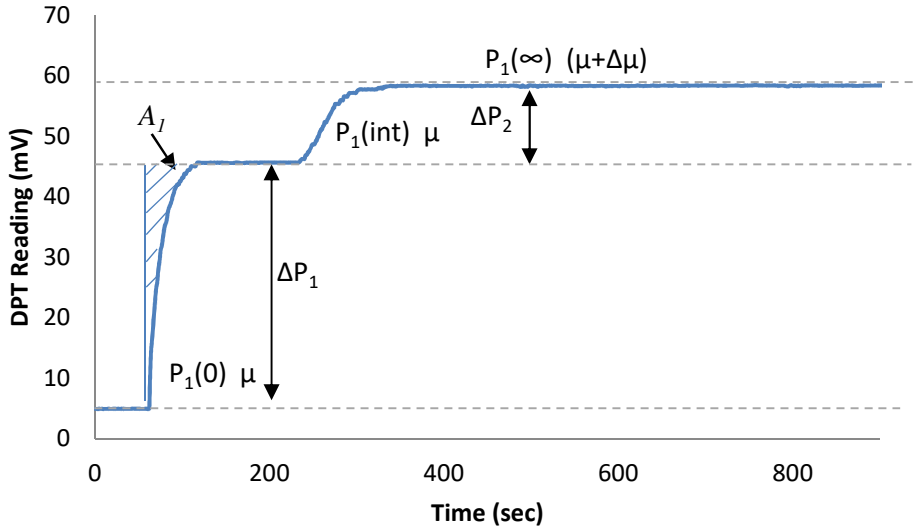

Figure 5.2 - Typical perturbation addition result graph

The area on the graph for the addition experiment is denoted A_1. This area is calculated from

$$A_1 = \int_0^\infty [P_1(\text{int}) - P_1(t)]\ dt \qquad 5.3$$

The size of the area depends on the main flow, the perturbation flow, the viscosity of the gases used and resistances used in the experimental arrangement. The infinity term in the equation denotes the intermediate steady state that is reached between the steps.

The changes in flow rates are quantified using the Hagen-Poiseuille equation as mentioned in Section 3.2. The system was broken down into two parts, upstream and downstream of where the perturbation is added (see Figure 5.1). Initially, before the perturbation is added, the equations governing the flow are:

Upstream of perturbation addition

$$P_{sys}^2 - P_1(0)^2 = 2k_A M_1(0)\mu RT \qquad 5.4$$

Downstream of perturbation addition

$$P_1(0)^2 - P_{at}^2 = 2k_B M_1(0)\mu RT \qquad 5.5$$

Adding these equations together gives the equation for the whole system:

Overall

$$P_{sys}^2 - P_{at}^2 = 2(k_A + k_B)M_1(0)\mu RT \quad 5.6$$

At the intermediate stage, after the pressure change due to flow, the equations are:

Upstream of perturbation addition

$$P_{sys}^2 - P_1(int)^2 = 2k_A M_1(int)\mu RT \quad 5.7$$

Downstream of perturbation addition

$$P_1(int)^2 - P_{at}^2 = 2k_B[M_1(int) + m]\mu RT \quad 5.8$$

Overall

$$P_{sys}^2 - P_{at}^2 = 2[(k_A + k_B)M_1(int) + k_B m]\mu RT \quad 5.9$$

Then finally, after the pressure change due to viscosity, the equations are:

Upstream of perturbation addition

$$P_{sys}^2 - P_1(\infty)^2 = 2k_A M_1(\infty)\mu RT \quad 5.10$$

Downstream of perturbation addition

$$P_1(\infty)^2 - P_{at}^2 = 2k_B(M_1(\infty) + m)(\mu + \Delta\mu)RT \quad 5.11$$

Overall

$$P_{sys}^2 - P_{at}^2 = 2k_A M_1(\infty)\mu RT + 2k_B(M_1(\infty) + m)(\mu + \Delta\mu)RT \quad 5.12$$

The ratio of the initial flow rate and the intermediate can be found by equating 5.6 and 5.9.

$$(k_A + k_B)M_1(0) = (k_A + k_B)M_1(int) + k_B m \quad 5.13$$

Rearranging 5.13 gives the flow rate ratio

$$\frac{M_1(int)}{M_1(0)} = 1 - \frac{k_B}{k_A + k_B}\frac{m}{M_1(0)} \qquad 5.14$$

This ratio will approach 1 as $\frac{k_B}{k_A}$ and/or $\frac{m}{M_1(0)}$ tends to 0.

Similarly, the ratio of the initial and final flow rates can be found by equating 5.6 and 5.12.

$$(k_A + k_B)M_1(0)\mu = k_A M_1(\infty)\mu + k_B(M_1(\infty) + m)(\mu + \Delta\mu) \qquad 5.15$$

Rearranging 5.15 gives

$$\frac{M_1(\infty)}{M_1(0)} = \frac{\mu(k_A + k_B)}{(k_A + k_B)\mu + k_B\Delta\mu} - \frac{m}{M_1(0)}\frac{k_B(\mu + \Delta\mu)}{(k_A + k_B)\mu + k_B\Delta\mu} \qquad 5.16$$

This ratio will approach 1 as $\frac{k_B}{k_A}$ and/or $\frac{m}{M_1(0)}$ tends to 0.

5.3.2. Removal of Perturbation Flow

Figure 5.3 below shows the schematic diagram of the system as the perturbation is removed.

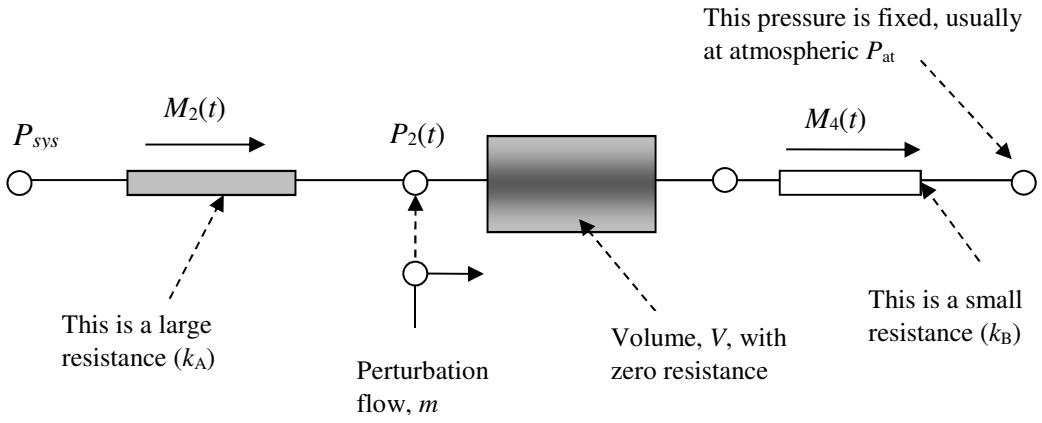

Figure 5.3 - Basic experimental arrangement with perturbation being removed from the system

The initial flow rate into the system is $M_2(0)$ and the flow rate out is $M_4(0)$ and the pressure is $P_2(0)$. The even numbered subscripts describe the perturbation removal experiment.

Initially, for this experiment the perturbation flow, m, is still flowing into the system so the flow rate is $(M_2(0)+m)$ and the viscosity is $(\mu+\Delta\mu)$. At time $t=0$, the perturbation is switched from flowing to the system to flowing to the vent. The pressure in the system then starts to decrease and levels at $P_2(int)$. Again, this represents the change in pressure due to the change in flow. At this point the flow rate is $M_2(int)$. The viscosity is still $(\mu+\Delta\mu)$. The pressure in the system decreases again. This is due to the change in viscosity so at the final stage the pressure is $P_2(\infty)$ and the viscosity is μ. The flow rate is $M_2(\infty)$ and should equal $M_1(0)$ from the addition experiment.

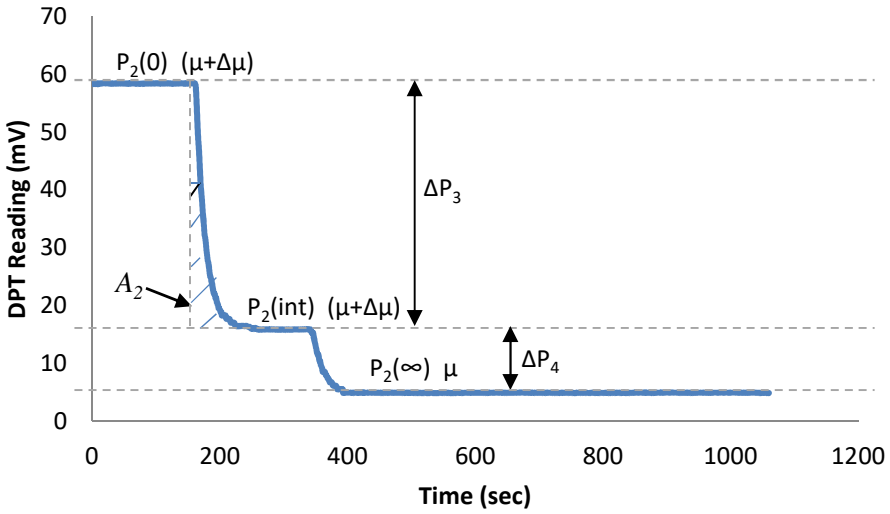

Figure 5.4 - Typical perturbation removal result graph

The area under the graph is denoted A_2. It is calculated from:

$$A_2 = \int_0^{\infty} [P_2(int) - P_2(t)]\ dt \qquad 5.17$$

It is expected that A_2 should be greater than A_1 This is because the initial flow rates, pressures and viscosities will be higher for the removal experiment. In the addition experiment, the initial flow rate is $M_1(0)$ and in the removal experiment, the initial flow rate is $(M_2(0) + m)$.

Initially, before the perturbation is removed, the Hagen-Poiseuille equations governing the flow are:

Upstream of perturbation removal

$$P_{sys}^2 - P_2(0)^2 = 2k_A M_2(0)\mu RT \quad 5.18$$

Downstream of perturbation removal

$$P_2(0)^2 - P_{at}^2 = 2k_B(M_2(0) + m)(\mu + \Delta\mu)RT \quad 5.19$$

Adding these equations together gives the equation for the whole system:

Overall

$$P_{sys}^2 - P_{at}^2 = 2k_A M_2(0)\mu RT + 2k_B(M_2(0) + m)(\mu + \Delta\mu)RT \quad 5.20$$

At the intermediate stage, after the pressure change due to flow, the equations are:

Upstream of perturbation removal

$$P_{sys}^2 - P_2(int)^2 = 2k_A M_2(int)\mu RT \quad 5.21$$

Downstream of perturbation removal

$$P_2(int)^2 - P_{at}^2 = 2k_B M_2(int)(\mu + \Delta\mu)RT \quad 5.22$$

Overall

$$P_{sys}^2 - P_{at}^2 = 2k_A M_2(int)\mu RT + 2k_B M_2(int)(\mu + \Delta\mu)RT \quad 5.23$$

Then finally, after the pressure change due to viscosity, the equations are:

Upstream of perturbation removal

$$P_{sys}^2 - P_2(\infty)^2 = 2k_A M_2(\infty)\mu RT \quad 5.24$$

Downstream of perturbation removal

$$P_2(\infty)^2 - P_{at}^2 = 2k_B M_2(\infty)\mu RT \quad 5.25$$

Overall

$$P_{sys}^2 - P_{at}^2 = 2(k_A + k_B)M_2(\infty)\mu RT \qquad 5.26$$

The ratio of the initial flow rate and the intermediate can be found by equating 5.19 and 5.22.

$$M_2(0)[k_A\mu + k_B(\mu + \Delta\mu)] + k_B m(\mu + \Delta\mu) = M_2(int)[k_A\mu + k_B(\mu + \Delta\mu)] \qquad 5.27$$

Rearranging 5.26 gives the ratio of the flow rates

$$\frac{M_2(int)}{M_2(0)} = 1 - \frac{k_B(\mu + \Delta\mu)}{k_A\mu + k_B(\mu + \Delta\mu)}\frac{m}{M_2(0)} \qquad 5.28$$

This ratio will approach 1 as $\frac{k_B}{k_A}$ and/or $\frac{m}{M_2(0)}$ tends to 0.

Likewise, the ratio of the initial and final flow rates can be found by equating 5.19 and 5.25.

$$M_2(0)[k_A\mu + k_B(\mu + \Delta\mu)] + k_B m(\mu + \Delta\mu) = M_2(\infty)\mu(k_A + k_B) \qquad 5.29$$

Rearranging 5.28 gives

$$\frac{M_2(\infty)}{M_2(0)} = \frac{k_A\mu + k_B(\mu + \Delta\mu)}{\mu(k_A + k_B)} + \frac{m}{M_2(0)}\frac{k_B(\mu + \Delta\mu)}{\mu(k_A + k_B)} \qquad 5.30$$

Again, this ratio will approach 1 as $\frac{k_B}{k_A}$ and/or $\frac{m}{M_2(0)}$ tends to 0.

5.3.3. Material Balance

As described in Section 4.3, the material balance over a system is

$$\text{Input} = \text{Accumulation} + \text{Output} \qquad 4.1$$

For this system, the material balance over a small time interval, *dt*, where the hold-up changes by *dH* is

$$M_1(t)dt + m\,dt = \ dH + M_3(t)dt \qquad 5.31$$

The accumulation term is the change in hold-up in the system caused by adding the perturbation flow. This is derived from the perfect gas equation as described in Section 4.3.

The change in hold-up is given by

$$dH = \frac{V}{RT}\,dP \qquad 3.29$$

Therefore,

$$\Delta H = \frac{V}{RT}\int dP \qquad 5.32$$

The material balance is

$$M_1(t)dt + m\,dt = \frac{V}{RT}\int dP + M_3(t)dt \qquad 5.33$$

We now consider how we might measure the areas under the steps in more detail. Firstly, we consider the perturbation addition experiment. We can use the time-varying Hagen-Poiseuille equations. Therefore, at any time, *t*, the Hagen-Poiseuille equations for the system are

Upstream of perturbation addition

$$P_{sys}^2 - P_1(t)^2 = 2k_A M_1(t)\mu RT \qquad 5.34$$

Downstream of perturbation addition

$$P_1(t)^2 - P_{at}^2 = 2k_B M_3(t)\mu RT \qquad 5.35$$

These equations are then rearranged for the variable molar flow rates, $M_1(t)$ and $M_3(t)$ respectively giving

$$M_1(t) = \frac{P_{sys}^2 - P_1(t)^2}{2k_A\mu RT} \qquad 5.36$$

$$M_3(t) = \frac{P_1(t)^2 - P_{at}^2}{2k_B\mu RT} \qquad 5.37$$

These can be inserted into the material balance.

We now consider the perturbation flow, *m*. Rearranging 5.8 gives

$$m = \frac{P_1(int)^2 - P_{at}^2}{2k_B\mu RT} - M_1(int) \tag{5.38}$$

Equation 5.7 can also be rearranged to give

$$M_1(int) = \frac{P_{sys}^2 - P_1(int)^2}{2k_A\mu RT} \tag{5.39}$$

These can also put into the material balance equation to give

$$\begin{aligned} &\frac{P_{sys}^2 - P_1(t)^2}{2k_A\mu RT}dt + \left[\frac{P_1(int)^2 - P_{at}^2}{2k_B\mu RT} - \frac{P_{sys}^2 - P_1(int)^2}{2k_A\mu RT}\right]dt \\ &= \frac{V\,dP}{RT} + \frac{P_1(t)^2 - P_{at}^2}{2k_B\mu RT}dt \end{aligned} \tag{5.40}$$

This can be simplified to

$$[P_1(int)^2 - P_1(t)^2]\,dt = V\mu\frac{k_Ak_B}{k_A + k_B}\,dP \tag{5.41}$$

$$[P_1(int) - P_1(t)]dt = V\mu\frac{k_Ak_B}{k_A + k_B}\,\frac{dP}{P_1(int) + P_1(t)} \tag{5.42}$$

The shaded area under the graph (Figure 5.2) is given by

$$A_1 = \int_0^\infty [P_1(int) - P_1(t)]\,dt \tag{5.3}$$

Also,

$$\int_{P_1(0)}^{P_1(int)} \frac{dP}{P_1(int) + P_1(t)} = [\ln[P_1(int) + P_1(t)]]_{P_1(0)}^{P_1(int)} \tag{5.43}$$

So,

$$\int_{P_1(0)}^{P_1(int)} \frac{dP}{P_1(int) + P_1(t)} = \ln\left[\frac{P_1(int) + P_1(int)}{P_1(int) + P_1(0)}\right] \tag{5.44}$$

Inserting these into the material balance, it becomes

$$A_1 = V\mu \frac{k_A k_B}{k_A + k_B} \ln\left[\frac{P_1(int) + P_1(int)}{P_1(int) + P_1(0)}\right] \quad 5.45$$

We know the limits for the integration of the pressure. Therefore, the change in hold-up is given by

$$\Delta H = \frac{V}{RT}\left[P_1(int) - P_1(0)\right] \quad 5.46$$

From the graph

$$P_1(int) - P_1(0) = \Delta P_1 \quad 5.47$$

The area under the graph is then calculated by

$$A_1 = V\mu \frac{k_A k_B}{k_A + k_B} \ln\left[1 + \frac{\Delta P_1}{P_1(int) + P_1(0)}\right] \quad 5.48$$

This can be simplified further to

$$A_1 = V\mu \frac{k_A k_B}{k_A + k_B} \ln\left[1 + \frac{\Delta P_1}{2P_1(0) + \Delta P_1}\right] \quad 5.49$$

A similar equation can be found for the perturbation removal experiment. The material balance for the removal experiment over a small time interval, *dt*, where hold-up changes by *dH* is

$$M_2(t)dt = dH + M_4(t)dt \quad 5.50$$

To be able to relate the material balance to the area under the graph, we need to include the molar flow rates for the intermediate stage.

$$[M_2(t) - M_2(int)]dt = \frac{V\, dP}{RT} + [M_4(t) - M_4(int)]\, dt \quad 5.51$$

At any time, *t*, the Hagen-Poiseuille equations for the system are

$$P_{sys}^2 - P_2(t)^2 = 2k_A M_2(t)\mu RT \quad 5.52$$

$$P_2(t)^2 - P_{at}^2 = 2k_B M_4(t)(\mu + \Delta\mu)RT \quad 5.53$$

These equations are then rearranged for the variable molar flow rates, $M_2(t)$ and $M_4(t)$ respectively giving

$$M_2(t) = \frac{P_{sys}^2 - P_2(t)^2}{2k_A\mu RT} \tag{5.54}$$

$$M_4(t) = \frac{P_2(t)^2 - P_{at}^2}{2k_B(\mu + \Delta\mu)RT} \tag{5.55}$$

At the intermediate stage, the Hagen-Poiseuille equations are

$$P_{sys}^2 - P_2(int)^2 = 2k_A M_2(int)\mu RT \tag{5.56}$$

$$P_2(int)^2 - P_{at}^2 = 2k_B M_4(int)(\mu + \Delta\mu)RT \tag{5.57}$$

These equations are then rearranged for the variable molar flow rates, $M_2(int)$ and $M_4(int)$ respectively giving

$$M_2(int) = \frac{P_{sys}^2 - P_2(int)^2}{2k_A\mu RT} \tag{5.58}$$

$$M_4(int) = \frac{P_2(int)^2 - P_{at}^2}{2k_B(\mu + \Delta\mu)RT} \tag{5.59}$$

These are then inserted into the material balance, Equation 5.51. The material balance is therefore

$$\left[\frac{P_{sys}^2 - P_2(t)^2}{2k_A\mu RT} - \frac{P_{sys}^2 - P_2(int)^2}{2k_A\mu RT}\right]dt = \frac{V\,dP}{RT} + \left[\frac{P_2(t)^2 - P_{at}^2}{2k_B(\mu + \Delta\mu)RT} - \frac{P_2(int)^2 - P_{at}^2}{2k_B(\mu + \Delta\mu)RT}\right]dt \tag{5.60}$$

This can be simplified to

$$[P_2(int)^2 - P_2(t)^2]\,dt = V\frac{k_A k_B\mu(\mu + \Delta\mu)}{k_A\mu + k_B(\mu + \Delta\mu)}\,dP \tag{5.61}$$

$$[P_2(int) - P_2(t)]dt = V\frac{k_A k_B\mu(\mu + \Delta\mu)}{k_A\mu + k_B(\mu + \Delta\mu)}\frac{dP}{P_2(int) + P_2(t)} \tag{5.62}$$

The shaded area under the graph (Figure 5.4) is given by

$$A_2 = \int_0^{\infty} [P_2(int) - P_2(t)]\, dt \qquad 5.17$$

Also,

$$\int_{P_2(0)}^{P_2(int)} \frac{dP}{P_2(int) + P_2(t)} = [\ln[P_2(t) + P_2(int)]]_{P_2(0)}^{P_2(int)} \qquad 5.63$$

So,

$$\int_{P_2(0)}^{P_2(int)} \frac{dP}{P_2(int) + P_2(t)} = \ln\left[\frac{P_2(int) + P_2(int)}{P_2(int) + P_2(0)}\right] \qquad 5.64$$

Substitutng these into the material balance gives

$$A_2 = V \frac{k_A k_B \mu(\mu + \Delta\mu)}{k_A \mu + k_B(\mu + \Delta\mu)} \ln\left[\frac{P_2(int) + P_2(int)}{P_2(int) + P_2(0)}\right] \qquad 5.65$$

We know the limits for the integration of the pressure. Therefore, the change in hold-up is given by

$$\Delta H = \frac{V}{RT} [P_2(int) - P_2(0)] \qquad 5.66$$

From the graph in Figure 5.4

$$P_2(int) - P_2(0) = \Delta P_3 \qquad 5.67$$

The area under the graph is then calculated by

$$A_2 = V \frac{k_A k_B \mu(\mu + \Delta\mu)}{k_A \mu + k_B(\mu + \Delta\mu)} \ln\left[1 + \frac{\Delta P_3}{P_2(int) + P_2(0)}\right] \qquad 5.68$$

This can be simplified further to

$$A_2 = V \frac{k_A k_B \mu(\mu + \Delta\mu)}{k_A \mu + k_B(\mu + \Delta\mu)} \ln\left[1 + \frac{\Delta P_3}{2P_2(0) + \Delta P_3}\right] \qquad 5.69$$

We now have equations for the areas under the graphs for both the addition and removal of the perturbation flow experiments.

For the perturbation addition experiment, ΔP_1 is positive. This means that the log expression will be more than 1 so will give a positive result. For the perturbation removal experiment, ΔP_3 is negative therefore the log expression will be less than 1 and so will give a negative result.

We can now consider the case where the main and the perturbation flows have the same composition.

Equation 5.17 for A_2 can be changed because the viscosity will not change when the perturbation is added, so $\Delta\mu$ can be omitted from the equation. Therefore,

$$A_2 = V\mu \frac{k_A k_B}{k_A + k_B} \ln\left[1 + \frac{\Delta P_3}{2P_2(0) + \Delta P_3}\right] \qquad 5.70$$

Also, in the results graph, there will only be one step change due to the change in flow as the main flow and perturbation flow have the same composition and so the viscosity will be the same. Thus,

$$\Delta P_1 + \Delta P_3 = 0 \qquad 5.71$$

and

$$A_2 = V\mu \frac{k_A k_B}{k_A + k_B} \ln\left[1 - \frac{\Delta P_1}{2P_2(0) - \Delta P_1}\right] \qquad 5.72$$

The ratio of the two areas under the graphs can be found from

$$Ratio\ of\ areas = \frac{A_2}{A_1} = \frac{\ln\left[1 - \frac{\Delta P_1}{2P_2(0) - \Delta P_1}\right]}{\ln\left[1 + \frac{\Delta P_1}{2P_1(0) + \Delta P_1}\right]} \qquad 5.73$$

For small step changes where ΔP_1 is small, $P_2(0) \approx P_1(0)$ and we can assume that both terms will have the same magnitude. Therefore, the ratio of areas $\rightarrow 1$.

However, for large step changes, where ΔP_1 is large, $P_2(0) \neq P_1(0)$ and the areas will not be the same.

5.3.4. Testing Validity of Area Equation

In the previous section, equations for the areas under the graph were derived. These equations were

$$A_1 = V\mu \frac{k_A k_B}{k_A + k_B} \ln\left[1 + \frac{\Delta P_1}{2P_1(0) + \Delta P_1}\right] \quad 5.49$$

and

$$A_2 = V \frac{k_A k_B \mu(\mu + \Delta\mu)}{k_A \mu + k_B(\mu + \Delta\mu)} \ln\left[1 + \frac{\Delta P_3}{2P_2(0) + \Delta P_3}\right] \quad 5.69$$

Both area equations show that the area is proportional to the volume, the viscosity, the resistances k_A and k_B and the changes in pressure. The volume is dependent on the length and diameter of the delay lines. The viscosity depends on the gases used in the experiment. The resistances are set by which flow elements are inserted into the steel blocks. The pressure changes depend on the flow rates and the viscosity of the main and perturbation gases.

The validity of equation can be tested in several ways including

- Add/take-away same perturbation flow
- Add increasing perturbation flows
- Change value of k_A or k_B
- Use different main flows
- Change volume

5.4.Experimental Arrangement and Procedure

Figure 5.5 shows the experimental arrangement used in this section. The system is two-sided. There is a reference side (bottom) and a measuring side (top where the perturbation is added) so that the change in pressure can be recorded using a differential pressure transducer (DPT).

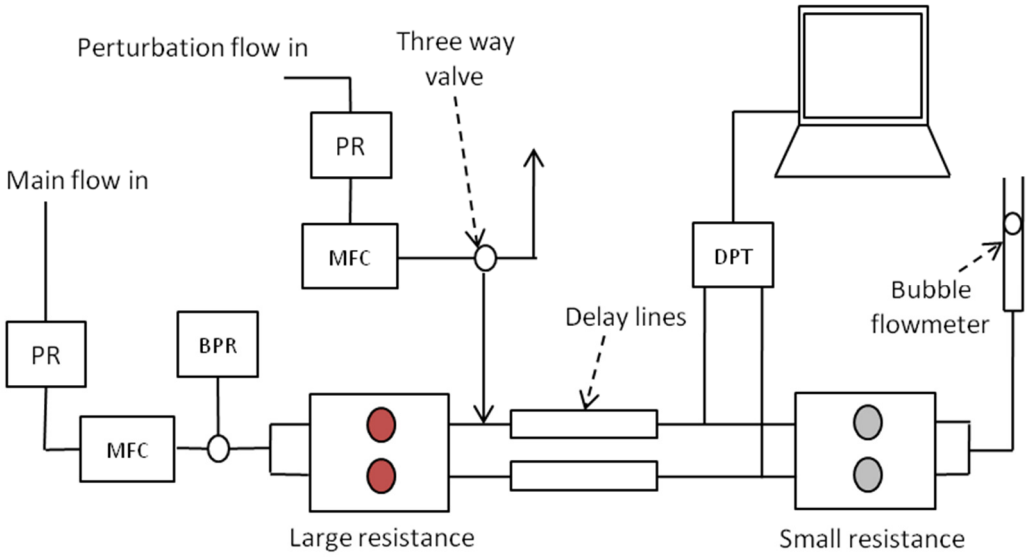

Figure 5.5 - Schematic Representation of Experimental Arrangement

The main flow enters the system. The flow rate and pressure are set by a mass flow controller (MFC) and a pressure regulator (PR) respectively. The main flow was set using a *Porter* VC1000 mass flow controller. The inlet pressure was set to 40 psi using a *Porter* 8286 pressure regulator.

The main flow splits into two equal streams. Each stream flows through the same sizes of resistances and volume to ensure that the flow rates through each side of the system are equal. Both sides initially flow through a large resistance. Here we used a steel block with two flow setting elements to create a high resistance in each stream. The flow elements used were red which allowed a maximum flow of 60 ml/min. These flow elements have sintered discs in them to restrict the amount of gas flowing through them. Here we assume that the flow is in the continuum regime and so the Hagen-Poiseuille equation still applies. The streams leaving the block then lead to the delay lines. The extra volume from the delay lines allow the pressure changes due to any change in flow and any change in viscosity to be seen separately. Finally, the gas streams leave the system by passing through another steel block. Flow elements (silver with green dots) were inserted into the steel block. These allow a maximum flow of 750 ml/min. Both flows leave the steel block and combine. The total flow leaving the arrangement can be measured using a bubble flow meter.

The perturbation flow is added to the measurement side of the system upstream of the delay lines. The perturbation flow was set in the same way as the main flow using a pressure regulator and mass flow controller. The flow was set using a *Porter* VC1000 mass flow controller and the inlet pressure was set to 40 psi using a *Porter* 8286 pressure regulator. A three-way valve is used to add the perturbation gas to the system. Initially, the perturbation flow is directed to vent. Experiments are carried out by switching the valve and directing the perturbation flow into the system.

The pressures, $P_1(t)$ and $P_2(t)$, are monitored using a Furness Controls Differential Pressure Transducer with an output of ±1000 mV corresponding to an input of ± 100 Pa and this is recorded using *Pico* 16-bit resolution software. The graphs are plotted using *Microsoft* Excel.

An experiment was conducted by switching the three-way valve so that the perturbation flow is directed into the system. A flow rate, m, was added to the system. The theory suggests that this will change $M_1(0)$ to $M_1(\text{int})$ and then eventually to $M_1(\infty)$. The infinity term represents the time taken for the system to reach the new steady state. The addition of the perturbation flow will also change the viscosity by $\Delta\mu$. When the system reaches the new steady state, the three way valve is switched back to the original position, removing the perturbation flow from the system. A typical result graph is shown below in Figure 5.6.

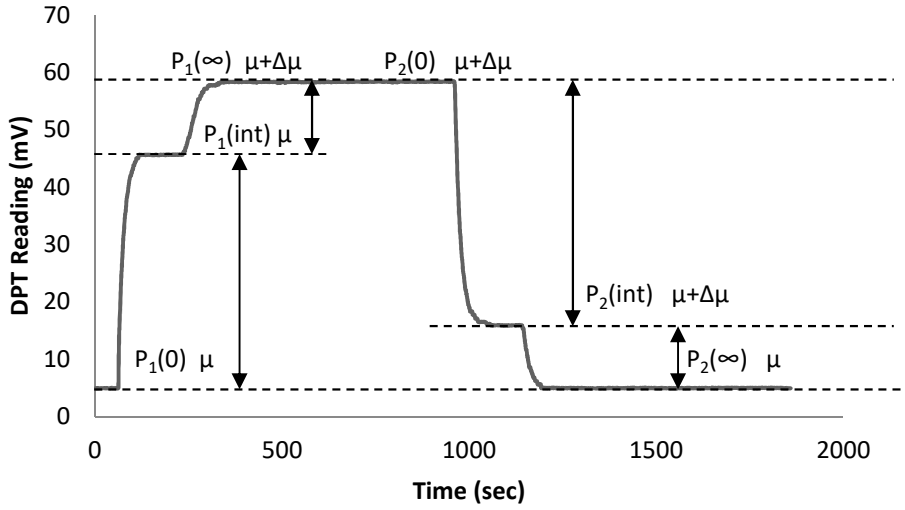

Figure 5.6 - Typical results graph when an argon perturbation flow is added to a nitrogen main flow

Four different experiments were carried out (see Table 5.1). For the first experiment, the baseline value of $P_1(t)$ was simply recorded for 500 seconds, with no perturbation being added. This was to determine the magnitude of any drifting in the baseline. The second experiment involved adding a nitrogen perturbation flow to a main flow of nitrogen. The perturbation flow was about 10% of the main flow. The third experiment also added a nitrogen perturbation flow to a main flow of nitrogen. The perturbation flow was about 1% of the main flow. Finally, the fourth experiment shows a similar experiment but using a different experimental arrangement.

Table 5.1 – Experiment carried out

Experiment	**Conditions**
1	Baseline determination
2	10% perturbation flow used
3	1% perturbation flow used
4	New experimental arrangement for better results

5.4.1. Calculation of Areas

The areas under the graphs were calculated using the trapezoidal rule. The difference between the baseline and each of the DPT readings were calculated using

$$\Delta DPT_t = DPT_t - DPT_B \tag{5.74}$$

where DPT_t and DPT_B are the DPT readings at any time, t and at the baseline respectively.

The trapezoidal rule was used to calculate the area in increments, therefore

$$A_p = \left(\frac{\Delta DPT_1 + \Delta DPT_2}{2}\right) \times \Delta t \tag{5.75}$$

The total graph area was then found by

$$A_T = \sum A_p \tag{5.76}$$

5.4.2. Interpretation of DPT Readings

The DPT gives reading in millivolts (mV). The DPT used has an output of ±1000 mV corresponding to an input of ± 100 Pa. This was large enough for detection of the perturbation flows that we were using.

1000 mV≡ 1000 mm H_2O = 10,000 Pa
Therefore 100 mV = 100 mm H_2O = 1000 Pa ≈ 0.01 bar = 10 mbar
In the results graph, a pressure change of 100 mV represents a pressure change of 10mbar.

5.5.Results

This section will present and interpret the results of the experiments described in Table 5.1 of Section 5.4 including the baseline determination and experiments using different perturbation flows and optimised experimental arrangement.

5.5.1. First Experiment - Baseline Test

As in the previous chapter, it is important that the baseline is constant. Any drifting in the baseline will affect the accuracy of the calculated areas. Figure 5.7 shows the baseline over a period of 500 seconds. Only nitrogen was added to the system.

The average DPT reading is 76.97±0.001 mV. Putting this DPT reading into perspective, a 0.1 mV baseline change corresponds to a pressure change of about 0.01 Pa. From Figure 5.7, it can be seen that the baseline does not change by a large amount. Therefore, the calculation of areas will not be affected greatly by drifting in the baseline.

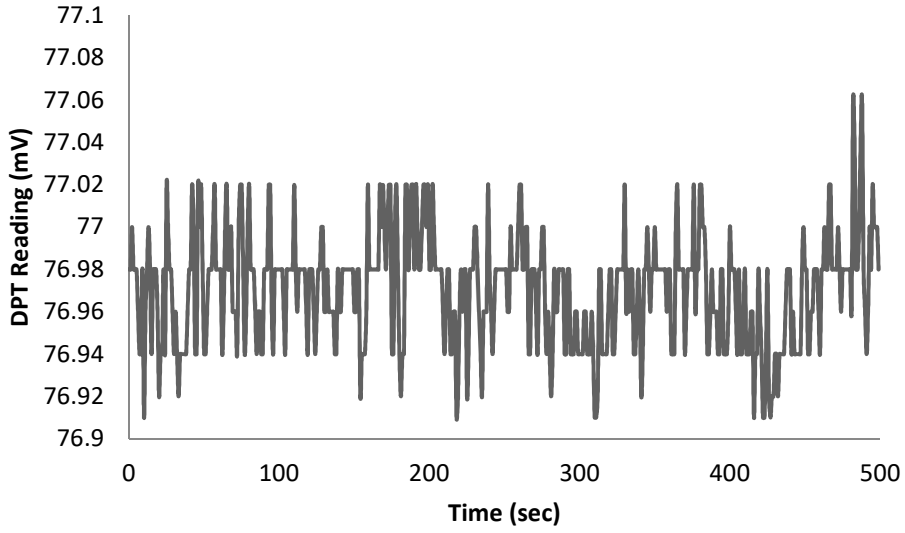

Figure 5.7 - Baseline of the DPT signal without the perturbation being added to the system

5.5.2. Second Experiment - Large Perturbation Flow (10% of main flow rate)

An experiment was conducted by adding a nitrogen perturbation flow at about 10% of the main flow to a main flow of nitrogen. The main flow was set to 100 ml/min therefore, the perturbation flow was about 10 ml/min. The DPT results are shown on the graph in Figure 5.8. The experiment was carried out by switching the three-way valve so that the perturbation flow is being added into the system. The addition of the perturbation flow causes an increase in pressure from $P_1(0)$ to $P_1(int)$. There is no change in pressure due to viscosity (as described in Section 5.3) because the same gas is being used for both the main and perturbation flows so $P_1(int) = P_1(\infty)$. Therefore, any change in pressure recorded from the DPT is solely due to the change in flowrate entering the system.

The areas under the graph, A_1 and A_2, were calculated using the trapezoidal rule (Equations 5.75 and 5.76) as described in the experimental procedure (Section 5.4.1). A_1 and A_2 were found to be 14380 mVs and 13231 mVs for the perturbation addition and removal respectively. It was expected that A_2 would be slightly greater than A_1 due to non-linearity of the flow detector. However, this is not the case here.

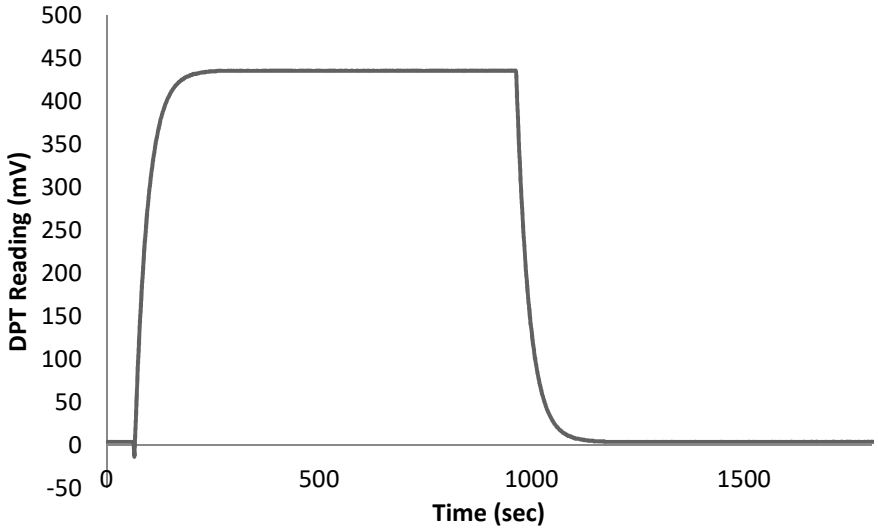

Figure 5.8 - DPT Readings for adding a 10% nitrogen perturbation(10ml/min) flow to a main flow of nitrogen (100 ml/min)

From Figure 5.8, it can be seen that there is a negative dip or pulse before the pressure increases. This negative pulse was found to be due to the method in which the perturbation flow is added to the system. There is a piece of tubing between the mass flow controller and the three way valve. Initially, this piece of tubing was at atmospheric pressure when the valve is positioned so that the perturbation flow is directed to the vent. When the valve is switched so that the perturbation flows to the system, the pressure in this piece of tubing needs to adjust and increase to the system pressure. This creates the negative peak. Therefore, the area under the graph increases. This is measured from the time the perturbation flow is added. Therefore, a correction must be made for this extra area. When the perturbation is removed from the system, the peak does not occur because this area of tubing is no longer involved in the system. Only the main flow is entering the system.

The extra area from the negative peak needs to be quantified. This is done by finding the ratio of the hold-up in the delay line and the extra tubing. This ratio and A_2 are then used to obtain the actual extra area that is added under the graph.

From the theory section, we know that the hold-up in the system is calculated from

$$dH = \frac{V}{RT}\, dP \qquad 3.29$$

The ratio of the hold-up in the delay-line and the tubing can be found from

$$\Delta H_{ratio} = \frac{\Delta H_{delay\ line}}{\Delta H_{tubing}} = \frac{V_{delay\ line}\,\Delta P_{delay\ line}}{V_{tubing}\Delta P_{tubing}} \qquad 5.77$$

The delay line is made from a 8 m length of 0.41 cm I.D nylon tubing. The tubing connecting the mass flow controller and the three-way valve is a 75 cm length of 0.23 cm I.D. nylon tubing. Therefore, the volume ratio is about 19.5.

The pressure drop along the delay line ($\Delta P_{delay\ line}$) is ΔP_1 from the DPT graph which is 0.0431 bar when the units are converted from mV. The pressure drop along the tubing was 0.16 bar. The pressure ratio was found to be 0.27. Therefore, the overall hold-up ratio was 9.38. This shows that the tubing between the mass flow controller and the three way valve accounts for quite a significant of hold-up in the system and hence a significant part of A_1.

The new area, $A_{1(new)}$, was calculated from

$$A_{1\,(new)} = A_{1\,(old)} - \left(\frac{A_2}{\Delta H_{ratio}}\right) \qquad 5.78$$

The new A_1 is therefore 12969.55 mVs. The ratio of areas is given by

$$Ratio\ of\ Areas = \frac{A_2}{A_{1(new)}} = \frac{13231}{12969.55} = 1.02 \qquad 5.79$$

This can be checked using the area equation derived in Section 5.3.3. From Equation 5.49

$$Area = V\mu\frac{k_A k_B}{k_A + k_B}\ln\left[1 + \frac{\Delta P_1}{2P_1(0) + \Delta P_1}\right] \qquad 5.49$$

The ratio of area can also be found as

$$Ratio\ of\ areas = \frac{A_2}{A_1} = \frac{\ln\left[1 - \frac{\Delta P_1}{2P_2(0) - \Delta P_1}\right]}{\ln\left[1 + \frac{\Delta P_1}{2P_1(0) + \Delta P_1}\right]} \qquad 5.80$$

The ratio of areas is 1.0187. There is a small difference in the area ratios. This could be due to many errors which could affect the areas including the sampling rate of the DPT or the mass flow controller not being accurate. These will be explored in the discussion section.

5.5.3. Third Experiment - Small Perturbation Flow (1% of main flow rate)

To ensure that this method was correct, the same procedure was followed to process the results of adding a smaller nitrogen perturbation (about 1% of the main flow) to a main flow of nitrogen. Figure 5.9 shows the results graph from this experiment. It can be clearly seen that the negative spike is a lot more significant here. This is because the pressure will be greater so will be more significant. Using the trapezoidal rule, A_1 and A_2 are calculated as 2363 mVs and 1098.5 mVs respectively.

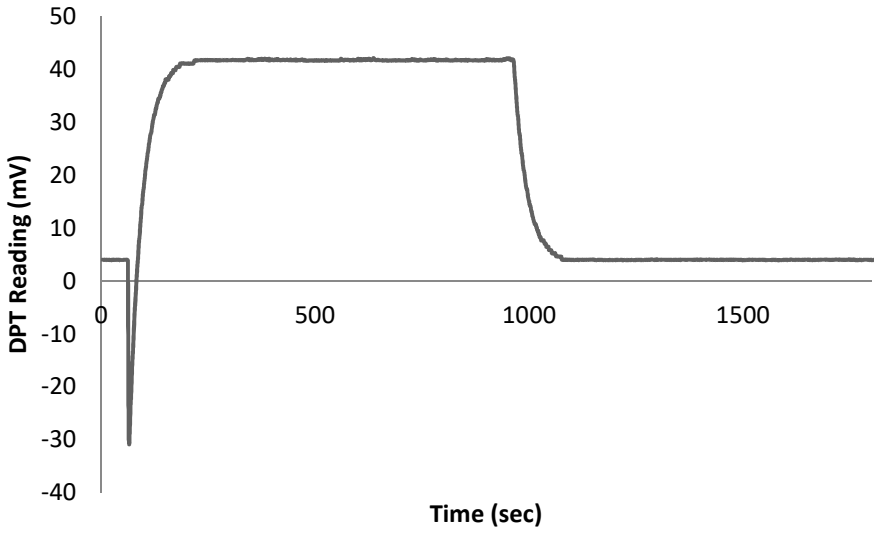

Figure 5.9 - DPT Readings for adding a 1% nitrogen perturbation flow(1ml/min) to a main flow of nitrogen(100ml/min)

From the result graph, ΔP_1 is 0.004 bar. The pressure drop along the tubing is constant at 0.16 bar and so the pressure ratio is 0.025. The volumes are the same for all the experiments so the hold-up ratio is 0.871. This gives a corrected A_1 of 1101 mVs.

The ratio of areas becomes

$$Ratio\ of\ Areas = \frac{A_2}{A_1} = \frac{1098.5}{1101} = 0.998 \qquad 5.81$$

To check this ratio, we use the area equation as before where ΔP_1 is 0.004 bar and $P_1(0)$ is 1.16 bar. The area ratio using this method is calculated to be 1.001. Again, there is a difference in the areas but these can be explained by the errors.

5.5.4. Fourth Experiment – New Equipment Arrangement

For this experiment, extra pieces of equipment were added to the system as shown in Figure 5.10. Similar issues and solutions were implimented by Mason *et al*. (1998) [38], Mason *et al.*(2000) [40] and Russell *et al.* (2005) [42]. In these works, a purge stream for the perturbation flow is added to the experimental arangement. The perturbation gas flows along this stream when not flowing in the measurement side of the system, allowing the flow in the system to remain constant when the perturbation flow is added.

In this experimental arrangement, the main flow was split into three streams instead of two. The third stream from the main flow was connected up to another steel resistance block shown in Figure 5.11. The block had one red flow element and one silver with a green dot flow element. The main flow enters and flows through the red element. The outlet of this is then connected to the inlet at the silver resistance. The vent flow from the three-way valve is also added to the inlet of the silver resistance instead of flowing to the atmosphere. This block mimics the system, as the resistances are the same as the main system and prevents the pressure difference between the system and the tubing from occuring. The outlet from the block is added to the reference and measurement sides and exits the system.

The same experimental procedure was followed. The perturbation flow was added and removed from the system by switching the three-way valve.

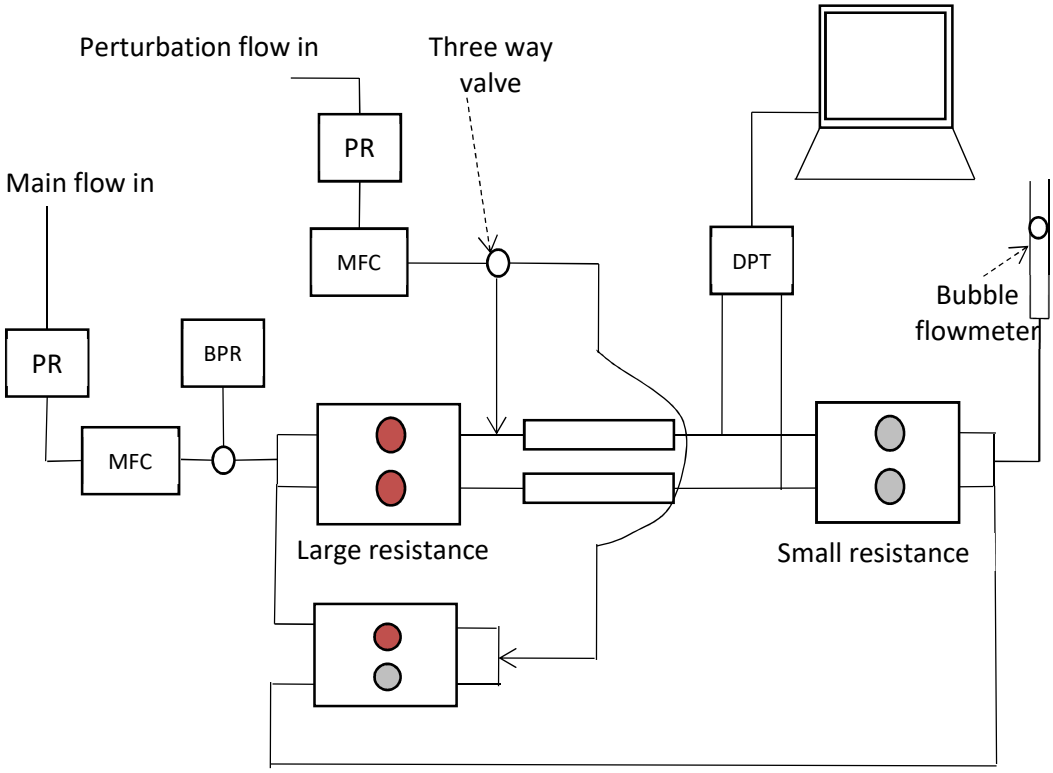

Figure 5.10 - Experimental Arrangement with extra block to eliminate the negative peak

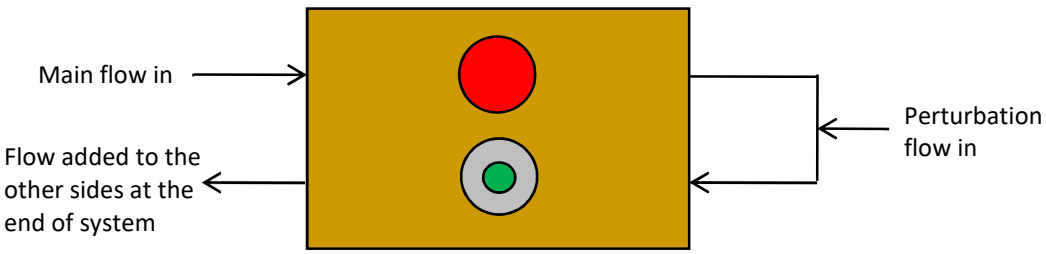

Figure 5.11 - Diagram of third block incorporated into the system

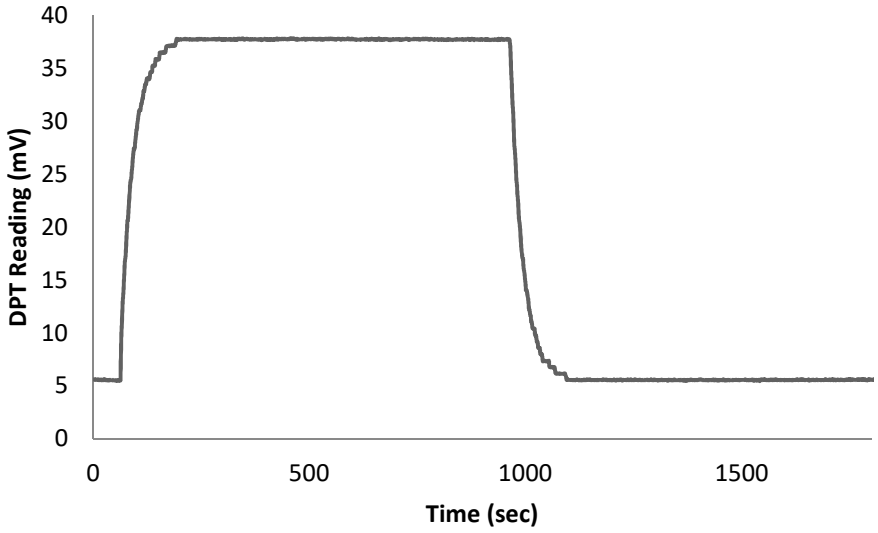

Figure 5.12 - DPT Readings for adding a 1.5% nitrogen perturbation (1ml/min) flow to a main flow of nitrogen (65ml/min)

Figure 5.12 shows a typical result after the extra block was added. The areas were calculated in the same way as before using the trapezoidal rule. The calculated areas for the experiment shown below were 889.98 and 942.32 mVs for A_1 and A_3 respectively. The ratio of areas is 1.06. By changing the arrangement, the negative has been eliminated but the areas are still not as close as expected. It seems that the pressure where the perturbation is added is now slightly higher than the system pressure. The higher pressure does not result in a positive peak. Instead it affects the area under the graph. This could be due to the slight differences in the flow resistances used or in the steel blocks.

5.6.Discussion

5.6.1. Baseline Test

As previously discussed in Section 4.6.1, it is important that the baseline in the experiments is relatively stable and free from noise and drift. As discussed in the previous chapter, any

drifting in the baseline will affect the accuracy of the area calculations. Figure 5.7 shows a DPT recording of the baseline for 500 seconds. The average DPT reading was 76.97 mV and the standard deviation was 0.001 mV. A DPT reading of 0.1 mV is equivalent to 0.01 Pa. Therefore, the baseline is adequately stable for the experiments.

5.6.2. Sampling Rate

During the experiments, a Furness Controls Differential Pressure Transducer was used and recordings were made using *Pico* 16-bit resolution software. Each of the experiments was run for 1860 seconds. The DPT recordings were plotted using Microsoft Excel and the areas were calculated using the trapezoidal rule. Due to constrictions with the data acquisition software, only one reading per second was recorded. This constriction could affect the area calculations. When the perturbation is added to the system, the pressure increases rapidly before levelling out. Therefore, the pressure will increase by a significant amount in one second. Due to the nature in which the areas are calculated using the trapezoidal rule (see Section 5.4.1), if the sampling rate could be reduced to one reading per 100 milliseconds or smaller than the area calculations would be more accurate.

5.6.3. Importance of selecting the correct baseline to determine areas

As described in the theory section, the area under the graph is calculated from

$$A_1 = \int_0^{\infty} [P_1(int) - P_1(t)]\ dt \qquad 5.3$$

$$A_2 = \int_0^{\infty} [P_2(t) - P_2(int)]\ dt \qquad 5.17$$

A_1 represents the perturbation addition experiment and A_2 represents the perturbation removal experiment. For these areas to be accurate, it is important that the correct value of $P_1(0)$, $P_1(int)$, $P_2(0)$ and $P_2(int)$ are used. The wrong value used in these integrals can affect the area calculations. A sensitivity analysis was carried out to examine how the calculated areas

depend on $P_1(int)$ and $P_2(int)$. The pressure drops and areas from experiment 4 were used to show how slight adjustments in either pressures can affect the area and hence the ratio of areas. The results are shown in Table 5.2.

Table 5.2 – Variation in area with pressures for Experiment 4

	Baseline P_1(int) (mV)	Area (mVs)		Baseline P_2(int) (mV)	Area (mVs)
A_1	132.18	895.73	A_2	164.38	936.75
A_1	132.2	893.13	A_2	164.4	939.37
A_1	132.22	890.53	A_2	164.42	941.99
A_1	132.24	887.93	A_2	164.44	944.61
A_1	132.26	885.33	A_2	164.46	947.23

It is expected that A_2 should be slightly greater than A_1 (see Section 5.6.4). The table shows that changing $P_1(int)$ or $P_2(int)$ by 0.02 mV will change the area by about 2.6 mVs.

Both the areas and the change in pressure, ΔP, are used to calculate the flow-rate retention time, τ_n as

$$\tau_n(s) = \frac{A_1(mVs)}{\Delta P_1(mV)} \qquad 5.82$$

The flow-rate retention time is a function of volume and so again, it is important that the baselines are as accurate as possible.

5.6.4. Comparison of Areas

It is expected that with larger perturbations, A_1 should be slightly greater than A_1. This is because of non-linearity of the flow detector. From the Hagen-Poiseuille equation,

$$P_1^2 - P_2^2 \propto 2kRT\mu M \qquad 5.83$$

Therefore, the flow rate M is not directly proportional to the pressure. If the perturbation flow is quite large, then the extra flow rate will affect the area as the pressures will be higher. If

the perturbation flow is small enough it will not make a significant effect on the area so the difference in areas should be negligible.

The theory tells us that

$$Area = V\mu \frac{k_A k_B}{k_A + k_B} \ln\left[1 + \frac{\Delta P_1}{2P_1(0) + \Delta P_1}\right] \quad 5.49$$

In the experiments conducted, the volume, viscosity and the resistances k_A and k_B are all constant. The only changes in the experiments are the flow rates and hence the pressures. The changes in pressure were used to check the accuracy of the calculated areas. So,

$$\frac{A_2}{A_1} = \frac{\ln\left[1 - \frac{\Delta P_1}{2P_2(0) - \Delta P_1}\right]}{\ln\left[1 + \frac{\Delta P_1}{2P_1(0) + \Delta P_1}\right]} \quad 5.73$$

Using a log series,

$$\ln[1 + x] = x - \frac{x^2}{2} + \frac{x^3}{3} \quad 5.84$$

If x is <<1 then $\ln[1 + x] \rightarrow x$ and so the area should be proportional to x.

In this case,

$$x = \frac{\Delta P_1}{2P_1(0) + \Delta P_1} \quad 5.85$$

Therefore, x is a function of ΔP_1 and $P_1(0)$ where ΔP_1 is the pressure change due to the change in flow-rate into the system. The change in flowrate is caused by the addition of the perturbation flow so if the perturbation flow is small, ΔP_1 will be small. When comparing the areas using the ratio as described in the results section, the smaller the perturbation flow, the closer the ratio is to 1.

To show a significant difference between the perturbation addition and removal experiments, a ΔP_1 value of approximately 0.1 bar is needed so that the step areas differ by about 5%.

The experiments have shown that the accuracy in the ratio of areas as calculated from the pressures is very high. Using this information is would be possible to rearrange the area equation to be used to find volumes or even the viscosity in the system.

5.6.5. The negative spike in the results

In the experiments, the integration is always started from the time at which the valve is switched. In experiments 2 and 3, there is a negative spike present after the perturbation is added which meant that the mass flow controller and associated tubing were at a lower pressure so the gas flows out of the mainstream and into the loop until this pressure increases to the system pressure. The integration is started when the perturbation enters the system, therefore the calculated area will include the extra contribution due to the extra length of tubing. It was necessary to correct the addition area, A_1, to remove the associated area from this effect. There were no peaks when the perturbation is removed from the system as the valve has been turned again and so the extra tubing is no longer part of the system.

The corrected area was calculated using the hold-up ratio of the delay line and the extra tubing from the mass flow controller. The hold-up in the system was calculated from

$$\Delta H = \frac{V}{RT}\, dP \qquad 3.29$$

This meant that the hold-up ratio was

$$\Delta H_{ratio} = \frac{V_{delay\ line}\, \Delta P_{delay\ line}}{V_{tubing} \Delta P_{tubing}} \qquad 5.77$$

The new addition area was then quantified from

$$A_{1\ (new)} = A_{1\ (old)} - \left(\frac{A_2}{\Delta H_{ratio}}\right) \qquad 5.78$$

The areas were then checked by calculating the ratio of areas and comparing it to the log equation (5.88).

To prevent the negative peak, an extra block was added to the system. This is shown in Figures 5.11 and 5.12. The extra block was set up so that instead of the three-way switching from the vent to the system resulting in a difference between the atmospheric pressure of the vent and the system pressure, it is switched from the extra block to the system. The extra block is there to mimic what is happening in the system with regards to the resistances. This should mean that the tubing between the mass flow controller and the valve should be at the same pressure as the system. The addition of the extra block means that the main flow is being split into 3 streams instead of 2. Therefore, the main flow rate will need to be increased in order to maintain the required flow rates. This solution of adding a third purge stream is similar to that used by Mason [38,40] and Russell [42].

Adding the extra block to the experimental arrangement resulted in the elimination of the negative peak after the valve is switched. The negative peak could also be reduced by ensuring that any extra tubing on the side-legs is kept to a minimum.

5.6.6. Future work

The theory tells us that

$$Area = V\mu \frac{k_A k_B}{k_A + k_B} \ln\left[1 + \frac{\Delta P_1}{2P_1(0) + \Delta P_1}\right] \qquad 5.86$$

This equation shows that the area is a function of volume, viscosity, the resistances k_A and k_B, and the pressure terms $P_1(0)$ and ΔP_1.

There are many different experiments that could be carried out to continue work using this equation. Firstly, experiments could be carried out using different gases. Using nitrogen as a main flow and argon as the perturbation flow should give results graphs similar to Figure 5.6. By using different gases, the pressure drop due to viscosity can now be considered and the viscosity term will become more significant.

Other work could also to carried by keeping the viscosity constant and varying the flow resistances, k_A and k_B. By keeping (k_A+ k_B) constant, this means that $\frac{k_A k_B}{k_A + k_B}$ has a maximum value when k_A= k_B.

It may also be useful to compare ΔP values. In the experiments that were carried out using nitrogen as the main and perturbation gases, it is more useful to look at the removal experiments as there were no peaks involved here. Plotting the perturbation percentage against ΔP_2 gives

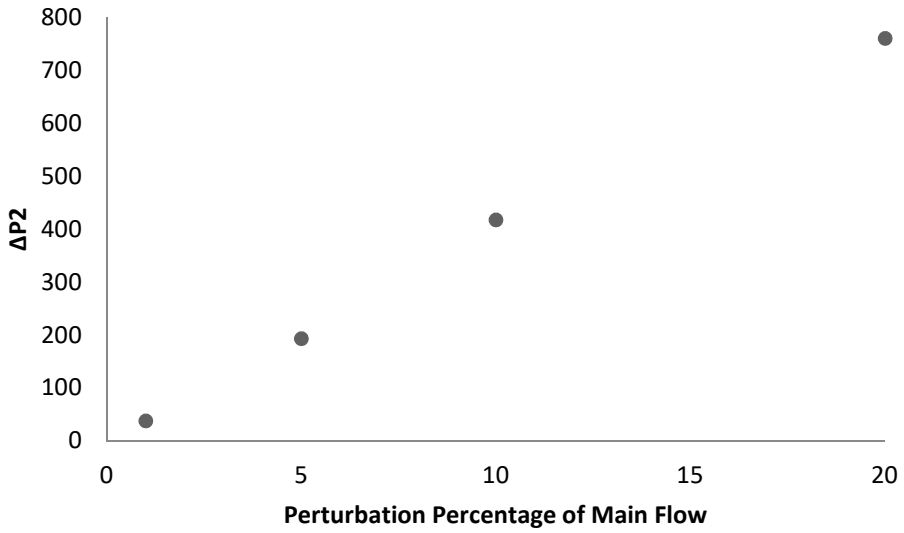

Figure 5.13 – Perturbation % of main flow versus ΔP_2 graph

Further work could be done on comparing the pressure changes using different gases as discussed previously.

5.7.Conclusions

It has been shown through a series of experiments that it is possible to calculate volumes by adding and removing a perturbation flow of gas into a system. A gas flows into the system at a constant rate. A perturbation flow is added to the system which changes the flow rate and thus the pressure in the system. This change in pressure can then be used to calculate volumes. There are a few limiting factors in the system including the reliability of the apparatus.

Further work could include using the theory developed here to find the viscosity when the volume is known or considering using different resistances whilst keeping the viscosity constant.

In this work, the main flow and perturbation flow have the same composition. In the next chapter, perturbations of different composition are added to the measurement side of the system. The effects of this are considered using a gas density detector as well as the differential pressure transducer.

6. Gas Density Detector

6.1. Introduction

This section looks to carry on work from the previous two chapters by considering binary components systems. Chapters 4 and 5 used single component systems and used pressure changes in a system and flow rate changes respectively. This chapter introduces the use of a gas density detector to be used in multi-component flux response systems.

The gas density detector (GDD) is compared to a hot-wire anemometer in constant temperature mode (see Section 6.2). Its operation is similar in that it operates using a pneumatic Wheatstone bridge arrangement where any imbalances results in an output response.

As in the previous chapters, a differential pressure transducer (DPT) will be used to measure flow rate and pressure changes. The GDD response will be used to measure changes in density of the gas mixture flowing through the system. It will also be used to aid in the composition determination of gas mixtures.

6.2. Background

Hot-wire anemometry is based on convective heat transfer to the surrounding fluid from an electrically heated wire or filament placed in a fluid flow. It is the principal research tool for most turbulent air/gas flow studies. It can be used to provide information related to the velocity and temperature of the flow, concentration changes in gas mixtures and phase changes in multi-phase flows [57,58].

A hot-wire anemometer is basically a thermal transducer. The principle of operation is an electric current is passed through a fine filament which is exposed to a cross flow. As the flow rate varies, the heat transfer from the filament varies. This causes a variation in the heat balance of the filament. The hot-wire sensor is made from a short length of resistance wire, circular in cross-section.

The filament is made from a material which possesses a temperature coefficient of resistance. If the temperature of the filament varies, so does its resistance. The variation in resistance is monitored by various electronic methods which give signals related to the variations in flow velocity or flow temperature. The hot-wire method can be used for measuring instantaneous velocities and temperature at a point in flow.

There are two modes of operation of a hot wire system, constant current mode and constant temperature mode [57-59]. In constant current mode, the current in the wire is kept constant and variations in wire resistance caused by the flow are measured by monitoring the voltage drop variations across the filament. In constant temperature mode, the filament is placed in a feedback circuit which tends to maintain the wire at constant resistance and hence constant temperature. Fluctuations in the cooling of the filament are seen as variations in wire current. The basic circuit for a constant temperature anemometer is shown in the Figure 6.1.

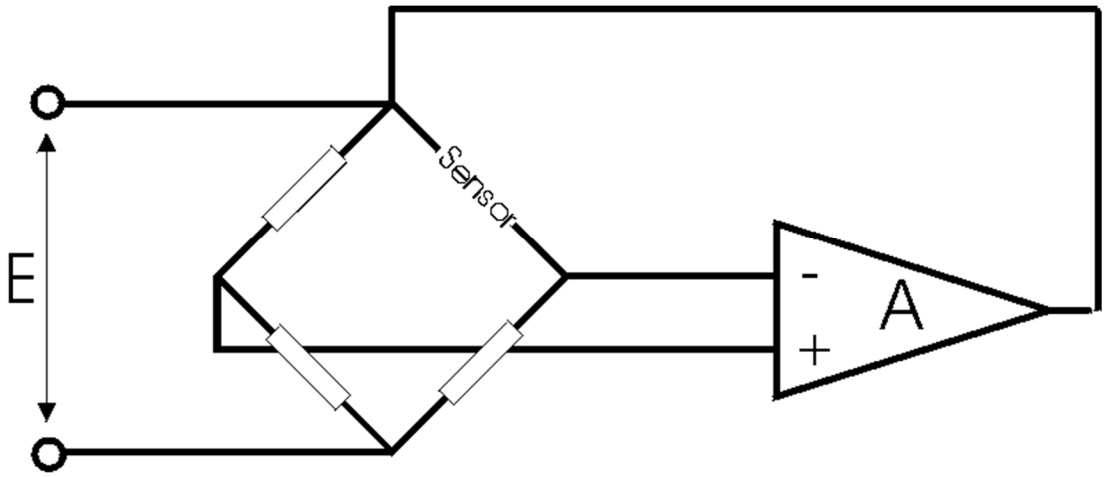

Figure 6.1 - Basic circuit for constant temperature hot-wire anemometer [59]

The gas density detector is basically a hot-wire anemometer operated in constant temperature mode. The operation of a hot-wire anemometer, and hence the gas density detector, is based on convective heat transfer and the basic principles of fluid flow.

The filaments are made of thin wire and are considered to be cylindrical sensors and so King's law can be applied when considering the operation of the hot-wire anemometer [60,61]. King

derived a solution for the heat transfer from an infinite cylinder in an incompressible, low Reynolds number flow. His equation is written as

$$Nu = A + B\,Re^{0.5} \tag{6.1}$$

where A and B are calibration constants.

The Nusselt number, Nu, can be determined using

$$Nu = \frac{h\,d}{k} \tag{6.2}$$

where h is the heat transfer coefficient $\left(\frac{W}{m^2 K}\right)$

d is the diameter of the filament (m)

k is the thermal conductivity of the fluid $\left(\frac{W}{m\,K}\right)$.

The heat transfer coefficient, h, is calculated by

$$h = \frac{q\ (heat)}{(\pi dL)(T - T_{amb})} \tag{6.3}$$

where $q\ (heat)$ is the heat loss (W)

(πdL) is the heat transfer area (m^2)

$(T - T_{amb})$ is the temperature difference (K).

This can be inserted into the equation for the Nusselt number giving

$$Nu = \frac{q\ (heat)}{\pi L\ k\ (T - T_{amb})} \tag{6.4}$$

In turn, this can be added to King's law to give the following equation

$$\frac{q\ (heat)}{\pi L\ k\ (T - T_{amb})} = A + B\left(\frac{\rho u d}{\mu}\right)^{0.5} \tag{6.5}$$

In a hot-wire anemometer in constant temperature mode, the rate of heat loss to the fluid by convection is equal to the electrical power input delivered to the sensor. The heat loss is related to the fluid properties and the wire resistance. Therefore, at a constant temperature,

$$q\ (heat) = \frac{V^2}{R} \qquad 6.6$$

where V is the voltage drop across the sensor
R is the electrical resistance

If the fluid properties and the wire resistance remain constant, the new King's law expression becomes

$$V^2 = A' + B'(u)^{0.5} \qquad 6.7$$

The hot wire anemometer measures the fluid velocity. The larger the velocity, the greater the heat loss. In the gas density detector, the heat loss and hence the voltage drop across the sensor depends on the flow rate of the reference flow over the sensor, Q and the density of the gas flowing over the sensor, ρ. Therefore, for the gas density detector the equation will become

$$V^2 = A' + B'(Q\rho)^{0.5} \qquad 6.8$$

At constant temperature and pressure, differentiating the above equation for flow rate, Q, and density, ρ, gives

$$2V\ dV = 0.5B'\rho^{0.5}\ Q^{-0.5}dQ \qquad 6.9$$

For the gas density detector work in this chapter, it is necessary to look at how the change in voltage in the detector affects the change in flow rate, $\frac{dV}{dQ}$, as a function of density and so it is beneficial to find out how, for a particular value of ($Q\rho$), the value of $\frac{dV}{dQ}$ varies with the density, ρ.

Rearranging

$$\frac{dV}{dQ} = \frac{1}{4}\frac{B'}{V}\left(\frac{\rho}{Q}\right)^{0.5} \qquad 6.10$$

The mass flow rate, M, is directly proportional to the volumetric flow rate, Q, and the density, ρ, and so if

$$M \propto (Q\rho) \rightarrow \frac{dV}{dQ} \propto \left[\frac{\rho^2}{M}\right]^{0.5} \rightarrow \frac{dV}{dQ} \propto \rho \qquad 6.11$$

This proves that the change in the voltage across the sensor as the fluid flow changes is directly proportional to the density.

6.3. Theory

Following on from the hot wire anemometry theory, the set-up and operation of the gas density detector will be considered. This section is looking to find a relationship in the gas density detector operation between the change in the flows within the system (Δq) and the change in the density of the gas mixture through the system (Δρ).

Firstly, the initial system will be considered without any perturbation being added to the sample flow. The pressure drops within the system will be derived using Bernoulli's equation and how the system resistances, flow rates and input gas properties are balanced around the internal loops in the GDD will be derived.

Secondly, the sample flow to the system will be perturbed by an additional flow, changing the sample composition. The pressure changes in the system caused by the altered composition will be considered along with the associated viscosity changes. It is assumed that the flow rate remains constant in order for the investigation of system pressure and viscosity changes with the change in sample flow composition can be examined. Material balances will be conducted around the GDD to understand how the change in the sample flow composition affects the GDD response.

Thirdly, the pressure, viscosity and flow rate changes will be investigated after a perturbation flow is added to the sample flow. In this section, it is assumed that the flow rate in the GDD has changed and looks at how this will affect the response from the GDD.

6.3.1. The Initial System

Figure *6.2* shows a diagram of the gas density detector with the reference and sample flows entering the system. Both the reference and the sample flows have the same composition.

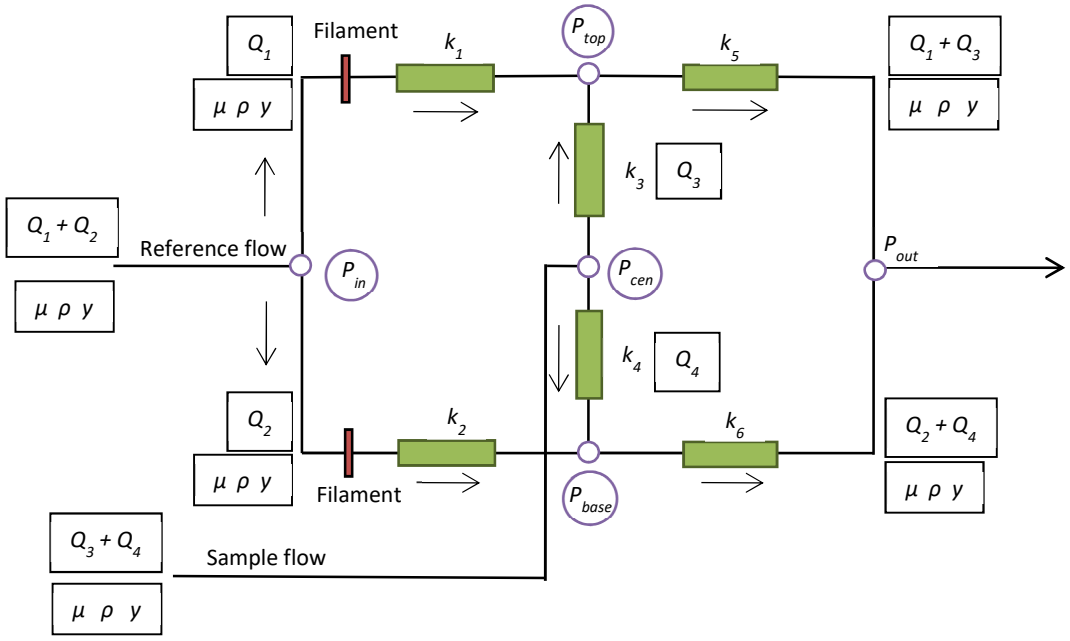

Figure 6.2 - Schematic diagram of the gas density detector before the perturbation flow is added

The reference flow ($Q_1 + Q_2$) enters the gas density detector and splits into two streams, one flowing up (Q_1) and one flowing down (Q_2). The sample flow ($Q_3 + Q_4$) enters the gas density detector and splits into an upper (Q_3) and lower (Q_4) stream. The density, viscosity and mole fraction of both flows are ρ, μ and y respectively. These remain constant throughout the experiment.

There are two filaments in the system, one in the upper stream and one in the lower stream. The filaments are set up in a Wheatstone bridge arrangement where the two filaments are part of a balanced bridge circuit. Any change in flow past the filaments will alter the filament temperature and the bridge circuit will become unbalanced. Here it will be considered how a change in density in the sample flow causes the flows (Q_1 and Q_2) to change. Initially, when the reference flow and sample flow (without any perturbation) are entering the gas density detector, the system is at equilibrium and any difference in filament temperatures should remain constant with time.

All the circled pressures can change as any adjustments are made to the system. The outlet pressure (P_{out}) remains constant as it is set by a back-pressure regulator.

It is essential to look at the pressure drops in the conduits of the detector to ensure that the system is balanced. To do this, the system is considered separately in three different loops, the initial loop, the sample flow loop and the reference flow loop. The initial loop incorporates the reference and sample flows entering the system. It is shown below in Figure *6.3* by the red dashed line.

The difference in elevation between the two pressure points being considered within the system is given by Δh. It is assumed to be an equal length in all conduits.

The reference and sample flows enter the loop at the points P_{in} and P_{cen} respectively. The loop flows in a clockwise direction from

$$P_{in} \rightarrow P_{top} \rightarrow P_{cen} \rightarrow P_{base} \rightarrow P_{in} \qquad 6.12$$

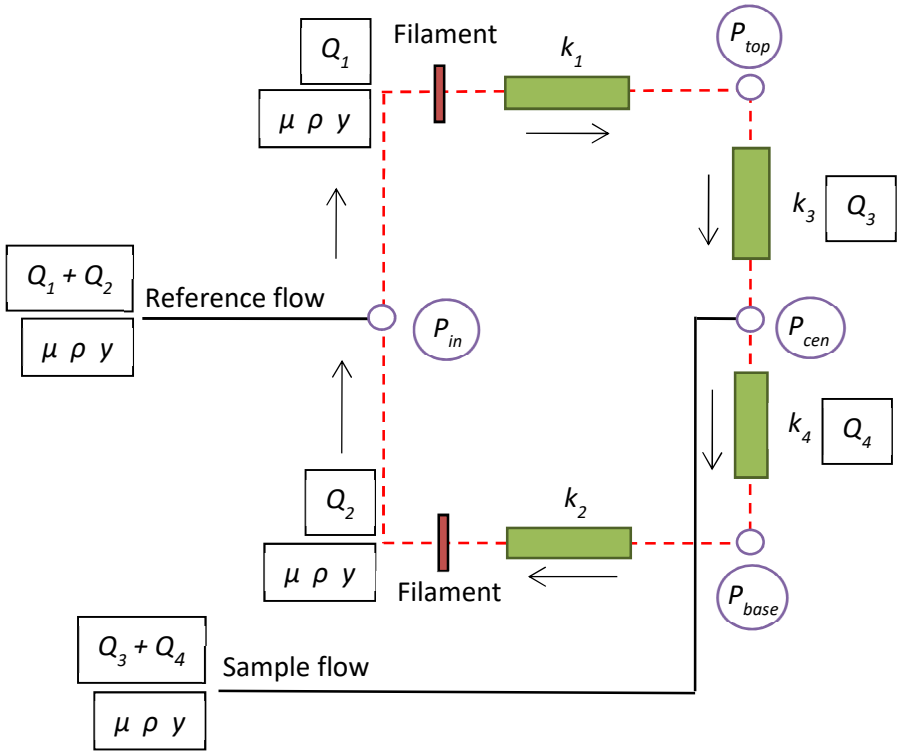

Figure 6.3 - The Initial Loop

Using Bernoulli's equation, the pressure drop around each section of the system is given by

$$P_{top} - P_{in} = -k_1 Q_1 \mu - \rho g \Delta h \quad 6.13$$

$$P_{cen} - P_{top} = k_3 Q_3 \mu + \rho g \Delta h \quad 6.14$$

$$P_{base} - P_{cen} = -k_4 Q_4 \mu + \rho g \Delta h \quad 6.15$$

$$P_{in} - P_{base} = k_2 Q_2 \mu - \rho g \Delta h \quad 6.16$$

The total pressure drop around the loop should be zero. Using these equations, the overall balance around the loop can be found.

$$\Delta P_{loop} = 0 = k_3 Q_3 - k_1 Q_1 + k_2 Q_2 - k_4 Q_4 \quad 6.17$$

This can be rearranged to give the overall balance around the initial loop

$$k_1 Q_1 + k_4 Q_4 = k_2 Q_2 + k_3 Q_3 \quad 6.18$$

It is assumed that there is symmetry in the resistances;

$k_1 = k_2 \qquad k_3 = k_4$

Therefore, equation 6.18 can be reduced to

$$k_1 (Q_1 - Q_2) = k_3 (Q_3 - Q_4) \quad 6.19$$

The sample flow loop around the system is shown below in Figure *6.4* by the red dashed line. Again, the loop flows in a clockwise direction from

$$P_{cen} \rightarrow P_{top} \rightarrow P_{out} \rightarrow P_{base} \rightarrow P_{cen} \quad 6.20$$

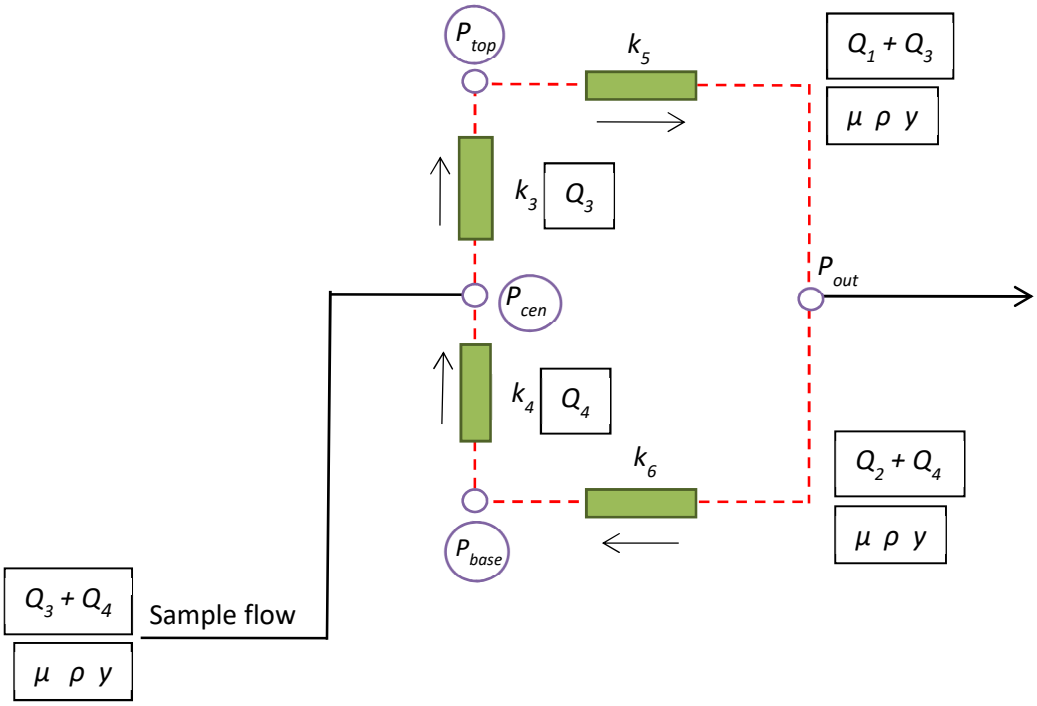

Figure 6.4 - The Sample Flow Loop

Using the Bernoulli's equation, the pressure drop around each section of the system is given by

$$P_{top} - P_{cen} = -k_3 Q_3 \mu - \rho g \Delta h \qquad 6.20$$

$$P_{out} - P_{top} = -k_5 (Q_1 + Q_3)\mu + \rho g \Delta h \qquad 6.22$$

$$P_{base} - P_{out} = k_6 (Q_2 + Q_4)\mu + \rho g \Delta h \qquad 6.21$$

$$P_{cen} - P_{base} = k_4 Q_4 \mu - \rho g \Delta h \qquad 6.24$$

The difference in elevation between the two pressure points being considered within the system is given by Δh. It is assumed to be an equal length in all conduits.

From these equations, the overall balance around the loop is

$$\Delta P_{loop} = 0 = -k_3 Q_3 - k_5 (Q_1 + Q_3) + k_4 Q_4 + k_6 (Q_2 + Q_4) \qquad 6.25$$

This can be rearranged to give the overall balance around the sample flow loop

$$k_3Q_3 + k_5(Q_1 + Q_3) = k_4Q_4 + k_6(Q_2 + Q_4) \qquad 6.26$$

The reference flow loop around the system is shown below in Figure *6.5* by the red dashed line. Again, the loop flows in a clockwise direction from

$$P_{in} \rightarrow P_{top} \rightarrow P_{out} \rightarrow P_{base} \rightarrow P_{in} \qquad 6.27$$

Using the Bernoulli's equation, the pressure drop around each section of the system is given by

$$P_{top} - P_{in} = -k_1Q_1\mu - \rho g\Delta h \qquad 6.28$$

$$P_{out} - P_{top} = -k_5(Q_1 + Q_3)\mu + \rho g\Delta h \qquad 6.229$$

$$P_{base} - P_{out} = k_6(Q_2 + Q_4)\mu + \rho g\Delta h \qquad 6.30$$

$$P_{in} - P_{base} = k_2Q_2\mu - \rho g\Delta h \qquad 6.31$$

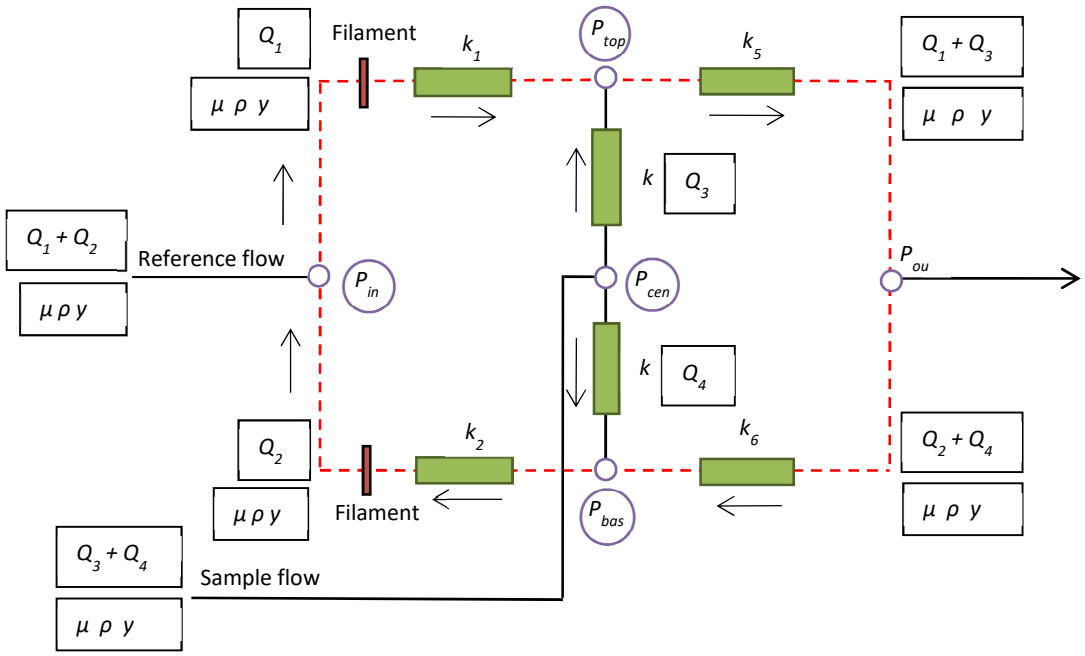

Figure 6.5 - The Reference Flow Loop

From these equations, the overall balance around the loop is

$$\Delta P_{loop} = 0 = -k_1 Q_1 - k_5(Q_1 + Q_3) + k_2 Q_2 + k_6(Q_2 + Q_4) \qquad 6.32$$

This can be rearranged to give the overall balance around the reference flow loop

$$k_1 Q_1 + k_5(Q_1 + Q_3) = k_2 Q_2 + k_6(Q_2 + Q_4) \qquad 6.33$$

To try to reduce some of the terms in the balances above, it is assumed that there is symmetry in the resistances;

$k_1 = k_2 \qquad k_3 = k_4 \qquad k_5 = k_6$

Therefore, the overall balances in Equations 6.25 and 6.32 become

$$k_3(Q_3 - Q_4) = k_5(Q_2 + Q_4 - Q_1 - Q_3) \qquad 6.23$$

$$k_1(Q_1 - Q_2) = k_5(Q_2 + Q_4 - Q_1 - Q_3) \qquad 6.24$$

Rearranging Equation 6.34 gives

$$(k_3 + k_5)(Q_3 - Q_4) = -k_5(Q_1 - Q_2) \qquad 6.25$$

If it is assumed that there is no resistance to flow after the reference and sample flows meet, then $k_5 = 0$, and Equation 6.36 above becomes $Q_3 = Q_4$. This can then be inserted into Equation 6.19 allowing this to become $Q_1 = Q_2$.

Therefore, in future calculations, it can be assumed that if $k_5 \ll k_1, k_3$ then $Q_1 + Q_3 = Q_2 + Q_4$.

6.3.2. Perturbation added to Sample Flow - Flow remains constant

This section considers the effect of a change being made to the system by perturbing the sample flow. It is assumed that the addition or removal of the perturbation causes the composition of the sample flow to change but the flow rate of the sample stream remains the same. Therefore, $(Q_1 + Q_2)$ and $(Q_3 + Q_4)$ remain the same. The effect on sample flow rate by the addition of a perturbation flow is considered in the next section.

6.3.2.1. Pressure Changes in the GDD

Figure 6.6 shows a diagram of the gas density detector after the composition has changed due to a perturbation to the sample flow. The changes in the gas properties and the system flow rates are considered.

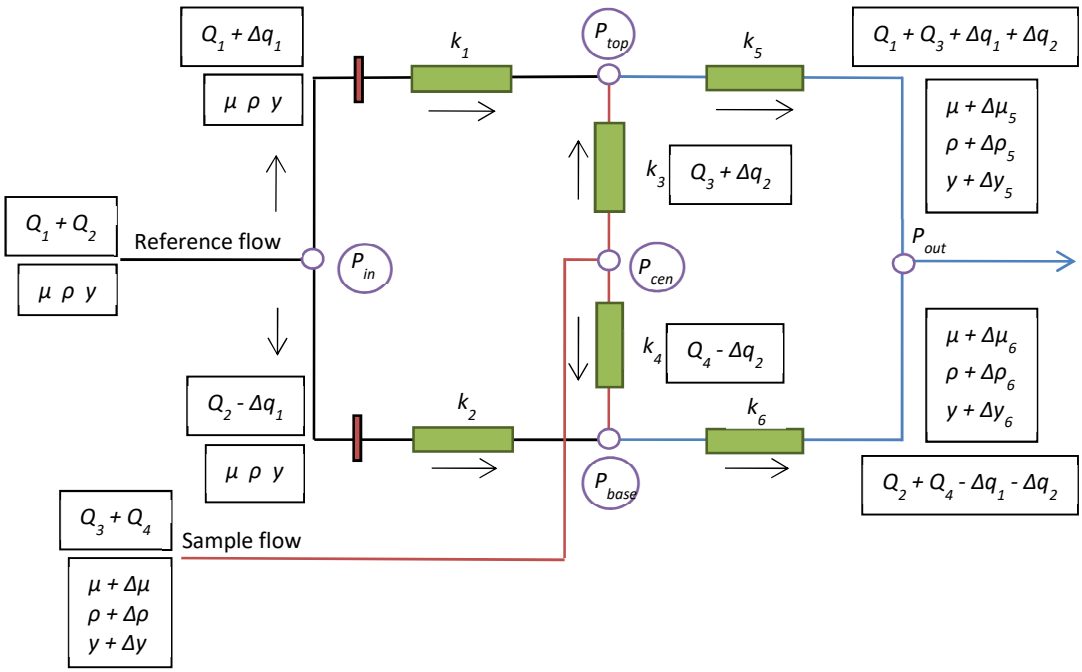

Figure 6.6 - Schematic diagram of the gas density detector after the perturbation is added but the flow stays constant

The reference and sample flows are still $(Q_1 + Q_2)$ and $(Q_3 + Q_4)$ respectively. The reference flow has density, ρ, viscosity, μ, and mole fraction, y. The density, viscosity and mole fraction of the sample stream are now $(\rho + \Delta\rho)$, $(\mu + \Delta\mu)$ and $(y + \Delta y)$ respectively.

When the perturbation is added to the sample stream, flow rates Q_1 and Q_2 change but the sum of the two flow rates will still be the same. These changes are dependent on the new density of the sample stream. If the density of the sample flow is greater than that of the reference flow, then when the sample stream splits, the lower stream will have a greater flow than the upper stream. This will result in reference flow streams changing. The upper stream will increase ($Q_1 + \Delta q_1$) and the lower stream will decrease ($Q_2 - \Delta q_1$). These changes in flow mean that the filament temperatures will change. The changes in filament temperatures are used to detect the change in density in the sample stream. The sample flows, Q_3 and Q_4, will change by Δq_2 which can be positive or negative depending on whether the sample flow density increases or decreases after the perturbation flow is added.

Like in Figure *6.2*, all the circled pressures change. P_{out} remains constant and is set by a back-pressure regulator to 0.05 bar.

After the perturbation is added, the pressures in the system will change to

$$P_{in} \rightarrow P_{in} + \Delta P_{in} \tag{6.26}$$

$$P_{top} \rightarrow P_{top} + \Delta P_{top} \tag{6.27}$$

$$P_{cen} \rightarrow P_{cen} + \Delta P_{cen} \tag{6.28}$$

$$P_{base} \rightarrow P_{base} + \Delta P_{base} \tag{6.29}$$

Applying Bernoulli's equation, the starting equations, before any perturbation is added, around P_{in}, P_{cen} and P_{out} are

$$P_{in} - P_{top} = k_1 Q_1 \mu + \rho g \Delta h \tag{6.30}$$

$$P_{in} - P_{base} = k_2 Q_2 \mu - \rho g \Delta h \tag{6.31}$$

$$P_{cen} - P_{top} = k_3 Q_3 \mu + \rho g \Delta h \tag{6.32}$$

$$P_{cen} - P_{base} = k_4 Q_4 \mu - \rho g \Delta h \quad 6.33$$

$$P_{top} - P_{out} = k_5 (Q_1 + Q_3) \mu - \rho g \Delta h \quad 6.34$$

$$P_{base} - P_{out} = k_6 (Q_2 + Q_4) \mu + \rho g \Delta h \quad 6.35$$

Each stream in the diagram will be looked at individually to see how changing the sample flow composition (and hence density) affects the pressures and the flows through the different branches of the system.

Firstly, the reference flow loop is investigated. To start, P_{in} is considered. The upper stream from P_{in} to P_{top} is initially represented by Equation 6.17. After the perturbation is added, pressures P_{in} and P_{top} and flowrate Q_1will change if the composition of the perturbation is different. The Bernoulli equation will become

$$(P_{in} + \Delta P_{in}) - \left(P_{top} + \Delta P_{top}\right) = k_1 (Q_1 + \Delta q_1) \mu + \rho g \Delta h \quad 6.36$$

The viscosity and density do not change as it is still only the reference flow flowing through the branch. Subtracting Equation 6.41 from 6.47 gives

$$\Delta P_{in} - \Delta P_{top} = k_1 \Delta q_1 \mu \quad 6.37$$

This gives an equation relating the changes in pressure at the inlet of the reference flow and the top stream to the change in flowrate going through the upper branch.

The lower stream from P_{in} is considered. The initial Bernoulli equation is shown in Equation 6.42. After the perturbation is added to the sample flow and the equation becomes

$$(P_{in} + \Delta P_{in}) - (P_{base} + \Delta P_{base}) = k_2 (Q_2 - \Delta q_1) \mu - \rho g \Delta h \quad 6.38$$

The viscosity and density remain constant. Subtracting Equation 6.42 from 6.49 gives

$$\Delta P_{in} - \Delta P_{base} = k_2(-\Delta q_1)\mu \qquad 6.39$$

This gives an equation relating the changes in pressure at the inlet and the bottom stream to the change in flowrate going through the lower branch.

Secondly, P_{out} is considered. The upper stream from $P_{top}$to P_{out} is initially represented by Equation 6.45. The perturbation flow is added and the equation becomes

$$\begin{aligned}(P_{top} + \Delta P_{top}) - \ & P_{out} \\ & = k_5(Q_1 + Q_3 + \Delta q_1 + \Delta q_2)(\mu + \Delta\mu_5) \\ & - (\rho + \Delta\rho_5)g\Delta h\end{aligned} \qquad 6.40$$

The composition change due to the addition of the perturbation means that the viscosity and density have changed by $\Delta\mu_5$ and $\Delta\rho_5$ respectively. The flowrate to P_{out} , $(Q_1 + Q_3)$ will change by $(\Delta q_1 + \Delta q_2)$. As previously mentioned, P_{out} is constant so subtracting Equation 6.45 from 6.51 gives

$$\Delta P_{top} = k_5[(Q_1 + Q_3 + \Delta q_1 + \Delta q_2)\Delta\mu_5 + (\Delta q_1 + \Delta q_2)\mu] - \Delta\rho_5\, g\Delta h \qquad 6.41$$

Therefore, there is an equation defining the pressure change in the top branch of the system after the perturbation is added to the system.

The lower branch from P_{base} to P_{out} is considered. This is initially represented in Equation 6.46. After the perturbation is added

$$\begin{aligned}(P_{base} + \Delta P_{base}) - \ & P_{out} \\ & = k_6(Q_2 + Q_4 - \Delta q_1 - \Delta q_2)(\mu + \Delta\mu_6) \\ & - (\rho + \Delta\rho_6)g\Delta h\end{aligned} \qquad 6.42$$

Again, the composition has changed due to the addition of the perturbation. P_{out} is constant so subtracting Equation 6.46 from 6.53 gives

$$\Delta P_{base} = k_6[(Q_2 + Q_4 - \Delta q_1 - \Delta q_2)\Delta\mu_6 - (\Delta q_1 + \Delta q_2)\mu] + \Delta\rho_6\, g\Delta h \quad 6.43$$

This results in an equation describing the pressure change in the lower branch after the perturbation is added to the system.

Pressure changes ΔP_{top} and ΔP_{base} have now been defined. Equations 6.48 and 6.50 can both be rearranged for ΔP_{in};

$$\Delta P_{in} = \Delta P_{top} + k_1\Delta q_1\mu = \Delta P_{base} - k_2\Delta q_1\mu \quad 6.44$$

The definitions for ΔP_{top} and ΔP_{base} from Equations 6.52 and 6.54 can then be inserted and equated to give

$$\begin{aligned} k_5[(Q_1 + Q_3 + \Delta q_1 + \Delta q_2)\Delta\mu_5 + (\Delta q_1 + \Delta q_2)\mu] - \Delta\rho_5\, g\Delta h \\ + k_1\Delta q_1\mu \\ = k_6[(Q_2 + Q_4 - \Delta q_1 - \Delta q_2)\Delta\mu_6 - (\Delta q_1 + \Delta q_2)\mu] \\ + \Delta\rho_6\, g\Delta h - k_2\Delta q_1\mu \end{aligned} \quad 6.45$$

If the reference and sample flows split equally to the upper and lower branches, $Q_1 + Q_3 = Q_2 + Q_4$, and assuming $k_5 = k_6$, the equation for the reference flow loop becomes

$$\begin{aligned} (\Delta\rho_5 + \Delta\rho_6)g\Delta h \\ = (k_1 + k_2 + k_5 + k_6)\mu\,\Delta q_1 + (k_5 + k_6)\mu\,\Delta q_2 \\ + k_5(Q_1 + Q_3)(\,\Delta\mu_5 - \Delta\mu_6) \\ + k_5(\Delta q_1 + \Delta q_2)(\,\Delta\mu_5 + \Delta\mu_6) \end{aligned} \quad 6.46$$

This results in an equation relating the change in flowrates (Δq_1 and Δq_2) within the system, from points $P_{in}$to P_{out} around the reference flow loop, to the change in density ($\Delta\rho_5$ and $\Delta\rho_6$) caused by adding the perturbation.

Finally, the sample flow loop and P_{cen} are considered. The upper stream from P_{cen} to P_{top} is initially represented in Equation 6.43. After the perturbation is added and the composition is changed, the equation becomes

$$(P_{cen} + \Delta P_{cen}) - \left(P_{top} + \Delta P_{top}\right) = k_3(Q_3 + \Delta q_2)(\mu + \Delta\mu) + (\rho + \Delta\rho)g\Delta h \quad 6.47$$

The composition change due to the addition of the perturbation means that the viscosity and density have changed by $\Delta\mu$ and $\Delta\rho$ respectively. The flowrate Q_3 will change by Δq_2. Subtracting Equation 6.43 from 6.58 gives

$$\Delta P_{cen} - \Delta P_{top} = k_3[(Q_3 + \Delta q_2)\,\Delta\mu + \mu\,\Delta q_2] + \Delta\rho\; g\Delta h \quad 6.48$$

This gives an equation relating the changes in pressure at the inlet of the sample flow and the top stream to the change in flowrate going through the upper branch, the change in viscosity and the change in density due to the addition of the perturbation to the sample stream.

The lower stream from P_{cen} to P_{base} is considered. Initially, this is represented by the Bernoulli Equation 6.44. The perturbation is added and the equation becomes

$$(P_{cen} + \Delta P_{cen}) - (P_{base} + \Delta P_{base}) = k_4(Q_4 - \Delta q_2)(\mu + \Delta\mu) - (\rho + \Delta\rho)g\Delta h \quad 6.49$$

Again, the flowrate, viscosity and density of the gas mixture have changed due to the addition of the perturbation. Subtracting Equation 6.44 from 6.58 gives

$$\Delta P_{cen} - \Delta P_{base} = k_4[(Q_4 - \Delta q_2)\,\Delta\mu - \mu\,\Delta q_2] - \Delta\rho\; g\Delta h \quad 6.50$$

This gives an equation relating the changes in pressure at the inlet of the sample flow and the bottom stream to the change in flowrate going through the lower branch, the change in viscosity and the change in density due to the addition of the perturbation to the sample stream.

Equations 6.59 and 6.61 can be rearranged for ΔP_{cen} ;

$$\Delta P_{cen} = \Delta P_{top} + k_3[(Q_3 + \Delta q_2)\,\Delta\mu + \mu\,\Delta q_2] + \Delta\rho\; g\Delta h = \Delta P_{base} + k_4[(Q_4 - \Delta q_2)\,\Delta\mu - \mu\,\Delta q_2] - \Delta\rho\; g\Delta h \quad 6.51$$

The definitions for ΔP_{top} and ΔP_{base} from Equations 6.52 and 6.54 can then be inserted and equated to give

$$\begin{aligned} k_5[(Q_1 + Q_3 + \Delta q_1 + \Delta q_2)\Delta\mu_5 + (\Delta q_1 + \Delta q_2)\mu] - \Delta\rho_5\, g\Delta h \\ + k_3[(Q_3 + \Delta q_2)\,\Delta\mu + \mu\,\Delta q_2] + \Delta\rho\, g\Delta h \\ = k_6[(Q_2 + Q_4 - \Delta q_1 - \Delta q_2)\Delta\mu_6 - (\Delta q_1 + \Delta q_2)\mu] \\ + \Delta\rho_6 g\Delta h + k_4[(Q_4 - \Delta q_2)\,\Delta\mu - \mu\,\Delta q_2] - \Delta\rho\, g\Delta h \end{aligned} \qquad 6.52$$

It is assumed that the reference and sample flows split equally to the upper and lower branches, so $Q_1 + Q_3 = Q_2 + Q_4$, and the resistances $k_3 = k_4$ and $k_5 = k_6$. The equation for the sample flow loop becomes

$$\begin{aligned} (\Delta\rho_5 + \Delta\rho_6 - 2\Delta\rho)\, g\Delta h \\ = (k_3 + k_4 + k_5 + k_6)\,\mu\Delta q_2 + (k_5 + k_6)\,\mu\Delta q_1 \\ + k_3(Q_3 + \Delta q_2)\Delta\mu - k_3(Q_3 - \Delta q_2)\Delta\mu \\ + k_5(Q_1 + Q_3)(\,\Delta\mu_5 - \Delta\mu_6) \\ + k_5(\Delta q_1 + \Delta q_2)(\,\Delta\mu_5 + \Delta\mu_6) \end{aligned} \qquad 6.53$$

An equation relating the change in flowrates within the system, from P_{cen} to P_{out} around the sample flow loop, to the change in density caused by adding the perturbation has been determined.

6.3.2.2. Viscosity Changes in the GDD

Both Equations 6.57 and 6.64 give equations relating the change in flowrates, Δq_1 and Δq_2, due to the addition of the perturbation, to the change in densities, $\Delta\rho_5$ and $\Delta\rho_6$. These equations have terms which include change in viscosity terms, $\Delta\mu_5$ and $\Delta\mu_6$. These viscosity terms will be looked at in this section.

Figure *6.7* shows a graph relating the viscosity and the mole fraction of the sample flow entering the gas density detector. Here it has been assumed that there is linear variation of viscosity with mole fraction.

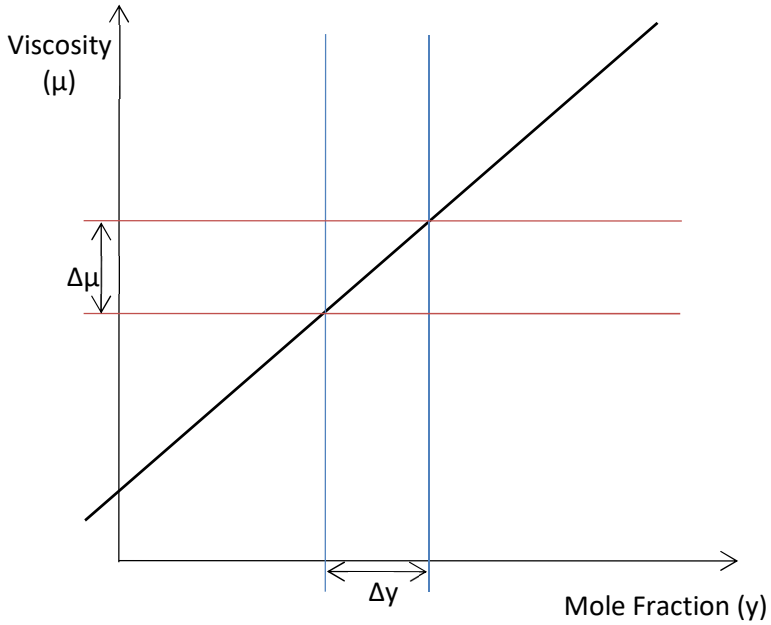

Figure 6.7 - Graph relating viscosity to mole fraction

The graph shows that if the viscosity changes by Δμ then the mole fraction will change by Δy. Therefore, the following equations can be assumed

$$\Delta\mu_5 = g_{visc}\,\Delta y_5 \qquad 6.54$$

$$\Delta\mu_6 = g_{visc}\,\Delta y_6 \qquad 6.55$$

where g_{visc} is the gradient of the line in the graph.

Equations for Δy_5 and Δy_6 can be derived from balancing the mole fractions at the points where the reference and sample flows meet in the upper and lower branches. Figure *6.8* shows the flows and mole fractions in the upper branch of the system.

A balance over the top branch gives

$$(Q_1 + \Delta q_1)y + (Q_3 + \Delta q_2)(y + \Delta y) = (Q_1 + Q_3 + \Delta q_1 + \Delta q_2)(y + \Delta y_5) \qquad 6.56$$

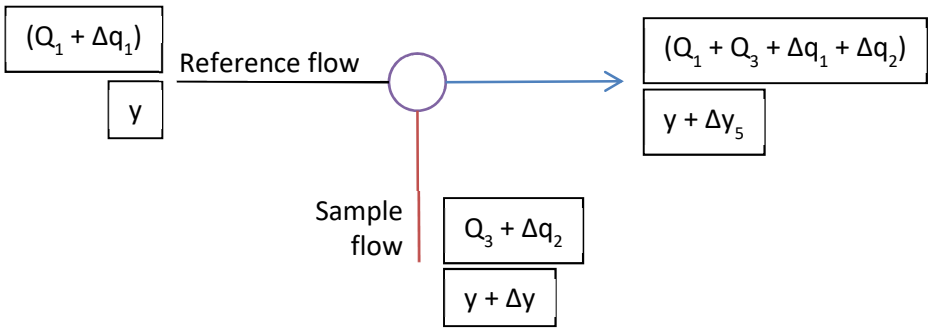

Figure 6.8 - Flows and mole fractions in the top branch of the system when the sample flowrate remains constant

This can be simplified to

$$\Delta y_5 = \frac{\Delta y(Q_3 + \Delta q_2)}{(Q_1 + Q_3 + \Delta q_1 + \Delta q_2)} \qquad 6.57$$

Similarly, Figure *6.9* shows the flows and mole fractions in the lower branch of the system.

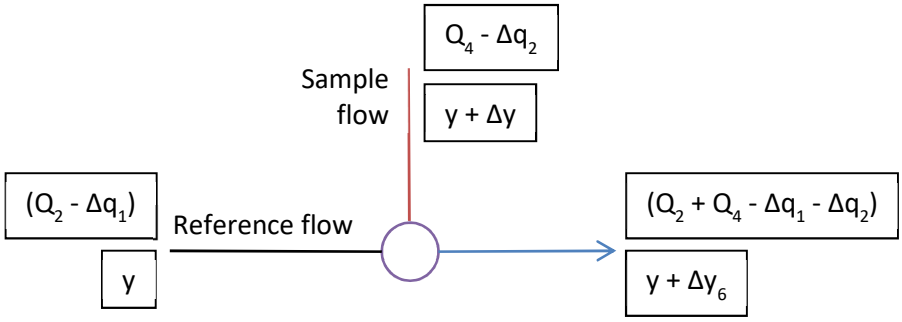

Figure 6.9 - Flows and mole fractions in the bottom branch of the system when the sample flowrate remains constant

A balance over the bottom branch gives

$$(Q_2 - \Delta q_1)y + (Q_4 - \Delta q_2)(y + \Delta y) = (Q_2 + Q_4 - \Delta q_1 - \Delta q_2)(y + \Delta y_6) \qquad 6.58$$

This can be rearranged and simplified to

$$\Delta y_6 = \frac{\Delta y(Q_4 - \Delta q_2)}{(Q_2 + Q_4 - \Delta q_1 - \Delta q_2)} \tag{6.59}$$

Equations 6.68 and 6.70 can be inserted into Equations 6.65 and 6.66 to give derivations for the change in viscosity

$$\Delta\mu_5 = g_{visc}\Delta y\left[\frac{(Q_3 + \Delta q_2)}{(Q_1 + Q_3 + \Delta q_1 + \Delta q_2)}\right] \tag{6.60}$$

$$\Delta\mu_6 = g_{visc}\Delta y\left[\frac{(Q_4 - \Delta q_2)}{(Q_2 + Q_4 - \Delta q_1 - \Delta q_2)}\right] \tag{6.61}$$

In Equation 6.57, the changes in viscosity terms associated with the change in flow in the reference flow loop are

$$k_5(Q_1 + Q_3)(\Delta\mu_5 - \Delta\mu_6) + k_5(\Delta q_1 + \Delta q_2)(\Delta\mu_5 + \Delta\mu_6) \tag{6.62}$$

An equation for $(\Delta\mu_5 + \Delta\mu_6)$ can be formed by inserting Equations 6.71 and 6.72

$$(\Delta\mu_5 + \Delta\mu_6) = g_{visc}\Delta y\left[\frac{(Q_3 + \Delta q_2)}{(Q_1 + Q_3 + \Delta q_1 + \Delta q_2)} + \frac{(Q_4 - \Delta q_2)}{(Q_2 + Q_4 - \Delta q_1 - \Delta q_2)}\right] \tag{6.63}$$

By assuming that the reference and sample flows split equally, $Q_1 = Q_2$ and $Q_3 = Q_4$, the equation becomes

$$(\Delta\mu_5 + \Delta\mu_6) = g_{visc}\Delta y\left[\frac{(Q_3 + \Delta q_2)}{(Q_1 + Q_3 + \Delta q_1 + \Delta q_2)} + \frac{(Q_3 - \Delta q_2)}{(Q_1 + Q_3 - \Delta q_1 - \Delta q_2)}\right] \tag{6.64}$$

This is rearranged to give

$$(\Delta\mu_5 + \Delta\mu_6) = g_{visc}\Delta y\left[\frac{2Q_3(Q_1+Q_3) - 2\Delta q_2(\Delta q_1 + \Delta q_2)}{(Q_1+Q_3)^2 - (\Delta q_1 + \Delta q_2)^2}\right] \quad 6.65$$

Similarly, $(\Delta\mu_5 - \Delta\mu_6)$ can be found by inserting 6.71 and 6.72

$$(\Delta\mu_5 - \Delta\mu_6) = g_{visc}\Delta y\left[\frac{(Q_3 + \Delta q_2)}{(Q_1+Q_3+\Delta q_1+\Delta q_2)} - \frac{(Q_4 - \Delta q_2)}{(Q_2+Q_4-\Delta q_1-\Delta q_2)}\right] \quad 6.66$$

Again, assuming that the reference and sample flows split equally, $Q_1 = Q_2$ and $Q_3 = Q_4$, the equation becomes

$$(\Delta\mu_5 - \Delta\mu_6) = g_{visc}\Delta y\left[\frac{(Q_3 + \Delta q_2)}{(Q_1+Q_3+\Delta q_1+\Delta q_2)} - \frac{(Q_3 - \Delta q_2)}{(Q_1+Q_3-\Delta q_1-\Delta q_2)}\right] \quad 6.67$$

This can be rearranged to

$$(\Delta\mu_5 - \Delta\mu_6) = g_{visc}\Delta y\left[\frac{2(Q_1\Delta q_2 - Q_3\Delta q_1)}{(Q_1+Q_3)^2 - (\Delta q_1 + \Delta q_2)^2}\right] \quad 6.68$$

These derivations, 6.74 and 6.79, can be inserted into the viscosity terms in equation 6.73 so the viscosity terms from Equation 6.57 become

$$k_5(Q_1+Q_3)\left[\frac{2(Q_1\Delta q_2 - Q_3\Delta q_1)}{(Q_1+Q_3)^2 - (\Delta q_1+\Delta q_2)^2}\right]g_{visc}\Delta y + k_5(\Delta q_1 + \Delta q_2)\left[\frac{2Q_3(Q_1+Q_3) - 2\Delta q_2(\Delta q_1+\Delta q_2)}{(Q_1+Q_3)^2 - (\Delta q_1+\Delta q_2)^2}\right]g_{visc}\Delta y \quad 6.69$$

By multiplying out the terms in the numerators, the viscosity terms reduce to

$$2\ k_5\ g_{visc}\ \Delta y \left[\frac{\Delta q_2(Q_1+Q_3)^2-(\Delta q_1+\Delta q_2)^2}{(Q_1+Q_3)^2-(\Delta q_1+\Delta q_2)^2}\right] \tag{6.70}$$

This can be reduced further

$$Viscosity\ terms = 2\ k_5\ g_{visc}\ \Delta y\ \Delta q_2 \tag{6.71}$$

This can then be inserted into Equation 6.57

$$\begin{aligned}(\Delta\rho_5+\Delta\rho_6)g\Delta h \\ = (k_1+k_2+k_5+k_6)\mu\ \Delta q_1+(k_5+k_6)\mu\ \Delta q_2 \\ +\ 2\ k_5\ g_{visc}\ \Delta y\ \Delta q_2\end{aligned} \tag{6.72}$$

This gives an equation relating the change in density to the change in flowrates in the system in the reference flow loop.

Similarly, for Equation 6.64, the changes in viscosity terms associated with the change in flow in the sample flow loop are

$$\begin{aligned}k_3(Q_3+\Delta q_2)\Delta\mu-k_3(Q_3-\Delta q_2)\Delta\mu+k_5(Q_1+Q_3)(\Delta\mu_5-\Delta\mu_6) \\ +\ k_5(\Delta q_1+\Delta q_2)(\Delta\mu_5+\Delta\mu_6)\end{aligned} \tag{6.73}$$

The sample loop contains more change in viscosity terms due to there being a change in viscosity, $\Delta\mu$, when the perturbation changes the sample flow viscosity as it enters gas density detector but before it mixes with the reference flow. The last two terms above are the same as in the reference loop and reduce to Equation 6.82. The first two terms can be reduced to

$$Viscosity\ terms = 2\ k_3\ \Delta q_2\ \Delta\mu \tag{6.74}$$

Remembering that $\Delta\mu = g_{visc}\ \Delta y$, the total of the viscosity terms in the sample flow loop are

$$Viscosity\ terms = 2(k_3+k_5)\ g_{visc}\ \Delta y\ \Delta q_2 \tag{6.75}$$

This can then be inserted into Equation 6.64

$$(\Delta\rho_5 + \Delta\rho_6 - 2\Delta\rho)\, g\Delta h = (k_3 + k_4 + k_5 + k_6)\, \mu\Delta q_2 + (k_5 + k_6)\, \mu\Delta q_1 + 2(k_3 + k_5)\, g_{visc}\, \Delta y\, \Delta q_2 \quad 6.76$$

This gives an equation relating the change in density to the change in flowrates in the system in the sample flow loop.

6.3.2.3. Material Balances around the GDD

Material balances are carried out around the points where the reference and sample flows join and mix together. These are carried out to establish equations for the change in density after the perturbation flow is added to the sample flow.

Figure *6.10* shows a diagram of the reference and the sample flows joining and mixing and then exiting the top branch of the system.

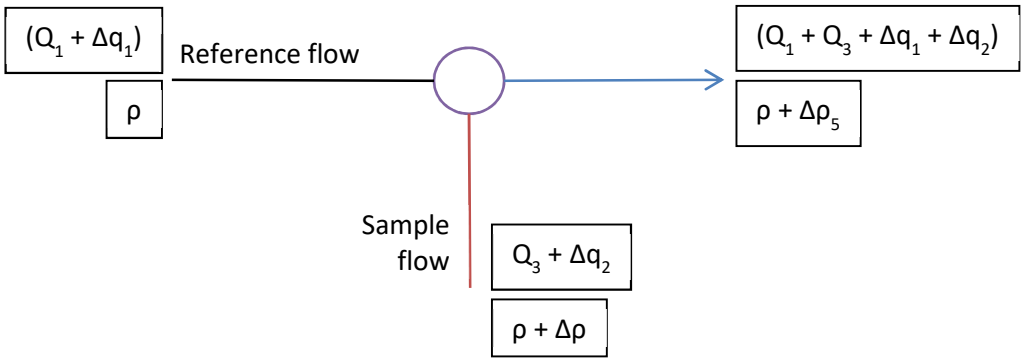

Figure 6.10 - Flows in the top branch of the system when the sample flowrate remains constant

For our purposes here, it is assumed that the mixture is ideal. The material balance is

$$\text{Input} = \text{Output} \quad 6.77$$

The material balance over the top branch gives

$$(Q_1 + \Delta q_1)\rho + (Q_3 + \Delta q_2)(\rho + \Delta\rho) = (Q_1 + Q_3 + \Delta q_1 + \Delta q_2)(\rho + \Delta\rho_5) \quad 6.78$$

This can be simplified to

$$\Delta\rho_5 = \frac{\Delta\rho(Q_3 + \Delta q_2)}{(Q_1 + Q_3 + \Delta q_1 + \Delta q_2)} \qquad 6.79$$

This results in an equation for the change in density when both the reference and the sample mix in the top branch before exiting the gas density detector.

Figure *6.11* shows a diagram of the reference and the sample flows joining and mixing and then exiting the bottom branch of the system.

The material balance over the bottom branch gives

$$(Q_2 - \Delta q_1)\rho + (Q_4 - \Delta q_2)(\rho + \Delta\rho) = (Q_2 + Q_4 - \Delta q_1 - \Delta q_2)(\rho + \Delta\rho_6) \qquad 6.80$$

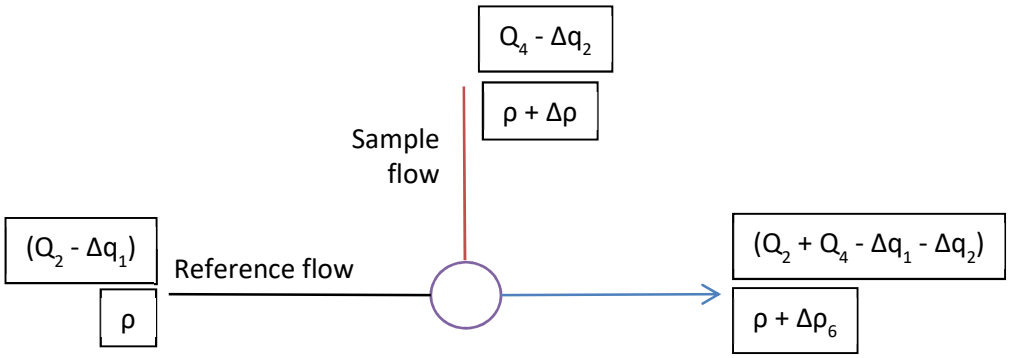

Figure 6.11 - Flows in the bottom branch of the system when the sample flowrate remains constant

This can be rearranged and simplified to

$$\Delta\rho_6 = \frac{\Delta\rho(Q_4 - \Delta q_2)}{(Q_2 + Q_4 - \Delta q_1 - \Delta q_2)} \qquad 6.81$$

It gives an equation for the change in density when both the reference and the sample mix in the bottom branch before exiting the gas density detector.

Equations for the change in density in the branches after the reference and sample flows join have been established which can be used in place of the density changes in Equations 6.83 and 6.87, the equations relating the change in flowrates to the change in density in the reference and sample flow loops respectively.

Inserting Equations 6.90 and 6.92 as part of Equation 6.83, and assuming $Q_1 = Q_2$ and $Q_3 = Q_4$ gives

$$\Delta\rho_5 + \Delta\rho_6 = \frac{(Q_3 + \Delta q_2)\Delta\rho}{(Q_1 + Q_3 + \Delta q_1 + \Delta q_2)} + \frac{(Q_3 - \Delta q_2)\Delta\rho}{(Q_1 + Q_3 - (\Delta q_1 + \Delta q_2))} \qquad 6.82$$

Rearranging gives

$$\Delta\rho_5 + \Delta\rho_6 = \Delta\rho\left[\frac{2Q_3(Q_1 + Q_3) - 2\Delta q_2(\Delta q_1 + \Delta q_2)}{(Q_1 + Q_3)^2 - (\Delta q_1 + \Delta q_2)^2}\right] \qquad 6.83$$

This can be inserted into 6.83 to give

$$\begin{aligned}\left[\frac{2Q_3(Q_1 + Q_3) - 2\Delta q_2(\Delta q_1 + \Delta q_2)}{(Q_1 + Q_3)^2 - (\Delta q_1 + \Delta q_2)^2}\right] \Delta\rho g \Delta h \\ = (k_1 + k_2 + k_5 + k_6)\mu\, \Delta q_1 + (k_5 + k_6)\mu\, \Delta q_2 \\ + 2\, k_5\, g_{visc}\, \Delta y\, \Delta q_2\end{aligned} \qquad 6.84$$

This can be simplified by assuming that the resistances k_5 and k_6 are negligible. The equation becomes

$$\left[\frac{2Q_3(Q_1 + Q_3) - 2\Delta q_2(\Delta q_1 + \Delta q_2)}{(Q_1 + Q_3)^2 - (\Delta q_1 + \Delta q_2)^2}\right] \Delta\rho g \Delta h = (k_1 + k_2)\mu\, \Delta q_1 \qquad 6.85$$

In this section, the flow remains constant, therefore if the addition of the perturbation causes the sample flow to increase by Δq_2, the reference flow in the top branch should decrease by the same flow rate and so $\Delta q_2 = -\Delta q_1$.

Therefore, by assuming that the sum of the change in flowrates, $\Delta q_1 + \Delta q_2 = 0$, the equation can be further reduced to

$$\left[\frac{2Q_3(Q_1+Q_3)}{(Q_1+Q_3)^2}\right]\Delta\rho g\Delta h = (k_1+k_2)\mu\,\Delta q_1 \qquad 6.86$$

This equation shows that the change in the reference stream flowrate, Δq_1 is proportional to the change in density of the sample flow when the perturbation is added.

Inserting Equations 6.90 and 6.92 as part of Equation 6.87, and assuming $Q_1 = Q_2$ and $Q_3 = Q_4$ gives

$$\begin{aligned}&(\Delta\rho_5+\Delta\rho_6-2\Delta\rho)g\Delta h\\&=\left[\frac{2Q_3(Q_1+Q_3)-2\Delta q_2(\Delta q_1+\Delta q_2)}{(Q_1+Q_3)^2-(\Delta q_1+\Delta q_2)^2}-\frac{2[(Q_1+Q_3)^2-(\Delta q_1+\Delta q_2)^2]}{(Q_1+Q_3)^2-(\Delta q_1+\Delta q_2)^2}\right]\Delta\rho g\Delta h\end{aligned} \qquad 6.87$$

This can be rearranged and inserted into Equation 6.87 to give

$$\begin{aligned}\left[\frac{-2Q_1(Q_1+Q_3)+2\Delta q_1(\Delta q_1+\Delta q_2)}{(Q_1+Q_3)^2-(\Delta q_1+\Delta q_2)^2}\right]\Delta\rho g\Delta h&\\=(k_3+k_4+k_5+k_6)\,\mu\Delta q_2+(k_5+k_6)\,\mu\Delta q_1&\\+2(k_3+k_5)\,g_{visc}\,\Delta y\,\Delta q_2&\end{aligned} \qquad 6.88$$

It can be further simplified by assuming that the resistances k_5 and k_6 are negligible. The equation becomes

$$\begin{aligned}\left[\frac{-2Q_1(Q_1+Q_3)+2\Delta q_1(\Delta q_1+\Delta q_2)}{(Q_1+Q_3)^2-(\Delta q_1+\Delta q_2)^2}\right]\Delta\rho g\Delta h&\\=(k_3+k_4)\,\mu\Delta q_2+2k_3\,g_{visc}\,\Delta y\,\Delta q_2&\end{aligned} \qquad 6.89$$

Again, by assuming that the flow in the system remains constant, the sum of the change in flowrates equal zero, $\Delta q_1 + \Delta q_2 = 0$, the equation can be further reduced to

$$\left[\frac{-2Q_1(Q_1+Q_3)}{(Q_1+Q_3)^2}\right]\Delta\rho g\Delta h = (k_3+k_4)\,\mu\Delta q_2+2k_3\,g_{visc}\,\Delta y\,\Delta q_2 \qquad 6.90$$

This equation shows that the change in the sample flowrate, Δq_2, is proportional to the change in density of the sample flow when the perturbation flow is added.

Comparing Equations 6.97 and 6.101 and ignoring the viscosity effects, it can be seen that

$$\frac{\Delta q_1}{\Delta q_2} = -\frac{Q_3}{Q_1}\frac{k_3 + k_4}{k_1 + k_2} \tag{6.91}$$

The reference flow, Q_1, is greater than the sample flow, Q_3 therefore $k_1 + k_2 < k_3 + k_4$ if $\Delta q_1 + \Delta q_2 = 0$.

6.3.3. Perturbation added to Sample Flow - Flow rate changes

A perturbation flow is added to the sample flow before it enters into the system. It is assumed that the addition of the perturbation flow causes the composition of the sample flow and the flowrate of the sample stream to change.

6.3.3.1. Pressure Changes in the GDD

Figure *6.12* shows a diagram of the gas density detector after the composition changes due to a perturbation flow being added to the sample flow. It also shows how the flow rates in the system and the gas mixture properties change.

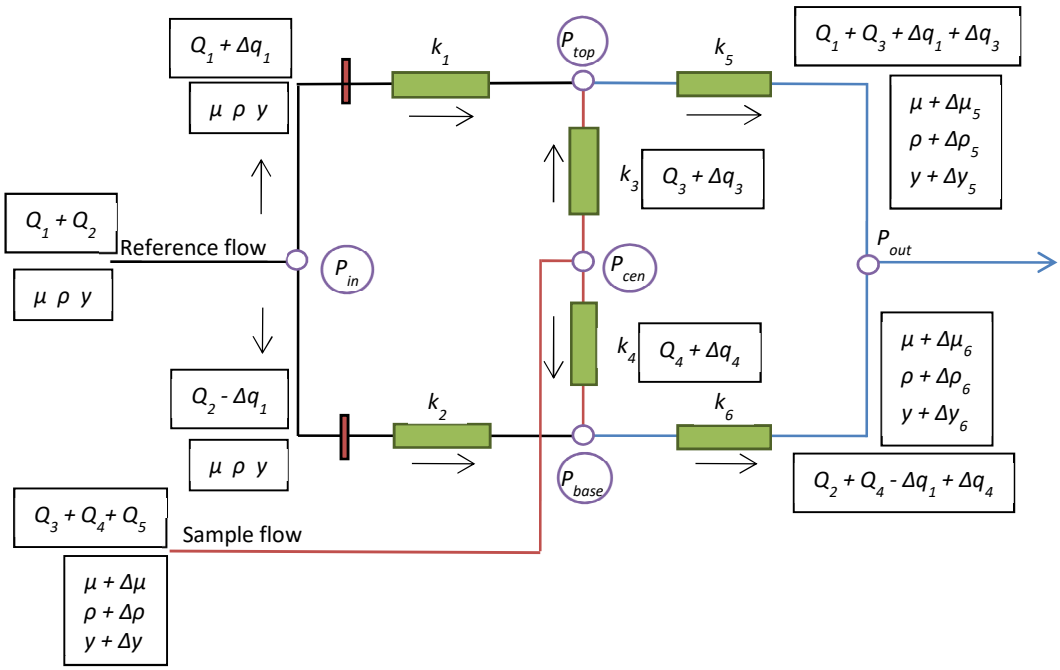

Figure 6.12 - Schematic diagram of the gas density detector after the perturbation flow is added – Flow changes

The reference flow entering the gas density detector is still the same at a flowrate of ($Q_1 + Q_2$) and has density, ρ, and viscosity, μ. A perturbation flow has been added to the sample flow at a flowrate, Q_5. The new sample flow into the system is now ($Q_3 + Q_4 + Q_5$). The density and viscosity of the sample stream is ($\rho + \Delta\rho$) and ($\mu + \Delta\mu$) respectively.

Like in the previous system where the flow remains constant, the addition of the perturbation flow to the sample flow causes flow rates Q_1 and Q_2 to change but, like before, the sum of the two streams will still be the same. Again, these changes are dependent on the new density of the sample stream.

The sample flow is greater due to the addition of the perturbation flow. The sample flows, Q_3 and Q_4, will change by Δq_3 and Δq_4 respectively. The changes in sample flow rates are equal to

$$Q_5 = \Delta q_3 + \Delta q_4 \qquad 6.92$$

The perturbation flow causes the density and viscosity of the sample stream to change to ($\rho + \Delta\rho$) and ($\mu + \Delta\mu$) respectively.

The pressure changes (Equations 6.37 - 6.40) and the starting Bernoulli equations (Equations 6.41 – 6.46) are the same as in the Section *6.3.2.1*.

Each stream will be looked at individually to see how the addition of the perturbation to the sample flow changes the pressures and the flows throughout the gas density detector.

Firstly, P_{out} is considered. The initial Bernoulli equation for the upper stream from P_{top} to P_{out} is shown in Equation 6.45.

$$P_{top} - P_{out} = k_5(Q_1 + Q_3)\mu - \rho g \Delta h \qquad 6.45$$

After the perturbation flow is added to the sample flow, the pressure in the upper branch, P_{top}, will change, along with the flowrates Q_1 and Q_3. The Bernoulli equation will then become

$$\begin{aligned}\left(P_{top} + \Delta P_{top}\right) - \ & P_{out} \\ & = k_5(Q_1 + Q_3 + \Delta q_1 + \Delta q_3)(\mu + \Delta\mu_5) \\ & - (\rho + \Delta\rho_5) g \Delta h\end{aligned} \qquad 6.93$$

The composition change due to the inclusion of the perturbation flow means that the viscosity and density have changed by $\Delta\mu_5$ and $\Delta\rho_5$ respectively. The flowrate to P_{out} , $(Q_1 + Q_3)$ will change by $(\Delta q_1 + \Delta q_3)$. As before, P_{out} is constant so subtracting Equation 6.45 from 6.104 gives

$$\Delta P_{top} = k_5[(Q_1 + Q_3 + \Delta q_1 + \Delta q_3)\Delta\mu_5 + (\Delta q_1 + \Delta q_3)\mu] - \Delta\rho_5 g \Delta h \qquad 6.94$$

There is now an equation for the pressure change in the top branch of the system.

The lower branch from P_{base} to P_{out} is considered. This is initially represented in Equation 6.46.

$$P_{base} - P_{out} = k_6(Q_2 + Q_4)\mu + \rho g \Delta h \qquad 6.46$$

After the perturbation flow is added, the equation becomes

$$(P_{base} + \Delta P_{base}) - P_{out} = k_6(Q_2 + Q_4 - \Delta q_1 + \Delta q_4)(\mu + \Delta\mu_6) + (\rho + \Delta\rho_6)g\Delta h \quad 6.95$$

Again, the composition and flowrates have changed due to the addition of the perturbation flow. P_{out} is constant so subtracting Equation 6.46 from 6.106 gives

$$\Delta P_{base} = k_6[(Q_2 + Q_4 - \Delta q_1 + \Delta q_4)\Delta\mu_6 + (-\Delta q_1 + \Delta q_4)\mu] + \Delta\rho_6 g\Delta h \quad 6.96$$

An equation describing the pressure change in the lower branch has been created. Therefore, equations for ΔP_{top} and ΔP_{base} have been obtained.

Secondly, the reference flow and hence P_{in} is considered. The upper stream from P_{in} to P_{top} is initially represented by Equation 6.41.

$$P_{in} - P_{top} = k_1 Q_1 \mu + \rho g \Delta h \quad 6.41$$

After the perturbation flow is added, pressures P_{in} and P_{top} and flowrate Q_1will change. The Bernoulli equation will become

$$(P_{in} + \Delta P_{in}) - \left(P_{top} + \Delta P_{top}\right) = k_1(Q_1 + \Delta q_1)\mu + \rho g \Delta h \quad 6.97$$

The viscosity and density do not change as it is still only the reference flow flowing through the branch. Subtracting Equation 6.41 from 6.108 gives

$$\Delta P_{in} - \Delta P_{top} = k_1 \Delta q_1 \mu \quad 6.98$$

This gives an equation relating the changes in pressure at the inlet of the reference flow and the top stream to the change in flowrate going through the upper branch.

The lower stream from P_{in} is considered. The initial Bernoulli equation is shown in Equation 6.42

$$P_{in} - P_{base} = k_2 Q_2 \mu - \rho g \Delta h \tag{6.42}$$

After the perturbation flow is added to the sample flow and the equation becomes

$$(P_{in} + \Delta P_{in}) - (P_{base} + \Delta P_{base}) = k_2 (Q_2 - \Delta q_1)\mu - \rho g \Delta h \tag{6.99}$$

The viscosity and density remains constant so subtracting Equation 6.42 from 6.110 gives

$$\Delta P_{in} - \Delta P_{base} = k_2 (-\Delta q_1)\mu \tag{6.100}$$

This gives an equation relating the changes in pressure at the inlet and the bottom stream to the change in flowrate going through the lower branch.

Equations 6.109 and 6.111 are the same as 6.48 and 6.50 as the reference flow is always constant. This is because the sample flow is added further upstream in the system and only affects the reference flow by restricting the flow along the branches and causes a difference in the flows, Δq_1.

Equations for ΔP_{top} and ΔP_{base} have previously been defined. Equations 6.109 and 6.111 can both be rearranged for ΔP_{in};

$$\Delta P_{in} = \Delta P_{top} + k_1 \Delta q_1 \mu = \Delta P_{base} - k_2 \Delta q_1 \mu \tag{6.101}$$

The definitions for ΔP_{top} and ΔP_{base} from Equations 6.105 and 6.108 can then be inserted and equated to give

$$\begin{aligned} k_5[(Q_1 + Q_3 + \Delta q_1 + \Delta q_3)\Delta\mu_5 + (\Delta q_1 + \Delta q_3)\mu] - \Delta\rho_5 g \Delta h \\ + k_1 \Delta q_1 \mu \\ = k_6[(Q_2 + Q_4 - \Delta q_1 + \Delta q_4)\Delta\mu_6 + (-\Delta q_1 + \Delta q_4)\mu] \\ + \Delta\rho_6 g \Delta h - k_2 \Delta q_1 \mu \end{aligned} \tag{6.102}$$

Assuming that the reference and sample flows split equally to the upper and lower branches, $Q_1 + Q_3 = Q_2 + Q_4$, the equation becomes

$$\begin{aligned}(\Delta\rho_5 + \Delta\rho_6)g\Delta h \\ &= (k_1 + k_2 + k_5 + k_6)\Delta q_1\mu + \mu(k_5\Delta q_3 - k_6\Delta q_4) \\ &+ k_6(Q_1 + Q_3)(\Delta\mu_5 - \Delta\mu_6) + k_6\Delta q_1(\Delta\mu_5 + \Delta\mu_6) \\ &+ k_6(\Delta q_3\Delta\mu_5 - \Delta q_4\Delta\mu_6)\end{aligned} \quad 6.103$$

An equation relating the change in flowrates ($\Delta q_1 + \Delta q_2$) within the system, from points P_{in} to P_{out} around the reference flow loop, to the change in density ($\Delta\rho_5$ and $\Delta\rho_6$) caused by adding the perturbation flow has been developed.

Finally, P_{cen} is considered. The upper stream from P_{cen} to P_{top} is initially represented in Equation 6.43.

$$P_{cen} - P_{top} = k_3 Q_3\mu + \rho g\Delta h \quad 6.43$$

After the perturbation flow is added and the composition is changed, the equation becomes

$$\begin{aligned}(P_{cen} + \Delta P_{cen}) - \left(P_{top} + \Delta P_{top}\right) \\ = k_3(Q_3 + \Delta q_3)(\mu + \Delta\mu) + (\rho + \Delta\rho)g\Delta h\end{aligned} \quad 6.104$$

The composition change due to the addition of the perturbation flow means that the viscosity and density have changed by $\Delta\mu$ and $\Delta\rho$ respectively. The flowrate Q_3 will change by Δq_3. Subtracting Equation 6.43 from 6.115 gives

$$\Delta P_{cen} - \Delta P_{top} = k_3[(Q_3 + \Delta q_3)\,\Delta\mu + \mu\,\Delta q_3] + \Delta\rho\; g\Delta h \quad 6.105$$

This gives an equation relating the changes in pressure at the inlet of the sample flow and the top stream to the change in flowrate going through the upper branch, the change in viscosity and the change in density due to the addition of the perturbation to the sample stream.

The lower stream from P_{cen} to P_{base} is considered. Initially, this is represented by the Bernoulli Equation 6.44.

$$P_{cen} - P_{base} = k_4 Q_4\mu - \rho g\Delta h \quad 6.106$$

The perturbation flow is added and the equation becomes

$$(P_{cen} + \Delta P_{cen}) - (P_{base} + \Delta P_{base}) = k_4(Q_4 + \Delta q_4)(\mu + \Delta\mu) - (\rho + \Delta\rho)g\Delta h \quad 6.107$$

Again, the flowrate, viscosity and density of the gas mixture have changed due to the addition of the perturbation flow. Subtracting Equation 6.44 from 6.117 gives

$$\Delta P_{cen} - \Delta P_{base} = k_4[(Q_4 + \Delta q_4)\,\Delta\mu - \mu\,\Delta q_4] - \Delta\rho\; g\Delta h \quad 6.108$$

This gives an equation relating the changes in pressure at the inlet of the sample flow and the bottom stream to the change in flowrate going through the lower branch, the change in viscosity and the change in density due to the addition of the perturbation to the sample stream.

Equations 6.116 and 6.118 can be rearranged for ΔP_{cen}

$$\begin{aligned}\Delta P_{cen} &= \Delta P_{top} + k_3[(Q_3 + \Delta q_3)\,\Delta\mu + \mu\,\Delta q_3] + \Delta\rho\; g\Delta h \\ &= \Delta P_{base} + k_4[(Q_4 + \Delta q_4)\,\Delta\mu - \mu\,\Delta q_4] - \Delta\rho\; g\Delta h\end{aligned} \quad 6.109$$

The definitions for ΔP_{top} and ΔP_{base} from Equations 6.105 and 6.107 can then be inserted and equated to give

$$\begin{aligned}k_5[(Q_1 + Q_3 + \Delta q_1 + \Delta q_3)\Delta\mu_5 + (\Delta q_1 + \Delta q_3)\mu] - \Delta\rho_5 g\Delta h \\ + k_3[(Q_3 + \Delta q_3)\,\Delta\mu + \mu\,\Delta q_3] + \Delta\rho\; g\Delta h \\ = \; k_6[(Q_2 + Q_4 - \Delta q_1 + \Delta q_4)\Delta\mu_6 + (-\Delta q_1 + \Delta q_4)\mu] \\ + \Delta\rho_6 g\Delta h + k_4[(Q_4 + \Delta q_4)\,\Delta\mu - \mu\,\Delta q_4] - \Delta\rho\; g\Delta h\end{aligned} \quad 6.110$$

Again, it is assumed that the reference and sample flows split equally to the upper and lower branches, $Q_1 = Q_2$ and $Q_3 = Q_4$, and that $k_3 = k_4$ and $k_5 = k_6$, the equation becomes

$$\begin{aligned}(\Delta\rho_5 + \Delta\rho_6 - 2\Delta\rho)g\Delta h \\ = (k_5 + k_6)\mu\Delta q_1 - (k_4 + k_6)\mu\Delta q_4 + (k_3 + k_5)\mu\Delta q_3 \\ + k_6(Q_1 + Q_3)(\Delta\mu_5 - \Delta\mu_6) + k_6\Delta q_1(\Delta\mu_5 + \Delta\mu_6) \\ + k_6(\Delta q_3\Delta\mu_5 - \Delta q_4\Delta\mu_6) + \; k_3\,\Delta\mu(\Delta q_3 - \Delta q_4)\end{aligned} \quad 6.111$$

Another equation relating the change in flowrates within the system, from points P_{in} to P_{cen} around the sample flow loop to the change in density caused by adding the perturbation flow has been found.

6.3.3.2. Viscosity Changes in the GDD

Equations 6.114 and 6.121 relate the change in flowrates, Δq_1 and Δq_2, due to the addition of the perturbation flow, to the changes in densities, $\Delta\rho_5$ and $\Delta\rho_6$. These equations have change in viscosity terms, $\Delta\mu_5$ and $\Delta\mu_6$. As explained in Section 6.3.2.2, it is assumed the viscosity, μ, varies linearly with mole fraction, y. From Equation 6.65 and 6.66 it is assumed that

$$\Delta\mu_5 = g_{visc}\,\Delta y_5 \qquad 6.65$$

$$\Delta\mu_6 = g_{visc}\,\Delta y_6 \qquad 6.66$$

where g_{visc} is the gradient of the line in the graph above.

Equations for Δy_5 and Δy_6 can be derived from balancing the mole fractions at the points where the reference and sample flows meet in the upper and lower branches of the detector.

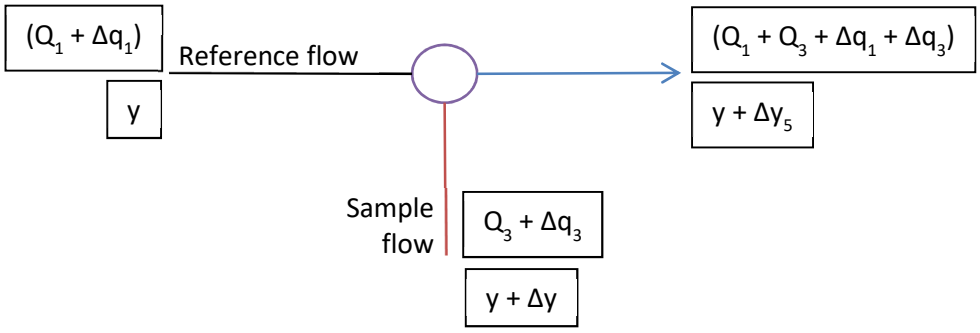

Figure 6.13 - Flows and mole fractions in the top branch of the system when the sample flowrate remains constant

Figure *6.13* above shows the flows and mole fractions in the upper branch of the system. A balance over the top branch gives

$$(Q_1 + \Delta q_1)y + (Q_3 + \Delta q_3)(y + \Delta y) = (Q_1 + Q_3 + \Delta q_1 + \Delta q_3)(y + \Delta y_5) \quad 6.112$$

This can be simplified to

$$\Delta y_5 = \frac{\Delta y(Q_3 + \Delta q_3)}{(Q_1 + Q_3 + \Delta q_1 + \Delta q_3)} \quad 6.113$$

Similarly, Figure *6.14* shows the flows and mole fractions in the lower branch of the system.

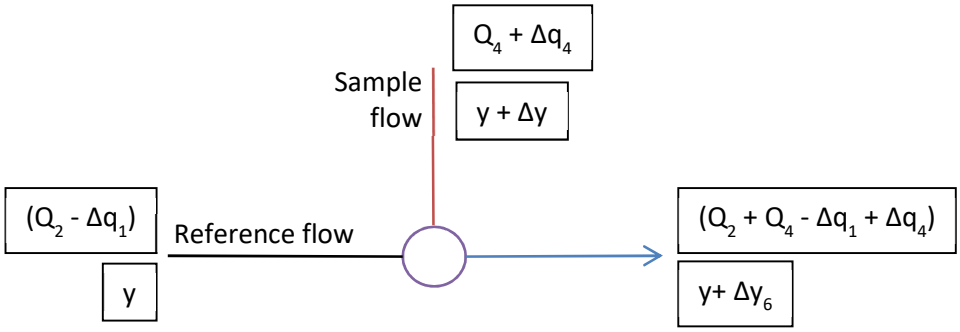

Figure 6.14 - Flows and mole fractions in the bottom branch of the system when the sample flowrate remains constant

A balance over the bottom branch gives

$$(Q_2 - \Delta q_1)y + (Q_4 + \Delta q_4)(y + \Delta y) = (Q_2 + Q_4 - \Delta q_1 + \Delta q_4)(y + \Delta y_6) \quad 6.114$$

This can be rearranged and simplified to

$$\Delta y_6 = \frac{\Delta y(Q_4 + \Delta q_4)}{(Q_2 + Q_4 - \Delta q_1 + \Delta q_4)} \quad 6.115$$

Equations 6.123 and 6.125 can be inserted into Equations 6.65 and 6.66 to give derivations for the change in viscosities

$$\Delta\mu_5 = g_{visc}\Delta y \left[\frac{(Q_3 + \Delta q_3)}{(Q_1 + Q_3 + \Delta q_1 + \Delta q_3)}\right] \quad 6.116$$

$$\Delta\mu_6 = g_{visc}\,\Delta y\left[\frac{(Q_4+\Delta q_4)}{(Q_2+Q_4-\Delta q_1+\Delta q_4)}\right] \tag{6.117}$$

Firstly, the equation for the change in flowrate with change in density in the reference flow loop will be considered. Assuming that $k_5 = k_6$, the viscosity terms in Equation 6.114 are

$$k_5(Q_1+Q_3)(\Delta\mu_5-\Delta\mu_6)+k_5\Delta q_1(\Delta\mu_5+\Delta\mu_6)+k_5(\Delta q_3\Delta\mu_5 - \Delta q_4\Delta\mu_6) \tag{6.118}$$

Viscosity changes $(\Delta\mu_5+\Delta\mu_6)$ can be found by inserting Equations 6.126 and 6.127

$$(\Delta\mu_5+\Delta\mu_6) = g_{visc}\Delta y\left[\frac{(Q_3+\Delta q_3)}{(Q_1+Q_3+\Delta q_1+\Delta q_3)} + \frac{(Q_4+\Delta q_4)}{(Q_2+Q_4-\Delta q_1+\Delta q_4)}\right] \tag{6.119}$$

By assuming that the reference and sample flows split equally, i.e. $Q_1 = Q_2$and $Q_3 = Q_4$, the equation becomes

$$(\Delta\mu_5+\Delta\mu_6) = g_{visc}\Delta y\left[\frac{(Q_3+\Delta q_3)}{(Q_1+Q_3+\Delta q_1+\Delta q_3)} + \frac{(Q_3+\Delta q_4)}{(Q_1+Q_3-\Delta q_1+\Delta q_4)}\right] \tag{6.120}$$

Remembering that $Q_5 = \Delta q_3+\Delta q_4$ and by rearranging

$$(\Delta\mu_5+\Delta\mu_6) = g_{visc}\Delta y\left[\frac{2Q_3(Q_1+Q_3)+(Q_1+2Q_3)Q_5+2\Delta q_3\Delta q_4+\Delta q_1(\Delta q_4-\Delta q_3)}{(Q_1+Q_3+\Delta q_1+\Delta q_3)(Q_1+Q_3-\Delta q_1+\Delta q_4)}\right] \tag{6.121}$$

Similarly, $(\Delta\mu_5-\Delta\mu_6)$ can be found by inserting 6.126 and 6.127

$$(\Delta\mu_5 - \Delta\mu_6) = g_{visc}\Delta y\left[\frac{(Q_3 + \Delta q_3)}{(Q_1 + Q_3 + \Delta q_1 + \Delta q_3)} - \frac{(Q_4 + \Delta q_4)}{(Q_2 + Q_4 - \Delta q_1 + \Delta q_4)}\right] \quad 6.122$$

By assuming that the reference and sample flows split equally $Q_1 = Q_2$ and $Q_3 = Q_4$, the equation becomes

$$(\Delta\mu_5 - \Delta\mu_6) = g_{visc}\Delta y\left[\frac{(Q_3 + \Delta q_3)}{(Q_1 + Q_3 + \Delta q_1 + \Delta q_3)} - \frac{(Q_3 + \Delta q_4)}{(Q_1 + Q_3 - \Delta q_1 + \Delta q_4)}\right] \quad 6.123$$

This can be rearranged to give

$$(\Delta\mu_5 - \Delta\mu_6) = g_{visc}\Delta y\left[\frac{Q_1(\Delta q_3 - \Delta q_4) - 2Q_3\Delta q_1 - \Delta q_1(\Delta q_3 + \Delta q_4)}{(Q_1 + Q_3 + \Delta q_1 + \Delta q_3)(Q_1 + Q_3 - \Delta q_1 + \Delta q_4)}\right] \quad 6.124$$

The derivations above in Equations 6.131 and 6.134 along with the equations for the viscosity changes in 6.126 and 6.127 can be inserted into the viscosity terms in Equation 6.128

$$\begin{aligned}
&\left(Q_1 + Q_3\right)\left[\frac{Q_1\left(\Delta q_3 - \Delta q_4\right) - 2Q_3\Delta q_1 - \Delta q_1(\Delta q_3 + \Delta q_4)}{\left(Q_1 + Q_3 + \Delta q_1 + \Delta q_3\right)(Q_1 + Q_3 - \Delta q_1 + \Delta q_4)}\right] g_{visc}\Delta y \\
&+ k_5\Delta q_1\left[\frac{2Q_3\left(Q_1 + Q_3\right) + \left(Q_1 + 2Q_3\right)Q_5 + 2\Delta q_3\Delta q_4 + \Delta q_1(\Delta q_4 - \Delta q_3)}{\left(Q_1 + Q_3 + \Delta q_1 + \Delta q_3\right)(Q_1 + Q_3 - \Delta q_1 + \Delta q_4)}\right] g_{visc}\Delta y \\
&+ k_5\Delta q_3\left[\frac{\left(Q_3 + \Delta q_3\right)}{\left(Q_1 + Q_3 + \Delta q_1 + \Delta q_3\right)}\right] g_{visc}\Delta y \\
&- k_5\Delta q_4\left[\frac{(Q_3 + \Delta q_4)}{\left(Q_1 + Q_3 - \Delta q_1 + \Delta q_4\right)}\right] g_{visc}\,\Delta y
\end{aligned} \quad 6.125$$

To simplify, the last two terms are changed so that they have the same denominator as the other terms

$$
\begin{aligned}
&k_5\left(Q_1+Q_3\right)\left[\frac{Q_1\left(\Delta q_3-\Delta q_4\right)-2Q_3\Delta q_1-\Delta q_1(\Delta q_3+\Delta q_4)}{\left(Q_1+Q_3+\Delta q_1+\Delta q_3\right)(Q_1+Q_3-\Delta q_1+\Delta q_4)}\right]g_{visc}\Delta y\\
&+k_5\Delta q_1\left[\frac{2Q_3\left(Q_1+Q_3\right)+\left(Q_1+2Q_3\right)Q_5+2\Delta q_3\Delta q_4+\Delta q_1(\Delta q_4-\Delta q_3)}{\left(Q_1+Q_3+\Delta q_1+\Delta q_3\right)(Q_1+Q_3-\Delta q_1+\Delta q_4)}\right]g_{visc}\Delta y\\
&+k_5\Delta q_3\left[\frac{\left(Q_3+\Delta q_3\right)\left(Q_1+Q_3-\Delta q_1+\Delta q_4\right)}{\left(Q_1+Q_3+\Delta q_1+\Delta q_3\right)\left(Q_1+Q_3-\Delta q_1+\Delta q_4\right)}\right]g_{visc}\Delta y\\
&-k_5\Delta q_4\left[\frac{(Q_3+\Delta q_4)\left(Q_1+Q_3+\Delta q_1+\Delta q_3\right)}{\left(Q_1+Q_3-\Delta q_1+\Delta q_4\right)\left(Q_1+Q_3+\Delta q_1+\Delta q_3\right)}\right]g_{visc}\,\Delta y
\end{aligned}
\qquad 6.126
$$

By multiplying out the brackets, the viscosity terms reduce to

$$
k_5 g_{visc}\Delta y\left[\frac{\left(2\Delta q_3-Q_5\right)\left[\left(Q_1+Q_3\right)^2-\left(\Delta q_1+\Delta q_3\right)^2+Q_5\left(Q_1+Q_3+\Delta q_1+\Delta q_3\right)\right]}{\left(Q_1+Q_3\right)^2-\left(\Delta q_1+\Delta q_3\right)^2+Q_5\left(Q_1+Q_3+\Delta q_1+\Delta q_3\right)}\right] \qquad 6.127
$$

Remembering that $Q_5=\Delta q_3+\Delta q_4$, this can be further reduced to

$$
Viscosity\ effects = k_5 g_{visc}\Delta y(\Delta q_3-\Delta q_4) \qquad 6.128
$$

This can be inserted into Equation 6.114

$$
\begin{aligned}
&(\Delta\rho_5+\Delta\rho_6)g\Delta h\\
&\qquad=(k_1+k_2+k_5+k_6)\Delta q_1\mu\\
&\qquad+\mu(k_5\Delta q_3-k_6\Delta q_4)+k_5 g_{visc}\Delta y(\Delta q_3-\Delta q_4)
\end{aligned}
\qquad 6.129
$$

This gives an equation relating the change in density to the changes in flowrates in the system in the reference flow loop.

Similarly, for Equation 6.121, assuming that $k_5=k_6$, the changes in viscosity terms associated with the change in flow in the sample flow loop are

$$
\begin{aligned}
&k_5(Q_1+Q_3)(\Delta\mu_5-\Delta\mu_6)+k_5\Delta q_1(\Delta\mu_5+\Delta\mu_6)+k_5(\Delta q_3\Delta\mu_5-\\
&\Delta q_4\Delta\mu_6)+\ k_3\,\Delta\mu(\Delta q_3-\Delta q_4)
\end{aligned}
\qquad 6.130
$$

The first three terms are the same as those in Equation 6.114 and will be the same as the viscosity effects in 6.138. Remembering that $\Delta\mu=g_{visc}\Delta y$, the viscosity terms can be inserted into Equation 6.121 to give

$$(\Delta\rho_5 + \Delta\rho_6 - 2\Delta\rho)g\Delta h = (k_5 + k_6)\mu\Delta q_1 - (k_4 + k_6)\mu\Delta q_4 + (k_3 + k_5)\mu\Delta q_3 + (k_3 + k_5)g_{visc}\Delta y(\Delta q_3 - \Delta q_4) \quad 6.131$$

This gives an equation relating the change in density to the changes in flowrates in the system in the sample flow loop.

6.3.3.3. Material Balances around the GDD

Material balances are carried out around the points where the reference and sample flows mix together to establish the relationship between the change in density and the flowrate changes after the perturbation flow has been added.

Figure *6.15* shows a diagram of the reference and the sample flows joining and mixing and then exiting the top branch of the system.

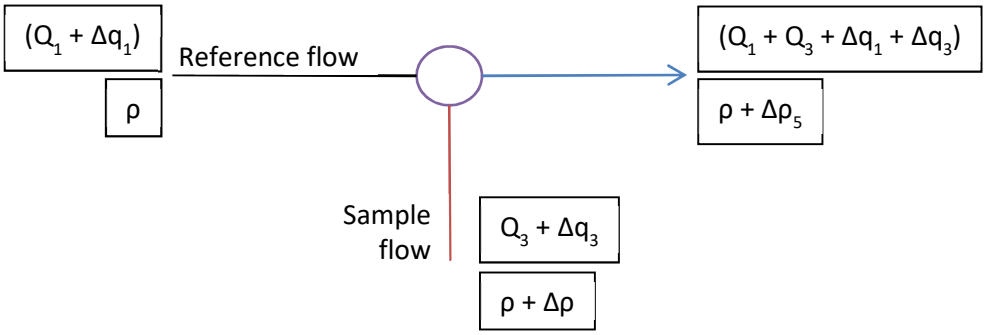

Figure 6.15 - Flows in the top branch of the system when the sample flowrate changes

The material balance over the top branch gives

$$(Q_1 + \Delta q_1)\rho + (Q_3 + \Delta q_3)(\rho + \Delta\rho) = (Q_1 + Q_3 + \Delta q_1 + \Delta q_3)(\rho + \Delta\rho_5) \quad 6.132$$

This can be simplified to

$$\Delta\rho_5 = \frac{\Delta\rho(Q_3 + \Delta q_3)}{(Q_1 + Q_3 + \Delta q_1 + \Delta q_3)} \qquad 6.133$$

This gives an equation for the change in density in the top exit stream after both the reference and the sample mix before exiting the gas density detector.

Another material balance is carried out on the bottom branch of the gas density detector where the reference and sample flows join. The diagram of this is shown below in Figure *6.16*.

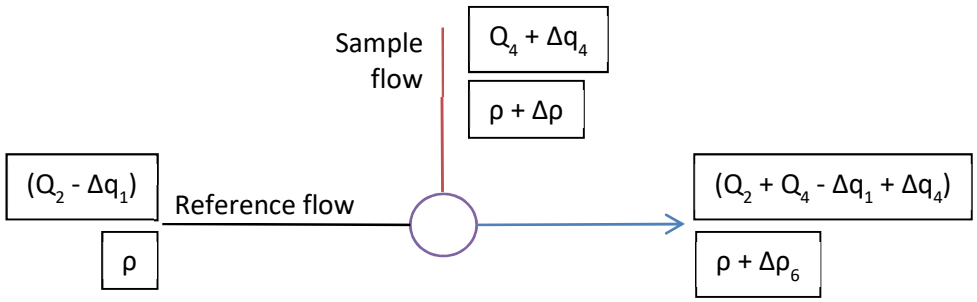

Figure 6.16 - Flows in the bottom branch of the system when the sample flowrate changes

The material balance over the bottom branch gives

$$(Q_2 - \Delta q_1)\rho + (Q_4 + \Delta q_4)(\rho + \Delta\rho) = (Q_2 + Q_4 - \Delta q_1 + \Delta q_4)(\rho + \Delta\rho_6) \qquad 6.134$$

This can be rearranged and simplified to

$$\Delta\rho_6 = \frac{\Delta\rho(Q_4 + \Delta q_4)}{(Q_2 + Q_4 - \Delta q_1 + \Delta q_4)} \qquad 6.135$$

It gives an equation for the change in density when both the reference and the sample mix in the bottom branch before exiting the gas density detector.

This results in equations for the change in density in the exit streams of the top and bottom branches after the reference and sample flows join together which can be used in Equations 6.139 and 6.141.

Inserting Equations 6.143and 6.145 as part of Equation 6.139, and assuming $Q_1 = Q_2$ and $Q_3 = Q_4$ gives

$$\Delta\rho_5 + \Delta\rho_6 = \frac{(Q_3 + \Delta q_3)\Delta\rho}{(Q_1 + Q_3 + \Delta q_1 + \Delta q_3)} + \frac{(Q_3 + \Delta q_4)\Delta\rho}{(Q_1 + Q_3 - \Delta q_1 + \Delta q_4)} \qquad 6.136$$

Remembering that $Q_5 = \Delta q_3 + \Delta q_4$, this can be rearranged to

$$\Delta\rho_5 + \Delta\rho_6 = \Delta\rho\left[\frac{2Q_3(Q_1 + Q_3) + (Q_1 + 2Q_3)Q_5 + \Delta q_4(\Delta q_1 + \Delta q_3) - \Delta q_3(\Delta q_1 - \Delta q_4)}{(Q_1 + Q_3 + \Delta q_1 + \Delta q_3)(Q_1 + Q_3 - \Delta q_1 + \Delta q_4)}\right] \qquad 6.137$$

This can be inserted into Equation 6.139 to give

$$\left[\frac{2Q_3(Q_1 + Q_3) + (Q_1 + 2Q_3)Q_5 + 2\Delta q_3\Delta q_4 + \Delta q_1(\Delta q_4 - \Delta q_3)}{(Q_1 + Q_3 + \Delta q_1 + \Delta q_3)(Q_1 + Q_3 - \Delta q_1 + \Delta q_4)}\right]\Delta\rho g\Delta h = (k_1 + k_2 + k_5 + k_6)\Delta q_1\mu + \mu(k_5\Delta q_3 - k_6\Delta q_4) + k_5 g_{visc}\Delta y(\Delta q_3 - \Delta q_4) \qquad 6.138$$

This can be simplified by assuming that the resistances k_5 and k_6 are negligible. The equation becomes

$$\left[\frac{2Q_3(Q_1 + Q_3) + (Q_1 + 2Q_3)Q_5 + \Delta q_4(\Delta q_1 + \Delta q_3) - \Delta q_3(\Delta q_1 - \Delta q_4)}{(Q_1 + Q_3 + \Delta q_1 + \Delta q_3)(Q_1 + Q_3 - \Delta q_1 + \Delta q_4)}\right]\Delta\rho g\Delta h = (k_1 + k_2)\Delta q_1\mu \qquad 6.139$$

By assuming that $\Delta q_3 + \Delta q_4 = 0 = Q_5$ and that $\Delta q_1 + \Delta q_3 = 0$, this equation can be further reduced to

$$\left[\frac{2Q_3(Q_1 + Q_3)}{(Q_1 + Q_3)^2}\right]\Delta\rho g\Delta h = (k_1 + k_2)\Delta q_1\mu \qquad 6.140$$

Inserting Equations 6.143 and 6.145 into Equation 6.141, and assuming $Q_1 = Q_2$ and $Q_3 = Q_4$ gives

$$\begin{aligned}&(\Delta\rho_5 + \Delta\rho_6 - 2\Delta\rho)g\Delta h \\ &= \left[\frac{2Q_3(Q_1 + Q_3) + (Q_1 + 2Q_3)Q_5 + \Delta q_4(\Delta q_1 + \Delta q_3) - \Delta q_3(\Delta q_1 - \Delta q_4)}{(Q_1 + Q_3 + \Delta q_1 + \Delta q_3)(Q_1 + Q_3 - \Delta q_1 + \Delta q_4)}\right. \\ &\left. - \frac{2(Q_1 + Q_3 + \Delta q_1 + \Delta q_3)(Q_1 + Q_3 - \Delta q_1 + \Delta q_4)}{(Q_1 + Q_3 + \Delta q_1 + \Delta q_3)(Q_1 + Q_3 - \Delta q_1 + \Delta q_4)}\right] \Delta\rho g\Delta h\end{aligned} \quad 6.141$$

This can be simplified and inserted into Equation 6.141 to give

$$\begin{aligned}&\left[\frac{-2Q_1\left(Q_1 + Q_3\right) - Q_1Q_5 - (2\Delta q_1 - \Delta q_4)\left(\Delta q_1 + \Delta q_3\right) - \Delta q_3(\Delta q_1 - \Delta q_4)}{\left(Q_1 + Q_3 + \Delta q_1 + \Delta q_3\right)(Q_1 + Q_3 - \Delta q_1 + \Delta q_4)}\right]\Delta\rho g\Delta h \\ &\quad = (k_5 + k_6)\mu\Delta q_1 - (k_4 + k_6)\mu\Delta q_4 \\ &\quad + (k_3 + k_5)\mu\Delta q_3 + (k_3 + k_5)g_{visc}\Delta y\left(\Delta q_3 - \Delta q_4\right)\end{aligned} \quad 6.142$$

This can be simplified by assuming that the resistances k_5 and k_6 are negligible. The equation becomes

$$\begin{aligned}&\left[\frac{-2Q_1\left(Q_1 + Q_3\right) - Q_1Q_5 - (2\Delta q_1 - \Delta q_4)\left(\Delta q_1 + \Delta q_3\right) - \Delta q_3(\Delta q_1 - \Delta q_4)}{\left(Q_1 + Q_3 + \Delta q_1 + \Delta q_3\right)(Q_1 + Q_3 - \Delta q_1 + \Delta q_4)}\right]\Delta\rho g\Delta h \\ &\quad = k_3\mu\Delta q_3 - k_4\mu\Delta q_4 + k_3 g_{visc}\Delta y\left(\Delta q_3 - \Delta q_4\right)\end{aligned} \quad 6.143$$

By assuming that $\Delta q_3 + \Delta q_4 = 0 = Q_5$ and that $\Delta q_1 + \Delta q_3 = 0$, this equation can be further reduced to

$$\begin{aligned}&\left[\frac{-2Q_1(Q_1 + Q_3)}{(Q_1 + Q_3)^2}\right]\Delta\rho g\Delta h \\ &\quad = k_3\mu\Delta q_3 - k_4\mu\Delta q_4 + k_3 g_{visc}\Delta y(\Delta q_3 - \Delta q_4)\end{aligned} \quad 6.144$$

This equation shows that the changes in the sample flowrate, Δq_3 and Δq_4, is proportional to the change in density of the sample flow when the perturbation flow is added.

6.4.Experimental Arrangement and Procedure

Figure *6.17* shows a representation of the experimental arrangement. The gases used in experiments in this figure are nitrogen and argon. The flow from the cylinder for each gas is split. For argon, one stream goes to the gas mixer while the other stream is used to perturb the system. For nitrogen, the flow is split into three streams, one to the gas mixer, another to be used as a perturbation gas and the third acts as an auxiliary flow to the gas mixer.

The diagram shows nitrogen and argon entering a gas mixer. The mixer is essentially a steel enclosure with mass flow controllers and rotameters for each gas that makes up the gas mixture. Each gas enters the enclosure from the cylinder via stainless steel tubing and flow rates are set using a *Porter* VC1000 mass flow controller and a rotameter. Each rotameter is specific for each gas being used.

As previously mentioned, the nitrogen and argon flows split before entering the mixer. The gas that does not enter the mixer is directed to a *Porter* 8286 pressure regulator, set to a gauge pressure of 40 psi. This stream leads to a *Porter* VC1000 mass flow controller and used as the perturbation gas flow into the system. Both flows are connected to a 4-way valve so that either gas can be entered into the system while the other is directed to the vent. The perturbation gas to enter the system flows to a three-way valve that allows the perturbation flow to be added to either the measurement side of the system or a bypass stream. The bypass stream contains another steel block which mimics the system. This eliminates any pressure difference in the system when the perturbation gas is added or removed.

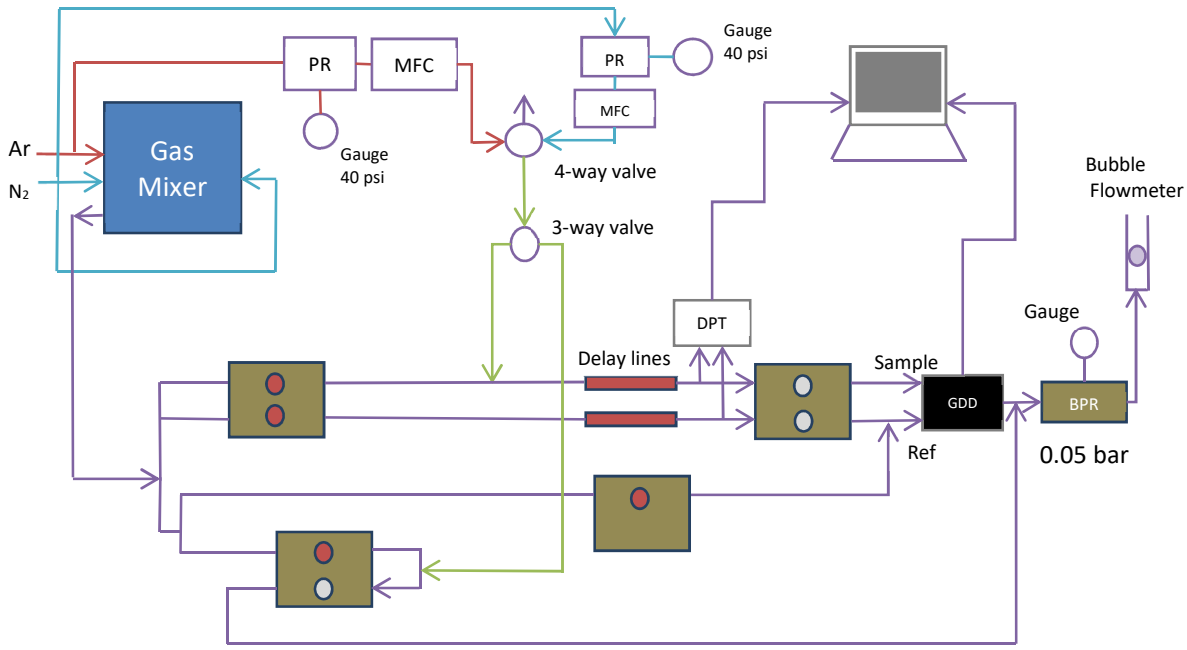

Figure 6.17 - Schematic diagram of the experimental arrangement including the gas density detector

The gas mixture leaving the mixer splits into three streams. Two of the streams flow through a double-sided arrangement, similar to that described in Section 5.4. One side is used as a reference while the other is a measurement side. Each of the stream flows through the same sizes of resistances and volumes to ensure that the flowrates through each side of the system are equal.

Both the reference and measurement sides initially flow through a large resistance. A steel, flow setting block, with two red flow setting elements is used to create a high resistance in each stream. Each red flow element allows a maximum flow of 60 ml/min to pass. The streams leaving the block then lead to the delay lines. The extra volume from the delay lines allow the pressure changes due to any change in flow and any change in viscosity to be seen separately. Finally, the gas streams leave the system by passing through another steel flow setting block. At this point silver flow elements with green dot were inserted into the steel block. These allow a maximum flow of 750 ml/min to pass. Both the reference and measurement flows leave the steel block and flow to the gas density detector as the reference and sample flows respectively. Any change in density between the reference and sample streams are recorded using *Pico* 16-bit resolution software. The graphs are plotted using *Microsoft* Excel.

The pressures along each side of the system are monitored using a Furness Controls Differential Pressure Transducer with an output of ±1000 mV corresponding to an input of ± 100 Pa and this is recorded using *Pico* 16-bit resolution software. The graphs are plotted using *Microsoft* Excel.

The other gas stream from the mixer splits again. One sub-stream flows to a steel flow setting block with a red flow element. The flow leaving the block combines with the reference flow entering the gas density detector. This is necessary as the reference flow entering the *Gow-Mac* gas density detector must be at least 20ml/min greater than the sample flow. By adding this extra flow, the reference flow will be greater than the sample flow and will have the same composition as that flowing through the double-sided part of the system.

The other sub-stream was connected to another steel flow setting block which had one red flow element and one silver flow element with a green dot. The main flow enters and passes through the red flow element. The outlet of this is then connected to the inlet at the silver flow element. The flow setting block with both elements mimics the system, as the resistances are the same as the main system and prevents any pressure difference between the system and the tubing from occuring. The outlet from the block is added to the outlet of the gas density detector and exits the system.

A back pressure regulator was added at the end of the system to keep the outlet pressure constant. It was set at 0.05 bar. The exit flowrate was measured using a bubble flowmeter.

Experiments are carried out by switching the 3-way valve and directing the perturbation flow into the system. When a new equilibrium is reached the perturbation flow is then removed from the system by switching the valve back to the original position.

Various experiments were carried out (see Table *6.1*). The first experiment involved determining the baseline of the DPT and GDD recorded over 24 hours. The second experiment involved changing the reference and sample flow rates and observing the changes in the DPT and GDD responses. The third experiments looked at adding a perturbation of a different gas component at different perturbation flow rates to see how the change in molecular weight of the sample gas affected the DPT and GDD results. The fourth set of experiments looked at the effect of changing the perturbation flow rate. The fifth set of experiments were conducted using the same reference, sample and perturbation flow rates but with different binary gas

combinations. Finally, the last set of experiments looked at using helium as the perturbation gas.

Table 6.1 – List of Experiments

Expt #	**Main Gas**	**Sample Gas**	**Perturbation Gas**	**Conditions**
1	N_2	N_2	-	Baseline determination
2	N_2	N_2	N_2	Effect of changing ref and sample flow rates
3	N_2 Ar	N_2 Ar	Ar N_2	Effect of molecular weights in gas combinations
4	He He	He He	Ar N_2	Effect of changing perturbation flow rate
5	N_2 He He	N_2 He He	Ar N_2 Ar	Effect of using different combinations of gases
6	Ar N_2	Ar N_2	He He	Adding helium as the perturbation

6.5. Results

This section will present and interpret the results of the experiments described in Table *6.1* of Section 6.4 including the baseline determination and experiments using different perturbation flow rates and gases.

6.5.1. Baselines

As the previous chapters have shown, it is important that the baseline readings of both the differential pressure transducer (DPT) and the gas density detector (GDD) are constant and relatively free from noise and drifting (Sections 4.5.1 and 5.5.1). Any drifting in the baseline can cause inaccurate calculations when processing the results.

Figure *6.18* shows the baselines recorded from the differential pressure transducer and the gas density detector with readings taken every 10 seconds over a 24-hour period. Only nitrogen

was added to the system. It can be seen that the GDD baseline varies over the recording time while the DPT baseline seems to only vary slightly.

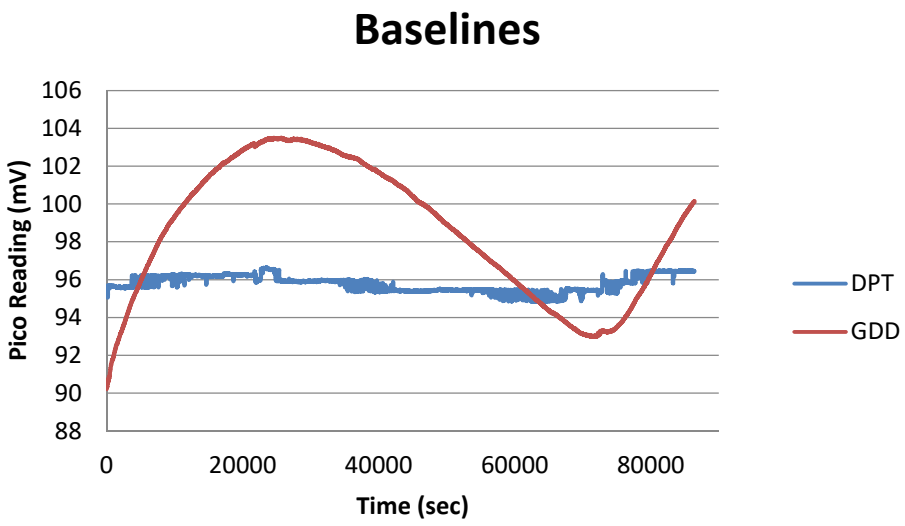

Figure 6.18 - Baselines of the DPT and GDD signals without any perturbation being added to the system

Looking at the DPT baseline more closely (Figure *6.19*), the baseline does change with time. When plotting the two baselines individually on a double axis, both baselines increase and decrease in synchronisation. The GDD makes a smoother transition as there are greater differences in the readings and the points recorded are over a larger range than the DPT readings. It is thought that the variances in the baselines are due to changes in the temperature in the environment around the equipment during the 24-hour period of recording, i.e. from air conditioning and heating.

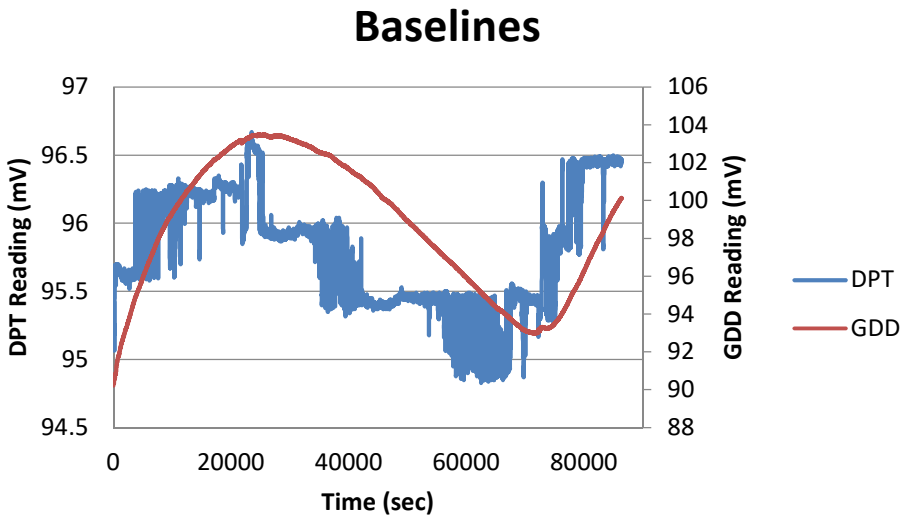

Figure 6.19 - Comparison of DPT and GDD baselines

The average DPT reading is 95.778±0.44 mV. From the graph it can be seen that there are long periods of time where the baseline is fairly constant. Therefore, any calculations can be made without being greatly affected by baseline drifting. This cannot be said for the GDD baseline. The average GDD reading is 98.615±3.548 mV. The standard deviation is much larger for the GDD and the graph does not level out as time passes.

6.5.2. Effect of Changing Reference and Sample Flows

In the gas density detector, it is important to also look at the effect of changing the flows into the detector. There are two input flows into the detector, a reference flow and a sample flow. It is expected that the GDD response will remain constant as the sample flow is changed but will change with the reference flow.

Experiments were carried out to verify if this is in fact the case. Nitrogen was used for both the reference and sample gas. The reference flow was set to 70 ml/min while the sample flow was set to 50 ml/min. Both were controlled by *Porter* instrument mass flow controllers. The GDD instruction manual stated that there must be at least a 20ml/min difference between the reference and sample flow rates. The back-pressure regulator was set to 0.05 bar. The GDD response was recorded using Picolog software recording one reading every second.

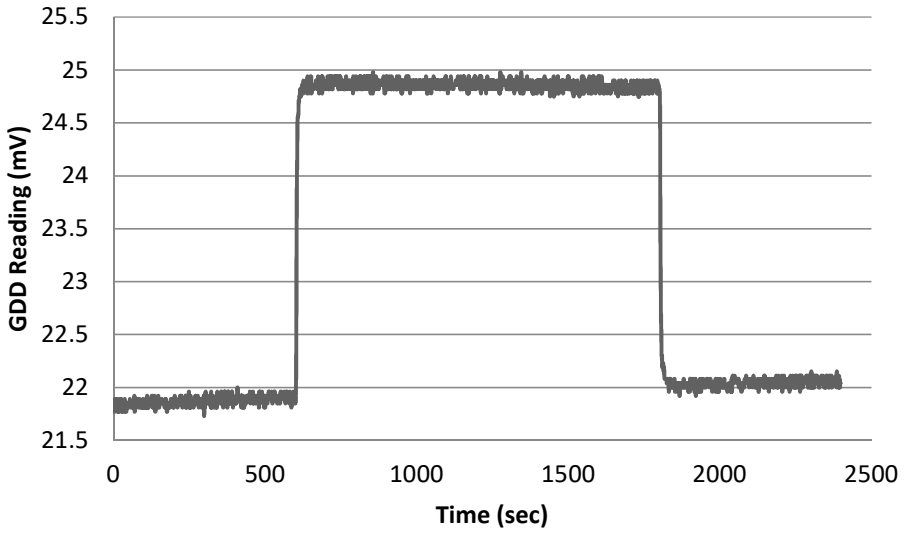

Figure 6.20 - GDD response from increasing and decreasing reference flow

Figure *6.20* shows the GDD response as the reference flow is changed. The reference flow was increased by about 5 ml/min to 75 ml/min after 10 mins and was then reduced to 70 ml/min after a further 20 mins had passed. This gave the response time to settle. When the flow was increased, there was an instantaneous increase in the GDD response as expected. Increasing the reference flow rate by 5 ml/min bring about a 3 mV increase the GDD response.

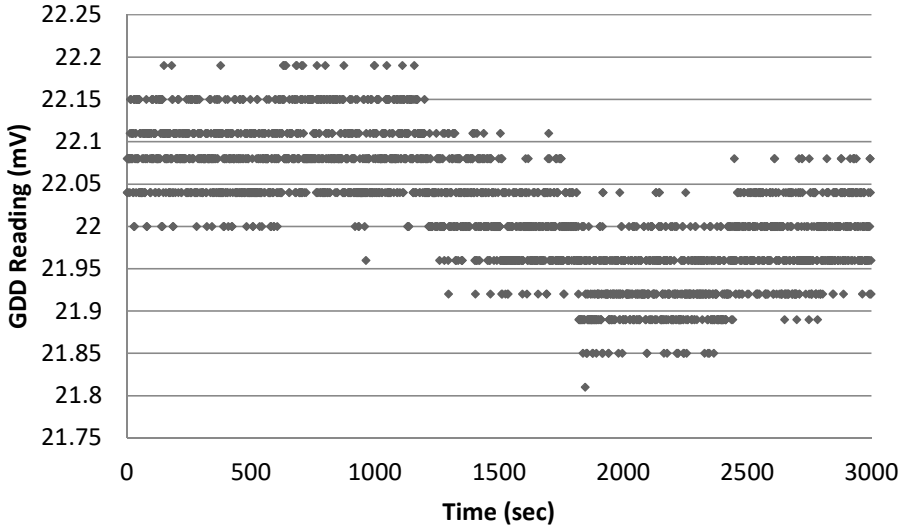

Figure 6.21 - GDD response from changing the sample flow

Figure *6.21* shows the GDD response as the sample flow is changed. The flow was increased by 5 ml/min after 600 seconds then returned to original flow rate after a further 600 seconds. Then the flow was reduced by 5 ml/min and increased again to the original flow rate. This confirms that the GDD response does not change greatly as the sample flow rate is changed.

From Figure *6.21,* it can be seen that an increase of 5 ml/min in the sample flow rate produces no response on the GDD response. A decrease of 5ml/min in the sample flow rate produces ~0.1 mV decrease the GDD response. The response seen is of a similar magnitude to baseline noise and so is considered negligible. As expected, the GDD response remained constant when the sample flow changed and shifted as the reference flow changed.

In such experiments when both the reference and sample loops are running on pure gas, the resistances in both loops should be balanced so the detector should not be affected by flow changes. For the sample loop, this is confirmed by Figure 6.21 suggesting that the loop resistances are in balance. However, Figure 6.20 shows a small response for the reference loop. This may also suggest that the resistances in this loop are out of balance. This will be further investigated in next sections.

6.5.3. Effect of Molecular Weight

To explore the effect of molecular weight, two different combinations of gases were looked at, adding a perturbation of argon to a main flow of nitrogen and adding a perturbation flow of nitrogen to a main flow of argon. This demonstrates the effect that the molecular weights of the components have on the response from the differential pressure transducer (DPT) and the gas density detector (GDD). The relationship between the DPT and the GDD responses will be investigated.

6.5.3.1. Adding Argon to Nitrogen

The molecular weight of argon is 40 g/mol and that of nitrogen is 28 g/mol. When nitrogen is the main gas flowing through the detector, adding a perturbation flow of argon will cause the overall molecular weight to increase and so the density of the sample flow through the detector will increase. The result of adding the perturbation flow can be seen below in Figure *6.22*.

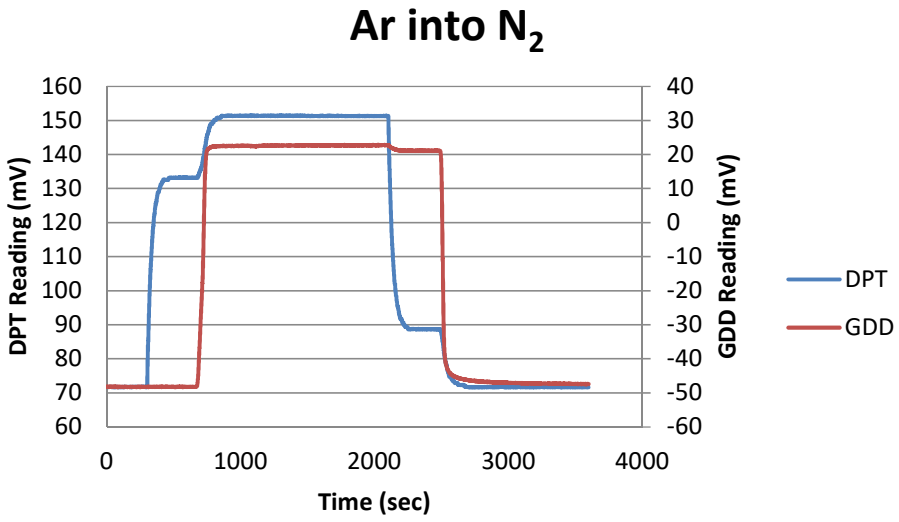

Figure 6.22 - Effects on DPT and GDD readings when adding an argon perturbation flow to main flow of nitrogen

The graph shows the readings from the DPT and GDD before the perturbation flow is added, after it is added and when it is removed again. The system is initially run without any perturbation being added so the baseline line can be seen to be stable. At time t = 300 secs, the perturbation is added to the sample flow. A new baseline is achieved after the changes due to the new flow and gas density have settled. At time t = 2100 secs, the perturbation is removed from the sample flow and again the system settles back to the original baseline. The reference stream into the gas density detector is a nitrogen flow of 50 ml/min while the sample stream is nitrogen stream of about 25 ml/min with a 1.5 ml/min flow of argon added as the perturbation flow.

The DPT response represented by the blue line on the graph shows when argon is added to nitrogen. As expected the changes in pressure due to changes in flow and viscosity can be seen separately. The first step shows the increase in pressure within the system due to the increase in flow caused by adding the perturbation flow. The second step shows the increase in pressure due to the change in viscosity from the addition of the perturbation flow.

The red line on the graph represents the GDD response to the addition and removal of the perturbation flow. As expected, the gas density detector does not show any initial response when the perturbation flow is added to the sample flow. It only shows a response when the density front reaches the detector. This can be seen clearly in Figure *6.22*. Also, the density increases as the argon perturbation is added to the sample flow as the gas mixture now has a greater overall density than the pure nitrogen flow. When the perturbation flow is removed, the GDD response decreases slightly and reaches a new plateau before decreasing more dramatically as the pure nitrogen density front reaches the detector. This is thought to be due to the presence of a gas mixture in the system.

The above experiment was repeated for different perturbation flow rates. The results for the DPT and GDD responses are shown separately below in Figures *6.23* and *6.24* respectively. For both detectors it can be seen that the step sizes increase with the perturbation flow rate. Even at very small perturbation flow rates, any changes in density in the sample flow can be clearly seen on both result graphs.

In Figure *6.24,* as the perturbation flow increases, so does the GDD response to the perturbation flow being removed. For larger perturbation flow rates, the response from the gas density detector to the perturbation flow being removed is greater.

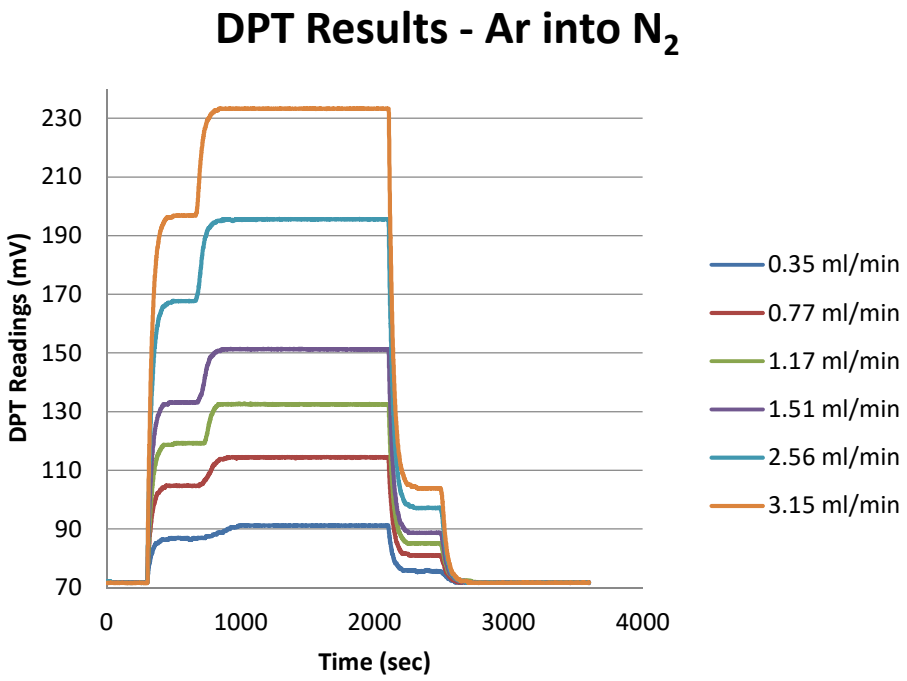

Figure 6.23 - DPT responses to different argon perturbation flows being added to a main flow of nitrogen

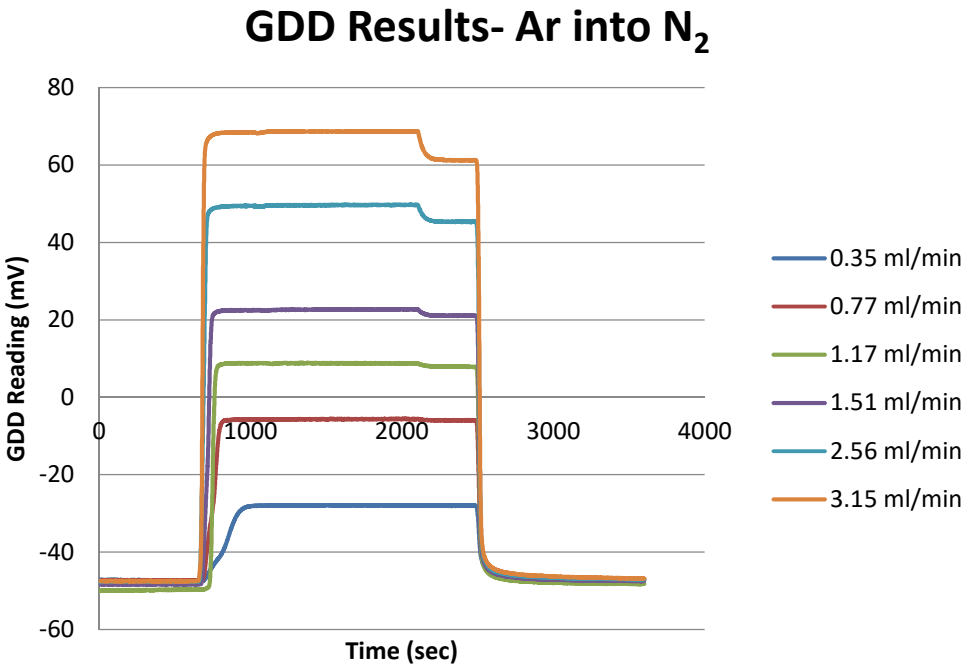

Figure 6.24 - GDD responses to different argon perturbation flows being added to a main flow of nitrogen

It is essential to look into the linearity of the flow step change, ΔP_1 (from Figure *5.2*), in the DPT reading and the increase in the GDD reading with the increase in perturbation flow. This is shown graphically below in Figures *6.25* and *6.26*. The step change in the DPT reading due to the change in flow corresponds to the perturbation flow rate, Q_5 in the theory section, while the change in the GDD reading corresponds to the change in density due to the addition of the perturbation flow, $\Delta\rho$.

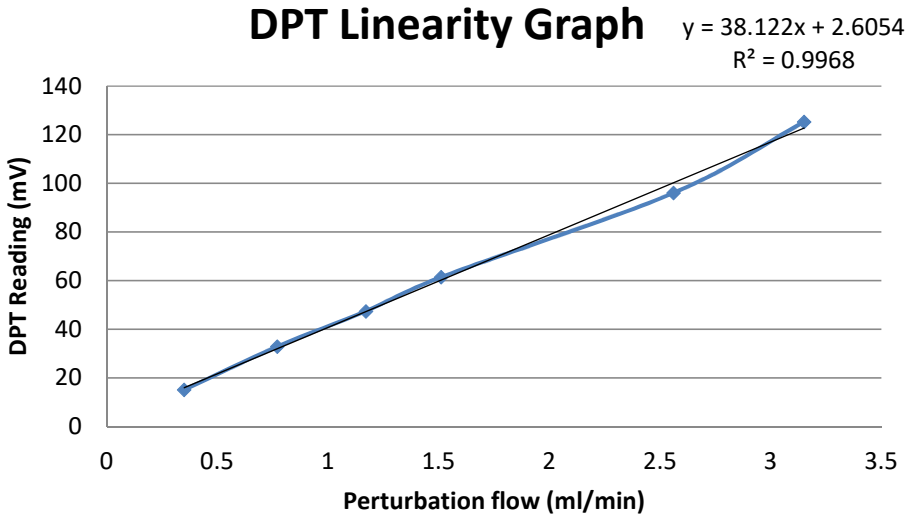

Figure 6.25 - Comparison between perturbation flow rate and DPT readings

It can be seen from Figure *6.25*, that the DPT step relating to the change in flow is linearly related to the perturbation flow. This is to be expected as the increase in flow causing the change in the DPT signal is due to the addition of the perturbation. The high R^2 value shows that the points follow closely to the regression line on the graph.

The GDD reading in Figure *6.26* follows a similar pattern. As the perturbation flow increases, so does the reading from the GDD. The R^2 value is lower for the GDD than the DPT results. It is still high at 98% so can still be considered as follows a linear relationship.

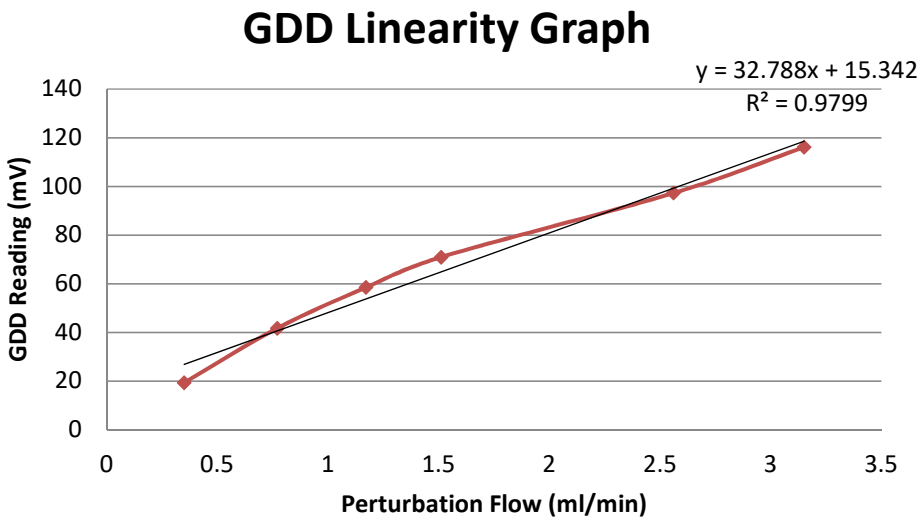

Figure 6.26 - Comparison between perturbation flow rate and GDD readings

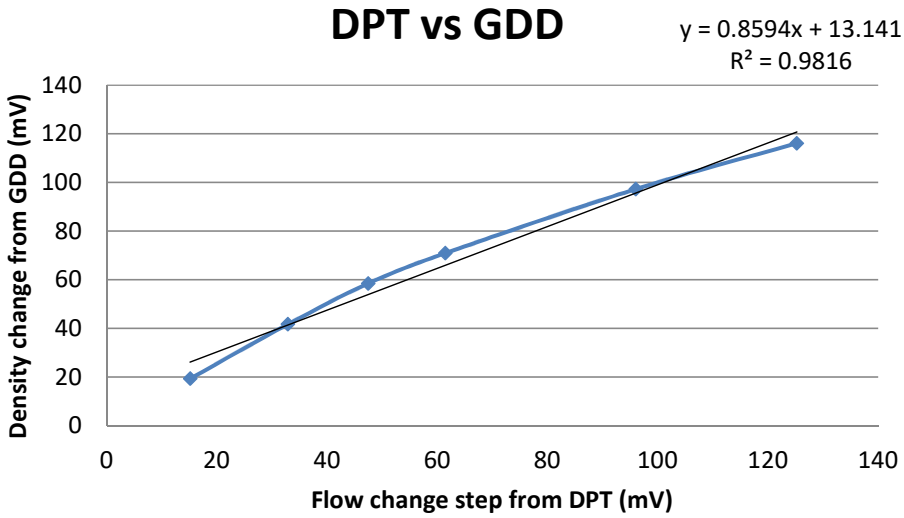

Figure 6.27 - Comparison of DPT and GDD step changes

Figure *6.27* plots the change in flow as detected by the DPT against the change in density as recorded from the GDD. The R^2 value is around 98% like the GDD results.

Overall, the results here have shown that, as expected, there is a linear relationship between the perturbation flow rate added to the system and the change in density identified by the gas density detector. Therefore, the GDD could be used to quantify the composition of a gas mixture.

6.5.3.2. *Adding Nitrogen to Argon*

This set of results looks at the addition of a lighter molecular weight perturbation gas, nitrogen, being added to the heavier main gas, argon. By adding nitrogen to the main flow of argon, it is expected that the sample flow will decrease in density. A typical result is shown in Figure *6.28*.

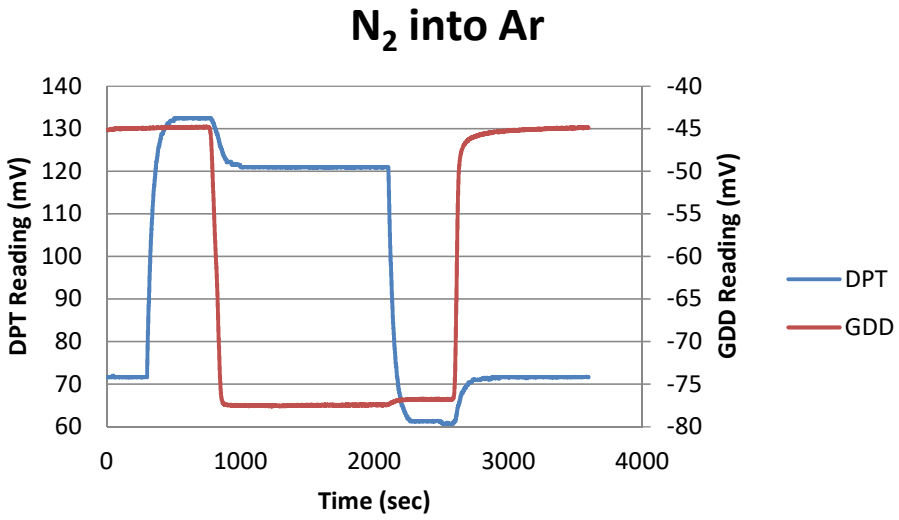

Figure 6.28 - Effects on DPT and GDD readings when adding nitrogen perturbation flow to a main flow of argon

Like in the previous experiments, the system is initially run with only argon flowing through both the reference and sample streams in the system. At time t=300secs, the perturbation flow was added to the system. A new baseline is achieved after changes due to flow and density have settled. At time t=2100secs, the perturbation flow is removed from the system and the signals are allowed time to settle back to the original baselines. The reference stream into the GDD is an argon flow rate of 50 ml/min. The sample stream is an argon flow of 25 ml/min with a 1.4 ml/min flow of nitrogen added as the perturbation flow.

The DPT response is represented by the blue line on the graph. It again shows the changes in pressure in the system due to the change in flow and the change in viscosity separately. As with the previous experiment adding argon to nitrogen, there is an increase in pressure in the system due to the addition of the perturbation flow. Unlike the previous experiments, the main gas through the system is heavier than the perturbation gas. As expected, when the viscosity front reached the DPT, it causes the pressure in the system to decrease due to the reduction in

viscosity and hence density as the argon and the nitrogen mix. This can be seen clearly in Figure *6.28*.

The GDD response to the addition and removal of the perturbation flow is shown by the red line on the graph. Again, the gas density detector shows no initial response when the perturbation is added to the system. A response is evident when the density front reaches the detector. It can be seen that the density decreases after the nitrogen perturbation is added to the sample flow as the gas mixture now has a lower density than the pure argon flow. Also, when the perturbation flow is removed there is an immediate response from the GDD.

The same experiment was repeated using different perturbation flow rates. The DPT and GDD responses are shown on Figures *6.29* and *6.30* respectively.

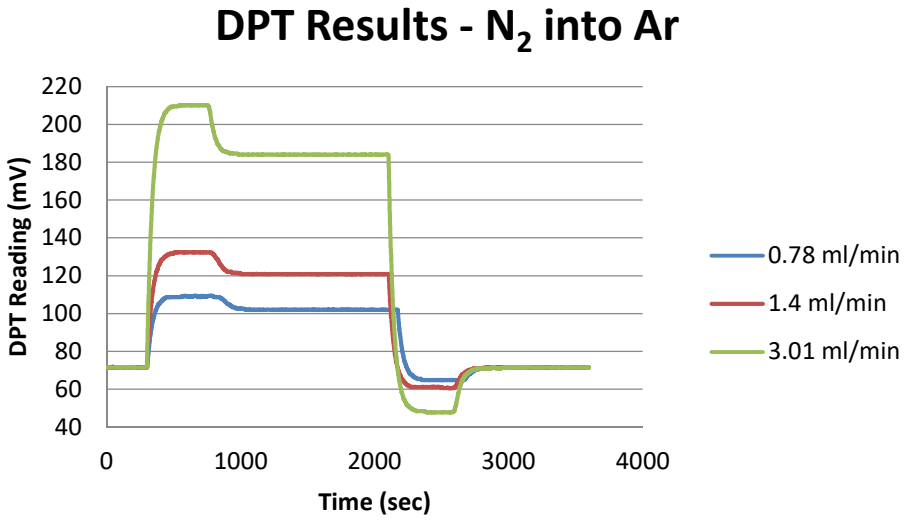

Figure 6.29 - DPT response to different nitrogen flow rates being added to a main flow of argon

The DPT results show that as the perturbation flow increases, so does the DPT response. A response can be clearly seen at low perturbation flow rates. The gas density detector also shows that the response increase with perturbation flow rate.

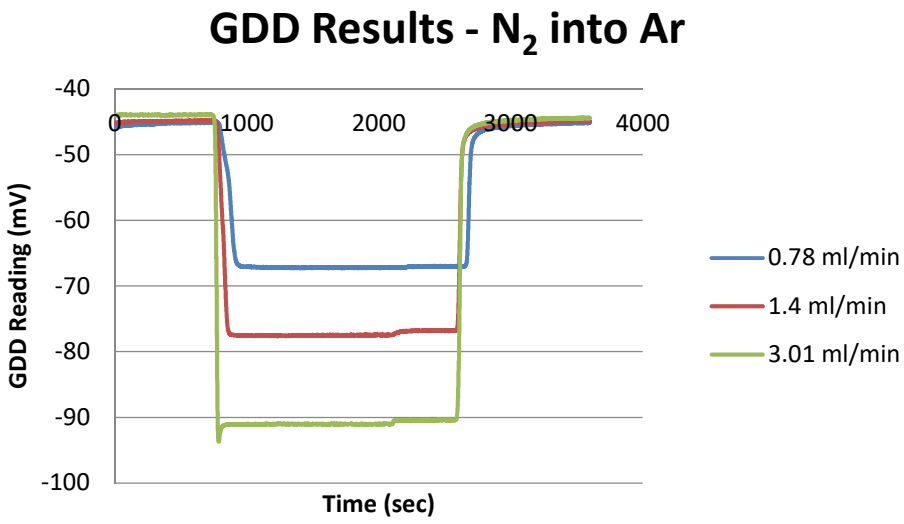

Figure 6.30 - GDD response to different nitrogen flow rates being added to a main flow of argon

The relationship between the perturbation flow rate and the DPT response is shown in Figure *6.31*. Like in the argon into nitrogen system, as expected, the nitrogen into argon system shows a good linear relationship (R^2 value of 99.7%) between the perturbation flow rate and the DPT results.

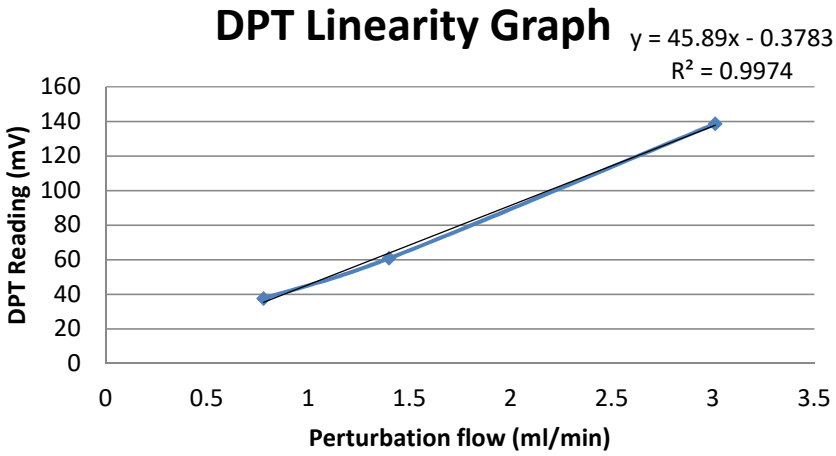

Figure 6.31 - Comparison between perturbation flow rate and DPT readings in nitrogen into argon system

Figure *6.32* shows the relationship between the perturbation flow rate and the gas density detector response.

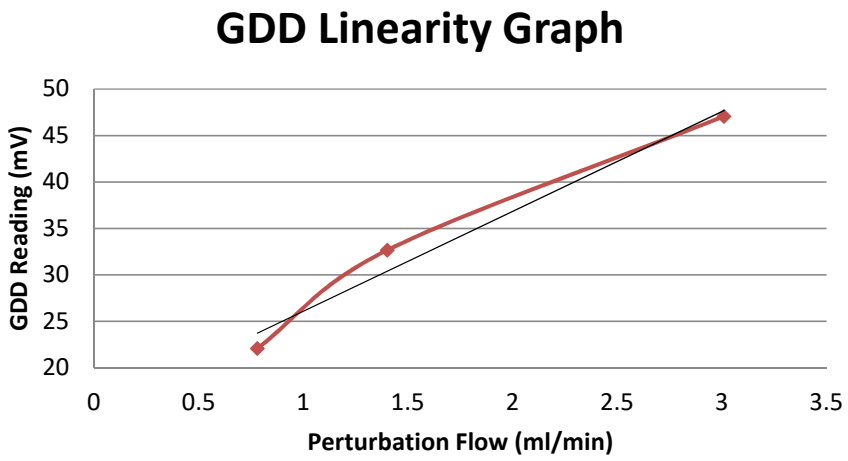

Figure 6.32 - Comparison between perturbation flow rate and GDD readings in nitrogen into argon system

The graph shows that the GDD response increases with perturbation flow rate but the line is more of a polynomial curve shape than a linear straight line. If more experiments were carried out using different perturbation flows then more points could be plotted and could give a more conclusive result.

The change in pressure due to the change in flow from the DPT was plotted against the change in density recorded from the GDD. The result is shown in Figure *6.33*.

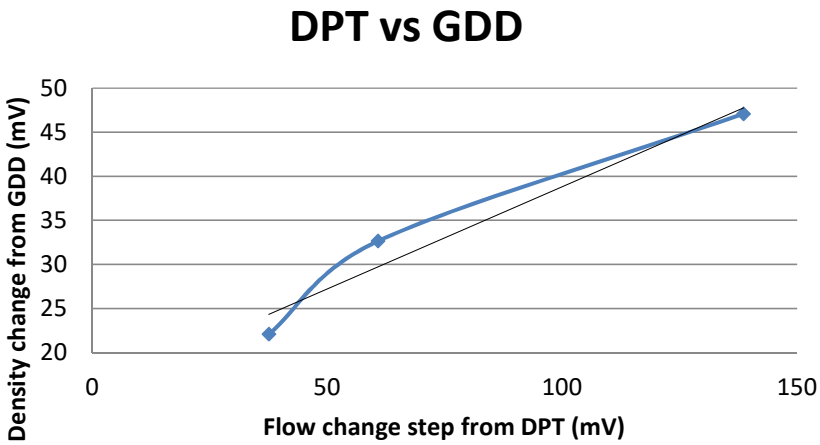

Figure 6.33 - Comparison of DPT and GDD steps

Like in Figure *6.32*, no linear relationship can be drawn from Figure *6.33* due to the limited number of points but it can be observed that as the flow step from the DPT increases, the density change from the GDD increases.

6.5.3.3. Conclusions

The differential pressure transducer results have shown that as the perturbation flow rate, Q_5, increases, the pressure in the system increases due to the change in flow and the change in viscosity. It has also been shown that the pressure change due to the increased flow increases linearly with the perturbation flow rate.

The gas density detector results have shown a linear response to increasing the perturbation flow rate. By adding the perturbation flow the composition of the sample gas is changed from a pure gas flow to a gas mixture. The change in density, $\Delta\rho$, caused by this composition modification is recorded by the GDD and increases with the perturbation flow rate.

This section has confirmed the relationship from theory Section 6.3.3.3, that the change in the sample flow rate is proportional to the change in density of the sample flow when the perturbation flow is added.

6.3.4. Effect of Changing Perturbation Flow Rate

The effect of changing the perturbation flow rate will be investigated using two different combinations of gases, adding a perturbation flow of argon to a main flow of helium and adding a perturbation flow of nitrogen to a main flow of helium. Both combinations will be tested at a perturbation flow rate of 2.0 ml/min and 2.6 ml/min. This will allow a comparison to be seen between the response from the differential pressure transducer (DPT) and the gas density detector (GDD) when the perturbation flow is changed and also when the perturbation gas is changed, each affecting the molecular weight of the gas mixture within the system.

6.3.4.1. DPT Readings at Different Perturbation Flow Rates

In these experiments, a pure component perturbation flow is added to a pure main flow. The gases used in different combinations are argon, nitrogen and helium. In all these experiments, the component with the higher molecular weight is added to that of the lower molecular weight. The main flow is 50ml/min, the sample flow is 25ml/min and the perturbation flow is either 2.0ml/min or 2.6ml/min. The DPT results can be seen in Figure *6.34*.

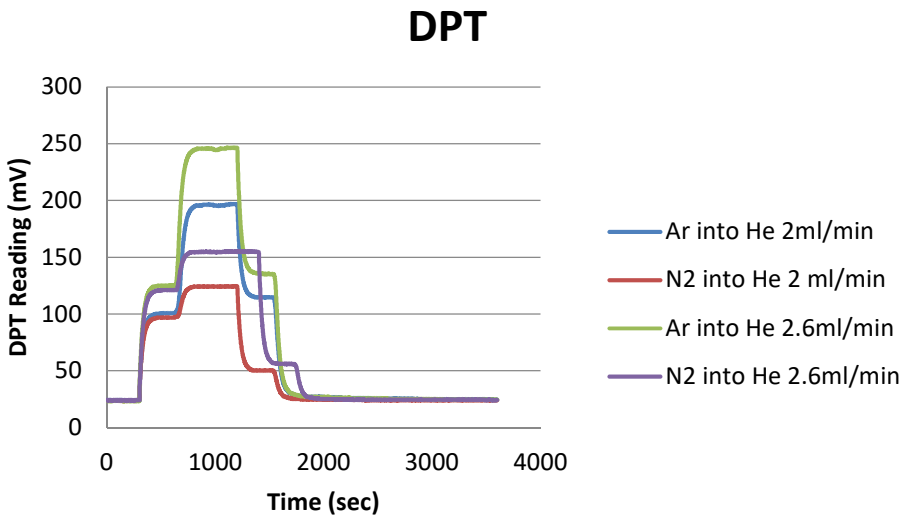

Figure 6.34 – DPT Reading for Nitrogen or Argon Perturbation Flow into a Main Flow of Helium

The first step in DPT results, ΔP_1, shows the response from the increase in pressure due to the addition of the perturbation flow. It was expected that the first steps for each perturbation flow rate would be the same size due to the main and perturbation flows all being equal.

The second step in the DPT results, ΔP_2, represents the pressure change due to the change in viscosity. It was expected, the pressure change due to the change in viscosity is greater when a larger perturbation flow is added. Figure *6.34* shows that this is indeed the case. The actual pressure differences caused by the change in flow and the change in viscosity are shown in Table *6.2*.

Table 6.2 – Actual DPT differences from different gas combinations and perturbation flow rates

Perturbation Flow Rate (ml/min)	Ar into He		N_2 into He	
	ΔP_1	ΔP_2	ΔP_1	ΔP_2
2	76.60	96.09	72.97	100.32
2.6	101.48	121.61	97.05	130.43
Percentage Difference				
76.923%	75.483%	79.015%	75.188%	76.915%

Table *6.2* compares the percentage difference between the perturbation flow rates, the ΔP_1 and ΔP_2. It shows that the difference in pressure changes due to change in flow and change in viscosity are all proportional to the change in perturbation flow rate.

6.3.4.2. GDD Readings at Different Perturbation Flow Rates

For the same experiments carried out in Section *6.5.3.1*, the GDD results are shown in Figure *6.35*. Like in previous experiments, the perturbation flow was added at *t*= 300 secs. There is no response due to the increase in flow rate when the perturbation flow is added so ΔD_1 is zero.

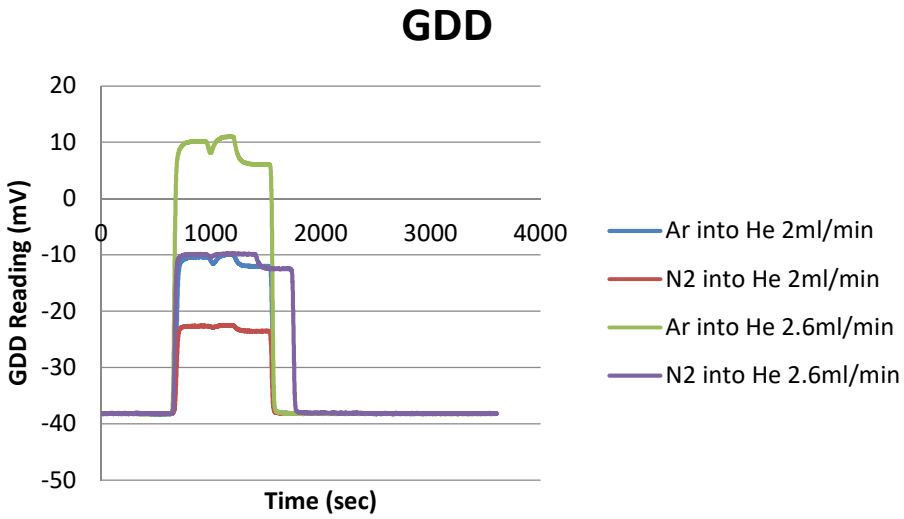

Figure 6.35 - GDD Reading for Nitrogen or Argon Perturbation Flow into a Main Flow of Helium

The step change that can be seen here, ΔD_2, represents the change in density as the gas mixture reaches the gas density detector. The actual density differences caused by the change in density are shown in Table *6.3*.

It was expected that the GDD would be most responsive adding a 2.6 ml/min argon perturbation flow to a main flow of helium due to these components having the greatest difference in molecular weights and the higher perturbation flow rate. Figure *6.35* shows that this is the case.

Table 6.3 – Actual GDD differences from different gas combinations and perturbation flow rates

Perturbation Flow Rate (ml/min)	**Ar into He**	**N_2 into He**
	ΔD_2	**ΔD_2**
2	28.27	15.49
2.6	49.21	28.35
Percentage Difference		
76.923%	57.448%	54.638%

Unlike the DPT results, the results for the pressure change due to the change in density in the GDD is not related to the change in flow rate. The actual pressure differences are recorded in Table *6.3*. These results will be discussed in Section 6.6.3. The shape of the results curves will also be discussed in this section.

6.3.4.3. Conclusions

The differential pressure transducer results have shown that as the perturbation flow rate, Q_5, increases, the pressure in the system increases due to the change in flow (ΔP_1) and the change in viscosity of the sample flow (ΔP_2) (see Table *6.4*). It has also been shown that the pressure difference due to the increased flow in the sample line and the pressure change due to the change in density is proportional to the perturbation flow rate being added to the system.

Table 6.4 – Actual DPT and GDD differences from different gas combinations and perturbation flow rates

Perturbation Flow Rate, Q_5 (ml/min)	**Ar into He**			**N_2 into He**		
	ΔP_1	**ΔP_2**	**ΔD_2**	**ΔP_1**	**ΔP_2**	**ΔD_2**
2	76.60	96.09	28.27	72.97	100.32	15.49
2.6	101.48	121.61	49.21	97.05	130.43	28.35
Percentage Difference						
76.923%	75.483%	79.015%	57.448%	75.188%	76.915%	54.638%

The gas density detector results have shown to increase with the perturbation flow rate (see Table *6.4*). By adding the perturbation flow, the composition of the sample gas is changed from a pure gas flow to a gas mixture. The change in density, $\Delta\rho$, caused by this composition modification is recorded by the GDD and increases with the perturbation flow rate, Q_5, but it is not proportional to Q_5.

This section has confirmed the relationship from Theory Section 6.3.3.3, that the change in the sample flow rate is proportional to the change in density of the sample flow when the perturbation flow is added. This can only be seen from the DPT results.

6.5.5. Binary Gas Systems

This section looks at using different combinations of gases to investigate the differences in the differential pressure transducer and gas density detector results.

6.5.5.1. Molecular Weight Differences-DPT Results

In these experiments, a pure component perturbation flow is added to a pure main flow. The gases used in different combinations are argon, nitrogen and helium. In all these experiments, the component with the higher molecular weight is added to that of the lower molecular weight. The main flow is 50ml/min, the sample flow is 25 ml/min and the perturbation flow is 2.5 ml/min. The DPT results can be seen in Figure *6.36*.

The first step in DPT results, ΔP_1, shows the response from the increase in pressure due to the addition of the perturbation flow. It was expected that the first steps in all lines would be the same size due to the main and perturbation flows all being equal.

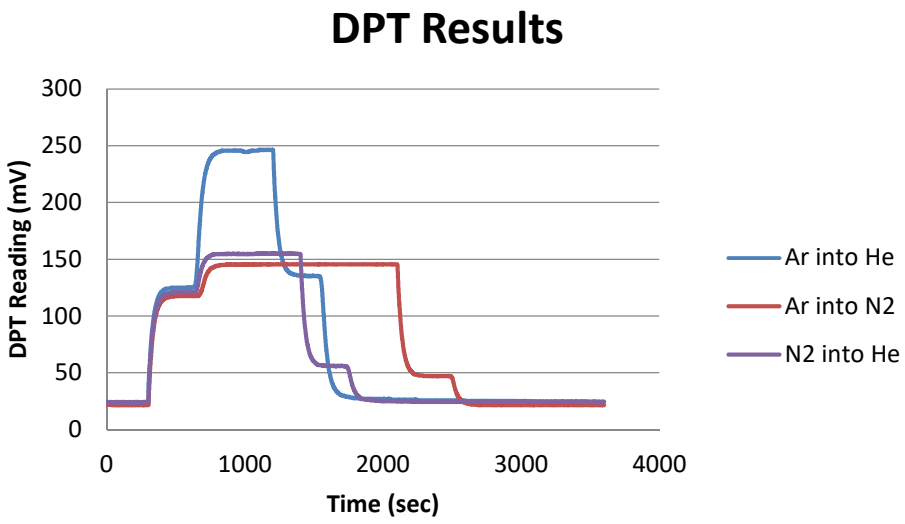

Figure 6.36 - DPT results from adding different combinations of pure components to the system

The second step in the DPT results, ΔP_2, represents the pressure change due to the change in viscosity. Argon has a molecular weight of 40 g/mol, nitrogen 28 g/mol and helium has a molecular weight of 4 g/mol. Argon and helium have the largest difference in molecular weights so it was expected that the viscosity change when argon was added to helium would be greatest. Figure *6.36* shows that this is indeed the case. The actual pressure differences caused by the change in flow and the change in viscosity are shown in Table *6.5*.

Table 6.5 – Actual DPT pressure differences from different gas combinations

Main Flow	***Perturbation Flow***	***Difference in Molecular Weights***	***ΔP_1 (mV)***	***ΔP_2 (mV)***
Nitrogen	Argon	12	96.08	27.85
Helium	Nitrogen	24	97.09	33.49
Helium	Argon	36	101.49	120.92

The pressure changes due to the change in viscosity did increase with the difference in molecular weight but the results show that there does not seem to be any relationship between the pressure difference due to addition of the perturbation flow and the molecular weights of the components involved.

6.5.5.2. *Molecular Weight Differences-GDD Results*

For the same experiments carried out in Section *6.5.3.1*, the GDD results are shown in Figure *6.37*. Like in previous experiments, the perturbation flow was added at t= 300 secs. There is no response due to the increase in flow rate when the perturbation flow is added so ΔD_1 is zero.

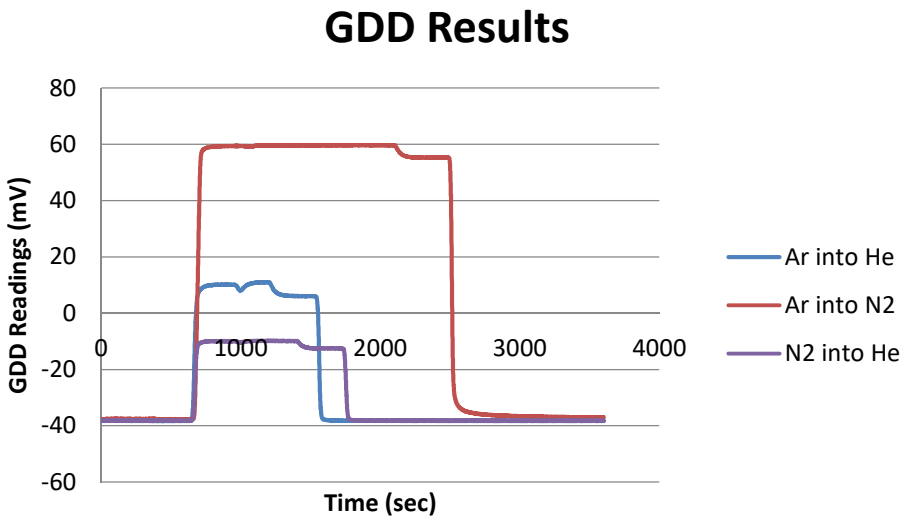

Figure 6.37 - GDD results from adding different combinations of pure components to the system

The step change that can be seen here, ΔD_2, represents the change in density as the gas mixture reaches the gas density detector. The actual density differences caused by the change in density are shown in Table *6.6*.

Table 6.6 – Actual GDD reading differences from different gas combinations

Main Flow	***Perturbation Flow***	***Difference in Molecular Weights***	***ΔD_2 (mV)***
Nitrogen	Argon	12	97.23
Helium	Nitrogen	24	25.68
Helium	Argon	36	49.21

It was expected that the greatest GDD reading would come from adding an argon perturbation flow to a main flow of helium due to these components having the greatest difference in molecular weights. This, however, was not the case. Again, no relationship was found between the GDD reading and the difference in molecular weight.

6.5.5.3. Conclusions

The differential pressure transducer results have shown that as the perturbation flow rate, Q_5, increases, the pressure increase in the system due to the change in flow (ΔP_1) is consistent when the perturbation flow rate remains the same with different pure gas combinations (see Section *6.3.3*). The change in pressure due to the change in viscosity, ΔP_2, does not follow what is expected.

From the GDD results, there is no relationship between the GDD response and the change in the density of the gas mixture created by adding the perturbation flows. It was expected that the greatest ΔD_2 value would be when a helium was perturbed with argon but this was not the case.

The experimental results obtained do not validate the theoretical relationship that were developed in the theory section.

6.5.6. Adding Helium as Perturbation Gas

This section looks at adding a perturbation gas of helium to a main flow of either argon or nitrogen. In these experiments, the component with the lower molecular weight is added to that of the higher molecular weight. The main flow is 50ml/min, the sample flow is 25 ml/min and the perturbation flow is 2.6 ml/min.

Helium has a lower molecular weight than both argon and nitrogen so it was expected that the DPT and GDD readings would follow the same pattern as adding nitrogen to argon (Section *6.5.3.2.*).

Figure *6.38* shows the DPT results from the experiments. As expected, ΔP_2 is positive due to the helium increasing the viscosity of the sample flow.

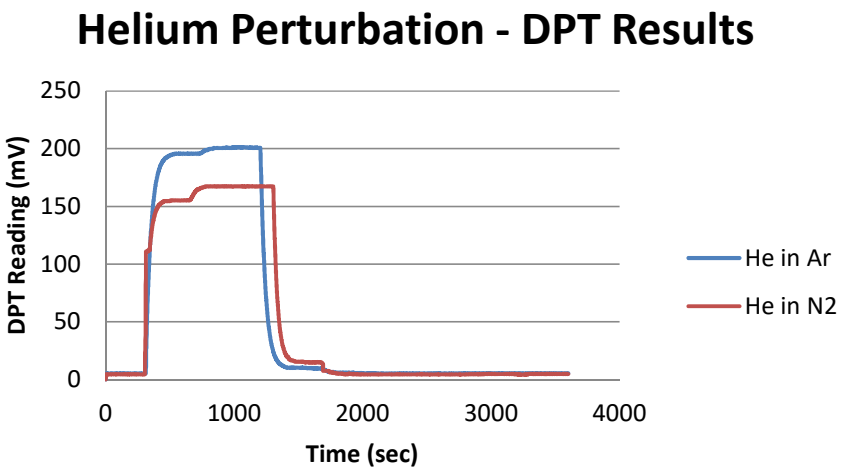

Figure 6.38 - DPT results from adding different combinations of pure components to the system

Figure *6.39* shows the GDD results from the experiments. It was expected that ΔD_2 would be negative due to the helium reducing the density of the sample flow but instead the GDD response has a positive ΔD_2 after initially decreasing the eventual response is that the GDD reading increases.

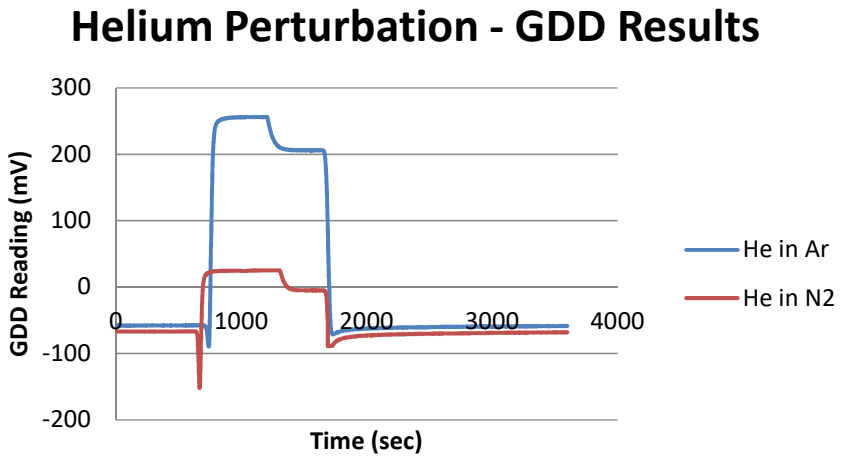

Figure 6.39 - GDD results from adding different combinations of pure components to the system

These results are difficult to explain and will be considered in the discussion (Section *6.6.4.*).

6.6. Discussion and Future Work

6.6.1. Baseline Test

As discussed in the previous two discussion sections, it is important that the baseline in the experiments is relatively stable and free from noise and drift. Any drifting in the baseline will affect the accuracy of the area calculations.

Figures *6.18* and *6.19* show a DPT recording of the baseline for 24 hours on different scales. The average DPT reading was 95.778 mV and the standard deviation was 0.44 mV. A DPT reading of 0.1 mV is equivalent to 0.01 Pa. The DPT baseline did increase and decrease, or drift, over the 24-hour period. This was thought to be due to changes in the environment of the experimental set-up is situated throughout the day and night, e.g. temperature changes from heating and cooling systems. The actual experiments last 40 minutes. The DPT baseline does not vary in that time. Therefore, the baseline is adequately stable for the experiments.

Figures *6.18* and *6.19* also show the GDD recording of the baseline for 24 hours. The average GDD reading was 98.615 mV but the standard deviation was 3.548 mV so there was a lot more variance in the GDD results over the 24-hour period. The GDD baseline did increase and decrease, or drift, over the 24-hour period and followed the same pattern as the DPT recording. As mentioned previously, the actual experiments last 40 minutes. During the experiments, the GDD baseline does vary in that time but not enough to make a significant difference to results. Once the baseline is stable enough (see *6.6.2.*), experiments can be carried out.

The variance in the GDD results could be minimised by sealing all the experimental equipment in an enclosure. By building an enclosure around the apparatus, it will be shielded from changes in the temperature of the external environment and could reduce the variability in GDD response.

6.6.2. GDD Baseline Settle Time

When carrying out the experiments, the GDD had to be switched on and left to equilibrate for 3-4 hours before the experiments could be conducted. The change over the course of a day in the baseline can be seen in Figure *6.40*.

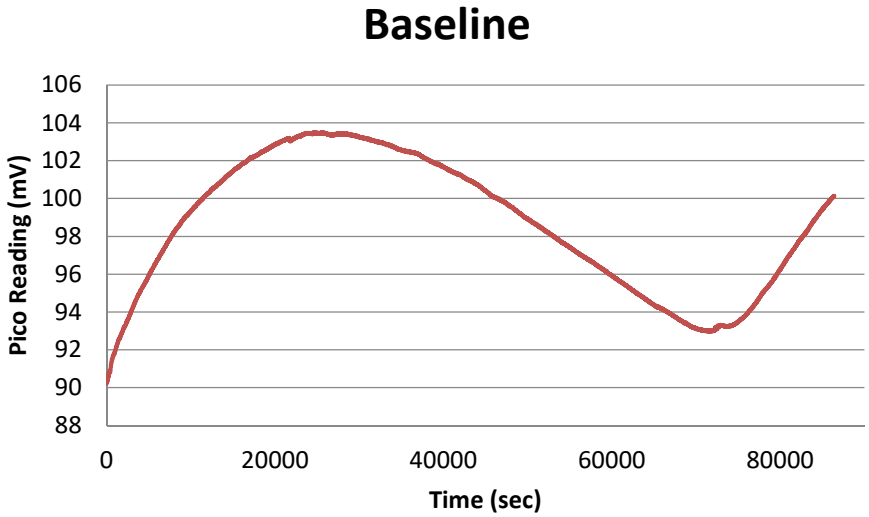

Figure 6.40 - GDD baseline recorded over 24 hours

Each experiment was run for a maximum of 40 minutes so it was found after running the equipment with just the main and sample gas flowing for 3-4 hours before a perturbation is added allowed the reading to be at such a level that it would return to the original baseline after the perturbation flow had stopped.

To reduce this set-up time, an enclosure set at a constant temperature to encompass all the experimental equipment would be advantageous and so could shield the apparatus from any environmental effects in the lab space.

6.6.3. Helium Experiments -Adding Perturbation to Helium Main Flow

In Section 6.5.4., a perturbation flow of either argon or nitrogen was added to a main flow of helium. The DPT results obtained were as expected (see Figure *6.34*). The increase in perturbation flow, Q_5, was proportional to the pressure change due to the increase in sample flow as the perturbation is added, ΔP_1, and the pressure change due to the change in gas density caused by the addition of the perturbation, ΔP_2.

The GDD results (Figure *6.35*) found that the change in density recorded, ΔD_2, was not proportional to the perturbation flow rate, Q_5. Helium has a much lower density than either

nitrogen and argon. This can be seen in Table *6.7*. The addition of the perturbation to the helium main flow would increase the density of the sample flow and so would create a response in the GDD. Further work could be conducted to establish a relationship between the change in density of the gas mixture and the GDD results.

Table 6.7 – Physical Properties of Components

Component	**Molecular Weight (g/mol)**	**Density (g/L)**
Helium	4	0.1786
Nitrogen	28	1.251
Argon	40	1.784

Similar issues were reported by Brandes *et al*. (1984) [19] where it was found that when helium was used as a carrier gas, results with some errors were obtained. This was thought to be due to back diffusion of the sample flow into the reference flow so higher flows would be required than those used in the experiments carried out in this work.

In all experiments conducted where helium was used as the main flow, there was a consistent, repetitive dip in pressure at the same time (about t=1000 secs) after the perturbation has been added in both the DPT and GDD readings. These can be seen clearly in Figures *6.34* and *6.35* below.

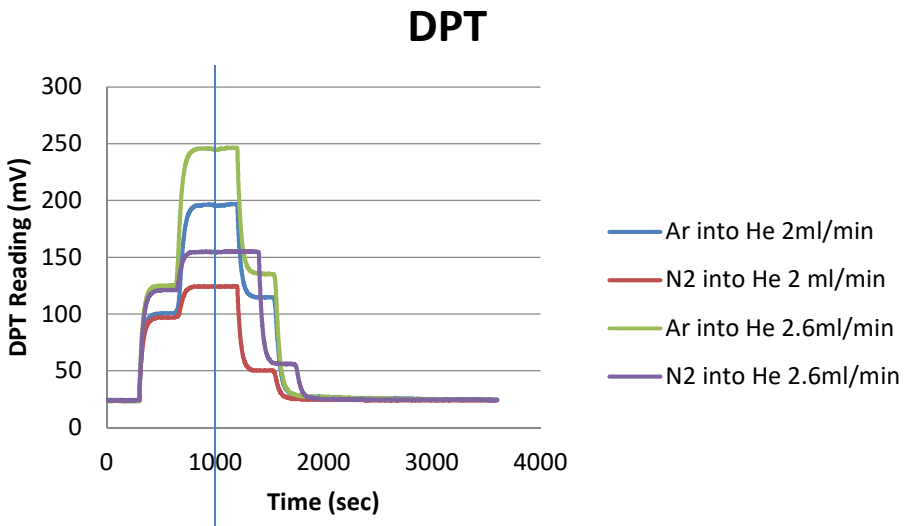

Figure 6.34 – DPT Reading for Nitrogen or Argon Perturbation Flow into a Main Flow of Helium

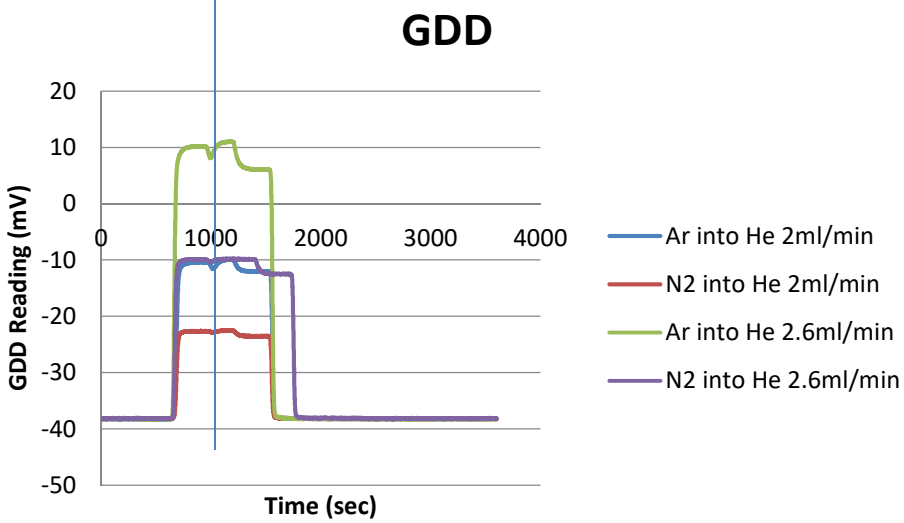

Figure 6.35- GDD Reading for Nitrogen or Argon Perturbation Flow into a Main Flow of Helium

The experiments were all conducted under the same conditions of flow rate and in the same environment with the same timings.

This type of effect has been seen before in viscosity measurements where a large composition effect (viscosity change) has passed through a back pressure regulator. It is symptomatic of the change in viscosity causing a change in resistance of the internal jet of the back pressure

regulator. This produces a spike because the regulator responds more slowly than the time taken for the composition front to pass through the device.

The same effect is not seen when the perturbation is removed from the system as the GDD is in balance and does not respond to flow changes. This suggests that the GDD responds to flow changes when the perturbation flow is added and the GDD on the sample flow loop is out of balance in terms of flow and composition. For this to happen, the resistances k_5 and k_6 must be significant. The previous assumption in the material balance of the system that k_5 and k_6 are negligible is incorrect. Further investigation into this effect is required.

6.6.4. Helium Experiments – Adding Helium as Perturbation Gas

When helium is added as a perturbation gas to a main flow of argon or nitrogen, the results were not as expected (see Section *6.5.6.*). It was expected that the results graph would be like those achieved when nitrogen was added as the perturbation to a main flow of argon (Figure *6.28*) where the perturbation gas with a lower molecular weight is added to a main flow with a higher molecular weight therefore decreasing the density of the gas mixture. When compared to argon perturbation into nitrogen and nitrogen perturbation into argon experiments which validate the derivations from Section 6.3, the theory does not hold true for the addition of nitrogen or argon perturbation into helium.

Figure *6.28* shows the DPT and GDD response of perturbing argon with nitrogen. As the perturbation flow is added to the sample flow, ΔP_1 on the DPT reading increases as expected due to the increase in the flow rate. ΔP_2 on the DPT reading is negative due to the decrease in the viscosity as nitrogen mixes with the argon and reduces the density of the sample flow. The GDD response when nitrogen perturbs the argon main flow is also as expected. When the perturbation flow is added there is no response to the change in the sample flow. The GDD response, ΔD_2, decreases when the new density front is detected due to the reduction in gas density as the nitrogen mixes with the main flow of argon. These results are expected and validate the theory derived in Section 6.3.

Figure *6.38* shows the DPT recordings when a helium perturbation flow is added to a main flow of nitrogen or argon. As the perturbation flow is added to the sample flow, ΔP_1 on the DPT reading increases as expected due to the increase in the flow rate. ΔP_2 on the DPT reading

is also positive. This was as expected due to the increase in the viscosity as helium mixes with the main flow.

Figure *6.41* shows the DPT results comparing different combinations of pure components, all with a main flow of 50ml/min, sample flow of 25ml/min and perturbation flow of about 2.5ml/min. The dashed lines show the experiments when the perturbation flow has a higher molecular weight and density than the main flow so follow the expected pattern. The solid lines show the helium experiments when the perturbation flow has a lower molecular weight and density than the main flow. Additional experiments using different components with different densities would be beneficial to further test the derived theory.

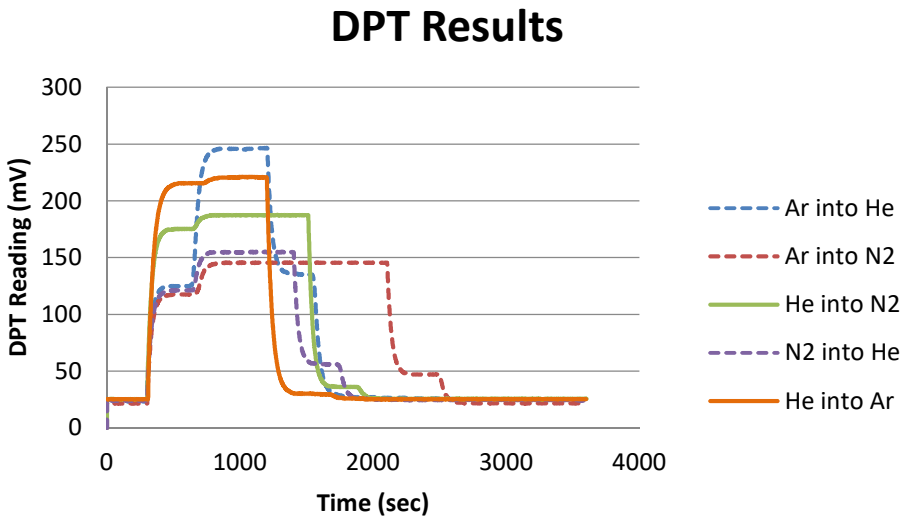

Figure 6.41 - DPT results from adding different perturbation to main flow combinations

Figure *6.39* shows the GDD recordings when a helium perturbation flow is added to a main flow of nitrogen or argon. The GDD response was not as expected. When the perturbation flow is added there is no response to the change in the sample flow. However, the GDD response, $\Delta D_{2,}$ increases overall when the new density front is detected. This is unexpected as it is though that there will be a reduction in gas density as the helium mixes with the main flow. In each combination of adding helium to either nitrogen or argon, the response starts to decrease as expected but then increases sharply after this spike downwards.

Figure *6.42* shows the GDD results comparing the same combinations of pure components as in Figure *6.41*. The dashed lines show the experiments when the perturbation flow has a higher molecular weight and density than the main flow so follow the expected pattern. The solid lines show the helium experiments when the perturbation flow has a lower molecular weight and density than the main flow. Again, the helium perturbation results are anomalies to the theory.

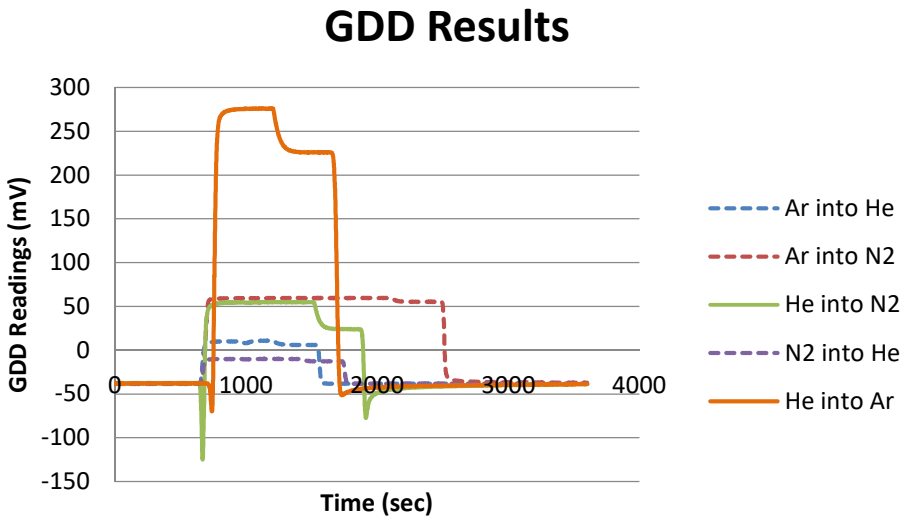

Figure 6.42 - GDD results from adding different perturbation to main flow combinations

Further work needs to be carried out to using different gases, perturbing the gas of the higher molecular weight with one of a lower molecular weight to find out if these results are anomalies. The use of a denser gas like xenon had been considered but were not completed.

Using helium as a component has been problematic when used as the main flow gas and the perturbation gas. It would be beneficial to repeat these experiments using hydrogen instead of helium.

6.6.5. Viscosity Effects on the GDD

The effect on the density of the gas mixture in the system when the perturbation is added is considered. The density of argon is 25% greater than nitrogen. When argon or nitrogen is added to helium, it is expected that the step height observed by the GDD response when adding argon will be 25% greater than adding nitrogen for the same flow rates. However, in the GDD trace in Figure *6.35*, the step height for argon is nearly double that of nitrogen. It can be seen from the DPT traces in Figure *6.34* that similar perturbation flows have been used therefore the reason for the over measurement in the GDD output must be due to a second effect taking place when the density is measured. The second effect could be the viscosity change since we have established the GDD is also sensitive to changes in flow as well as density. The results in Table 6.5 shows that this is true given the viscosity effect for adding argon as a perturbation (ΔP_2) is almost 4 times that of using nitrogen as a perturbation. If the viscosity and density are being measured together then it is entirely possible that the observed effect is correct.

The most convincing evidence for the GDD responding to both viscosity and density at the same time are the experiments of helium perturbations into argon and nitrogen. Figure *6.38* shows the results from experiments where helium is added argon or nitrogen are compared on the next page. As previously discussed in Section 6.6.3, it can be seen that the steps in the GDD are not as expected. The GDD response follows the same trend as the viscosity steps in the DPT trace suggesting that the GDD is responding to viscosity. This implies that the resistance in the GDD sample loop is significant.

From the theory derived in this work, the density should produce a negative step. However, a positive step is observed. In Figure *6.38*, it can be seen that in both cases the viscosity effects are positive and could be offsetting the density measurement. The lines added to the figures shows that the effects on both the DPT and GDD match up. The viscosity step is slightly behind the density effect which is consistent with the position of each in the system loop.

The original designers of the GDD did not consider the possibility that viscosity change could affect the results obtained for the GDD. This work has shown that viscosity is very important to the operation of the GDD.

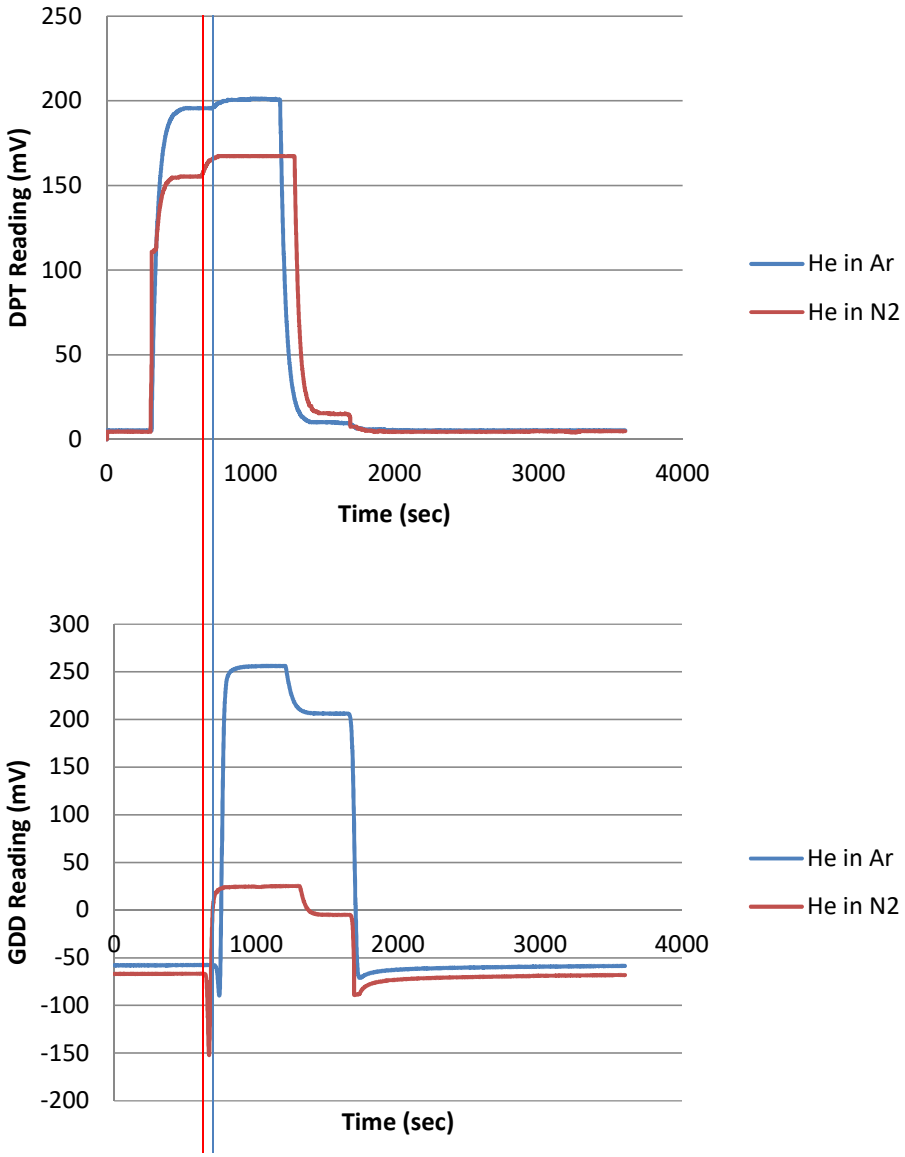

Figure 6.43 – DPT and GDD results from adding different combinations of pure components to the system

Further work is required to determine the size of the resistances in the sample loop and to establish the sizes of resistances which cause this effect from the viscosity change. Further experiments should be conducted to establish if the viscosity steps are correct for the perturbations that have been used here. Measurements should be taken with and without the GDD to determine if the additional resistance caused by the GDD is having an effect. If the measurements with and without the GDD are the same, it will be seen if the additional resistance due to the GDD is having an effect.

The additional flow in the reference side could be affecting the DPT result if there is a significant resistance in this stream due to the GDD. Additional work should be carried out to ascertain this.

It would be beneficial to check the pressure drop across the GDD loop and verify if they are significant and if they compare to the pressure drop across the measuring resistance in the flux response detector.

6.6.6. Future Work

6.6.6.1. Helium Experiments

Many issues have arisen with the use of helium in the gas density detector. The DPT and GDD experiments do not confirm the concepts derived. This could be due to many causes.

It could be due to the flow rates used in the experiments not being high enough to avoid back diffusion of helium from the sample flow into the reference flow. It would be beneficial in future work to investigate the flow rate required to inhibit back diffusion of helium into the reference flow.

Another reason could be an imbalance in the resistances in the GDD loops as described in Section 6.5.2. It may be caused by a change in viscosity causing a change in resistance of the internal jet of the back pressure regulator as discussed in Section 6.6.3. Or it may be due to the GDD reacting to the viscosity change when the perturbation has been added as previously considered in Section 6.6.5.

New experiments could be conducted to extend the length of time that the perturbation can flow into the system and establish a new steady state before the perturbation is removed from the system.

Experiments using different flow rates could also aid in determining a pattern to develop a relationship between the DPT and GDD results and the composition of components used.

Also, new experiments using hydrogen instead of helium could be conducted to compare using gases with low molecular weight.

All of the work described in this section will aid in the understanding of the operation and assembly of the GDD and find its limitations. This could help in revising the current design to make a more user friendly device.

6.6.6.2. Gas Mixtures using pure components as perturbation gas

If the gas density detector is to be used for industrial applications, it will need to able to be able to work with gas mixtures. Experiments could be performed using binary gas mixtures of known composition to determine if the system can be used for the determination of gas mixtures. The perturbation gas can be either of the components and the results analyzed to determine if they follow the theory.

6.6.6.3. Gas Mixture perturbed by a different gas

To further the previously proposed work, binary gas mixtures could be perturbed by a gas of a different component. If the perturbation gas is of a known density, then it is possible it can be used to aid in the determination of the components in the gas mixture.

6.6.6.4. Ternary Gas mixtures

Previous work by Heslop *et al*. (2000) [62] had looked at the determination of the composition of binary gas mixtures by the addition of one of the known components to a system. By incorporating the gas density into the system as an extra detector there is the potential to expand this to ternary mixtures. Further work could include this addition to the system.

6.7. Conclusions

In this chapter, theory has been derived to find a relationship in the operation of the gas density detector operation between the change in flows within the system (Δq) and the change in the density of the gas mixture through the system ($\Delta \rho$). The pressure drops around the system have been derived, an understanding of how the change in sample flow composition affects the GDD response and an investigation into how the addition of a perturbation flow affects the system have been explored.

Experiments have been carried out to validate these theories using various gas components and flow rates. It has been proved that the reference flow into the system needs to be consistent. When using nitrogen and argon as perturbation and main flow and vice versa, the theories are confirmed. However, when helium is used as either the main flow or the perturbation flow, the results are not as expected. The results obtained imply that the GDD is affected by viscosity change as well as flow and density changes. There is also evidence from the helium experiments which suggest that the resistances in the GDD are not balanced. This was one of the assumptions made when developing the fundamental theory. Extra work with other gases will be required to further confirm these concepts.

Further work will also need to be completed to investigate how the gas density detector can be used to quantify the effect of gas density changes in flux response systems.

7. Conclusions and Future Work

In this thesis, work has been carried out to look at different ways in which density change will affect flux response systems. Flux response technology uses differential measurements and so can be beneficial in gas chromatography for measuring very small differences in flow rates leaving the column.

The apparatus used throughout is similar to that used in perturbation viscometry since delay lines are used to separate the effect of a change in flow rate and a change in density in a system when a perturbation flow applied. The apparatus is a twin-sided arrangement for differential measurements to be made between the reference and sample flows.

The first project investigated the measurement of volume using perturbations in pressure. The experimental set-up allowed a constant flow of nitrogen into the system. A valve was switched and the gas then flowed through a channel of higher resistance until a new steady state was achieved. At this point the valve was switched to its original position and allowed to reach steady state again. A new pneumatic Wheatstone bridge arrangement of resistances was designed and implemented so that these changes could be measured using a differential pressure transducer. The area under the resulting graphs were used to determine the volume in the system.

Additional work could be performed to further this project. This includes the possibility of encasing the apparatus in an enclosure to shield the equipment from any environmental influences like temperature or pressure. This should reduce any variation in results due to these factors. An improved means of delivering a constant mass flow rate could also be considered and the inclusion or a back pressure regulator instead of discharging to atmospheric pressure could be pursued to improve accuracy and external effects.

Another option could be to use needle valves to provide the change in pressure instead of lengths of tubing. These could be more accurate while reducing the increase in system volume and will eliminate the use of the 3-way valve creating points in the experiment where flow is restricted when the valve it switched.

Further experiments could be carried out to try this theory on a bigger scale so that it could be used in industrial applications. Also, experiments could be conducted without the test volume or with very small volumes to determine the limits of the apparatus.

The second project involved the measurement of volume by perturbing the gas flow into the system with another perturbation gas flow. This work aimed to improve the existing arrangement from the first work by incorporating existing flux response technology to measure volume. Twin-sided apparatus was set up with delay lines and flux response measurements were taken using a differential pressure transducer. The delay lines were added so that there can be a distinction between flux response due to the change in flow caused by adding the perturbation flow and due to the change in density. The results in this project differed from those in the first project in that the step changes after the perturbation flow is added and measured instead of the area under the curve. These were used to determine the volume measurement in the system.

In the work conducted in this section, only single component systems were used in experiments. Future work using multi-component systems would be beneficial to obtain graphs with both the pressure change steps due to the change in flow rate and the change in composition and density. Further experiments could be conducted using different gases to compare the pressure changes with different viscosities.

It would also be interesting to use the theory developed in the second section to find the viscosity when the volume is known or to consider using different resistances while keeping the viscosity constant.

The third project involved the use of a gas density detector in the system used in the second project to allow multicomponent systems to be considered. A twin-sided apparatus was set up with delay lines. The delay lines were in the system to separate the pressure change due to the change in flow rate and the change in density after the perturbation flow was added to the system. Flux response measurements were taken using a differential pressure transducer. The resulting change in composition causing by the addition of the perturbation flow was also measured using the gas density detector. Theoretical equations were derived for the expected response from the differential pressure transducer and the gas density detector. Experiments were carried out to validate the theoretical equations. The results obtained when using nitrogen and argon as reference and perturbation flow and vice versa were as expected.

When helium was used in the system, the results did not follow what was expected. It was suspected that this was due to the reference flow rate being too low and so back diffusion in to the reference flow affected the result. Further work would be advantageous to find the minimum reference flow rate to avoid any issue with back diffusion.

It would be beneficial to look at alternative arrangements for the apparatus used in this work. The gas density detector might give more useful results if it were situated in a different section of equipment. The equipment throughout the experimental work was situated on the benchtop in the laboratory. It would be beneficial to have the equipment enclosed in an environment that could be controlled and will not be affected by the atmosphere around the system.

Additional experiments using different gas components would be of value to further validate the theoretical expressions derived in this section. Also, experiments using binary and ternary gas mixtures could be considered for this apparatus.

Upon further investigation, it appears that the gas density detector is affected by changes in viscosity as well as density. This has never been explored before and would be interesting to complete additional experiments with different gases and flow rates to confirm this hypothesis.

In this section of work is was assumed that the resistances in the GDD loops were balanced. This may not be the case. Further investigation should be completed to verify if this the situation. The effect of the GDD to the resistance in the system should be looked at. Measurements should be taken with and without the GDD to determine if the additional resistance caused by the GDD is having an effect. If the measurements with and without the GDD are the same, it will be seen if the additional resistance due to the GDD is having an effect.

To conclude this thesis, the three main aims set out in the introduction were met:

1. A new pneumatic Wheatstone bridge arrangement of resistances which allows a pressure perturbation to be used to measure system volumes was developed.
2. Existing flux response technology was used to improve the arrangement developed initially by building a two-sided apparatus where changes were made by adding a perturbation flow to one side of the system in order for volumes to be measured.

3. The operation of the gas density detector was investigated and a new method of measurement through the inclusion of the gas density detector to the experimental arrangement was introduced, allowing binary component systems to be considered.

As can be seen above, there are many areas where it would be valuable to continue this work and potential applications.

8. Appendices

8.1. Appendix 1: Conference Proceedings of CHISA 2006: 17th International Conference of Chemical and Process Engineering

Experimental determination of volumes from flow rate measurements

M.J. Heslop, A. McDonald, and E. Knotts
Department of Chemical and Process Engineering, University of Strathclyde, James Weir Building, 75 Montrose Street, Glasgow, G1 1XJ, United Kingdom; tel: + 44 141 548 2825, email: mark.heslop@strath.ac.uk

8.2. Appendix 2: Paper accepted for Adsorption Journal 2008

New experimental method for the determination of single-component isotherms: an application of the flow-rate retention time

M.J. Heslop[1], G. Mason[2], B.A. Buffham[2], A. McDonald[1] and R. Low[3]

[1]Department of Chemical and Process Engineering, University of Strathclyde, James Weir Building, 75 Montrose Street, Glasgow, G1 1XJ, United Kingdom; tel: + 44 141 548 2825, email: mark.heslop@strath.ac.uk; [2]Department of Chemical Engineering, Loughborough University, Loughborough, Leicestershire, LE11 3TU, United Kingdom; [3]INEOS Fluor Limited, PO Box 13, The Heath, Runcorn, Cheshire, WA7 4QF, United Kingdom.

8.3. Appendix 3: Conference Proceedings of CHISA 2016: 22nd International Conference of Chemical and Process Engineering

Measurement of volume, voidage and porosity: a novel application of the material balance

M.J Heslop and [1]A. McDonald
University of Sheffield, Department of Multidisciplinary Education, 32 Leavygreave Road, Sheffield S3 7RD, United Kingdom; tel. +44 114 222 7601, m.j.heslop@sheffield.ac.uk; [1]University of Strathclyde, Department of Chemical Engineering, 75, Montrose Street, Glasgow, United Kingdom

9. References

1. Phillips C. *Gas Chromatography.* Butterworths; 1956.
2. Grob RL. *Modern Practice of Gas Chromatography*. John Wiley & Sons; 1985.
3. Purnell H. *Gas Chromatography.* John Wiley & Sons; 1962.
4. Knox JH. *Gas Chromatography.* Butterworths; 1962.
5. McNair HM. *Basic Gas Chromatography*. Varian Aerograph; 1969.
6. Littlewood AB. *Gas Chromatography: Principles, Techniques and Applications*. Academic Press; 1962.
7. Paryjczak T. *Gas Chromatography in Adsorption and Catalysis*. Halsted Press; 1986.
8. Martin AJP and James AT. Gas-Liquid Chromatography: a New Apparatus for the Detection of Vapours in Flowing Gas Streams. *Biochem. J.* 1956; 65: 138-143.
9. Nerheim AG. A Gas-Density Detector for Gas Chromatography. *Analytical Chemistry.* 1963; 35: 1640-1644.
10. Guillemin CL and Auricourt MF. Gas Phase Chromatography- Study of the Gow-Mac Gas Density Balance – Application to Quantitative Analysis. *J. Gas Chromatog.* 1963; 1: 24-29.
11. Guillemin CL and Auricourt MF. Choice of Carrier Gas for the Gas Density Balance. *J. Gas Chromatog.* 1964; 2: 156-159.
12. Guillemin CL, Auricourt MF and Blaise P. Operation of the Gow-Mac Gas Density Balance. *J. Gas Chromatog.* 1966; 4: 338-342.
13. Vermont J and Guillemin CL. Gas Density Balance Calibration Technique – Application to Relative Response Factors for Thermal Conductivity Detectors. *Analytical Chemistry*. 1973; 45: 775-781.
14. Walsh JT and Rosie DM. Studies of the Gas Density Cell. *J. Gas Chromatog.* 1967; 5: 232-240.
15. Vermont J and Guillemin CL. Gas Density Balance Calibration Technique – Application to relative Response Factors for Thermal Conductivity Detectors. *Analytical Chemistry*. 1973; 45: 775-781.
16. Heggie DT and Reeburgh WS. Measurements of Dissolved Permanent Gases with a Gas Density Balance Detector. *J. Chromatogr. Sci.*1974; 12: 7-10.

17. Barry EF and Rosie DM. Rapid Determination of Response Factors for the Gas Chromatographic Thermal Conductivity Detector. *J Chromatography*. 1975; 103: 180-181.
18. Kiran E and Gillham JK. The Gas Density Balance and the Mass Chromatograph. *Analytical Chemistry*. 1975; 47: 983-995.
19. Brandes E, Kirchner HH and Richter W. Gas Analysis Using a Gas Density Detector. *Fresenius Z. Anal. Chem.* 1984; 319: 898-902.
20. Coulson JM, Richardson JF, Backhurst JR, Harker JH. *Coulson and Richardson's Chemical Engineering Volume 2 – Particle Technology and Separation Processes*. Butterworth-Heinemann; 1991.
21. http://www.npl.co.uk/science-+-technology/analytical-science/trace-analysis-and-electrochemistry/chromatogram
22. Dimbat M, Porter PE and Stross FH. Apparatus Requirements for Quantitative Application of Gas-Liquid Partition Chromatography. *Analytical Chemistry*. 1956; 28: 290-297.
23. Sevcik J. *Detectors in Gas Chromatography.* Elsevier Science Publishers; 1976.
24. https://en.wikipedia.org/wiki/Thermal_conductivity_detector#/media/File:Thermal_Conductivity_Detector_1.svg
25. Liberti A, Conti L and Crescenzi V. Molecular Weight Determination of Components by Gas-Phase Chromatography. *Nature.* 1956; 178: 1067-1069.
26. Phillips CSG and Timms PL. Molecular Weight Determination with the Martin Density Balance. *J. Chromatog.* 1961; 5: 131-136.
27. Guillemin CL, Auricourt MF, Du Crest J and Vermont J. Accurate and Rapid Method for Obtaining Substance-Specific Correction Factors Usable in Quantitative Analysis by Gas Chromatography. *J. Chromatogr. Sci* 1969; 7: 493-499.
28. Nerheim AG. Gas-Density Detector – Effects of Reference Flow and Outlet Tube Design on response and Accuracy. *J. Chromatogr. Sci.* 1977; 15: 465-468.
29. Bosanquet CH and Morgan GO. The Concentration Factor in Vapour Phase Partition Chromatography, *Vapour Phase Chromatography* (ed. D.H. Desty), pp 35-50, Butterworth; 1957.
30. Buffham BA, Mason G and Meacham RI. Sorption-Effect Chromatography. *Journal of Chromatographic Science.* 1986; 24: 265-269.
31. Meacham RI, Buffham BA and Mason G. The Role of Viscosity in Sorption-Effect Chromatography. *Journal of Chromatographic Science*. 1990; 28: 34-41.

32. Buffham BA, Mason G and Meacham RI. (1993) Absolute Gas Chromatography. *Proc. R. Soc. Lond. A*. 1993; 440: 291-301.

33. Buffham BA. (1978) Model-Independent Aspects of Perturbation Chromatography Theory. *Proc. R. Soc. Lond. A.* 1978; 364: 443-455.

34. Buffham BA, Mason G and Yadav GD. Retention Volumes and Retention Times in Binary Chromatography: Determination of Equilibrium Properties. *J. Chem. Soc. Faraday Trans. I*. 1985; 81: 171-173.

35. Mason G and Buffham BA. Gas Adsorption Isotherms from Composition and Flow-Rate Transient Times in Chromatographic Columns I. Basic Theory and a Binary Experimental Test. *Proc. R. Soc. Lond. A*. 1996a; 452: 1263-1285.

36. Mason G and Buffham BA. Gas Adsorption Isotherms from Composition and Flow-Rate Transient Times in Chromatographic Columns III. Effect of Gas Viscosity Changes. *Proc. R. Soc. Lond. A.* 1997; 453: 1569-1592.

37. Mason G and Buffham BA. Gas Adsorption Isotherms from Composition and Flow-Rate Transient Times in Chromatographic Columns II. Effect of Pressure Changes. *Proc. R. Soc. Lond. A.* 1996b; 452: 1287-1300.

38. Mason G, Buffham BA, Heslop MJ and Zhang B. Capillary Viscometry by Perturbation of Flow and Composition. *Chemical Engineering Science.* 1998; 53: 2665-2674.

39. Russell PA, Buffham BA, Mason G and Heslop MJ. Perturbation Viscometer to Measure the Viscosity Gradients of Gas Mixtures. *AIChE* 2003; 49: 1986-1994.

40. Mason G, Buffham BA, Heslop MJ, Russell PA and Zhang B. Perturbation Viscometry of Gas Mixtures. Addition and Removal of Finite Perturbations. *Chemical Engineering Science*. 2000; 55: 5747-5754.

41. Buffham BA, Mason G, Heslop MJ and Russell PA. Perturbation Viscometry of Gas Mixtures: Fitting a Model to Logarithmic Viscosity Gradients. *Chemical Engineering Science.* 2002; 57: 4493-4504.

42. Russell PA, Buffham BA, Mason G and Heslop MJ. The Effect of Very Large Perturbation Flows on a Perturbation Viscometer. *Chemical Engineering Science*. 2005; 60: 2943-2954.

43. Russell PA, Buffham BA, Mason G, Richardson DJ and Heslop MJ. Perturbation Viscometry Measurement of Viscosity Ratios for Ternary Gas Mixtures and Quantification of the Errors. *Fluid Phase Equilibria*. 2004; 215: 195-205.

44. Russell PA, Buffham BA, Mason G and Hellgardt K. Measurement of the Gradient of Viscosity with Composition of Mixtures of Non-Ideal Gases. *Chemical Engineering Science*. 2006; 61: 6604-6615.

45. Buffham BA, Hellgardt K, Heslop MJ and Mason G. Remote Sensing of the Flux Responses of a Gas-Solid Catalytic Micro-Reactor. *Chemical Engineering Science*. 2000; 55: 1621-1632.

46. Rathor MN, Buffham BA and Mason G. Determination of the Volumes of Void Zones in Packed Chromatographic Columns. *Journal of Chromatography.* 1988; 445: 37-48.

47. Buffham BA, Mason G and Koash K. Composition-Front Scanning of Porous Media. *Transactions of the Institute of Chemical Engineers A*. 1996; 74: 627-634.

48. Buffham BA, Hellgardt K, Heslop MJ, Mason G and Richardson DJ. Modelling and Simulation of the Flux Responses of a Gas-Solid Catalytic Micro-Reactor. *Chemical Engineering Science*. 2002; 57: 953-966.

49. Coulson JM and Richardson JF. *Coulson and Richardson's Chemical Engineering Volume 1 – Fluid Flow, Heat Transfer and Mass Transfer*. Butterworth-Heinemann; 1996.

50. Schaschke C. *Fluid Mechanics – Worked Examples for Engineers*. IChemE; 1998.

51. Segnini S, Pedreshi F and Dejmek P Volume measurement method of potato chips. *International Journal of Food Properties.* 2004; 7: 37–44.

52. Drazeta L, Lang A, Hall AJ, Volz RK, and Jameson PE. Air volume measurement of 'Braeburn' apple fruit. *Journal of Experimental Botany.* 2004; 55: 1061–1069.

53. Frattolillo A. New simple method for fast and accurate measurement of volumes. *Review of Scientific Instruments.* 2006; 77: 045107.

54. Palmer C, Sasegbon A and Hellgardt K. In situ measurement of gas adsorption processes using Flux Response Technology. *Adsorption*. 2011; 17: 783-794.

55. Kobata T, Ueki M, Ooiwa A and Ishii Y. Measurement of the volume of weights using an acoustic volumeter and the reliability of such measurement. *Metrologia.* 2004; 41: S75–S83.

56. Tosti S and Bettinali L. Volume measurements by means of membranes. *Desalination.* 2006; 200: 140–141.

57. Bruun HH. *Hot-Wire Anemometry – Principles and Signal Analysis*. Oxford University Press; 1995.

58. Perry AE. *Hot-Wire Anemometry.* Claredon Press Oxford; 1982.

59. http://www-g.eng.cam.ac.uk/whittle/current-research/hph/cta-circuit/cta-circuit.html

60. King LV. On the Convection of Heat from Small Cylinders in a Stream of Fluid: Determination of the Convection Constants of Small Platinum Wires with Applications to Hot-Wire Anemometry. *Philosophical Transactions of the Royal Society of London, Series A*. 1914; 214: 373-432.

61. http://www-g.eng.cam.ac.uk/whittle/current-research/hph/hot-wire/hot-wire.html

62. Heslop MJ, Mason G and Buffham BA. Absolute Determination of the Composition of Binary Gas Mixtures by Admixture of Known Components. *IChemE.* 2000; 78: 1061-1065.

10. Nomenclature

Chapter	Symbol	Description
2, 4, 5	A, A', A_1, A_1'	Area
2	M, M_1, m, m'	Molecular weights
2, 3, 4, 5, 6	P, p	Pressure
2, 3	V	Volume
2	K	Constant
2	$\Delta(\Delta P)$	Change in Pressure Drop
2	$\Delta\rho$	Change in Density
2	$(X_B - X_D)$	Height of gas in vertical conduit
2	F	Constant for Friction
2	ΔU	Change in flow rate
2, 3, 4, 5, 6	μ, μ', μ''	Viscosity
2	L/l	Length of conduit
2, 6	g	Gravitational constant
2	D	Diameter of conduit
2	S_d	Sensitivity factor
2	F	Carrier Gas flow rate
2	R	Recorder sensitivity
2	C	Reciprocal chart speed
2	E	Vapour volume
2	ΔM	Density difference
2	Kn	Knudsen number
2	λ	Mean free path
2	Ma	Mach number
2, 3 ,6	v	Fluid velocity
2	c	Velocity of sound in fluid
2	$\Delta\rho/\rho_0$	Relative change in density
2	Re	Reynolds number
2, 6	h	Height of conduit
2	R_1	Conduit radius
2, 3, 6	ρ, ρ', ρ''	Density
2, 3, 4, 6	Q	Volumetric flow rate
2, 3	π	pi
3	ΔP	Change in pressure
3	r	Radius of tube
3	l, z	Length of tube
3	k	Tubing constant
3, 4, 5	M, m	Molar flow rate
3, 4, 5	R	Universal gas constant

Chapter	Symbol	Description
3	V	Total specific volume
3	v_A, v_B	Specific volume of components
3	x_A, x_B	Mass fractions
3	w_A, w_B	Molecular weights
3, 4	n	Number of moles
3, 4, 5	T	Absolute temperature
3	Z	Compressibility factor
3, 4, 5	H	Hold-up
3	h	Statis head
4, 5	V	Volume
4, 5, 6	k	Resistance
4, 5	t	Time
4	Δk	Change in resistance
5	R_{add}, R_{rem}	Pressure ratio when perturbation is added/removed
6	Nu	Nusselt number
6	h	Heat transfer coefficient
6	d	Diameter
6	k	Thermal conductivity
6	q	Heat loss
6	πdL	Heat transfer area
6	V	Voltage drop
6	R	Resistance
6	Δq	Perturbation flow